


6-30-2021

High and Low Toxin Producing Strains of *Karenia Brevis* Differ Significantly in the Redox Proteome, Lipid Profiles, and Xanthophyll Cycle Pigments

Ricardo Colon
rcolo030@fiu.edu

Follow this and additional works at: <https://digitalcommons.fiu.edu/etd>

 Part of the [Biochemistry Commons](#), [Cellular and Molecular Physiology Commons](#), [Environmental Chemistry Commons](#), [Environmental Health Commons](#), [Marine Biology Commons](#), and the [Molecular Biology Commons](#)

Recommended Citation

Colon, Ricardo, "High and Low Toxin Producing Strains of *Karenia Brevis* Differ Significantly in the Redox Proteome, Lipid Profiles, and Xanthophyll Cycle Pigments" (2021). *FIU Electronic Theses and Dissertations*. 4746.

<https://digitalcommons.fiu.edu/etd/4746>

This work is brought to you for free and open access by the University Graduate School at FIU Digital Commons. It has been accepted for inclusion in FIU Electronic Theses and Dissertations by an authorized administrator of FIU Digital Commons. For more information, please contact dcc@fiu.edu.

FLORIDA INTERNATIONAL UNIVERSITY

Miami, Florida

HIGH AND LOW TOXIN PRODUCING STRAINS OF *KARENIA BREVIS* DIFFER
SIGNIFICANTLY IN THE REDOX PROTEOME, LIPID PROFILES, AND
XANTHOPHYLL CYCLE PIGMENTS

A dissertation submitted in partial fulfillment

of the requirements for the degree of

DOCTOR OF PHILOSOPHY

in

CHEMISTRY

by

Ricardo Colon

2021

To: Dean Michael R. Heithaus
College of Arts, Sciences and Education

This dissertation, written by Ricardo Colon, and entitled High and Low Toxin Producing Strains of *Karenia Brevis* Differ Significantly in the Redox Proteome, Lipid Profiles, and Xanthophyll Cycle Pigments, having been approved in respect to style and intellectual content, is referred to you for your judgement.

We have read this dissertation and recommend that it be approved.

John Landrum

Kevin O'Shea

Joongho Moon

Jose Eirin-Lopez

Kathleen Rein, Major Professor

Date of Defense: June 30, 2021

The dissertation of Ricardo Colon is approved.

Dean Michael Heithaus
College of Arts, Sciences and Education

Andrés Gil
Vice President for Research and Economic Development and
Dean of the University Graduate School

Florida International University, 2021

Figure 1.2 on page 4 was reproduced with permission from John Wiley and Sons (Lic No. 4983171465273, Jan 06, 2021) as found in “Diversity and evolutionary history of plastids and their hosts” originally published in the American Journal of Botany

Figure 1.10B on page 25 and Figure 1.11 on page 26 were reproduced with permission from John Wiley and Sons (Lic. No. 507606013966, May 26, 2021) as found in “Brevetoxin, the Dinoflagellate Neurotoxin, Localizes to Thylakoid Membranes and Interacts with the Light-Harvesting Complex II (LHCII) of Photosystem II” originally published in ChemBioChem

Figure 5.2 on page 134 was reproduced with permission from John Wiley and Sons (Lic. No. 5062471298218, May 05, 2021) as found in “Semisynthesis of cytotoxic proteins using a modified protein splicing element” originally published in Protein Science.

© Copyright 2021 by Ricardo Colon

All rights reserved.

DEDICATION

I dedicate this work to my family. You all are the reason I want to succeed. My nieces and nephews who I love so much, I hope to set an example that you can achieve what ever you set your mind to. To Damian, who left us too young, you will always be in my heart. To my beautiful and caring mother, who taught me how to hustle for what I want. To my loving dad, who taught me how to think outside the box and gave me my curiosity and resourcefulness. To my big sisters and brother who set examples for me along the way. To my aunts and uncles, who always took care of me along the way. To my grandparents who sacrificed so much to give us everything.

I love you all from the bottom of my heart.

ACKNOWLEDGMENTS

I would like to humbly thank all of those who have helped me accomplish this journey.

First, I would like to thank Dr. Kathleen Rein for her 7 years of support for me as an undergraduate and a graduate student. Dr. Rein has been like a mother to me, and I will always remember the fire she ignited within me and her relentless work ethic. If not for her, I would not have started this journey. Although I may not have always been the easiest to mentor, I will have eternal gratitude for the effort she put into guiding me along my way.

A special thank you to my fellow classmates and lab mates, if it were not for the laughter, tears, and beers we have shared, grad school would have been the end of me. I am thankful for the support of my committee members, who have challenged and supported me along the way. Our graduate secretary Maggie Autie, a wonderful human being with a heart of gold, thank you for all your help along the way. Dr. William Louda for his assistance and collaboration on detecting and quantitating the xanthophylls in *K. brevis*. Dr. Rob Hondal for his help in training and collaboration on the purification of *KbTrxR*.

A huge thanks to FIU for the funding for professional development in the form of conferences, workshops, and my employment at the FIU Health Aux Lab.

Of course, my family who has kept me going and kept me fed when I was too tired... or lazy to cook for myself.

My fiancé Gaby and her family, who has shown me nothing but love and support along the way.

ABSTRACT OF THE DISSERTATION

HIGH AND LOW TOXIN PRODUCING STRAINS OF *KARENIA BREVIS* DIFFER
SIGNIFICANTLY IN THE REDOX PROTEOME, LIPID PROFILES, AND
XANTHOPHYLL CYCLE PIGMENTS

by

Ricardo Colon

Florida International University, 2021

Miami, Florida

Professor Kathleen Rein, Major Professor

The dinoflagellate *Karenia brevis*, blooms annually in the Gulf of Mexico, producing a suite of neurotoxins known as the brevetoxins. The cellular toxin content of *K. brevis*, however, is highly variable between or even within strains. I investigated biochemical differences between high (*KbHT*) and low (*KbLT*) toxin producing cultures both derived from the Wilson strain, related to energy-dependent quenching (qE) by photosystem II, and the content of reduced thiols of the proteome. By characterizing the xanthophyll content of the two strains I was able to determine that *KbLT* performs qE inconsistently. To investigate the source of the differences in qE, RT-qPCR was utilized to examine gene expression of the xanthophyll cycle enzyme diadinoxanthin de-epoxidase (Dde), however no differences in expression were found. Furthermore, using redox proteomics the protein expression of Dde and monogalactosyldiacylglycerol (MGDG)

synthase were determined to not be significantly different in the two cultures. Also reported are significant differences in the lipidomes of *KbHT* and *KbLT* with respect to MGDG, which facilitates the xanthophyll cycle. Redox proteomics experiments detected a significantly higher proportion of proteinogenic cysteine thiols in the reduced thiol state in the low toxin proteome, including plastid localized thioredoxin (Trx), which can result in inactivation of Dde and activation of MGDG synthase. Moreover, recombinant *K. brevis* thioredoxin reductase (*KbTrxR*) was produced in order to characterize the interaction of this enzyme with brevetoxin. Brevetoxin was found to inhibit reductase activity towards various substrates. Using mass spectrometry, I was able to detect an adduct of *KbTrxR* and brevetoxin on a cysteine residue at the N-terminal redox center. This supports the hypothesis that brevetoxin could mediate redox homeostasis by interacting with thiol-disulfide centers in thioredoxin reductase.

TABLE OF CONTENTS

CHAPTER	PAGE
Chapter 1: The marine dinoflagellate <i>Karenia brevis</i> , a special type of phytoplankton	1
1.1 A brief overview of phytoplankton and the importance of endosymbiosis	1
1.2 Primary and secondary metabolites of phytoplankton origin.....	7
1.2.1 Biofuels and consumer products.....	7
1.2.2 Phycotoxins	11
1.3 Harmful algal blooms.....	18
1.4 The economic and public health issues of <i>Karenia brevis</i> and the brevetoxins	20
1.5 Investigating the role of brevetoxin	22
1.5.1 Brevetoxin binding to LHC-II indicates a role in photosynthesis	25
1.5.2 The thioredoxin system links redox homeostasis and photosynthesis	29
1.6 Significant biochemical differences in high and low toxin producing strains of <i>K. brevis</i>	35
1.7 Project overview and specific aims.....	37
1.7.1 Research Objectives	38
Chapter 2: Comparative analysis of the NPQ-essential, xanthophyll cycle pigments in high and low toxin <i>K. brevis</i> under varying light conditions.....	39
2.1 The xanthophyll cycle plays an essential role in NPQ.....	39
2.2 Results and Discussion.....	41
2.3 Materials and methods	44
2.3.1 Reagents.....	44
2.3.2 Culture growth conditions	44
2.3.3 Extraction and analysis of carotenoids	44
2.4 Conclusion.....	46
Chapter 3. Evaluation of essential components of NPQ in high and low toxic strains of <i>K. brevis</i>	48

3.1.1 Xanthophyll de-epoxidase activity is dependent on pH, redox status, and lipid content	48
3.1.2 Lipid-pigment-protein interactions.....	50
3.1.3 SQDG; a negatively charged lipid required for the proper functioning of PS-II.....	52
3.1.4 <i>Karenia brevis</i> allelopathy disrupts photosynthetic capabilities and lipid biosynthesis of competitors.	53
3.2 Results and discussion.....	54
3.2.1 The relative levels of expression of four Dde homologues in <i>KbHT</i> and <i>KbLT</i>	54
3.2.2 Comparison of thylakoid lipids in high and low toxic strains of <i>K. brevis</i>	57
3.3 Materials and methods	58
3.3.1 General.....	58
3.3.2 q-RT-PCR of DDE in <i>KbHT</i> and <i>KbLT</i>	58
3.3.2.1 RNA extraction	58
3.3.2.2 RNA purification and analysis.....	59
3.3.2.3 q-RT-PCR of <i>K. brevis</i> DDE	60
3.3.3 Lipid analysis of <i>KbHT</i> and <i>KbLT</i>	60
3.3.3.1 Lipid extraction and analysis	60
3.3.3.2 Protein extraction.....	62
3.4 Conclusion.....	63
3.4.1 mRNA expression of DDE shows little variation between <i>KbLT</i> and <i>KbHT</i> ..	63
3.4.2 Thylakoid lipid content varies between <i>KbHT</i> and <i>KbLT</i>	64
 Chapter 4. Redox proteomics characterization of the high and low toxic strains of <i>K. brevis</i> using fourplex IodoTMT labeling.....	66
4.1.1 Thiol-disulfide exchange plays a key role in regulation of thylakoid proteins	66
4.1.1.1 Dde and MGDG synthase are disulfide regulated	67
4.1.1.2 Thioredoxins, glutaredoxins, and peroxiredoxins; important redox active proteins needed for ROS detoxification and regulation of enzyme activity.	68
4.1.1.3 Kinases and phosphatases	69
4.1.2 Polyketide synthases.....	71
4.1.3 Redox proteomics.....	73
4.1.4 Multiplex labeling using IodoTMT	75

4.2 Results and Discussion.....	77
4.2.1 Simultaneous duplex IodoTMT labeling of the <i>K. brevis</i> proteome reveals that <i>KbLT</i> contains significantly more reduced cysteine residues than <i>KbHT</i>	77
4.2.2 Cellular organelle localization of proteins.....	79
4.2.2.1 DeepLoc.....	79
4.2.2.2 ChloroP, TargetP, and SignalP; protein prediction tools.....	82
4.2.3 Functional Annotation	83
4.2.4 Differences in redox state are consistent across cellular organelles.....	84
4.2.5 The significance of expression differences between <i>KbHT</i> and <i>KbLT</i>	87
4.2.6 The significance of redox differences in <i>KbHT</i> and <i>KbLT</i>	89
4.2.7 Diadinoxanthin de-epoxidase, and MGDG synthase are expressed similarly, but have significant differences in redox status.....	91
4.2.8 Redox homeostasis mediating enzymes in the thioredoxin system, and glutaredoxin system, are significantly different in redox status.....	95
4.2.8.1 Thioredoxins	95
4.2.8.2 Glutaredoxins.....	96
4.2.8.3 Peroxiredoxins	98
4.2.8.4 Glutathione reductases.....	99
4.2.8.5 Thioredoxin reductases	100
4.2.9 Redox status among kinases and phosphatases are significantly different. ...	102
4.2.9.1 Kinases.....	102
4.2.9.2 Phosphatases	106
4.2.10 Proteins believed to be related to the biosynthesis of toxins are differentially expressed in <i>KbHT</i> and <i>KbLT</i>	109
4.2.10.1 Polyketide synthases: differences in expression and redox status	109
4.2.10.2 Cellular localization of PKS	110
4.3 Materials and methods	114
4.3.1 General.....	114
4.3.2 Culture growth conditions	114
4.3.3 Fourplex IodoTMT redox proteomics of <i>KbHT</i> and <i>KbLT</i>	114
4.3.3.1 Generation of a <i>K. brevis</i> protein database	114
4.3.3.2 Lysis, protein precipitation and quantitation	114
4.3.3.3 Fourplex IodoTMT labeling, trypsin digestion and enrichment of labeled peptides	116

4.3.3.4 Mass spectrometry and data processing.....	117
4.3.4 Bioinformatics tools and data analysis	118
4.3.4.1 Functional annotation using NCBI BLASTp, NCBI CDD, Pfam and BLASTKoala	118
4.3.4.2 Cellular localization and prediction tools	118
4.3.4.3 Homology model of Dde4	119
4.4 Conclusion.....	119
4.4.1 Multiplex labeling of the <i>K. brevis</i> proteome.....	120
4.4.2 Enzymes related to the xanthophyll cycle and qE.....	121
4.4.2.1 Diadinoxanthin de-epoxidase.....	121
4.4.2.2 MGDG synthase.....	124
4.4.3 Select plastid targeted proteins	125
4.4.3.1 Thiol oxidoreductases	125
4.4.3.2 Kinases and phosphatases	126
4.4.4 Polyketide synthases.....	129
4.4.4.1 Polyketide synthases are overexpressed in <i>KbHT</i>	129
 Chapter 5. Expression of recombinant <i>K. brevis</i> NTR and characterization of its enzymatic activity in the presence of PbTx-2.....	 131
5.1 Thioredoxin reductase activity is influenced by α , β -unsaturated carbonyl containing compounds and other electrophiles	 131
5.1.1 Brevetoxin is an effector of mammalian thioredoxin reductase.....	132
5.1.2 Semisynthesis of TrxR variants allows for exploration into the functionality of the C-terminus.....	134
5.2 Results and Discussion.....	137
5.2.1 Optimization of recombinant <i>KbTrxR</i> expression.....	137
5.2.2 Inhibition assays with <i>KbTrxR</i> and PbTx-2	140
5.2.3 <i>KbTrxR</i> forms a covalent adduct with PbTx-2 at the N-terminal redox center	142
5.3 Materials and methods	144
5.3.1 General.....	144
5.3.2 Cloning of <i>KbTrxR</i>	144
5.3.3 <i>KbTrxR</i> inhibition assays	146
5.3.3.1 DTNB reduction.....	146

5.3.3.2 H ₂ O ₂ reduction	146
5.3.3.3 Trx reduction.....	147
5.3.3.4 GSSG reduction	147
5.3.3.5 Preparation of PbTx-2/ <i>Kb</i> TrxR adducts	147
5.3.3.6 Mass spectrometry data analysis.....	148
5.4 Conclusion.....	148
5.4.1 <i>Kb</i> TrxR activity is inhibited by PbTx-2	149
5.5 Summary	149
References.....	153
APPENDIX.....	185
VITA.....	196

LIST OF TABLES

TABLE	PAGE
Table 1.1 Examples of algal toxins, their producers, mechanism of toxicity and class. ¹ -n-acetyl choline receptor, ² -protein phosphatase, ³ -cyclic adenosine monophosphate. .	14
Table 1.2 Putative NTRs found in the <i>K. brevis</i> using tBLASTn algorithm.	33
Table 1.3 Analysis of the <i>K. brevis</i> transcriptome library identified the machinery required to biosynthesize selenoproteins.	34
Table 2.1 Xanthophylls detected in <i>KbHT</i> and <i>KbLT</i> under varying light conditions (n=5), $p^{\text{Ddx}} = 0.05$, $p^{\text{Dtx}} = 0.04$	42
Table 2.2 Xanthophylls with significant differences on average between the strains (n=7, unless otherwise noted).	43
Table 3.1 Query origins, accession numbers and E values for the four corresponding loci from the <i>K. brevis</i> transcriptome library	55
Table 3.2. Primer sequences used to amplify each of the four <i>K. brevis</i> DDE homologues	55
Table 4.1 The global redox status of the proteomes of <i>KbHT</i> and <i>KbLT</i> , and the ratio of redox status for the four biological replicates (ρ shown is for paired t-test).	79
Table 4.2 Localization predictions of all proteins identified by fourplex IodoTMT	80
Table 4.3 Summary of predicted N-terminal presequences by ChloroP, TargetP (plant and non-plant), and SignalP.	82
Table 4.4 Relative expression of Dde and MGDG synthase expressed as ratio of total IodoTMT intensities for Dde and MGDG synthase relative to total intensities of all peptides (Light+Heavy-enzyme/Total) for each replicate of <i>KbLT</i> and <i>KbHT</i>	92
Table 4.5 Redox status of Dde and MGDG synthase expressed as ratio of IodoTMT intensities of Light / Light+Heavy for each replicate of <i>KbLT</i> and <i>KbHT</i>	93

Table 4.6 Diatoxanthin epoxidase expression (IodoTMT Light+Heavy for Dep over abundance for all peptides*10 ⁴), and redox status (IodoTMT Light/(Light+Heavy)). Ratios are shown for both expression and redox status.	95
Table 4.7 List of loci to which peptides detected in MS/MS analysis were mapped and their multiplicity (N), PKS match, cellular localization, cTP prediction, and expression ratio. E-value's shown are for BLASTp search. References: 1) Monroe et al., 2010, 2) Kohli et al., 2017.....	113
Table 5.1 Initial rates (v_0) of reduction of substrates by <i>KbTrxR</i> in the presence and absence of PbTx-2 (40 μ M)	141
Table 5.2 Brevetoxin adducted peptides in tryptic digest of <i>KbTrxR</i>	143
Table S3.1 Relative expression ratio vs RIN calculations	186
Table S3.2 All lipid species quantified (nmol per mg protein).....	186
Table S3.3 All SQDG species analyzed (signal per mg protein).....	187
Table S4.1 Ratios of IodoTMT intensities for plastid localized Trx in <i>KbLT</i> and <i>KbHT</i>	189
Table S4.2 Ratios of IodoTMT intensities for plastid localized Grx in <i>KbLT</i> and <i>KbHT</i>	190
Table S4.3 Ratios of IodoTMT intensities for plastid localized Prx in <i>KbLT</i> and <i>KbHT</i>	190
Table S4.4 Ratios of IodoTMT intensities for plastid localized GR in <i>KbLT</i> and <i>KbHT</i>	191
Table S4.5 Ratios of IodoTMT intensities for non-plastid localized GR in <i>KbLT</i> and <i>KbHT</i>	191
Table S4.6 Ratios of IodoTMT intensities for plastid localized TrxR in <i>KbLT</i> and <i>KbHT</i>	191
Table S4.7 Ratios of IodoTMT intensities for plastid localized TrxR in <i>KbLT</i> and <i>KbHT</i>	192

Table S4.8 Ratios of IodoTMT intensities for plastid localized kinases in KbLT and KbHT 194

LIST OF FIGURES

FIGURE	PAGE
Figure 1.1 Venn diagram describing differences and similarities between the three primordial algal species to arise from primary endosymbiosis.	3
Figure 1.2 A chart demonstrating algal endosymbiosis as shown in Keeling et al., 2004. Cyanobacteria are represented as blue organisms, while glaucophytes contain blue plastids. Red and green algae are shown containing plastids in their respective colors.	4
Figure 1.3 Structures of various algal natural products. A) astaxanthin: a reddish pigment used as a food additive, B) phycocyanobilin: a blueish pigment that has been used as a fluoroprobe for immunochemical detection, C) pheophorbide a: a chlorophyll derivative photosensitizer with medicinal functions used for producing ROS to target malignant cells	10
Figure 1.4 The hepatotoxic A) microcystin-LR and B) nodularin commonly found in cyanobacterial blooms	12
Figure 1.5 Structure of A) palytoxin and B) maitotoxin.....	13
Figure 1.6 A) Saxitoxin B) domoic acid and C) anatoxin-a	15
Figure 1.7 The structures of several polyether toxins. Linear polyethers A) azaspiracid-1 and B) okadaic acid. Polyether ladders C) ciguatoxin-1 and D) yessotoxin.	16
Figure 1.8 A) Brevetoxin A-type frame B) brevetoxin B-type frame, and their respective names and substituents.	17
Figure 1.9 A) Blooms of <i>M. aeruginosa</i> in Lake Okeechobee B) Extension east and west through the canals and rivers to Port St. Lucie and Cape Coral (Rosen et al., 2018)	19
Figure 1.10 A) Fluorescent brevetoxin probe B) <i>K. brevis</i> cells incubated with PbTx-2 probe (yellow), and autofluorescence of the chloroplast (red).	25
Figure 1.11 A) Brevetoxin photoaffinity probe B) protein binding of the photoaffinity probe is pH dependent with LHC-II binding at low pH and Trx and neutral/alkaline pH (used with permission from (Cassell, Chen, Thomas, Liu, & Rein, 2015).....	26

Figure 1.12 The xanthophyll cycle in A) plants and green algae B) dinoflagellates and diatoms. Vde/Dde – violaxanthin and diadinoxanthin de-epoxidase, Zep/Dep – zeaxanthin and diatoxanthin epoxidase, respectively.	27
Figure 1.13 A) NPQ of KbHT vs KbLT showing differences in observed functioning of NPQ. B) Reactive oxygen species production between KbHT and KbLT.	29
Figure 1.14 Electron flow from NADPH to protein disulfide bridges, via TrxR and Trx. Trx reduces many proteins and is returned to the active reduced state by TrxR in a NADPH dependent reaction. The C-terminal redox center (in the box) in high M _w TrxR can be composed of two cysteine residues or a cysteine and a selenocysteine.	31
Figure 3.1 A) Average (n=5) RIN-corrected expression of each gene target and control normalized to total RNA ($\rho = 0.011$, <i>DDE3</i>). Error bars represent the standard deviation for biological replicates. B) <i>KbHT/KbLT</i> C _t ratios of the target gene/RuBisCO. Error bars represent the standard deviation for technical replicates for the ratios of C _t ratios (<i>KbHT/KbLT</i>) of each DDE on individual days and were calculated as propagation of error of multiple variables.....	56
Figure 3.2 A) DGDG, MGDG, PG and total lipids (nmol/mg protein) in <i>KbHT</i> and <i>KbLT</i> . DGDG ($\rho = 0.138$), MGDG ($\rho = 1.7 \times 10^{-4}$), PG ($\rho = 0.012$), TOTAL ($\rho = 5.0 \times 10^{-4}$). B) Total lipid distribution for <i>KbLT</i> and <i>KbHT</i> . MGDG ($\rho = 2.7 \times 10^{-3}$), DGDG ($\rho = 1.9 \times 10^{-3}$). SQDG is not included in total lipids as it could not be accurately quantitated. C) SQDG in <i>KbHT</i> and <i>KbLT</i> ($\rho = 7.7 \times 10^{-3}$).....	58
Figure 4.1 ICAT reagent depicting the three different functionalities of the molecule. In red, the biotin linker which allows for affinity purification and is cleavable. In black, the isotope coded linker (which contains either 9x ¹² C or ¹³ C) and in blue the cysteine reactive group.....	74
Figure 4.2 Mechanism of cysteine reactive reagents used in proteomics. A) nucleophilic substitution of cysteine with iodoacetamide. B) Michael reaction (addition) to NEM. Both reactions yield irreversible thioether bonds which effectively block any further modification of cysteine.....	75
Figure 4.3 A) Isobaric iodoTMT cysteine labeling reagent. The mass of the reporter is balanced by the mass equalizer such that each label has the same nominal mass. Locations of labels are shown for TMT ¹³¹ (●) and TMT ¹²⁶ (*). B) Redox proteomics workflow. 1. Cysteine residues were labeled with the light label. (iodoTMT ¹²⁶ and iodoTMT ¹²⁷ for <i>KbHT</i> and <i>KbLT</i> respectively). 2. Unlabeled cysteine residues were reduced with TCEP. 3. Heavy tags (iodoTMT ¹³⁰ and iodoTMT ¹³¹ for <i>KbHT</i> and <i>KbLT</i> , respectively) were used to label newly reduced cysteine residues. 4. Equal amounts of labeled proteins (according to Bradford assay) were combined, trypsinized and purified	

using Immobilized anti-TMT resin (dark triangles represent unlabeled peptides which will not bind to the resin). 5. Purified, labeled peptides were eluted from the resin and analyzed via LC-MS/MS.	76
Figure 4.4 The thiol concentration of isolated proteins before labeling for each replicate. Error bars represent standard deviation of technical replicates (n=3).....	77
Figure 4.5 Distribution of cellular localizations translated from Table 4.2. ‘All criteria’ signifies $N \geq 3$, with ρ value for permutation tests ≤ 0.05 for both expression and redox.	81
Figure 4.6 Totals of functional annotation by algorithm	84
Figure 4.7A Distribution of redox status for the global proteome, plastid, mitochondrion and nucleus represented as $\log_2(\text{Redox Ratio H/L})$	85
Figure 4.7B Distribution of redox status for the cell membrane, cytoplasm, lysosome/vacuole, peroxisome, extracellular, and endoplasmic reticulum + golgi apparatus represented as $\log_2(\text{Redox Ratio H/L})$	86
Figure 4.8 Volcano plot showing significant differences in expression as a function of fold changes in expression ($N \geq 3$, 1093 proteins total). Green represents lower expression in KbHT and red represents higher expression in KbHT. The x-axis is presented on a \log_2 scale, so values of 1 and -1 represent 2-fold and 0.5-fold, respectively. Solid black lines represent the log values for permutation ρ values <0.05 and <0.01 . All permutation ρ values = 0 were set to equal 4 due to inability to calculate the $-\log_{10}$. Dashed vertical line represents the average expression ratio (0.19).....	89
Figure 4.9 Volcano plot showing significant differences in redox status as a function of fold changes in redox status ($N \geq 3$, 1093 proteins total). Green represents proteins more oxidized in KbHT and red represents more reduced in KbHT. The x-axis is presented on a \log_2 scale, so values of 1 and -1 represent 2-fold and 0.5-fold, respectively. Solid black lines represent the log values for permutation ρ values <0.05 and <0.01 . All permutation ρ values = 0 were set to equal 4 due to inability to calculate the $-\log_{10}$. Dashed vertical line represents the average redox ratio (-0.333).	91
Figure 4.10 Alignment of soybean NP_001240949.1 (Soy), spinach XP_021853497.1 (Spi) and tobacco AFP57681.1 (Tob) Vde with the four translated DDE homologues identified in the <i>K. brevis</i> transcriptome library. Multiple sequence alignments were generated using Clustal Omega, and visualized using BoxShade (Sievers et al., 2011). Red and blue amino acids represent greater than 50% identity and similarity between aligned sequences, respectively. The 12 conserved cysteine residues are highlighted in yellow. The peptide fragment identified by MS/MS (vide infra) is underlined.	94

Figure 4.11 A) Average expression for plastid localized Trx. B) Average redox status for plastid localized Trx peptides.....	96
Figure 4.12 A) Average expression for plastid localized Grx. B) Average redox status for plastid localized Grx peptides	97
Figure 4.13 A) Average expression for plastid localized Prx. B) Average redox status for plastid localized Prx peptides.....	99
Figure 4.14 A) Average expression for GR. B) Average redox status for GR peptides. ** represents non-plastid localized, both other GR were localized to the plastid based on either DeepLoc or ChloroP	100
Figure 4.15 A) Average expression for plastid localized TrxR. B) Average redox status for plastid localized TrxR peptides	102
Figure 4.16A Average expression for plastid localized kinases. *represents a different frame translation of Locus 15581.	104
Figure 4.16B Average redox status for plastid localized kinases. *represents a different frame translation of Locus 15581.	105
Figure 4.17A Average expression for plastid localized phosphatases.....	107
Figure 4.17B Average redox status for plastid localized phosphatases.....	108
Figure 4.18 A) Average expression for all polyketide synthases. B) Average redox status for polyketide synthases.....	112
Figure 4.19 Homology model of the lipocalin domain of Dde4 based on the lipocalin domain of Arabidopsis thaliana Vde, indicating in yellow, the disulfide bridge formed between Cys ²⁵⁴ and Cys ³⁸⁸	124
Figure 5.1 Sel-green probe reaction with selenocysteine (Sec) generates a fluorescent coumarin derivative. The inhibition of this reaction in the presence of PbTx-2 provides evidence of the reactivity of PbTx-2 with Sec residues.....	133
Figure 5.2 Intein mediated peptide ligation technique used to prepare TrxR. (Evans Jr, Benner, & Xu, 1998).....	136

Figure 5.3 SDS-PAGE of PTXB3 (2-6) and PTYB3 (7-13) +KbTrxR expressed in T7 Express cells. 1: MW Ladder, 2: PTXB3 uninduced cells, 3: whole cell 16°C, 4: lysate 16°C, 5: whole cell 37°C, 6: lysate 37°C. 7: PTYB3 uninduced cells, 8: whole cell 16°C, 9: lysate 16°C, 10: whole cell 37°C, 11: lysate 37°C, 12: whole cell 16°C+heatshock, 13: lysate 16°C+heatshock..... 138

Figure 5.4 A) Pre-cleavage fractions of chitin agarose column. 1: MW Ladder, 2: Flow-through, 3-6: washes with Chitin Buffer , 7: MW Ladder, 8-9: washes with Chitin Buffer B, 10: Chitin resin pre-cleavage fraction. Red box signifies the fusion protein ~110 kDa. B) Post-cleavage fractions of chitin agarose column. 1: MW ladder, 2: Cleavage with BME (RT), 3: Resin fraction BME (RT), 4: Cleavage with BME 37°C, 5: resin fraction BME (37), 6: MW Ladder, 7: Cleavage with NMA (RT), 8: Resin fraction NMA (RT), 9: Cleavage with NMA 37°C, 10: resin fraction NMA (37). 139

Figure 5.5 Absorbance spectra of purified KbTrxR shows the characteristic $\lambda_{\max} = 460$ nm. 140

Figure 5.6 PbTx-2 exhibits a dose dependent inhibition of H₂O₂ reduction by *KbTrxR*. IC₅₀ = 56.0 (± 4.67) μM..... 141

Figure 5.7 Cysteine adduct formed by *KbTrxR* and PbTx-2 via Michael addition followed by reduction with NaBH₄..... 143

Figure S3.1 Capillary electrophoresis data for each q-RT-PCR sample demonstrating the RIN values calculated 185

Figure S3.2 RIN Correction of relative expression for q-RT-PCR. RIN correction was performed by plotting a linear regression of relative expression ratio (RER) for all biological replicates of both low and high toxic vs RIN. RER was found using the equation $RER_n = Ct(RuBisCO)_n / Ct(RuBisCO)_\alpha$ for each technical replicate within the 5 pairs of biological replicates ($y = 0.1509x - 0.1308$). Where n = sample number, and α = sample number H4 (the sample with the highest quality RNA). The RER(calculated) was found by substituting the RIN for x in the above equation. RER(calculated) was used as a coefficient for each samples C_i to account for differing RNA quality. 185

ABBREVIATIONS AND ACRONYMS

¹ Chl*	singlet chlorophyll
¹ Dtx*	singlet diatoxanthin
¹ O ₂ *	singlet oxygen
2CPrx	2-cys-peroxiredoxin
³ Chl*	triplet chlorophyll
ACN	acetonitrile
ACP	acyl carrier protein
Adda	3-amino-9-methoxy-2,6,8-trimethyl-10-phenyl-4,6-decadienoic acid
ADP	adenosine diphosphate
AMP	adenosine monophosphate
AT	acyl transferase
ATP	adenosine triphosphate
Ax	antheraxanthin
BLAST	Basic Local Alignment Search Tool
BME	betamercaptoethanol
BSA	bovine serum albumin
C	carbon
Car	carotenoid
Chl	chlorophyll
CID	collision induced dissociation
CO ₂	Carbon dioxide
cTP	chloroplast transit peptide

CTX	ciguatoxins
Cys	cysteine
Da	Daltons
DCMU	3-(3, 4-dichlorophenyl)-1, 1-dimethylurea
Dde	Diadinoxanthin de-epoxidase (protein)
<i>DDE</i>	Diadinoxanthin de-epoxidase (gene)
Ddx	Diadinoxanthin
Dep	diatoxanthin epoxidase
DEPC	diethyl pyrocarbonate
DGDG	digalactosyl diacylglycerol
DH	dehydratase
DHA	docosaehaenoic acid
DMSO	dimethyl sulfoxide
DNA	deoxyribonucleic acid
DTNB	5,5-dithio-bis-(2-nitrobenzoic acid)
DTT	dithiothreitol
Dtx	Diatoxanthin
EDTA	ethylenediamine tetraacetic acid
EGT	endosymbiotic gene transfer
EPA	eicosapentaenoic acid
EPS	epoxidation site
ER	enoyl reductase
FAS	fatty acid synthase
FBPase	fructose-1,6-bisphosphatase

FCP	fucoxanthin-chlorophyll <i>a/c</i> binding protein
FDA	Food and Drug Administration
Fe	iron
FTR	ferredoxin thioredoxin reductase
Fx	fucoxanthin
g	grams
GR	glutathione reductase
Grx	glutaredoxin
GSH	reduced glutathione
GSSG	oxidized glutathione
GSx	total glutathione
Gt	Gigatonnes
H	hydrogen
HAB	harmful algal bloom
HCF164	high chlorophyll protein 164
HCl	hydrochloric acid
HPLC	high-performance liquid chromatography
IAM	iodoacetamide
ICAT	isotope coded affinity tags
ISC	intersystems crossing
<i>KbHT</i>	<i>Karenia brevis</i> high toxic
<i>KbLT</i>	<i>Karenia brevis</i> low toxic
KCl	potassium chloride
KR	ketoreductase

KS	ketosynthase
L	liters
LHC-II	light harvesting complex II
LTO1	lumen-thiol oxidoreductase
luTP	thylakoid lumen transit peptide
mg	milligrams
MGDG	monogalactosyl diacylglycerol
mL	milliliters
MS	mass spectrometry
mTP	mitochondrial transit peptide
MTX	maitotoxin
M _w	molecular weight
N	Nitrogen
N ₂	Nitrogen (gas)
NaBH ₄	sodium borohydride
NCBI	National Center for Bioinformatics Information
NEM	N-ethylmaleimide
ng	nanograms
NMA	N-methyl mercaptoacetamide
NO ₃ ⁻	Nitrate
Nod	nodularin
NPQ	Non-photochemical quenching
NSP	neurotoxic shellfish poisoning

NTR	NADPH dependent thioredoxin reductase
NTRC	Chloroplastic NADPH dependent thioredoxin reductase
O	oxygen
O ₂	molecular oxygen (gas)
ORF	open reading frame
PbTx	brevetoxin
PC	phosphatidyl choline
PCR	polymerase chain reaction
PE	polyether
pg	picograms
PG	phosphotidyl glycerol
PKS	polyketide synthase
P-LHC-II	phosphorylated LHC-II
PITx	palytoxin
PO ₄ ⁻³	Phosphate
ppb	parts per billion
ppm	part per million
PQ	plastoquinone
PQH ₂	plastoquinol
Prx	peroxiredoxins
PS-I	photosystem I
PS-II	photosystem II
PUFA	polyunsaturated fatty acid

Q _B	bound quinone
qE	energy-dependent non-photochemical quenching
qI	photo-inhibition quenching
q-RT-PCR	quantitative reverse transcription polymerase chain reaction
qT	transition state quenching
RIN	RNA integrity number
RNA	ribonucleic acid
RNS	reactive nitrogen species
ROS	reactive oxygen species
RuBisCO/rbcL	ribulose-1,5-bisphosphate carboxylase/oxygenase (large subunit)
SBPase	seduloheptose-1,7-bisphosphatase
Sec/U	selenocysteine
SECIS	selenocysteine insertion sequence
Ser	serine
SN ₂	nucleophilic substitution
SP	signal peptide
SQDG	sulfoquinovosyl diacylglycerol
SSU rRNA	small subunit ribosomal RNA
STX	saxitoxins
TBAA	tetrabutyl ammonium acetate
tBLASTn	translated nucleotide BLAST
TCA	trichloroacetic acid

TCEP	tris carboxylethyl phosphine
TE	thioesterase
TMT	iodoacetamide tandem mass tags
tRNA	transfer RNA
Trx	thioredoxin
TrxR	thioredoxin reductase
UTR	untranslated region
Vde	violaxanthin de-epoxidase (protein)
VDE	violaxanthin de-epoxidase (gene)
VGSC	voltage-gated sodium ion channel
Vx	Violaxanthin
WHO	World Health Organization
Zep	zeaxanthin epoxidase
Zx	Zeaxanthin
Δ pH	transmembrane proton gradient
μ g	micrograms
μ L	microliters

Chapter 1: The marine dinoflagellate *Karenia brevis*, a special type of phytoplankton

1.1 A brief overview of phytoplankton and the importance of endosymbiosis

Phytoplankton are small, photosynthetic organisms which may be found in nearly all bodies of water, from lakes and estuaries to marine coastal areas and open ocean. There are several classes of phytoplankton and there are continuing discussions over their classification; however, most phytoplankton are eukaryotic except for the prokaryotic cyanobacteria. The eukaryotic group is polyphyletic and their classification schemes are constantly being modified based on newly acquired genetic information redefining early hypotheses regarding their evolution (Rengefors, Kremp, Reusch, & Wood, 2017).

Phytoplankton are estimated to produce between 50 and 80% of the planet's oxygen (Chapman, 2013). They play an integral role in the Earth's carbon cycle. Of the 39,100 Gigatonnes (Gt) of the world's carbon stored in the ocean, phytoplankton are considered to absorb nearly 4 Gt through photosynthesis and CO₂ fixation (Hallegraeff, 2010). Much of this phytoplankton derived carbon is pumped deep into ocean sediment and is stored for millions of years (Basu & Mackey, 2018). Like all organisms, phytoplankton require carbon (C), nitrogen (N) and phosphorous (P), to build biomolecules such as proteins, adenosine triphosphate (ATP), and nucleic acids. They span various trophic levels, many being able to perform photosynthesis and take up soluble nutrients such as nitrates (NO₃⁻) and phosphates (PO₄⁻³) or even fix nitrogen gas (N₂).

Most phytoplankton reside near surface waters in what is called the euphotic zone. Here the flux of light governs the depth at which any given species of phytoplankton is comfortable and can thrive. Phytoplankton have developed ways of moving throughout the water column as a strategy to adapt to different light intensities. Cyanobacteria have gas vesicles which can modulate their buoyancy (Walsby, 1981). Dinoflagellates rely on a tail-like flagella which helps them move around in a gyre like motion. Diatoms on the other hand, rely on ocean currents to carry them aloft (Witman, 2017).

Cyanobacteria represent the class of phytoplankton about which much genetic information is available. These prokaryotes are hypothesized to have played a fundamental role in the evolution of photosynthetic life on earth as we know it (Gray & Spencer, 1996). Through a process known as primary endosymbiosis, a prehistoric cyanobacterium was engulfed by a heterotrophic protist, resulting in what is the ancestor of all Plantae (Figure 1.2). The cyanobacterium was then adopted as the equivalent of the modern-day chloroplast, leading to the first photosynthetic eukaryote (Reyes-Prieto, Yoon, & Bhattacharya, 2009). This ancestral alga evolved into the three major classes of eukaryotic phytoplankton: rhodophyta (red algae), chlorophyta (green algae) and glaucophyte. All of these contain a chloroplast with two membranes inherited from the cyanobacteria inner and outer cell membranes (Jarvis & Soll, 2002). The classes are distinguished by their pigment profiles and certain physiological characteristics; with green algae containing chlorophyll *a* and *b* while storing starch in the plastid (Lewis & McCourt, 2004). Red algae, on the other hand contain chlorophyll *a*, phycobilisomes and

phycobilins (unique light harvesting complexes which contain phycobiliproteins, pigment molecules which absorb in the 450 – 670 nm range) (Graham & Wilcox, 2000; Singh, Sonani, Rastogi, & Madamwar, 2015). Glaucophytes also contain chlorophyll *a*, phycobilisomes and phycobilins, as well as a peptidoglycan layer which is a remnant of the cyanobacterial ancestor (Steiner & Löffelhardt, 2002) (Figure 1.1).

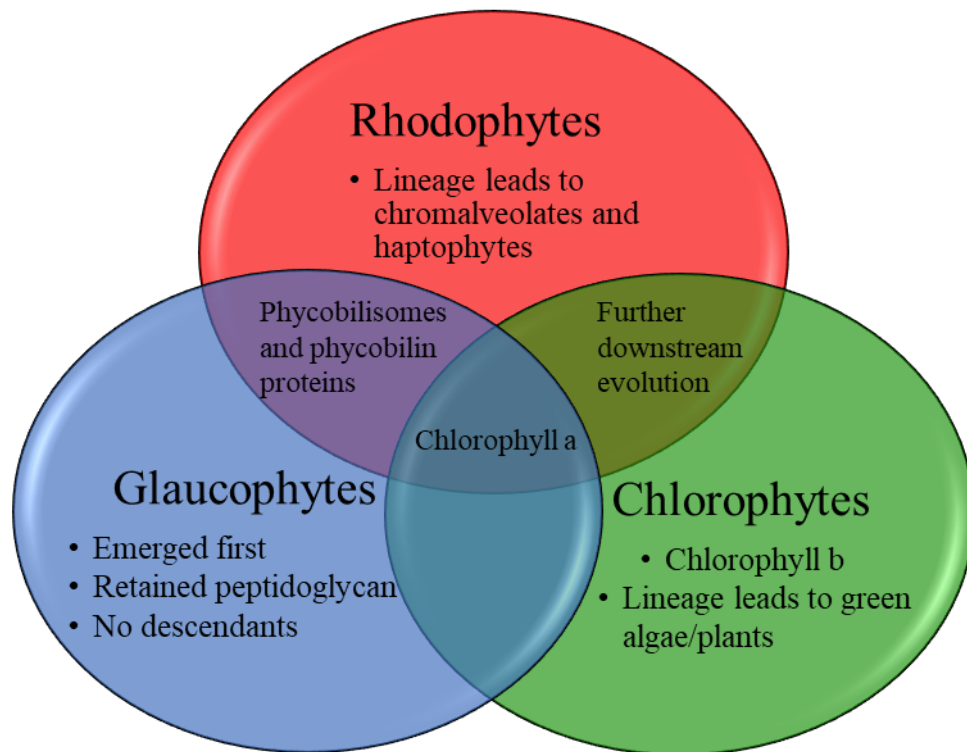


Figure 1.1 Venn diagram describing differences and similarities between the three primordial algal species to arise from primary endosymbiosis.

A primary endosymbiotic event leaves the organisms with a predicament. What is to be done with all the duplicative genetic material from the symbiont (cyanobacteria)? Studies on the plastid of plants and red algae show the number of plastid-encoded proteins were found to be between 80-200, while the number of proteins encoded by the genome of the cyanobacteria *Synechocystis* is over 3000 (Martin & Herrmann, 1998).

This reduction of genetic information within the organelle has been explained by the hypothesis of endosymbiotic gene transfer (EGT). EGT allows an organelle (symbiont) to import its genes to the nucleus of the host, which then exports the products back to the organelle with the help of organelle guided transit peptides, such as N-terminal chloroplast transit peptides and special protein import machinery, or envelope machinery (Blanchard & Lynch, 2000).

The evolution of phytoplankton, however, does not stop there. Of the three classes of primary endosymbionts, only glaucophytes have not been reported to have undergone

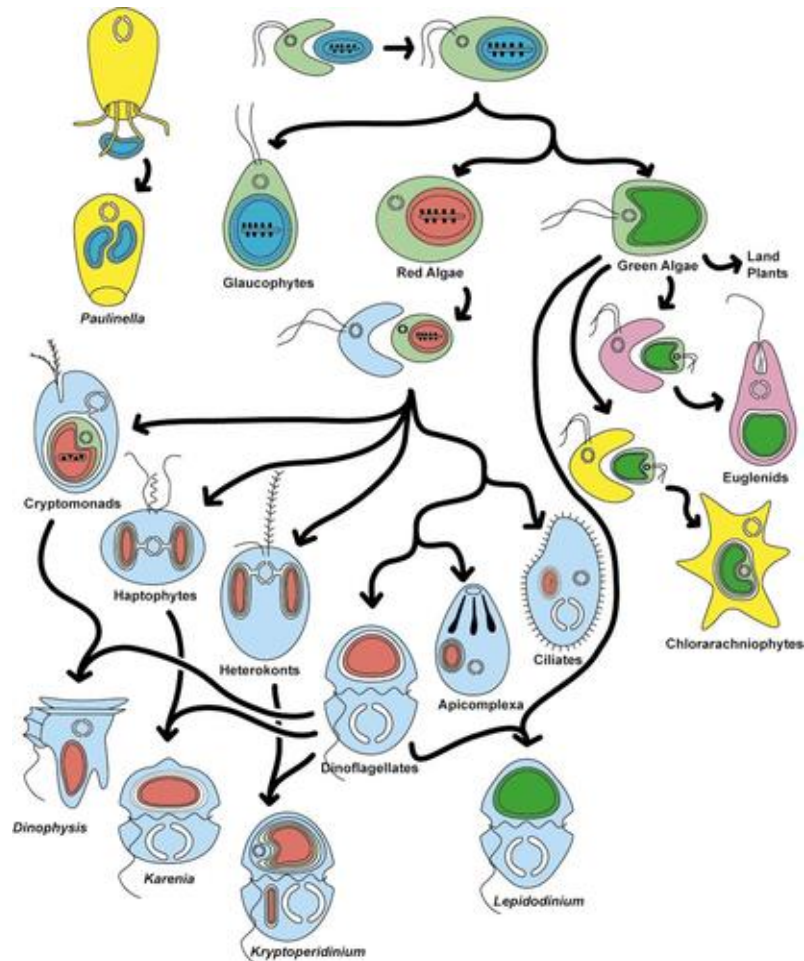


Figure 1.2 A chart demonstrating algal endosymbiosis as shown in Keeling et al., 2004. Cyanobacteria are represented as blue organisms, while glaucophytes contain blue plastids. Red and green algae are shown containing plastids in their respective colors.

any further symbiotic events (Kim, 2015). Both green and red algae were subject to endosymbiotic events in which they were engulfed by a eukaryotic host, leading to chloroplasts with three or four membranes (McFadden, 2001). In fact, a vast majority of algae are the result of secondary endosymbiosis, although the exact details of the mechanism of secondary endosymbiosis are a topic of much rigorous discussion (Chan & Bhattacharya, 2010). Green algae are considered to have given rise to two algal lineages the chlorarachniophytes and euglenoids (Figure 1.2). The Cabozoa hypothesis suggests a single common secondary endosymbiosis (Cavalier-Smith, 1999); although, analysis of plastid encoded proteins supports the hypothesis that two independent symbiotic events lead to these two lineages (Rogers, Gilson, Su, McFadden, & Keeling, 2007).

Red algal descendants are much more diverse and span a range of range of lineages. Currently the most supported hypothesis of red algal evolution, the chromalveolate hypothesis, describes six major lineages and several smaller lineages (Keeling, 2009). This hypothesis postulates a single chromalveolate ancestor results from a secondary endosymbiotic event that led to all the descendants containing red algal plastids (Cavalier-Smith, 1999). There are several chromalveolate lineages that are worth discussing in this text, namely apicomplexans, dinoflagellates, and haptophytes.

Apicomplexans are non-photosynthetic parasitic microorganisms. Probably the most infamous of which is *Plasmodium falciparum*, the malaria causing parasite. Apicomplexans have a special organelle known as the apicoplast, which discovered retains functions of fatty acid, isoprenoid and haem biosynthesis, but does not produce

chlorophyll (Ralph et al., 2004). It has been postulated that dinoflagellates and apicomplexans are sisters, having a common photosynthetic ancestor (Keeling, 2009).

Dinoflagellates are a complex and diverse group of protists with photosynthetic, heterotrophic, and parasitic members (Sibbald & Archibald, 2020). A unique characteristic of dinoflagellates is the ability to incorporate and swap endosymbionts with higher frequency than other secondary endosymbiotic algae. Comparison of small subunit ribosomal RNA (SSU rRNA) of 28 photosynthetic and 4 non-photosynthetic species suggest that at least 8 independent plastid removals and 3 plastid replacements have occurred in the dinoflagellate lineage (Saldarriaga, Taylor, Keeling, & Cavalier-Smith, 2001).

Haptophytes are a group of secondary endosymbionts, nearly all of which are photosynthetic and possess a unique chloroplast that contains chlorophyll c_1 and c_2 , as well as the accessory pigment derivatives of fucoxanthin (Fx) (Yoon, Hackett, & Bhattacharya, 2002). Haptophytes are important primary producers and are thought to be the primary source of carbon for petroleum products derived from ocean sediments (Andersen, 2004).

Several species of dinoflagellates arose because of a tertiary endosymbiosis (where a secondary endosymbiont is engulfed by a secondary plastid containing eukaryotic host cell, see bottom left of Figure 1.2). This leads to an even larger increase in the complexity of the nuclear genome and makes it difficult to accurately propose the lineage of phytoplankton species due to the amount of EGT that relocates genes from organelles to the nucleus (Burki et al., 2014). Advances in phylogenetic classification have

been made by looking at structural characteristics such as the number of membranes surrounding the chloroplasts. Investigating the pigment profiles of tertiary endosymbionts *Karenia* and *Karlodinium* suggest a common haptophyte ancestor that contained a chlorophyll-*c*/fucoxanthin producing chloroplast, unlike the more common chlorophyll-*a*/peridinin (Tengs et al., 2000). There have also been advances in phylogenetic analyses of the large subunit of ribulose-1,5-bisphosphate carboxylase/oxygenase (RuBisCO or *rbcL*) and photosystem proteins (*psaA* and *psbA*) which demonstrate that the fucoxanthin containing dinoflagellates obtained their haptophyte plastid prior to the deviation of the two tertiary plastid containing dinoflagellate lineages (peridinin vs. fucoxanthin) (Yoon et al., 2002)

1.2 Primary and secondary metabolites of phytoplankton origin

1.2.1 Biofuels and consumer products

Phytoplankton produce a diverse array of metabolites. Their fast growth rate, potentially high lipid content and ability to grow in areas which may be inhospitable for agricultural use make them a prime candidate for use in the generation of biofuels (Menetrez, 2012). Currently the most limiting factor of widespread algal biofuel use is the post-production costs which can be anywhere from \$300-2600 per barrel, while petroleum estimates are as low as \$40-80 (Hannon, Gimpel, Tran, Rasala, & Mayfield, 2010). Currently, 95% of biodiesel originates from land-based crops such as corn and soy. However, these crops require large amounts of land, fertilizer, pesticides, and water.

These crops are also sources of high value products in areas such as the food industry, which creates competition over feedstock sources (Rawat, Ranjith Kumar, Mutanda, & Bux, 2013). Using algae as the feedstock for biodiesel can circumvent the problems that arise from traditional biodiesel production (Cooney, Young, & Nagle, 2009). Similarly, it is reported that algae can produce up to 10 times more extractable oil per acre than traditional biofuel crops such as corn, or soy (Chisti, 2007). Another interesting approach is the possibility of growing algae in nutrient rich wastewater as a method to increase the economic viability, and also decrease the costs of nutrient removal from urban and agricultural wastewater (Pittman, Dean, & Osundeko, 2011).

Long-chain polyunsaturated fatty acids (PUFA) such as docosahexaenoic acid (DHA) and eicosapentaenoic acid (EPA) are commonly used as nutritional supplements. While EPA and DHA are omega-3 fatty acids essential to human growth, mammals are unable to produce them naturally, except during lactation. Phytoplankton such as *Nannochloropsis* sp., *Phaeodactylum tricorinitum*, *Dunaliella salina*, and *Pavlova lutheri* are sources of these PUFA (Adarme-Vega et al., 2012; Bhosale, Rajabhoj, & Chaugule, 2010; Guihéneuf, Mimouni, Ulmann, & Tremblin, 2009; Hu & Gao, 2003) and are supplemented into the feed of chickens and cows to produce omega-3 enriched eggs and milk (de Jesus Raposo, de Morais, & de Morais, 2013; Herber & Van Elswyk, 1996).

Commercial production of biologically active compounds derived from algae has become popular since algal communities produce an array of lucrative natural products. This can increase the return on investment per acre of crop, relative to land crops. Pigments such as β -carotene, astaxanthin, and phycobilins are commonly used in

cosmetics (Guedes, Amaro, & Malcata, 2011; Hannon et al., 2010; Ramesh Kumar, Deviram, Mathimani, Duc, & Pugazhendhi, 2019; Schoepp et al., 2014; Spolaore, Joannis-Cassan, Duran, & Isambert, 2006). *Arthrospira* sp., marketed as Spirulina, are widely used as a nutritional supplement because of their high protein content (Spolaore et al., 2006).

Carotenoids are lipophilic tetraterpene pigments found in the thylakoid membrane of all photosynthetic organisms. They are pigments that serve to prevent photooxidative damage of the light harvesting complex under excess light stress and broaden the range of wavelengths of light available for photochemistry (Yen et al., 2013). Furthermore, oxygenated carotenoids, or xanthophylls, such as astaxanthin (Fig 1.3A) have been found to be an efficient quencher of reactive oxygen and nitrogen species (ROS and RNS, respectively) (Fassett & Coombes, 2011). In 1987, astaxanthin was approved by the FDA as a food additive for the aquaculture industry used to give salmon their characteristic color, and in 1999 as a nutritional supplement for human consumption (Yen et al., 2013).

Phycobilins, linear tetrapyrroles that are bound to peptides to form phycobiliproteins (Figure 1.3B), are most commonly used as a fluoroprobe in immunochemical detection (Spolaore et al., 2006). They have also been used in cosmetics formulations as a natural colorant due to their red color (Glazer, 1994). Chlorophylls are green pigments containing a magnesium centered porphyrin and a phytol tail. A derivative of chlorophyll in which the magnesium atom and phytol tail have been removed, pheophorbide (Figure 1.3C) is used in photodynamic therapy for its photosensitizing abilities (Busch, Cengel, & Finlay, 2009; Ruiz-González et al., 2017).

Pheophorbide has the unique ability to produce ROS that can kill malignant cells by treating with light at a specific wavelength in the presence of the photosensitizer, avoiding some of the side effects associated with traditional cancer therapies (Chen et al.,

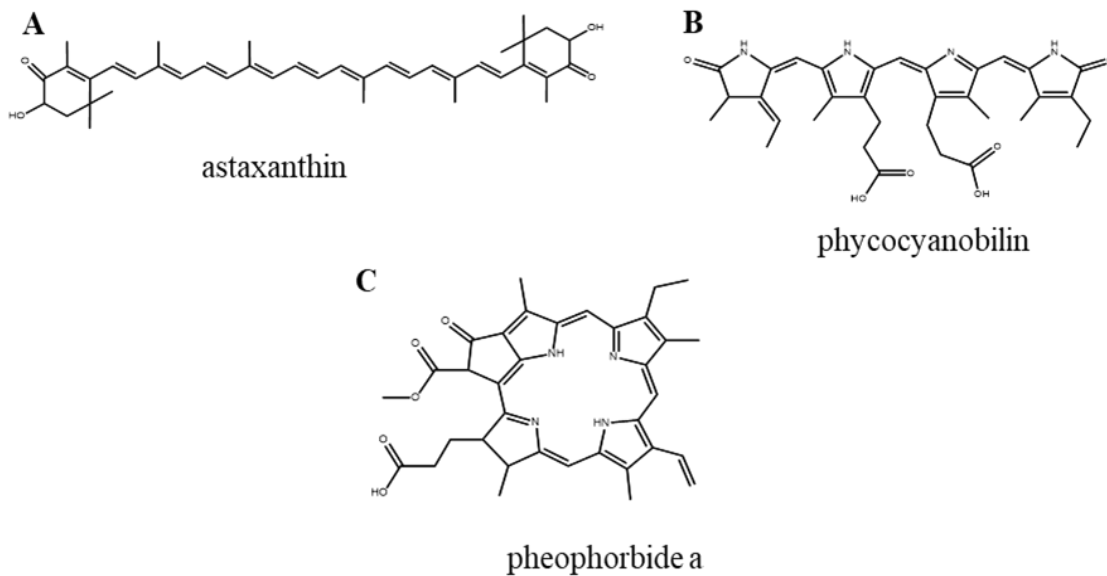


Figure 1.3 Structures of various algal natural products. A) astaxanthin: a reddish pigment used as a food additive, B) phycocyanobilin: a blueish pigment that has been used as a fluoroprobe for immunochemical detection, C) pheophorbide a: a chlorophyll derivative photosensitizer with medicinal functions used for producing ROS to target malignant cells

2002).

1.2.2 Phycotoxins

Of the thousands of species of algae that populate our marine and freshwater ecosystems, less than one percent produce toxins that can have detrimental effects on wildlife and humans (NOAA, 2021). The vast majority of harmful algal blooms are cyanobacterial and several cyanobacteria produce a variety of heptapeptide hepatotoxins known as the microcystins (MC) (Figure 1.4A) named for the infamous *Microcystis aeruginosa*. The first cyanobacteria in which the toxin was detected. Episodes of high *Microcystis* concentrations affect freshwater reservoirs across the entire continental US (Loftin et al., 2016). Another commonly found freshwater cyanobacterial hepatotoxin class are nodularins (Nod, Figure 1.4B). These potent pentapeptide toxins share structural similarities with MCs such as the 3-amino-9-methoxy-2,6,8-trimethyl-10-phenyl-4,6-decadienoic acid (Adda) moiety and both MC and Nod are protein phosphatase inhibitors (Chen, Shen, & Fang, 2013) although their mechanisms of toxicity differ (Bagu, Sykes, Craig, & Holmes, 1997; Rinehart et al., 1988). Both toxin classes consist of several variants depending on amino acid composition, substitution and configuration, but the most commonly found in nature are shown in Figure 1.4.

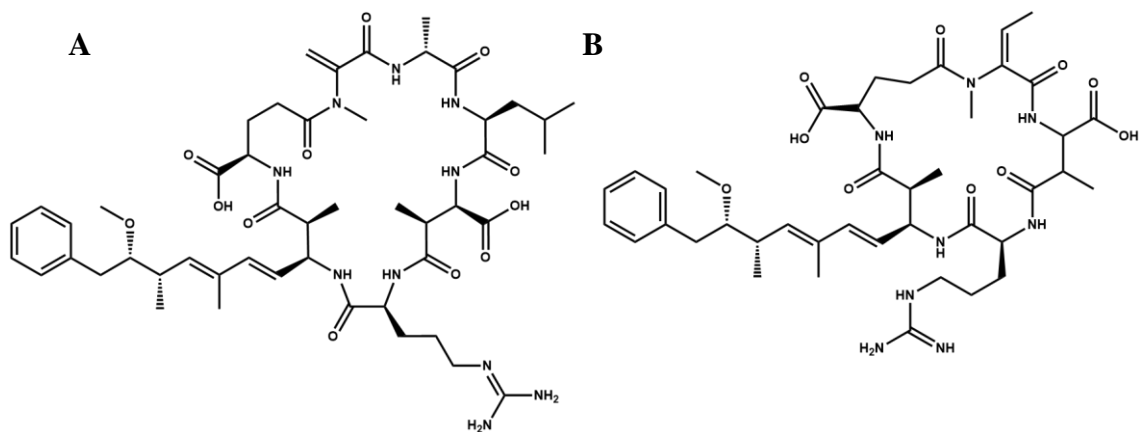


Figure 1.4 The hepatotoxic **A**) microcystin-LR and **B**) nodularin commonly found in cyanobacterial blooms

Algal toxins span a wide range of size, structural classes, and biological activities (Table 1.1). Algal toxins can vary in size from just over 150 Daltons (Da) in the case of anatoxin-a to 1500 Da, with special cases such as the palytoxins (PITX and maitotoxins (MTX) which are 2677 and 3422 Da, respectively (Figure 1.5) (Rossini & Hess, 2010). It is typical for a structural class of toxins to be comprised of several congeners with varying oxidation, alkylation, and stereochemistry.

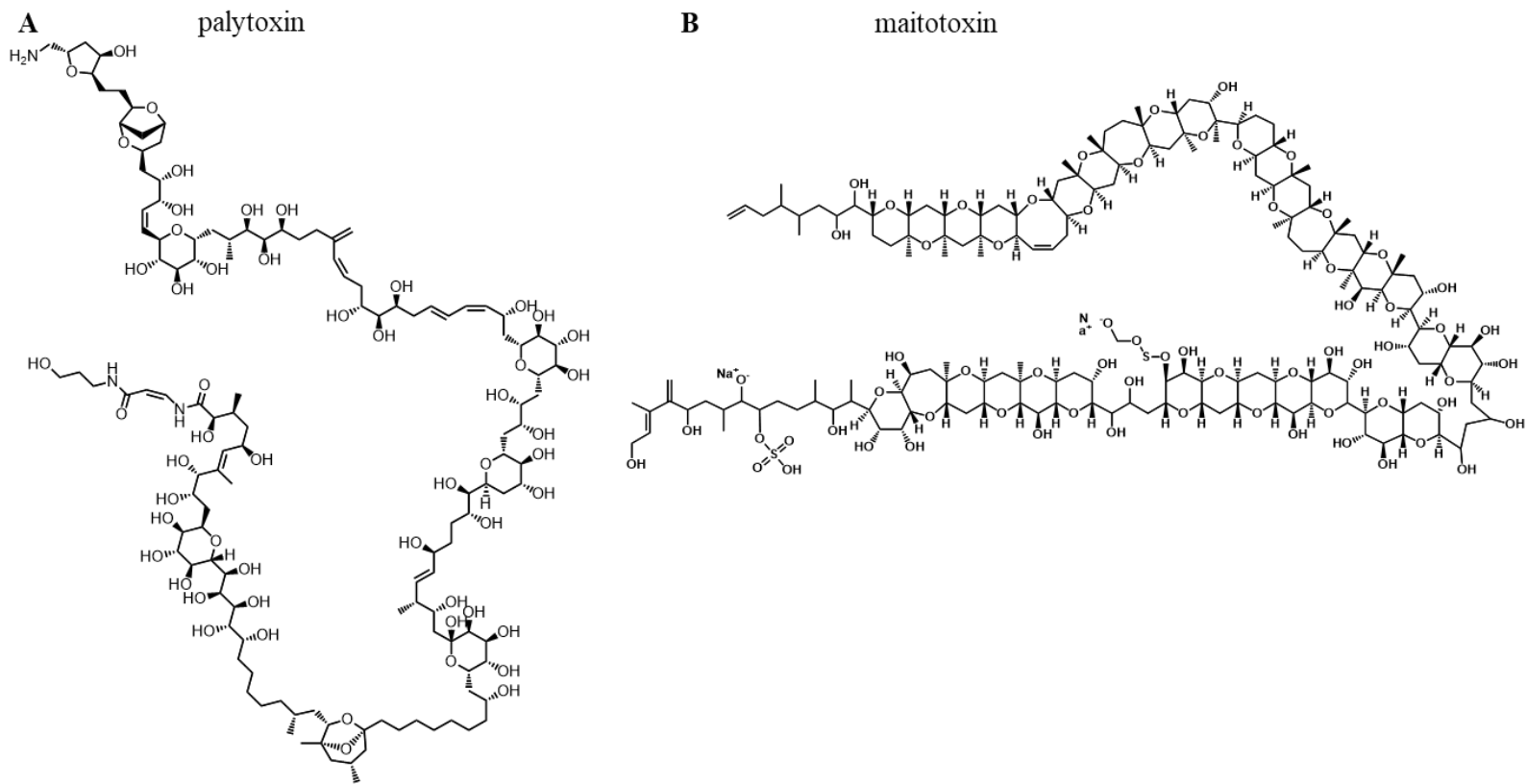


Figure 1.5 Structure of **A)** palytoxin and **B)** maitotoxin

Table 1.1 Examples of algal toxins, their producers, mechanism of toxicity and class. ¹-n-acetyl choline receptor, ²-protein phosphatase, ³-cyclic adenosine monophosphate.

Toxin	Produced Primarily By	Toxicity	Toxin Class	Figure/Reference
Anatoxins	<i>Anabaena</i> sp./ cyanobacteria	nAChR ¹ inhibitor	Amino acid-derived	Figure 1.6C (Christensen & Khan, 2020)
Azaspiracids	<i>Azadinium</i> sp.	PP inhibitor ²	Linear polyether	Figure 1.7A (Twiner, Rehmann, Hess, & Doucette, 2008)
Brevetoxins	<i>Karenia brevis</i>	Na ⁺ channel activator	Polyether ladder	Figure 1.8
Ciguatoxins	<i>Gambierdiscus toxicus</i>	Na ⁺ channel activator	Polyether ladder	Figure 1.7C (Dechraoui, Naar, Pauillac, & Legrand, 1999)
Domoic Acid	<i>Pseudo-nitzschia</i> sp.	Glu receptor agonist	Amino acid-derived	Figure 1.6B (Pulido, 2008)
Dinophysistoxins/ Okadaic Acid	<i>Dinophysis</i> sp., <i>Prorocentrum</i> sp.	PP1/PP2A inhibitor	Linear polyether	Figure 1.7B (Reguera et al., 2014)
Karlotoxin/Karmit oxin	<i>Karlodinium</i> sp.	Ichthyotoxic	Polyketide	(Binzer et al., 2020)
Lyngbyatoxins	<i>Lyngbya</i> sp.	Protein kinase C activator	Amino acid-derived	(Ito, Satake, & Yasumoto, 2002)
Maitotoxin	<i>Gambierdiscus toxicus</i>	Ca ²⁺ channel disruptor	Polyether ladder	Figure 1.5B (Sinkins et al., 2009)
Microcystins	<i>Microcystis</i> sp./ cyanobacteria	PP1/PP2A inhibitor	Heptapeptide	Figure 1.4A (Bagu et al., 1997)
Nodularins	<i>Nodularia</i> sp.	PP inhibitor	Pentapeptide	Figure 1.4B (Chen et al., 2013)
Palytoxin	<i>Ostreopsis</i> sp./ <i>Palythoa</i> corals	Na ⁺ /K ⁺ ATPase disruptor	Polyether ladder	Figure 1.5A (Ramos & Vasconcelos, 2010)
Saxitoxins	Dinoflagellates/cyano bacteria	Na ⁺ channel blocker	Polyether ladder	Figure 1.6A (Christensen & Khan, 2020)
Yessotoxins	Dinoflagellates	Ca ²⁺ / cAMP effector ³	Polyether ladder	Figure 1.7D (Glazer, 1994)

Algal toxins belong to numerous structural classes. For example, saxitoxins (Figure 1.6A) (STX) are tetrahydropurine alkaloids produced by dinoflagellates belonging to the genus *Alexandrium* and various cyanobacteria. Currently scientists have identified nearly 60 naturally occurring saxitoxin analogues with different hydroxylation and sulfonation patterns (Wiese, D'Agostino, Mihali, Moffitt, & Neilan, 2010). Domoic acid and anatoxin, on the other hand are both toxins with biosynthetic origins stemming from glutamate (Figure 1.6B and C, respectively) (Brunson et al., 2018; Namikoshi et al., 2004).

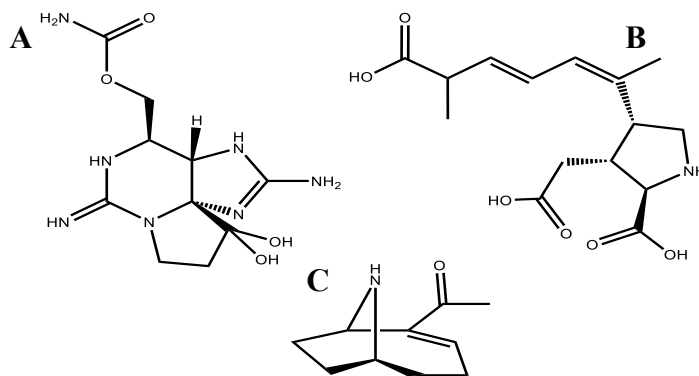


Figure 1.6 A) Saxitoxin B) domoic acid and C) anatoxin-a

While the aforementioned toxins are all nitrogen containing, derived in part from amino acids, a significant number of algal toxins consist almost entirely of carbon, hydrogen (H), and oxygen (O), except for the rare occurrence of a functional group addition such as sulfonation (Figure 1.7). These toxins have a unique polyether (PE) character which is postulated to be polyketide in origin, although the biosynthetic pathways for these toxins have not been elucidated (Wan, Yao, Liu, Chen, & Jiang, 2019). Two types of polyether toxins have been characterized: linear polyether, and

polyether ladders (Figure 1.7A and B and Figure 1.7C and D, respectively). *Karenia brevis* is responsible for producing its own suite of polyether ladder toxins, known as the brevetoxins (PbTx).

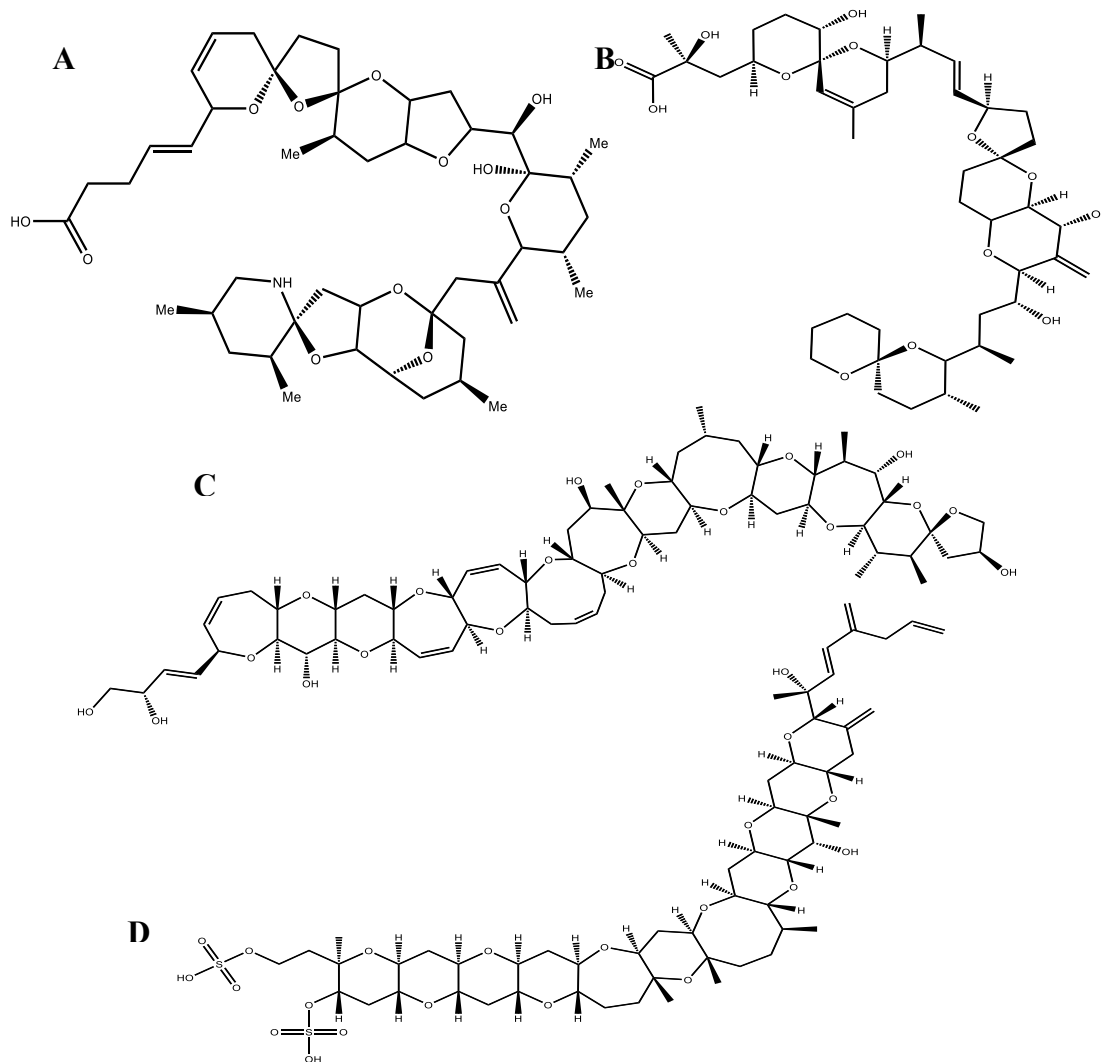


Figure 1.7 The structures of several polyether toxins. Linear polyethers **A)** azaspiracid-1 and **B)** okadaic acid. Polyether ladders **C)** ciguatoxin-1 and **D)** yessotoxin.

The brevetoxins share common structural features of other PE ladders produced primarily by marine dinoflagellates. These structural features include a series of *trans*-

fused ether rings, with the ether functionality on alternating sides of the ladder. Two skeletal backbones of the brevetoxins have been characterized (A and B) with several congeners resulting from variations on the J-ring (A-type) or K-ring (B-type) of the parent structures (Figure 1.8). At least 14 variants of these two backbones (Baden, Bourdelais, Jacocks, Michelliza, & Naar, 2005) and other minor PE ladders from *K. brevis* have also been described (Bourdelais, Jacocks, Wright, Bigwarfe, & Baden, 2005; Prasad & Shimizu, 1989). The most abundant of the brevetoxins, PbTx-2 has the B-type backbone with an α , β -unsaturated aldehyde K-ring side chain and comprises roughly 85% of the total toxin content in bloom samples (Pierce, Henry, & Blum, 2008; Pierce, Henry, Blum, & Payne, 2000).

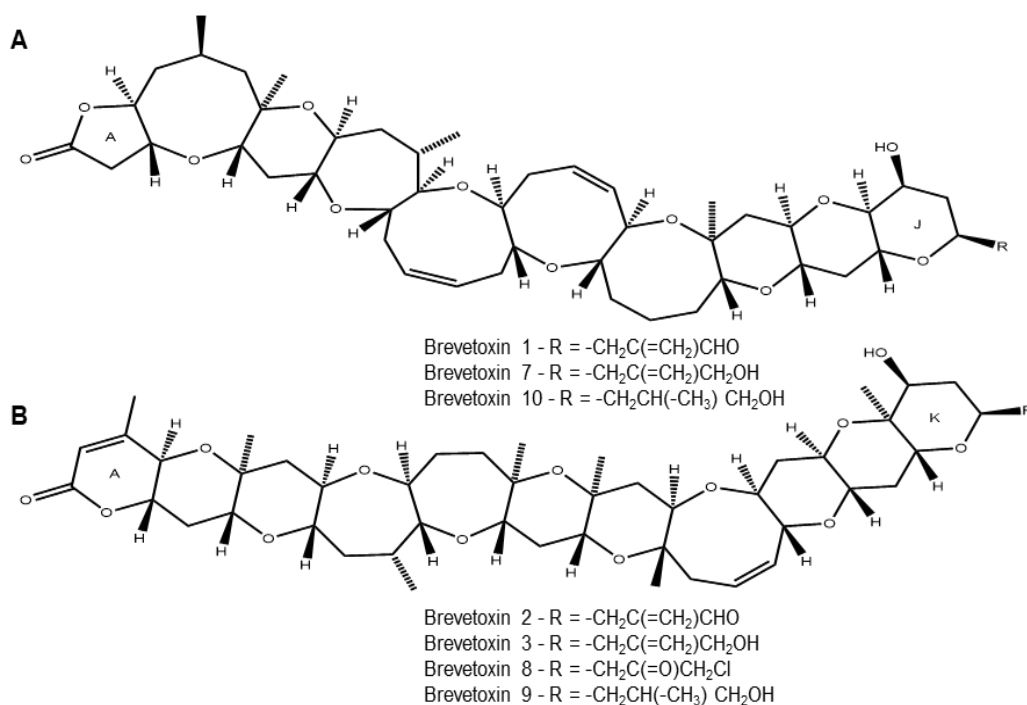


Figure 1.8 A) Brevetoxin A-type frame B) brevetoxin B-type frame, and their respective names and substituents.

1.3 Harmful algal blooms

Harmful algal blooms (HABs) are occurrences of rapidly growing algae concentrations that negatively impact the ecosystem. HABs may lead to massive fish kills as a result of anoxic conditions or the presence of toxins. In South Florida, residents suffer HABs from primarily two different species of algae: the toxic freshwater cyanobacteria, *Microcystis aeruginosa*, and the red tide forming marine dinoflagellate, *K. brevis*.

Significant cyanobacterial blooms which include primarily *M. aeruginosa*, have been observed in Lake Okeechobee and the surrounding estuaries in the last 20 years (Oehrle, Rodriguez-Matos, Cartamil, Zavala, & Rein, 2017; Philips, Badylak, Nelson, & Havens, 2020; Rosen, Davis, Gobler, Kramer, & Loftin, 2017). These blooms have extended to the east and west coasts of Florida from Port St. Lucie to Cape Coral, respectively (Figure 1.9A). In 2016 and 2018 *M. aeruginosa* blooms that started in Lake Okeechobee (Figure 1.9B) have created particularly unpleasant conditions for residents living along the Caloosahatchee River and the St. Lucie Estuary. These two estuaries were particularly high in bloom biomass and as the large algal mats began to die off noxious odors were reported by homeowners who live on these canals and beachfronts. A state of emergency was declared in four surrounding counties in 2016 as a result of this bloom. Microcystin levels in the water reached 495 ppb in the St. Lucie estuary during August of the 2018 bloom, furthermore the toxin levels are vastly underreported because the Florida Department of Environmental Protection filters their algal samples and only tests the filtrate, not accounting for intracellular toxin content (FLDEP, 2021). The World

Health Organization (WHO) maintains a recreational use guideline for microcystins of 2-4 ppb and a limit of 1 ppb for drinking water (Chorus & Welker, 2021) and proposed various action levels for recreational use to mitigate risks involved with exposure to toxin. The 2018 bloom expanded west to the Gulf of Mexico and cooccurred with a *K. brevis* bloom that was already present on the southwest coast of Florida. A state of emergency was declared in July and August 2018 for *M. aeruginosa* and *K. brevis*, respectively.

Some of the most damaging algal blooms occur in coastal regions, where population densities are the highest, and present a nuisance to public health while cause significant losses in the tourism and aquaculture industries (Anderson et al., 2008; Bechard, 2020a, 2020b). While coastal regions, and continentally bound seas represent only 15% of the ocean's surface area they account for up to 50% of total primary production and resultant carbon and nitrogen flux (Wollast, 1991). In addition to watershed runoff, phytoplankton populations have been shown to be positively correlated with atmospheric deposition of nutrients such as iron (Fe) and nitrogen. Furthermore, the

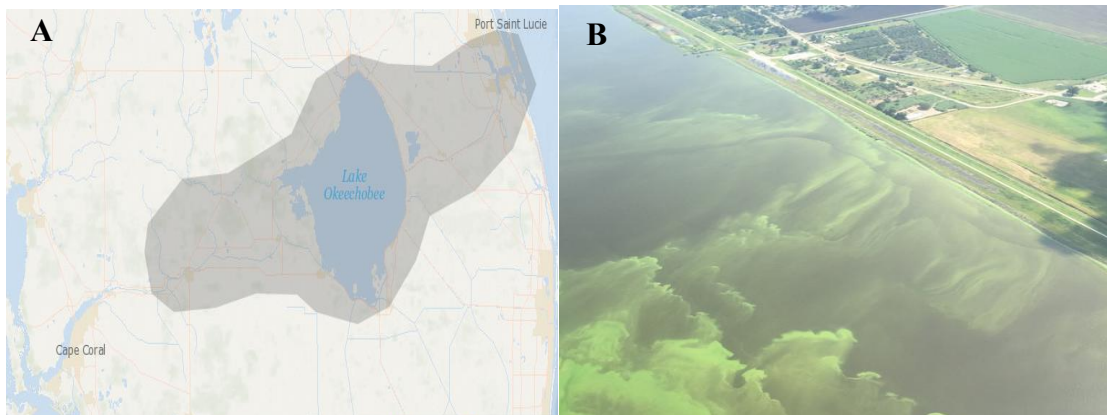


Figure 1.9 A) Blooms of *M. aeruginosa* in Lake Okeechobee B) Extension east and west through the canals and rivers to Port St. Lucie and Cape Coral (Rosen et al., 2018)

regions with the Fe enriched rainfall tend to be urbanized areas or regions near the tropical mid-Atlantic which are affected by the deposition of Saharan dust (Duce & Tindale, 1991; Paerl, 1997). Unchecked algal growth can lead to problems in drinking water reservoirs, fisheries, and recreational areas. These HABs can be caused by a variety of species and be accompanied by discoloration of the water, which has given rise to terms such as red tide, and brown tide. HABs are predicted to occur more often as a result of changing environmental conditions (Townhill et al., 2018).

1.4 The economic and public health issues of *Karenia brevis* and the brevetoxins

Annual blooms of *K. brevis*, known as the Florida red tide, that occur in the Gulf of Mexico, are a bane to the shellfish and tourism industries and can precipitate public health and environmental catastrophe (Fleming et al., 2011). In 2018, an extended bloom killed thousands of fish, and over 100 manatees (Bechard, 2020b). Millions of dollars in damages to coastal economies have been linked to harmful algal blooms in the past (Hoagland & Scatasta, 2006). From 1995-1999 coastal counties in southwestern Florida were estimated to have lost 32.3% of their monthly revenue due to red tide events (~\$6,500,000) which dwarfs the economic loss resulting from tropical weather events (approx. 5% or \$532,000) (Larkin & Adams, 2007).

An unfortunate result of *K. brevis* blooms is the increased levels of potent neurotoxins, the brevetoxins. Brevetoxins activate the voltage-gated sodium channel (VGSC) of excitable membranes, lowering the activation threshold and prolonging channel opening, resulting in membrane depolarization, thus affecting both the central and peripheral nervous systems as well as skeletal muscle (Jeglitsch, Rein, Baden, &

Adams, 1998). To further complicate the problem, bioaccumulation of brevetoxin occurs in shellfish, planktivorous fish and marine mammals. Flewelling and colleagues found that deceased dolphins suspected of having been in contact with brevetoxins had acutely toxic stomach contents. In this study, 50% of deceased dolphins tested contained the planktivorous fish *Breveoortia* sp., the undigested fraction of these fish contained high toxin levels (2126 ng/g, n=30). Furthermore, fish collected two weeks after the dolphin deaths were contaminated with brevetoxin (10-6,000 ng/g) (Flewelling et al., 2005).

Deceased manatees associated with a 1996 *K. brevis* bloom, demonstrated significant respiratory lesions, as well as brevetoxin in pulmonary macrophages, detected by immunohistochemical methods, indicating inhalation of brevetoxins. (Bossart, Baden, Ewing, Roberts, & Wright, 1998) Brevetoxin exposure via aerosols can cause severe acute respiratory distress, particularly in asthmatics (Bean et al., 2011). About 15% of the global asthma trigger response, or 45 million people, in 2004 was estimated to have been caused by exposure to aerosolized brevetoxins or palytoxins (Walsh et al., 2017).

The most common occurrences of brevetoxin poisoning in humans is via inhalation or through consumption of contaminated shellfish in areas afflicted by red tide. Neurotoxic shellfish poisoning (NSP) occurs as a result of ingesting shellfish with high levels of brevetoxins. Kirkpatrick and coworkers found that emergency room visits in Florida which resulted from selected gastrointestinal disorders, such as duodenitis, colitis, gastritis, and non-infectious enteritis, were 40% higher during bloom years suggesting under-diagnosis of NSP (Kirkpatrick et al., 2010). The last 30 years of research into brevetoxin have demonstrated the public health and economic burden that *K. brevis* can

play on the state of Florida. Recent events such as the 2018 bloom demonstrate just how severe the damages can be and how important research into phytoplankton is for developing mitigation strategies for HABs (Bechard, 2020a, 2020b; Philips et al., 2020; Tominack, Coffey, Yoskowitz, Sutton, & Wetz, 2020).

1.5 Investigating the role of brevetoxin

The endogenous function of brevetoxin remains unknown. Like most toxins, it has been suggested that brevetoxins primary role is as a grazing deterrent. However, Early experiments exposing copepods to different concentrations of *K. brevis* culture did not result in any observable differences in the behavior of copepods (Tester, Turner, & Shea, 2000). More recently, three species of copepods were exposed to both *K. brevis* and dissolved brevetoxins resulting in varying accumulation of toxins, and behavioral effects, suggesting species specific behavioral effects (Cohen, Tester, & Forward, 2007). There has been increasing support for the hypothesis that algal toxin production works as a grazing deterrent, citing differences in feeding behaviors and egg production among copepods (Hong et al., 2012; Waggett, Hardison, & Tester, 2012). Exposure of the copepod *Temora longicornis*, to *K. brevis* as well as 11 other species of toxic dinoflagellates produced a notable decrease in grazing in response to 10 of the 12 toxic algae relative to a nontoxic control (Xu & Kiørboe, 2018). Grazing avoidance of toxic algae by copepods demonstrates the important role toxins can play for phytoplankton, suggesting that grazers may have the ability to distinguish toxic prey via olfactory mechanisms prior to contact with the toxic cell, however this has yet to be directly observed (Tiselius, Saiz, & Kiørboe, 2013). Although it may seem obvious that toxins

work as a feeding deterrent, this function is not an endogenous role that can be observed free of predator-prey interactions.

Several hypotheses regarding the physiological role of brevetoxins have been proposed. A report of changes in brevetoxin production in response to changes in salinity was published recently (Errera & Campbell, 2011). However, other laboratories have disputed these findings (Sunda et al., 2013) citing errors in the experimental methodology. Observations of an inverse relationship between toxin content and nutrient availability with phosphorous limitation increasing brevetoxin content 2.3- to 7.3-fold (Hardison, Sunda, Shea, & Litaker, 2013) suggest an allelopathic roles for brevetoxin. It has recently been discovered that *K. brevis* allelopathy compromises lipid biosynthesis and photosynthetic efficiency of competitors (Poulin et al., 2018; Prince, Myers, & Kubanek, 2008). This suggests that *K. brevis* may utilize brevetoxins to outcompete competitors for resources.

Laboratory strains of *K. brevis* have been reported to have sustained differences in toxin content by up to 10-fold (Errera et al., 2010). Some strains can produce up to 68 pg/cell of PbTx, while others produce less than 1 pg/cell (Hardison, Sunda, Tester, Shea, & Litaker, 2014; Sunda et al., 2013). The reason for the observed differences in toxin content is not well understood, it is possible that genetic variation or a response to environmental conditions could be the source of these differences.

An important step in understanding the role that toxins play in dinoflagellates is investigating where they are localized within the organism. Early research into toxin localization in marine dinoflagellates using immunocytochemical techniques proposed

that saxitoxin in *Gonyaulax tamarensis* was primarily localized in the nucleus (Anderson & Cheng, 1988), suggesting a role in genome structure and function. Similar studies found okadaic acid antibodies localized to the chloroplast of toxin producing *Prorocentrum lima* and *Prorocentrum maculosum*, while a non-toxic *Prorocentrum micans* lacked labeling (Zhou & Fritz, 1994). Recently, Cassell et al., reported that a fluorescently labeled brevetoxin-derivative (Figure 1.10A) localized to the chloroplast of *K. brevis* (Figure 1.10B) (Cassell et al., 2015). It is important to mention that although the localization of a fluorescent brevetoxin probe to the chloroplast provides strong evidence of the role it may play in *K. brevis*, experiments performed by the Van Dolah lab focusing on detection of brevetoxin in isolated chloroplasts using mass spectrometry did not find any brevetoxins (Van Dolah et al., 2013). Our previous study also contradicts a published abstract which used fluorescent anti-brevetoxin antibodies and reported the localization in secretory vesicles (Vigna, Quesada, & Verdugo, 2012). However, no follow up work has been published on the latter research. With the discovery of brevetoxin localization to the chloroplast our lab began to search for brevetoxin binding partners, or receptors which could provide additional clues for the role it plays for the dinoflagellate. A brevetoxin photoaffinity probe (Figure 1.11A) captured two chloroplast proteins: light harvesting complex II (LHC-II) and a thioredoxin (Trx) like protein (Figure 1.11B)

1.5.1 Brevetoxin binding to LHC-II indicates a role in photosynthesis

LHC-II is a plastid transmembrane protein which functions in the harvesting of light, and its subsequent transfer of energy to the reaction centers of photosystem II (PS-II). In plants and green algae LHC-II binds fourteen chlorophyll molecules, four carotenoid molecules and two lipids (Standfuss, Terwisscha van Scheltinga, Lamborghini, & Kühlbrandt, 2005). Under high light conditions, a transmembrane proton gradient (ΔpH) is formed by the splitting of 2 H_2O molecules into oxygen O_2 and 4 H^+ . These protons are then able to interact within the thylakoid lumen and set in motion a series of processes that include photo-protective mechanisms, and enhanced ATP synthase activity (Järvi, Gollan, & Aro, 2013). It was observed that the binding of brevetoxin to its protein targets was pH dependent, with higher affinity for LHC-II at an acidic pH (conditions which simulate high light).

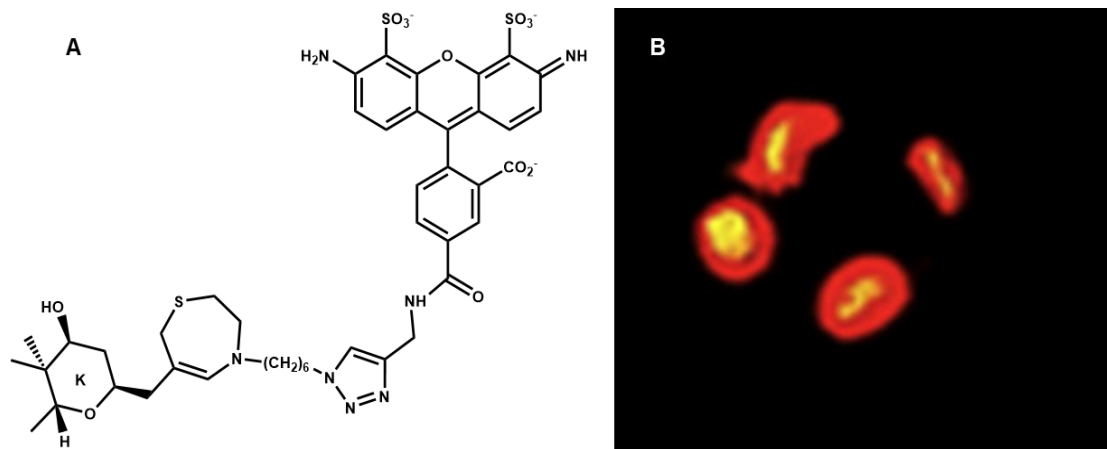


Figure 1.10 A) Fluorescent brevetoxin probe B) *K. brevis* cells incubated with PbTx-2 probe (yellow), and autofluorescence of the chloroplast (red).

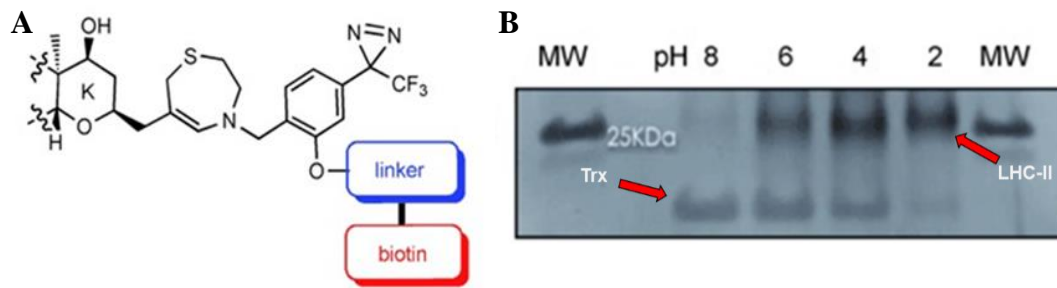


Figure 1.11 A) Brevetoxin photoaffinity probe B) protein binding of the photoaffinity probe is pH dependent with LHC-II binding at low pH and Trx and neutral/alkaline pH (used with permission from (Cassell, Chen, Thomas, Liu, & Rein, 2015))

One of the most crucial functions of LHC-II is the binding of the xanthophyll cycle pigments (violaxanthin (Vx)/zeaxanthin (Zx), in plants/green algae, and diadinoxanthin (Ddx)/diatoxanthin (Dtx) in marine dinoflagellates/diatoms) (see Figure 1.12). The binding of the LHC-II complex to the latter pigments in each respective pair (Zx/Dtx) is a result of the Δ pH dependent activation of a xanthophyll de-epoxidase enzyme and the aggregation of LHC-II into trimers. This aggregation releases the epoxide forms of each pigment pair (Vx/Ddx) into the thylakoid membrane allowing for the de-epoxidation. The xanthophyll cycle provides the foundation for the dissipation of excess light energy via a form of non-photochemical quenching (NPQ) (Liu et al., 2004). The binding of the xanthophylls to the light harvesting complex regulates photochemistry in a two-fold manner. First, under light limiting conditions, xanthophylls absorb light at wavelengths (450 – 525 nm) where chlorophyll is unable. Light energy absorbed by the xanthophyll pigments is transferred to chlorophyll: a process known as light harvesting which is analogous to fluorescence resonance energy transfer (FRET). Second, once de-epoxidized Zx/Dtx function to accept excess light from chlorophyll under light-saturating

conditions. This process is an important component of NPQ, allowing for the efficient de-excitation of singlet chlorophyll ($^1\text{Chl}^*$). Without this de-excitation, increased $^1\text{Chl}^*$ populations can allow for intersystem crossing (ISC) to triplet chlorophyll ($^3\text{Chl}^*$) which is an effective photosensitizer of molecular oxygen (O_2) producing singlet oxygen ($^1\text{O}_2^*$) (Jahns, Latowski, & Strzalka, 2009). Singlet oxygen is a powerful reactive oxygen species which can cause lipid peroxidation and lead to cell death (Krieger-Liszkay, 2004).

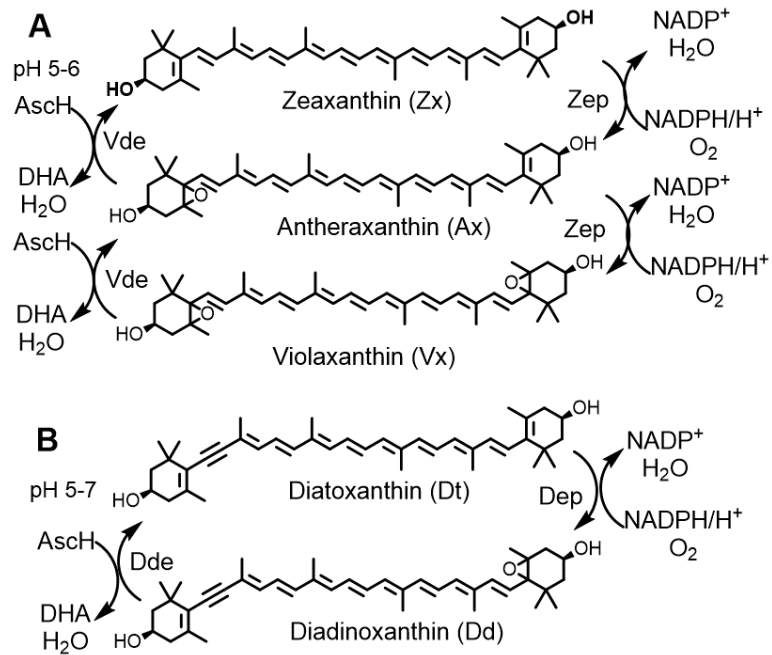


Figure 1.12 The xanthophyll cycle in **A)** plants and green algae **B)** dinoflagellates and diatoms. Vde/Dde – violaxanthin and diadinoxanthin de-epoxidase, Zep/Dep – zeaxanthin and diatoxanthin epoxidase, respectively.

LHC-II has been called the most abundant membrane protein on the planet and is part of the LHC superfamily of photosynthetic antennae proteins (Barros & Kühlbrandt, 2009). These proteins have diverged through evolution in different organisms to optimize

the photosynthetic efficiency involved in light harvesting. The LHC-associated proteins of phytoplankton have evolved mechanisms to regulate photo-oxidative stress and the use of light energy more efficiently for photochemistry, such as using various forms of chlorophyll and other accessory pigments (Tengs et al., 2000). In certain diatoms and dinoflagellates including *K. brevis*, a special type of LHC protein family has evolved known as the fucoxanthin-chlorophyll *a/c* binding protein (FCP). These proteins bind Fx and its esters (19'-butanoyloxy-Fx, and 19'-hexanoyloxy-Fx), in a carotenoid:Chl ratio of near 1:1, much higher than that found in green algal and plant LHC (Beer, Gundermann, Beckmann, & Büchel, 2006). The increased Car:Chl ratio allows for the absorption of light in the blue-green range which is critical for photosynthesis in aquatic environments (Premvardhan, Robert, Beer, & Büchel, 2010). Similarly, it is postulated that the higher concentration of Fxs in these proteins is required to lower photosynthetic yield of the light harvesting apparatus, this would allow for the more efficient de-excitation of ¹Chl* leading to reduced ROS production under conditions of high light stress (Gundermann & Büchel, 2012).

The binding of brevetoxin to LHC II at low pH, conditions simulating high light stress, indicates that the toxin may be playing a role in the regulation of photo-protection. High and low toxin containing strains of *K. brevis*, henceforth referred to as *KbHT* and *KbLT*, respectively, were tested for their ability to perform NPQ (Figure 1.13A). NPQ was consistently observed in cultures of *KbHT* whereas *KbLT* performs NPQ sporadically. The inability to effectively perform NPQ is correlated with an increase in ROS production and it was found that *KbLT* produced ROS at nearly twice the rate of

KbHT (Figure 1.13B) (Cassell et al., 2015). While the correlation is clear, correlation is not cause and the reason for the correlation is unknown. Is a high toxin content required for proper functioning of NPQ in *K. brevis*, or does sporadic functioning of NPQ result in reduced cellular toxin content?

While LHC-II binding of brevetoxin at acidic pH indicates the possibility of a photoprotective role, the Trx binding was more pronounced under neutral and alkaline conditions, simulating low-light or darkness (see Figure 1.11B), which may indicate the involvement of brevetoxin in biochemical processes unrelated to light-harvesting (Cassell et al., 2015).

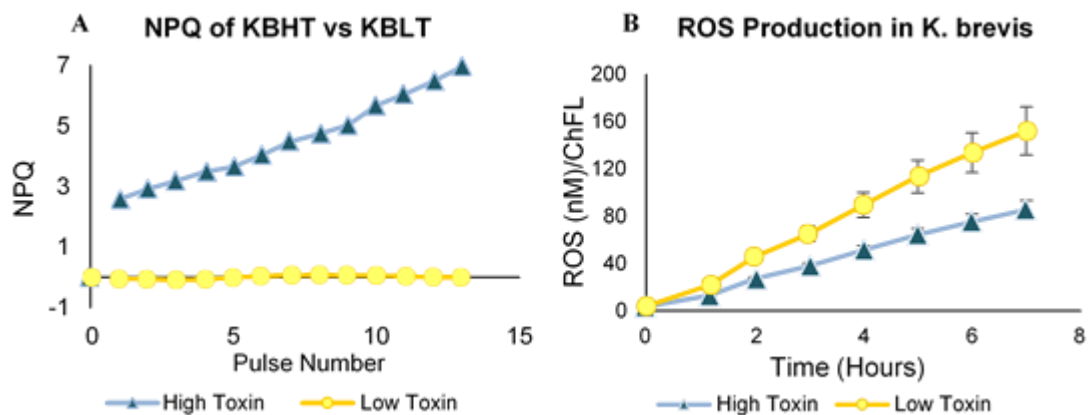


Figure 1.13 A) NPQ of *KbHT* vs *KbLT* showing differences in observed functioning of NPQ. B) Reactive oxygen species production between *KbHT* and *KbLT*.

1.5.2 The thioredoxin system links redox homeostasis and photosynthesis

The redox mechanisms of the chloroplast are multifaceted pathways which regulate electron flow as a result of oxygenic photosynthesis. Upon irradiance of PS-II by 4 photons, a pH gradient (ΔpH) is formed by the oxidation of water into oxygen and 4 protons. This oxidation also provides 4 electrons to PS-II which sets in motion a cascade

of redox reactions which are facilitated by the plastoquinone pool (PQ) and eventually generate 3 ATP molecules, and 2 nicotinamide adenine dinucleotide phosphate hydrogenase molecules (NADPH). These two molecules play important roles in biosynthetic pathways: ATP being the energy source for primary and secondary metabolism and NADPH being an important part of anabolic metabolism, providing reducing power during biosynthesis.

Chloroplasts contain two distinct redox cascades which exist as transmitters of light signals and regulators of chloroplast function. First, the ferredoxin-thioredoxin reductase (FTR)/thioredoxin pathway. FTRs are heterodimers which contain an iron-sulfur center, and a disulfide bridge which receive reducing equivalents from light dependent electron transport via ferredoxin. It was originally thought that the FTR pathway was the only way chloroplasts regulated redox status. However, the discovery of a chloroplast thioredoxin reductase which receives its reducing equivalents from NADPH revealed an alternative path for photosynthetic organisms to alter their redox status in response to changing environmental conditions (Serrato, Pérez-Ruiz, Spínola, & Cejudo, 2004). Both pathways work to regulate enzymatic activity via a network of thiol disulfide exchange reactions which are in part facilitated by the enzyme thioredoxin.

Trx is the parent of a family of redox regulatory enzymes (Hanschmann, Godoy, Berndt, Hudemann, & Lillig, 2013; Holmgren & Bjornstedt, 1995). Thioredoxins are present in almost all living organisms. In photosynthetic organisms, Trxs are commonly located within the chloroplast stroma and over 400 confirmed or potential targets of Trx have been identified within the chloroplast (Hall et al., 2010; Nikkanen & Rintamäki,

2014). Trx is converted from its inactive (disulfide) form to the active (dithiol) via thioredoxin reductase (TrxR) (Figure 1.14). In plants and algae, the two types of TrxR typically present are FTR and NADPH dependent thioredoxin reductase (NTR). The two types of TRs are thought to be selective for different forms of Trx. The discovery that FTRs are dependent on photo-reduced ferredoxin was the first direct link between light and redox regulation in the chloroplast (Schürmann & Buchanan, 2008).

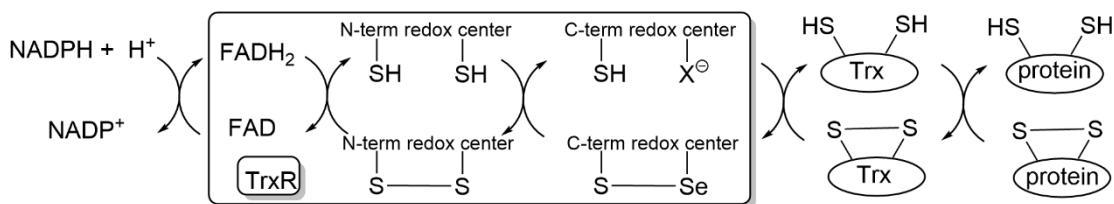


Figure 1.14 Electron flow from NADPH to protein disulfide bridges, via TrxR and Trx. Trx reduces many proteins and is returned to the active reduced state by TrxR in a NADPH dependent reaction. The C-terminal redox center (in the box) in high M_w TrxR can be composed of two cysteine residues or a cysteine and a selenocysteine.

Structurally, FTR and NTR are very different; NTRs utilize the coenzyme FAD to accept reducing equivalents from NADPH, they also possess a TrxR domain and a Trx domain, essentially serving as their own reductase which then transfers equivalents to the target protein (Jacquot et al., 1994; Serrato et al., 2004). NTRs fall into two categories, small and large NTR (Jacquot, Eklund, Rouhier, & Schürmann, 2009). Small or low M_w NTRs are homodimers of 35 kDa subunits often found in bacteria and yeast having similarities to plant NTR (Dai et al., 1996; Jacquot et al., 1994). While the large or high M_w NTRs are homodimers of 55 kDa subunits which are sometimes referred to as mammalian NTR, although they are widespread in the animal kingdom, including organisms such as green algae, diatoms, haptophytes and dinoflagellates including *K.*

brevis (Araie, Suzuki, & Shiraiwa, 2008; Novoselov & Gladyshev, 2003). Large NTRs may contain a unique C-terminal selenosulfide active site (xCUx). Selenocysteine (Sec) is incorporated into proteins by a unique UGA codon, usually recognized as a stop codon, accompanied by an mRNA selenocysteine insertion sequence (SECIS) in the 3'-untranslated region (UTR). A stem loop structure formed by the SECIS element is recognized by a SECIS binding protein which positions a Sec-tRNA for incorporation of Sec at the UGA codon (Gladyshev, Jeang, & Stadtman, 1996).

Analysis of the *K. brevis* (Wilson strain) transcriptome library (Ryan, Pepper, & Campbell, 2014) utilizing tBLASTn (Altschul, Gish, Miller, Myers, & Lipman, 1990) and chloroplast located large NTRs from *Emiliania huxleyi* and *Arabidopsis thaliana* as queries (NCBI accession numbers: BAH20464.1 and AEE86518.1, respectively) each produced two transcripts with significant ($<1E^{-10}$) homology to the query (Loci: 29890, 38966 for *E. huxleyi* and 21233, and 67462 for *A. thaliana*) (Chen et al., 2018). As shown in Table 1.2 the N-terminal redox centers containing CxxxxC motif typical of large NTRs all shared similarities with the haptophyte *E. huxleyi*. NTRs 1-3 which resulted from Locus 29890, a polycistronic mRNA containing 5 ORFs coding for 3 NTRs. (NTR 1: ORF 1 and 3, NTR 2: ORF 2 and 4, NTR 3: ORF 5 which did not appear to contain an N-terminal redox center) found using NCBI ORFfinder (Wheeler et al., 2003). Furthermore, NTR 4, of was revealed to be a 968 amino acid protein containing an unusual 5 possible redox centers (4 of which correspond to typical large NTRs and one small NTR), none of which could be confidently considered as the C-terminal redox center. However, this NTR does contain a CGGGKC redox center similar to that found in

apicomplexans such as *P. falciparum* (McCarty et al., 2015), which presents an interesting question regarding their shared chromalveolate lineage. While the N-terminal redox centers containing CxxC motifs typical of small NTRs both appear more similar to *A. thaliana*, which is consistent with the origins of these plant-like NTRs (Jacquot et al., 2009).

Table 1.2 Putative NTRs found in the *K. brevis* using tBLASTn algorithm.

Locus	NTR	Redox center N-terminal	Redox center C-terminal	Small /large?	3' UTR SECIS
29890	NTR1	CVNVGC	CC	large	yes
	NTR2	CVNVGC	CU	large	yes
	NTR3	absent	CU	unknown	yes
38966	NTR4	CVGQAC, CVGNAC, CIPC, CVNVGC, CGGGKC		unknown	no
21223	NTR5	CGPC	CATC	small	no
67462	NTR6	CAAC	absent	small	no

Analysis of the *K. brevis* transcriptome for the proper machinery for selenocysteine insertion using the program SECISearch3 (Mariotti, Lobanov, Guigo, & Gladyshev, 2013) shows promising results for the possibility of *K. brevis* having a Sec containing NTR (Table 1.2). Analysis of locus 28980 found a 73 nucleotide SECIS immediately following the TAA stop codon of ORF2,4 and 5. Additional searches of the Wilson transcriptome library revealed DNA sequences coding for the requisite enzymes for selenoprotein biosynthesis (Table 1.3). Briefly, the SECIS binding protein (locus 14693) which recruits translation and assembly factors and positions the Sec-tRNA. Selenocysteine tRNA synthase (locus 48280) and selenophosphate synthetase (loci 41392, 52141, 18903) which work together to take the serine residue which is preloaded

on Sec tRNA and, using selenophosphate synthesized from selenide and ATP, convert it to Sec.

Table 1.3 Analysis of the *K. brevis* transcriptome library identified the machinery required to biosynthesize selenoproteins.

Loci	Putative Function
14693	SECIS binding protein
48280	SeC tRNA synthase
41392	Selenophosphate synthetase
52141	Selenophosphate synthetase
18903	Selenophosphate synthetase

NTRs localized in the chloroplast are referred to as NTRC to avoid confusion with FTR which is always found in the chloroplast, and NTRs that may be found in other cellular compartments, such as the cytosol or mitochondria. Early experiments characterizing *NTRC* knockout mutants of *A. thaliana* showed increased sensitivity in response to the photo-oxidant methyl viologen suggesting the involvement of NTRC in oxidative stress mitigation (Serrato et al., 2004). It has also been shown that *A. thaliana* *NTRC* knockout mutants have drastically different photochemical parameters, such as reduced total chlorophyll, increased NPQ, greater ΔpH in response to light, and higher zeaxanthin levels (Naranjo et al., 2016). Furthermore, significant decreases in reduced glutathione and reduced ascorbate have been observed in *NTRC* knockout mutants of *A. thaliana* (Pérez-Ruiz, Naranjo, Ojeda, Guinea, & Cejudo, 2017). This evidence suggests that NTRC is strongly linked to photosynthetic activity and redox regulation. Similarly, experiments with *Trx-f* (an isoform of Trx responsible for regulating fructose-1,6-

biphosphatase (FBPase) activity) deficient and NTRC deficient mutants demonstrated that the pathways cooperate in some aspects of the regulation of the Calvin-Benson cycle, starch metabolism, and growth under varying light conditions. Thus, implying that light-dependent and NADPH-dependent thiol redox systems are closely linked in function with Trx-*f* and NTRC being colocalized to the same substructure of the chloroplast (Thormählen et al., 2015).

Brevetoxin binding to a Trx-like protein at neutral-alkaline pH indicates the possibility that one of the toxin's endogenous functions may be to regulate the disulfide reducing activity of the enzyme under light-limiting conditions. As shown by the *A. thaliana* mutants above, under conditions of compromised, or downregulated NTR/Trx activity, it may be observed that the growth rate, and photoprotective mechanisms may be sustained even when the organism is not experiencing light stress. *KbLT* may experience the opposite effect where, lacking adequate toxin production may lead to an inability to regulate NTR/Trx activity effectively and may inhibit the photoprotective response under sustained light, leading to the observed differences in NPQ and ROS production between the two strains.

1.6 Significant biochemical differences in high and low toxin producing strains of *K. brevis*

Recent analysis of biochemical parameters (total and reduced glutathione, small and low MW thiol concentration, thioredoxin/glutaredoxin activity, ascorbate concentration and antioxidant capacity) of *KbHT* and *KbLT* by Chen et al., have provided a more comprehensive picture of how PbTx content correlates with *K. brevis*' redox status (Chen

et al., 2018). Total glutathione (GSx) does not differ between *KbHT* and *KbLT*. However, reduced glutathione (GSH) was consistently higher in *KbLT*, ranging from 1.5 to 2.3-fold. Similarly, proteins from *KbLT* had more cysteines in the reduced state in *KbLT* when compared to *KbHT*, possibly influencing the activities of enzymes that are regulated by the redox status of cysteines.

Other important comparisons were the differences in ascorbate concentration and antioxidant capacity observed between the two strains. On one hand, *KbHT* contained a significantly higher antioxidant capacity (16 – 23 %) on 3 out of 4 days tested, however *KbLT* had higher ascorbate concentration (up to 4.5-fold) on all 4 days measured. Ascorbate is an important part of the antioxidant system of cells, it is also an important co-factor in the de-epoxidation of violaxanthin/diadinoxanthin in photosynthetic organisms. Furthermore, differences in Trx and glutaredoxin (Grx) activity were measured and found to be higher in the low toxic (3-fold and 1.6-fold, respectively). The observation that ascorbate concentrations are higher in the low toxic, in conjunction with higher measurements of GSH, high MW thiols, Trx and Grx activities indicate a significant difference in the redox status of the two strains. The observed differences suggest that the low toxic cell is existing in a more reduced state with a high amount of stored reduction potential. Considering the importance of the NTR/Trx system, and the other antioxidant systems tested in the mitigation of oxidative stress, it's possible the compromised redox status of the low toxic may result in the two strains' observed differences in ROS production, and NPQ.

1.7 Project overview and specific aims

The primary goal of the research project is to develop a more comprehensive understanding on the endogenous biochemical function of brevetoxin in *K. brevis* as it relates to photoprotection and redox homeostasis. By testing the hypothesis that brevetoxin content is linked to redox dependent photoprotective mechanisms in the chloroplast. Further comparison and characterization of the two strains' carotenoid concentration, gene expression, and lipid profiles will be performed to understand the biochemical basis for the inefficient functioning of NPQ in *KbLT*, as it relates to the xanthophyll cycle. Furthermore, experiments will be conducted to expand our understanding on the differences in thiol concentrations and redox status between the two strains and the implications that brevetoxin may have on the plastid redoxome. Finally, a recombinant *K. brevis* NTR will be expressed and characterized for activity in the presence of brevetoxin to assess any influence brevetoxin may have on it's ability to reduce various substrates.

1.7.1 Research Objectives

1. Comparative analysis of the NPQ-essential, xanthophyll cycle pigments in high and low toxin *K. brevis* under varying light conditions.
2. Determining the source of the differences in NPQ between *KbHT* and *KbLT* by comparing:
 - a. Relative mRNA levels of diadinoxanthin de-epoxidase DDE in *K. brevis* high and low toxin cultures.
 - b. Relative levels of vital lipids (MGDG, DGDG and SQDG) related to the xanthophyll cycle and plastid membrane integrity.
3. Redox proteomics characterization of *KbHT* and *KbLT* using IodoTMT labeling of *K. brevis* total protein.
4. Expression of recombinant *K. brevis* NTR and characterization of its enzymatic activity in the presence of PbTx-2.

Chapter 2: Comparative analysis of the NPQ-essential, xanthophyll cycle pigments in high and low toxin *K. brevis* under varying light conditions

Portions of this chapter have been published as an original research article in the journal *Harmful Algae*. Adopted with permission from Chen, W., Colon, R., Louda, J. W., del Rey, F. R., Durham, M., & Rein, K. S. (2018). Brevetoxin (PbTx-2) influences the redox status and NPQ of *Karenia brevis* by way of thioredoxin reductase. *Harmful Algae*, 71, 29-39.

Objective

Our hypothesis that brevetoxin may play a more important role in photoprotection than previously considered stems from the observed differences in the ability of the two strains of *K. brevis* (*KbHT* and *KbLT*) to perform NPQ and production of ROS, coupled with the binding of the fluorescent brevetoxin probe to LHC-II. By analyzing the xanthophyll cycle pigment content of *K. brevis* in response to intense light (>1,200x100 Lux) and darkness it is possible to assess the relative efficiency of the xanthophyll cycle, an important component of NPQ, in the two strains of *K. brevis*.

2.1 The xanthophyll cycle plays an essential role in NPQ

Photosynthetic organisms have developed mechanisms for regulating the utilization of light energy in order to more efficiently perform photochemistry and prevent photooxidative damage. NPQ plays a pivotal role in protecting the photosynthetic apparatus. NPQ is a photophysical process, which can be broken down into three components: energy-dependent quenching (qE), state-transition quenching (qT), and

photo-inhibition quenching (qI). During photosynthesis, light energy enters the photosynthetic apparatus and excites chlorophyll molecules to a singlet state ($^1\text{Chl}^*$). This excited species can relax via fluorescence emission, photochemistry, intersystem crossing (ISC), or thermal dissipation (NPQ). The quantum yields of these processes strongly depends on the lifetime of $^1\text{Chl}^*$.

qT is caused by the uncoupling of LHC-II from PS-II, and the subsequent binding of LHC II to PSI (Iwai, Kato, & Minagawa, 2007). Similarly, qI is involved in long term down-regulation of PSII, which can relax in terms of hours (Murata, Takahashi, Nishiyama, & Allakhverdiev, 2007). Electron transport creates a luminal ΔpH that triggers qE, which relaxes (de-excites) in seconds to minutes. Protonation of PSII proteins induces specific binding of xanthophylls to form pigment-protein complexes. This binding causes a conformational change in PS-II which results in a decreased $^1\text{Chl}^*$ lifetime (Müller, Li, & Niyogi, 2001). Previous studies by Cassell et al., demonstrated that the low toxic strain of *K. brevis* is qE deficient. Understanding how brevetoxin and qE are related will be our principal focus.

An effective way of analyzing the qE potential of *K. brevis* is by following the distribution of xanthophyll cycle pigments in response to changing light conditions (Evens, Kirkpatrick, Millie, Chapman, & Schofield, 2001). During high light adaptation, qE initiated by the ΔpH of the thylakoid lumen triggers the de-epoxidation of diadinoxanthin to diatoxanthin via the enzyme Dde. This process increases the number of conjugated π -orbitals in the xanthophyll and lowers the singlet excited state of diatoxanthin ($^1\text{Dtx}^*$) below that of $^1\text{Chl}^*$ (Frank et al., 1994; Lohr & Wilhelm, 1999).

$^1\text{Dtx}^*$ is then able to accept energy from $^1\text{Chl}^*$ and prevent ISC. If the NPQ deficiency of *KbLT* is a result of a compromised xanthophyll cycle, then *KbLT* should have reduced Dtx concentrations under high light conditions relative to *KbHT*.

2.2 Results and Discussion

HPLC analysis of *KbHT* and *KbLT* identified seventeen known and 3 unidentified carotenoids/xanthophylls as well as chlorophyll-*a*, -*c*₃ and -*c*₂ (Table 2.1). Carotenoid concentrations normalized to total chlorophyll did not show any significant differences between the strains, in either the light-adapted ($n = 5, \rho = 0.25$) or dark-adapted cultures ($n = 7, \rho = 0.86$). Nonetheless, differences in the distribution of carotenoids were observed. In *KbHT*, when comparing the light and dark-adapted samples, significant differences were observed only between the two xanthophyll cycle pigments: diatoxanthin ($n = 5, \rho = 0.04$) and diadinoxanthin ($n = 5, \rho = 0.05$). This difference between Ddx and Dtx in the *KbHT* light vs. *KbHT* dark samples translated to a significant difference ($n = 5, \rho = 0.04$) in epoxidation state ($\text{EPS} = \text{Ddx}/(\text{Ddx}+\text{Dtx})$). These fluctuations in Ddx and Dtx in *KbHT* are consistent with the proper functioning of the xanthophyll cycle. On the other hand, light and dark adapted *KbLT* showed no significant difference in these two xanthophylls or in any other carotenoid.

Table 2.1 Xanthophylls detected in *KbHT* and *KbLT* under varying light conditions (n=5), $p^{\text{Ddx}} = 0.05$, $p^{\text{Dlx}} = 0.04$.

Pigment*	mole% (SD) <i>KbHT</i>		mole% (SD) <i>KbLT</i>	
	light	dark	light	dark
19'-but-Fuco [A]	12.21 (1.91)	12.96 (1.81)	8.39 (3.55)	7.43 (2.58)
19'-but-Fuco [B]	12.56 (1.50)	11.68 (1.63)	7.66 (2.86)	6.70 (2.30)
19'-but-Fuco [C]	5.723 (1.10)	4.99 (1.46)	6.89 (3.83)	6.54 (1.02)
Fucoxanthin (Fx)	2.564 (1.04)	2.26 (1.17)	5.47 (3.13)	5.92 (1.93)
19'-hex-Fuco [A]	13.44 (2.94)	14.33 (2.22)	12.21 (6.42)	15.83 (0.61)
19'-hex-Fuco [B]	15.82 (2.46)	15.11 (1.64)	13.20 (7.04)	17.10 (2.55)
19'-hex-Fuco [C]	2.666 (1.23)	2.34 (1.10)	5.67 (3.56)	6.26 (2.99)
DiaDinoChrome	0.12 (0.27)	ND	0.32 (0.72)	0.26 (0.59)
Diadinoxan (Ddx)	15.43 (5.72)¹	21.63 (5.41)	19.54 (6.42)	22.68 (5.19)
Diato (Dtx)	6.18 (3.68)	1.22 (0.35)	5.56 (5.29)	2.32 (1.50)
Gyroxanthin	9.59 (1.21)	9.49 (1.34)	8.21 (1.75)	6.81 (0.74)
Alpha-carotene	0.19 (0.43)	0.87 (1.07)	ND	0.40 (0.63)
Tns-B-Car	1.66 (1.74)	1.38 (0.79)	2.16 (1.83)	0.78 (0.75)
Cis-B-Car	ND	0.48 (1.06)	ND	ND
UNKN#1	1.04 (1.20)	0.67 (0.91)	1.26 (1.21)	0.49 (1.10)
UNKN#2	0.43 (0.77)	0.30 (0.67)	1.37 (2.50)	ND
UNKN#3	0.57 (0.83)	ND	0.92 (1.28)	ND
Zeaxanthin (Zx)	0.33 (0.75)	0.28 (0.63)	1.14 (1.22)	0.46 (1.03)
Ddx+Dtx	21.61 (5.46)	22.86 (5.56)	25.11 (7.84)	25.01 (5.14)
Epoxidation State	0.71 (0.16)	0.94 (0.018)	0.80 (0.19)	0.90 (0.06)
Total Fuco	64.44 (6.56)	63.67 (5.78)	59.49 (10.55)	65.78 (6.48)
But Fuco	30.48 (2.00)	29.63 (3.43)	22.95 (7.82)	20.66 (5.38)
Hex Fuco	31.39 (5.49)	31.78 (4.05)	31.08 (15.98)	39.19 (1.38)

1: Shown in bold are carotenoids with significant differences *within* a strain under light and dark adaptation.

Comparison of the light and dark-adapted samples within the high or the low toxin *K. brevis* indicated that most carotenoids (except for Ddx and Dtx in *KbHT*) do not vary in the light vs dark. For this reason, both light and dark-adapted samples (n = 7) were used in the analysis comparing carotenoids between the strains (Table 2.2). Significant differences were observed for the fucoxanthins, with more 19'-butanoyl fucoxanthin A and B and less fucoxanthin and 19'-hexanoyl fucoxanthin C. However, these differences in individual fucoxanthins appear to offset one another, as there was no

significant difference in total fucoxanthins. Conversely, a significantly higher amount of Ddx was observed in the *KbLT* (19.54 mol %, EPS = 0.8), which results in a higher EPS in the light-adapted samples when compared to *KbHT* (15.43 mol %, EPS = 0.71, $\rho^{\text{Ddx}} = 2.75 \times 10^{-2}$). There was also a significantly higher amount of total xanthophyll cycle pigments (Ddx+Dtx) in *KbLT*.

Table 2.2 Xanthophylls with significant differences on average between the strains (n=7, unless otherwise noted).

Pigment*	mole% (SD)		<i>p</i> (T-test)	H-L
	<i>KbHT</i>	<i>KbLT</i>		
19'-but-Fuco [A]	12.58 (1.73)	8.11 (2.81)	1.17 E ⁻⁵	4.68
19'-but-Fuco [B]	12.31 (1.47)	7.24 (2.31)	3.37 E ⁻⁵	5.07
Fucoxanthin	5.53 (1.03)	5.73 (2.54)	1.17 E ⁻³	-3.48
19'-hex-Fuco [C]	2.25 (1.03)	5.93 (2.88)	1.45 E ⁻³	-3.39
Diadino (Ddx) light (n=5)	15.43 (5.72)	19.54 (6.42)	2.75 E ⁻²	-4.11
Gyroxanthin	9.50 (1.13)	7.48 (1.35)	1.36 E ⁻³	2.02
But Fuco Total	30.62 (2.76)	22.00 (6.00)	6.08 E ⁻⁴	8.62
Ddx+Dtx	21.28 (5.51)	24.73 (6.47)	1.04 E ⁻²	-3.45
Epox. State (EPS) (n=5)	0.71 (0.16)	0.80 (0.18)	2.80 E ⁻²	-0.09

2.3 Materials and methods

2.3.1 Reagents

All reagents were purchased from Thermo Fisher Scientific Co. or Sigma-Aldrich unless otherwise specified.

2.3.2 Culture growth conditions

Cultures of *K. brevis* (Wilson strains) were obtained from Mote Marine Laboratory (Sarasota, Florida) and maintained in L1-Si medium, with the exception that the NH 15 vitamin supplement (Gates and Wilson, 1960) replaced the L-1 supplement. Cultures were maintained in a growth chamber at ~20°C under artificial light (40 W, 3.4×10^3 Lux; PFD ca. $46 \mu\text{mol photons}\cdot\text{m}^{-2}\cdot\text{sec}^{-1}$).

2.3.3 Extraction and analysis of carotenoids

Log phase cultures of *K. brevis* were both light or dark adapted and extracted for carotenoids and chlorophyll on each of five different days. Cultures were light-adapted by placing the culture under 1.2×10^5 Lux (full sun: PFD ca. $2,220 \mu\text{mol photons}\cdot\text{m}^{-2}\cdot\text{sec}^{-1}$) for 25 minutes. Cultures were dark-adapted by placing culture in the dark for 25 minutes. On two of the 5 days, cultures were filtered through a pre-conditioned (according to the manufacturer's instructions, 100 mL of methanol followed by 50 mL of water) Varian C-18 disc (47 mm). Disks were washed with water (10 mL) and eluted with methanol (10 mL). The methanol was evaporated in vacuo and resuspended in aqueous methanol (10% NH₄OAc, 50 mM, pH 7.0, 1.5 mL). Samples

were immediately stored at -80°C . On three of the five days, cultures were vacuum filtered through Whatman GF/F #30 and stored at -80°C .

Frozen filters were added to a 10 mL Potter-Elvehjem tissue grinder and 3.0 mL of extraction solvent (methanol:acetone:dimethylformamide:water, 30:30:30:10, v/v/v/v) containing a known amount of an internal standard (IS = copper-mesoporphyrin-IX dimethyl ester) was added. The pestle of the tissue grinder was modified by carving off bits of the PTFE tip to make it somewhat pointed rather than round in order to aid disruption of the glass fiber filter. The Pestle was inserted into the chuck of a motorized mixer and the filter in the mortar (aka tube) was ground at moderate rpm while maintaining the glass mortar in an ice filled Teflon beaker. Following grinding, the extract within the mortar was sonicated in a water bath several times in short (< 3 sec) spurts. The tube (mortar) was then covered with aluminum foil and placed in the refrigerator ($\sim 4^{\circ}\text{C}$) to steep for 1–2 hours (Hagerthey, William Louda, & Mongkronsri, 2006). All procedures were performed at ice-bath temperatures under dim yellow light to avoid photooxidative and/or thermal alterations of the pigments. The tube was then centrifuged for 2–3 minutes, the extract decanted and filtered using a syringe filter ($0.45\ \mu\text{m}$). The UV-Vis spectrum of the crude extract was recorded between 350–800nm for estimating total chlorophyll at ca. 662-4 nm (e.g. $a = 87.7\ \text{L}\cdot\text{g}^{-1}\cdot\text{cm}^{-1}$) (Egeland et al., 2011) and to ensure that the extract was not too concentrated (highest peak over < 1.2 AU) for injection into the liquid chromatograph. Prior to injection, 0.125 mL of an aqueous ion pairing (aka ion suppression) solution consisting of 15.0 g of tetrabutylammonium acetate (TBAA) and 77.0 g ammonium acetate per liter final

volume (Louda, Li, Liu, Winfree, & Baker, 1998; Mantoura & Llewellyn, 1983) was added to 1.0 mL of the filtered extract.

High performance liquid chromatography (HPLC) –photodiode array detection (PAD) involved the injection of 100 or 500 μ L of the prepared injectate onto a 3.9 \times 300mm Waters NovaPak C18 column using a ternary gradient (Louda et al., 1998; Louda, Liu, & Baker, 2002) provided by Thermo-Separations-Products P4000 quaternary pump. Pigments were detected and PDA generated UV-Vis spectra recorded by a Waters 990 or 996 photodiode array detector with Waters software. Pigment identifications by retention times and UV-Vis spectra (Louda et al., 2002) were verified versus known mixed and pure (e.g. fucoxanthin, 19'-hexanoyloxyfucoxanthin, 19'-butanoyloxyfucoxanthin etc.) standards purchased from DHI Lab Products (Agern Allé 5, 2970 Hørsholm, Denmark). Quantitation of separated pigments involved integration of the peak area and application of millimolar or specific extinction coefficients given in the literature (Egeland et al., 2011).

2.4 Conclusion

Analysis of the carotenoid content of *KbHT* and *KbLT* under varying light conditions demonstrated that *KbLT* does not consistently perform xanthophyll de-epoxidation, a necessary step of the xanthophyll cycle for the efficient quenching of excess light energy. As shown by Table 1.2 significant differences are found in *KbHT*'s concentration of xanthophyll cycle pigments Ddx, and Dtx, between light and dark adaptation ($p = 0.05$, and 0.04 , respectively). This demonstrates a functioning xanthophyll cycle for *KbHT*, a significant difference was not observed in *KbLT* between

the two light conditions. In fact, a large amount of variation in the amount of Dtx under high light exposure is observed ($CV = 0.95$). This is consistent with findings of inconsistent NPQ performance in *KbLT* reported by (Cassell et al., 2015). We conclude that the poorly functioning xanthophyll cycle in *KbLT* leads to the observed disparities in NPQ between the two strains.

Chapter 3. Evaluation of essential components of NPQ in high and low toxic strains of *K. brevis*.

Portions of this chapter have been published as an original research article in the journal *Harmful Algae*. Adopted with permission from Colon, R., & Rein, K. S. (2021). Essential components of the xanthophyll cycle differ in high and low toxin *Karenia brevis*. *Harmful Algae*, 103, 102006.

Objective

Proper functioning of the xanthophyll cycle requires an active Dde enzyme. Dde activity in turn, is dependent on the presence of specific classes of thylakoid lipids. Therefore, DDE expression and thylakoid lipid content and distribution among classes was compared between *KbHT* and *KbLT*. From the data presented in the previous chapter it is evident that *KbLT* possesses the xanthophylls required to perform the de-epoxidation required for qE. However, the inconsistency of the observed Dtx concentration indicates that Dde activity may be compromised in *KbLT*.

3.1.1 Xanthophyll de-epoxidase activity is dependent on pH, redox status, and lipid content

Violaxanthin de-epoxidase (Vde) and zeaxanthin epoxidase (Ze) are lipocalin proteins which assist photosynthetic organisms' (primarily plants and secondary algae) acclimation to varying light intensities. In addition to the lipocalin domain, Vde contains an N-terminal cysteine rich domain and a highly charged C-terminus enriched in glutamyl residues. Similarities between plant/green algal Vde and dinoflagellate Dde

exist, specifically in the conservation of the N-terminal cysteine residues which are required for activity (Saga et al., 2010), as well as in the presence of a highly charged C-terminal domain. Studies characterizing the lipocalin-flanking domains of Vde have demonstrated the importance of the charged C-terminus for pH dependence. It is postulated that the principal function of the C-terminus of Vde is to provide binding sites for the enzyme to the lipid rich thylakoid membrane (Hieber, Bugos, Verhoeven, & Yamamoto, 2002).

Differences however do exist between plant and algal orthologues, especially in the C-terminal charged domain. Where plant Vde contains an average of 47% charged residues, ~25% are glutamic acid, while diatoms' *Phaeodactylum tricornutum* and *Thalassiosira Pseudonana* Dde contain 29 and 37% charged residues, 13 and 18% glutamic acid, respectively (Coesel, Oborník, Varela, Falciatore, & Bowler, 2008). The implications of these differences in the charged domain (C-terminus) have been demonstrated by the difference in pH dependence of Dde relative to Vde, with the former having a pH optimum 0.7 pH units higher (Grouneva, Jakob, Wilhelm, & Goss, 2006; Jakob, Goss, & Wilhelm, 2001).

Furthermore, experiments performed by (Hieber et al., 2002) using thylakoid extracts of *A. thaliana* expressing either WT or truncated mutants of Vde demonstrate that removal of the C-terminal residues of Vde inhibits the ability to bind to lipid micelles, but does not significantly inhibit the specific activity of the enzyme (pH < 5.0) when removing up to 64% of glutamic acid residues. However, it is important to note that at pH > 5.0 the activity is reduced by at least half, indicating that the lack of charged

residues influences the ability of the enzyme to interact with the native lipid-pigment interface.

Similarly, mutation of any of the N-terminal cysteine residues also compromises the enzymatic activity of Vde (Niyogi, Grossman, & Björkman, 1998). NPQ deficient mutants of *Arabidopsis thaliana* and *Chlamydomonas reinhardtii* have been reported to sustain high concentrations of violaxanthin under high light conditions and produce very little zeaxanthin (*npq1*). The *npq1* mutants of *A. thaliana* were found to be defective in the genes encoding VDE, with a signal nucleotide change from G to A, which would change a conserved cysteine residue to a tyrosine (Niyogi et al., 1998). Furthermore, deletion of the first 4 amino acids of Vde renders the enzyme completely inactive (Hieber et al., 2002), highlighting the importance of this N-terminal region for activity.

3.1.2 Lipid-pigment-protein interactions

Characterization of the xanthophyll cycle dates back to the 1960's, with experiments on isolated chloroplasts of spinach (Hager, 1969). Yamamoto (Yamamoto H.Y., 1974; Yamamoto, 1978) first showed that the addition of the galactolipid monogalactosyldiacylglycerol (MGDG) as well as ascorbate was required for de-epoxidase activity, postulating that the role of the lipid was to solubilize the substrate violaxanthin in micelles to facilitate the de-epoxidation. Yamamoto later proposed that a second function of the lipid was to satisfy a structural requirement that allowed for proper functioning of the de-epoxidase (Yamamoto, 1978).

Studies conducted over the past 20 years documenting the activity of Vde/Dde in various lipid environments, have demonstrated that xanthophyll de-epoxidases require the presence of lipid inverted hexagonal phases (H_{II}) for full activity (Goss & Latowski, 2020; Goss et al., 2005). The de-epoxidation of violaxanthin in the presence of the H_{II} phase forming phospholipid; phosphatidylethanolamine (PE) was found to occur at rates similar to those in the presence of MGDG. Using the bilayer forming lipids phosphatidylcholine and digalactosyldiacylglycerol (DGDG) no Vde activity was detected (Goss et al., 2007; Goss et al., 2005; Latowski, Åkerlund, & Strzałka, 2004; Latowski, Kostecka, & Strzałka, 2000; Latowski et al., 2002). This dependence on a specific structural component of MGDG supports Yamamoto's hypothesis that the role of MGDG is two-fold.

More recently, xanthophyll de-epoxidase activity has been investigated in the presence of lipid compositions attempting to mimic *in vivo* environments as well as in the presence of LHC-II (Schaller et al., 2010; Yamamoto, 2006). In the presence of the negatively charged lipids; sulfoquinovosyldiacylglycerol (SQDG) and phosphatidylglycerol (PG), as well as MGDG and DGDG, the activity of Dde reached only 25% relative to Dde activity in a binary mixture of MGDG and DGDG. Thus, it was proposed that the lipid composition of the thylakoid is not the only factor in efficient de-epoxidation but the separation of these lipids into domains must also occur (Goss et al., 2009).

The specific binding of Vde/Dde to the MGDG rich domains of the thylakoid membrane has been proposed to be a result of the docking of the charged domain of the

de-epoxidase on the polar head groups of the H_{II} lipid phase (Latowski et al., 2004; Latowski et al., 2002). Similarly, the interactions observed between MGDG and LHC-II further highlight the importance of the lipid-protein interactions within the thylakoid membrane. Recently, it has been shown that MGDG stabilizes LHC-II trimers from unfolding (Seiwert, Witt, Janshoff, & Paulsen, 2017). This coincides with the observation that upon illumination, aggregation of LHC-II trimers releases V_x/D_x into the thylakoid membrane, thus making it available to interact with V_{de} in these MGDG rich domains (Liu et al., 2004; Siefermann & Yamamoto, 1974; Yamamoto, 2006).

3.1.3 SQDG; a negatively charged lipid required for the proper functioning of PS-II

Much like the role MGDG plays in photoprotection and NPQ, the anionic lipids SQDG and PG play an important role in the functioning of PS-II. For many cyanobacterium SQDG and PG are partially interchangeable and can compensate for each other under sulfur and phosphorous limitations, respectively. However, that is not the case for all algae. For example, SQDG deficient mutants of *Chlamydomonas reinhardtii* have been reported to have 40% decreased PS-II activity and a higher sensitivity to 3-(3, 4-dichlorophenyl)-1, 1-dimethylurea (DCMU, an inhibitor of electron transport in the quinone pool). These mutants were able to replenish their activity in the presence of exogenous SQDG, but not in the presence of PG, or sulfonate-methylated SQDG (Minoda et al., 2002), indicating the sulfonate group played a particularly important role.

Similar studies using SQDG deficient mutants of *Thermosynechococcus elongatus* observed a 10% and 30% reduction in PS-II activity, as well as a significant

reduction in chlorophyll content, relative to WT under P-sufficient and P-limited conditions, respectively (Endo, Kobayashi, & Wada, 2016). PS-II dimers from this mutant of *T. elongatus* were later analyzed by X-ray crystallography. Results showed that of the four SQDG molecules which interact with the PS-II dimer in the WT, SQDG-1 and SQDG-2 are most responsible for the stabilization of the dimer via hydrogen bonding with residues on both monomers. It is shown that replacement of these two SQDGs with other lipids (PG, or beta-dodecylmaltoside) removed almost all hydrogen bonding and destabilized the dimer. Similarly, the hydrogen bonding, which is not present in the mutant, that occurs between SQDG-3 and a serine residue of PS-II (Ser-267) is proximal to hydrogen bonding that occurs between a separate serine residue (Ser-264) and the headgroup of bound quinone (Q_B) which may affect the exchange with free plastoquinone. SQDG-4 seems to be the least consequential, being proximal to the tail end of Q_B. Replacing this lipid with PG leaves most of the hydrogen bonding intact, and the hydrophobic tail of PG interacts similarly with Q_B as does SQDG (Nakajima et al., 2018).

3.1.4 *Karenia brevis* allelopathy disrupts photosynthetic capabilities and lipid biosynthesis of competitors.

The effects of allelopathic interactions between *K. brevis* and other marine phytoplankton competitors has been shown to weaken cell membrane integrity, alter lipid composition, reduce photosynthetic efficiency and result in increased indicators of oxidative stress in its algal competitors (Poulin et al., 2018; Poulson-Ellestad et al., 2014; Prince et al., 2008). Alterations in lipid composition will influence cell membrane

integrity, and photosynthetic efficiency is also highly dependent on the composition of thylakoid lipids (Schaller et al., 2011).

Recent *K. brevis* allopathy studies revealed important thylakoid lipid classes such as MGDG, DGDG, SQDG, PG, and phosphatidylcholine (PC) all experienced fold changes between -2.8 and -5.8 in the competitor *T. pseudonana*. These decreases in lipids were attributed to lipid degradation rather than decreases in lipid biosynthesis as increases in lipid biosynthetic enzymes were observed (Poulin et al., 2018).

3.2 Results and discussion

3.2.1 The relative levels of expression of four Dde homologues in *KbHT* and *KbLT*

In order to compare the expression of Dde in the high and low toxic strains, the transcriptome library of *K. brevis* was searched for Dde homologues. Using the National Center for Bioinformatics Information's (NCBI) Basic Local Alignment Search Tool for protein to translated nucleotide (tBLASTn) (Altschul et al., 1990), the protein sequences of various haptophytes, diatoms, dinoflagellates, and other marine phytoplankton were used as queries in the search of the *K. brevis* Wilson transcriptome (Ryan et al., 2014). From this search, four homologous loci meeting the criteria (E value < 1E⁻¹⁰) were identified (Table 3.1). The validity of the open reading frames of these loci was confirmed using NCBI Open Reading Frame Finder (ORFFinder) (Wheeler et al., 2003).

Table 3.1 Query origins, accession numbers and E values for the four corresponding loci from the *K. brevis* transcriptome library

Organism (CCMP* strain number when available)	NCBI Accession #	E values for four Loci			
		2514	42818	34174	9995
<i>Chrysochromulina</i> sp. (291)	KOO30092	2e-124	2e-5	2e-16	2e-19
<i>Nannochloropsis oceanica</i>	ANT70525	6e-84	0.019	2e-10	3e-19
<i>Phaeodactylum tricornutum</i>	XP_00217864	5e-76	0.016	2e-13	2e-18
<i>Symbodinium microadriaticum</i>	OLP87372	9e-70	N/A	4e-11	5e-15
<i>Thalassiosira pseudonana</i> (1335)	XP_002292080	8e-81	N/A	1e-12	6e-17
<i>Emiliana huxleyi</i> (1516)	EOD35102	1e-110	N/A	1e-13	7e-15
<i>Emiliana huxleyi</i> (1516)	EOD39239	3e-11	4e-9	8e-131	4e-46
<i>Karlodinium veneficum</i>	ARG42302	2e-12	1e-4	1e-106	3e-38
<i>Karlodinium veneficum</i>	ARG42303	5e-19	0.005	6e-41	5e-179

KbLT and *KbHT* cultures were diluted to 2×10^6 cells/L and mRNA was extracted on days 8, 14, 16, 18 and 21 post dilution. The expression levels were compared using quantitative reverse-transcription polymerase chain reaction (q-RT-PCR), using primer sets shown in Table 3.1 with RuBisCO as a housekeeping gene control (Yoon et al., 2002). Figure 3.1A shows the average relative expression as cycle threshold normalized to total RNA. Differences in RNA quality were accounted for using RIN-based correction of relative expression (Ho-Pun-Cheung et al., 2009). The only significant differences in average expression were observed for the weakest expressed homologue, *DDE3* ($\rho = 0.011$).

Table 3.2. Primer sequences used to amplify each of the four *K. brevis* DDE homologues

DDE# (Loci)	Forward Primer 5'-3'	Reverse Sequence 5'-3'	Product Length (bp)
<i>RuBisCO</i> *	GCAGCCTTTTATGCGGTATCG	CACCAGCCATTCGCATCCATTT	341
<i>DDE1</i> (2514)	GGTGGTGCCTTCCTCTACAC	TGCAGACGTTGTTTCGTCAGT	124
<i>DDE2</i> (42818)	GGTGGTTGCTGGATGAGACA	GACCAGCCGACTCCTTGAAA	179
<i>DDE3</i> (34174)	GGAAGACGCAACTGAATCGC	ATTGTGGTCCGCTTAGGAGC	250
<i>DDE4</i> (9995)	GCAAAGCCTCAATGACGGTG	GCCATCATATGGCCCCTGTT	134

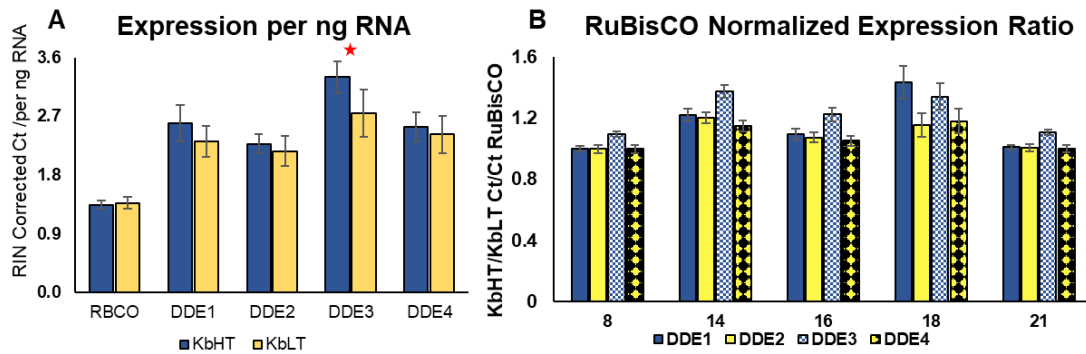


Figure 3.1 **A)** Average (n=5) RIN-corrected expression of each gene target and control normalized to total RNA ($\rho = 0.011$, *DDE3*). Error bars represent the standard deviation for biological replicates. **B)** *KbHT/KbLT* C_t ratios of the target gene/*RuBisCO*. Error bars represent the standard deviation for technical replicates for the ratios of C_t ratios (*KbHT/KbLT*) of each *DDE* on individual days and were calculated as propagation of error of multiple variables.

The C_t ratios of the four *DDE* homologues were calculated using *RuBisCO* as the normalizing gene. For both *KbHT* and *KbLT* the relative expression for the four *DDE* mRNA transcripts was $DDE2 > DDE3 > DDE4 > DDE1$. The results shown in Figure 3.1B represent the ratio of C_t ratios for *KbHT/KbLT* (C_{tHT}/C_{tLT}). As a lower C_t ratio indicates higher expression, a value for (C_{tHT}/C_{tLT}) of > 1 represents higher expression of the mRNA for *KbLT*. The mRNA expression for *DDE3* was higher in *KbLT* on all days that samples were taken. The ratio of C_t ratios ranged from 1.09 on days 8 and 21 to 1.37 on day 14. The mRNA expression for *DDE1*, 2 and 4 were higher in *KbLT* on three of the five days that samples were taken (days 14, 16 and 18). For these three homologues, the difference in *DDE* mRNA levels in *KbLT* and *KbHT* was not statistically significant on days 8 and 21. The largest difference in expression was observed for *DDE1* corresponding to Locus_2514 of the transcriptome library.

3.2.2 Comparison of thylakoid lipids in high and low toxic strains of *K. brevis*

Since the gene expression did not result in any obvious explanations for the differences observed in NPQ, a comparison of the thylakoid lipid profile between *KbHT* and *KbLT* was conducted. The MGDG, DGDG, SQDG and PG content for both strains were analyzed over a 25-day period with lipid extracts being prepared every fifth day. When expressed as nmol lipid/mg protein, total lipid content was 1.5-fold higher and MGDG and PG content were both 1.9-fold higher in *KbLT* than *KbHT* (Figure 3.2A). These differences were statistically significant. The small difference in DGDG when expressed as nmol lipid/mg protein was not significant (see Figure 3.2 legend). When expressed as a percentage of total lipid content, the trends hold for MGDG and PG, although the differences are smaller, with MGDG 1.3-fold higher and PG 1.28-fold higher in *KbLT* relative to *KbHT* (see Figure 3.2B). On the other hand, *KbHT* had 1.3-fold higher DGDG content than *KbLT*. SQDG could not be accurately quantified due to unreliable response factors. Nonetheless, it was found in 1.28-fold higher intensity when normalized to protein concentration in *KbHT* relative to *KbLT* (Figure 3.2C).

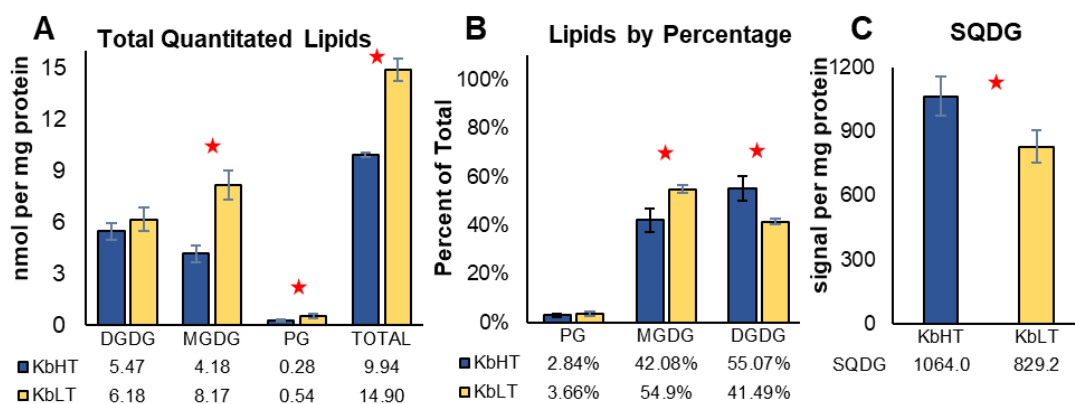


Figure 3.2 **A)** DGDG, MGDG, PG and total lipids (nmol/mg protein) in *KbHT* and *KbLT*. DGDG ($\rho = 0.138$), MGDG ($\rho = 1.7 \times 10^{-4}$), PG ($\rho = 0.012$), TOTAL ($\rho = 5.0 \times 10^{-4}$). **B)** Total lipid distribution for *KbLT* and *KbHT*. MGDG ($\rho = 2.7 \times 10^{-3}$), DGDG ($\rho = 1.9 \times 10^{-3}$). SQDG is not included in total lipids as it could not be accurately quantitated. **C)** SQDG in *KbHT* and *KbLT* ($\rho = 7.7 \times 10^{-3}$).

3.3 Materials and methods

3.3.1 General

Reagents and solvents were purchased from Fisher Scientific and used without further purification. Mass spectrometry of lipid samples was performed by Kansas State University Lipidomics Research Center using a 4000 QTRAP LC-MS/MS in positive ion mode. *KbHT* and *KbLT* cultures were grown under identical conditions as previously described above in section 2.3.2 (Chen et al., 2018).

3.3.2 q-RT-PCR of DDE in *KbHT* and *KbLT*

3.3.2.1 RNA extraction

RNA extraction was performed as described previously (Sun et al., 2016) with some modifications. Briefly, *K. brevis* culture (100 mL) was harvested by centrifugation (1000 g @ 4 °C for 10 min) in two 50 mL conical tubes, and the supernatant discarded.

The pellet was resuspended in diethyl pyrocarbonate (DEPC) treated water, the suspension was subjected to four freeze/thaw cycles by freezing in liquid nitrogen and thawing in a 25 °C water bath and vortexing. After the last freeze, 600 µL of cold denaturing solution (5 M guanidinium thiocyanate, 50 mM Tris pH 8, 25 mM sodium citrate, 0.5% w/v Sarkosyl, 2% PEG-8000, 0.1 M DTT) was added and the solution was vortexed until the pellet was resuspended and allowed to sit on ice for 10 min. The solution was separated into two tubes and 1/10 volume of 3M NaOAc (pH 5.2) was added and mixed briefly. An equal volume of acid-phenol-chloroform-isoamyl alcohol (125:24:1, pH 4.3) was added and the mixture was vortexed vigorously, and allowed to sit on ice for 5 min before centrifugation (17,000 g @ 4 °C for 15 min.) The aqueous (top) layer was carefully removed and an equal volume of chloroform:isoamyl alcohol (24:1) was added, vortexed and centrifuged (17,000 g @ 4 °C for 15 min.). The aqueous layer was removed, and 2.5 volumes of cold absolute ethanol was added. The solution was allowed to precipitate overnight at -20 °C.

3.3.2.2 RNA purification and analysis

The ethanol precipitated RNA was centrifuged (17,000 g @ 4 °C for 30 min) and washed with cold 70% ethanol. The pellet was then resuspended in warm (37 °C) DEPC-treated water and treated for DNA contamination using a *Turbo* DNA-free kit (Pierce Biotechnology) following the manufacturer's instructions for heavy contamination as a precaution. RNA concentrations were measured using Qubit 2.0 and samples were validated for RNA integrity using Bioanalyzer Pico (Figure S3.1) (Agilent Technologies). Samples were used for q-RT-PCR if RNA Integrity Numbers (RIN) were > 5.5 (Fleige et al., 2006).

3.3.2.3 q-RT-PCR of *K. brevis* DDE

Primers for DDE (Table 3.2) were developed using Primer3 software (Untergasser et al., 2012). The primer set for RuBisCO, which was used as a normalizing gene, was previously reported (Sun et al., 2016). Verso 1-Step RT-PCR SYBR Green master mix was employed for the analysis of genes of interest using manufacturer's instructions in a final volume of 20 μ L. Forward and reverse primer were present in the reaction at 80 nM (each) and each reaction contained 0.5 ng/ μ L RNA template. Nuclease free water was added instead of template for no template controls, and no RT controls were employed to ensure contaminating DNA was not amplified. q-RT-PCR was performed using an MJ Opticon under the following conditions: Reverse-transcription at 50 °C for 30 min, inactivation and denaturation at 95 °C for 15 min, followed by 40 cycles of denaturation at 95 °C for 15 s, annealing at 55 °C for 30 s, and extension at 72 °C for 30 s. Relative expression of DDE homologues was calculated as the average Ct value normalized to ng total RNA in each reaction (RIN corrected) or normalized to the Ct of RuBisCO. To confirm their identity, the PCR products were directly ligated into pGEM-T Easy (Promega) vectors, transformed into *E. coli* TOP10 (following the manufacturer's instructions), purified using QIAGEN miniprep kit and sent to Eurofins Genomics for sequencing using SP6 and T7 sequencing primers.

3.3.3 Lipid analysis of *KbHT* and *KbLT*

3.3.3.1 Lipid extraction and analysis

Lipid extraction was performed using a modified Bligh and Dyer method (Bligh & Dyer, 1959). *K. brevis* culture (100 mL) was harvested by centrifugation (1,000 g @ 4 °C

for 10 min) in two 50 mL conical tubes, and the supernatant discarded. Water (100 μ L) was added to the pellets and the suspension was transferred to a 1.5 mL microcentrifuge tube. Pellets were subsequently flash frozen in liquid nitrogen and, while thawing, grinded for 30 seconds using a hand-held plastic tissue homogenizer (Kontes). The process was repeated three times. Water was added to a final volume of 400 μ L and the homogenate was transferred to a 15 mL glass test tube with a Teflon lined screw cap.

To the homogenate, 0.5 mL chloroform and 1 mL methanol were added, and the mixture was vortexed briefly. An additional 0.5 mL chloroform and 0.5 mL methanol were added, vortexed and centrifuged (4,000 g @ 4 °C for 10 min). The lower chloroform layer was removed and set aside into a new glass test tube. Chloroform (0.5 mL) was added to the remaining methanol:water mixture, vortexed and centrifuged as described above; this process was repeated twice more. Finally, the combined chloroform fraction (2 mL) was washed once with 1M KCl (0.5 mL) and once with water (0.5 mL). The chloroform layer was added to a 2.0 mL glass vial with a Teflon lined screw cap and evaporated under nitrogen and stored at -80 °C until analysis.

Internal standards for PGs (phosphatidylglycerols) were PG (14:0/14:0) and diphytanoyl PG [which has formula of PG(20:0/20:0)]; for MGDG, MGDG(18:0/16:0) and MGDG(18:0/18:0); for DGDG, DGDG(18:0/16:0) and (18:0/18:0); and for SQDG (sulfoquinovosyl diacylglycerols), MGDG(18:0/16:0). When two internal standards were used, the internal standard intensity was determined from both peaks as a function of m/z. No additional response factor was used for PG, because the standards and biological analytes respond similarly. Unsaturated MGDG and DGDG values calculated in

comparison with the internal standard were divided by a response factor of 2.8, which corrects for the average mass spectral response of unsaturated glycolipids species in comparison to the response of the fully saturated standards. Because SQDGs were compared to an MGDG internal standard, which is a poor match, SQDGs could not be accurately quantified, and normalized signal is reported. This allows for sample-to-sample comparisons only.

PG, MGDG, and DGDG were analyzed by triple quadrupole (nominal mass) mass spectrometry, using neutral loss as described by Xiao et al. (2010; see the paper's supplemental data for complete methods description) (Xiao et al., 2010), and SQDG was analyzed with a scan for precursors of 225.0 in negative mode. In each precursor or neutral loss spectrum, the analytes were identified by the m/z of the precursor ion, so that analyte identifications were based on the presence of a characteristic fragment and the intact ion m/z . Annotations are consistent with potential molecular species, based on published fatty acid compositions of related dinoflagellate species, which contain highly polyunsaturated 18-, 20-, and 22-carbon species (Leblond, Evans, & Chapman, 2003; Leblond & Lasiter, 2009).

3.3.3.2 Protein extraction

To normalize lipid content, protein extractions were performed concurrently using the same culture. Briefly, *K. brevis* culture (50 mL) was harvested by centrifugation (1,000 g @ 4 °C for 10 min.) in a 50 mL conical tube, and the supernatant discarded. Lysis buffer, 500 μ L, (50 mM Tris, 1 mM EDTA, 0.1% Triton X-100 pH 8.0) was added to the pellet and vortexed. The mixture was stored on ice until analysis. Protein concentration was

measured in a 384 well microplate reader using 1:10 dilution of lysate and Bradford reagent against a standard curve of BSA. Lipid content was represented as nmol/mg protein or signal intensity/mg protein (in the case of SQDG for which internal standards do not provide accurate quantitation).

3.4 Conclusion

3.4.1 mRNA expression of DDE shows little variation between *KbLT* and *KbHT*

Four homologous *DDE* transcripts were identified by searching the transcriptome library (Ryan et al., 2014) of *K. brevis* using NCBI tBLASTn. Using q-RT-PCR the mRNA expression levels of *KbHT* and *KbLT DDE* were compared over 5 days. Expression levels were normalized to *RuBisCO* (Yoon et al., 2002) as well as RIN-corrected total RNA (Schroeder et al., 2006). The only significant difference found in average mRNA expression between *KbLT* and *KbHT* over a growth cycle was in *DDE3* (Figure 3.1A). When comparing each individual homologue on separate days it is apparent that fluctuations in expression occur over the growth cycle (Figure 3.1B). However, the slight differences in expression are not enough to explain the differences previously observed in qE and xanthophyll cycle activity (Cassell et al., 2015; Chen et al., 2018) especially since they seem to suggest a slightly higher expression in *KbLT*. The similarities in *DDE* mRNA were not surprising and are consistent with the currently accepted notion that dinoflagellate gene expression is governed by translational mechanisms (Jones, Williams, Bachvaroff, Place, & Jagus, 2015; Morey & Van Dolah, 2013; Roy, Jagus, & Morse, 2018; Roy & Morse, 2013), as differences in gene

expression are observed in the proteomes of dinoflagellates (Lee, Morse, & Lo, 2009; Liu, Lo, Matton, Lang, & Morse, 2012).

3.4.2 Thylakoid lipid content varies between *KbHT* and *KbLT*

One important aspect of xanthophyll de-epoxidase activity has been shown to be the presence of H_{II} structure forming lipids in the thylakoid membrane, specifically MGDG (Goss et al., 2007; Goss et al., 2005; Latowski et al., 2004). These lipids influence de-epoxidase activity in two ways: by stabilizing the LHC-II trimer upon light-induced aggregation, as well as by providing a matrix for xanthophylls to interact with their respective de-epoxidase (Goss & Latowski, 2020; Seiwert et al., 2017). By examining the lipidome of *KbHT* and *KbLT* with respect to the MGDG and DGDG content we observed significant differences not only in the total galactolipid content but also in the distribution of thylakoid lipids. When normalized to protein content and compared to *KbHT*, *KbLT* produced 50% more lipids (DGDG+MGDG+PG) and perhaps more importantly, it produced nearly twice the MGDG, which is critical to the proper functioning of the xanthophyll cycle. We may therefore conclude that the NPQ insufficiency of *KbLT* is not a result of insufficient MGDG.

The difference in DGDG between the two cultures was not statistically significant when quantified relative to protein content. When expressed as a percent of the total lipids, what *KbHT* is lacking in MGDG, is made up for in DGDG and SQDG, which have not been shown to be essential for qE. Also noteworthy is the observation that *K. brevis* allelopathy has been shown to weaken cell membrane integrity, alter lipid composition, reduce photosynthetic efficiency and result in increased indicators of

oxidative stress in its algal competitors (Poulin et al., 2018; Poulson-Ellestad et al., 2014; Prince et al., 2008). Alterations in lipid composition will influence cell membrane integrity, and photosynthetic efficiency is also highly dependent on the composition of thylakoid lipids. Exposure to *K. brevis* resulted in decreases in MGDG. Thus, like our results, brevetoxin is correlated with lower MGDG. However, several other lipid classes including, DGDG, SQDG and PG were also reduced in algal competitors upon exposure to *K. brevis*. As some *K. brevis* allelopathy studies revealed increases in lipid biosynthetic enzymes in competitors, these decreases in lipids were attributed to increases in lipid degradation rather than decreases in lipid biosynthesis. It is however, difficult to make comparisons as these allelopathy experiments were conducted with *K. brevis* cells rather than isolated PbTx-2.

Although the functioning of qE in *KbLT* is not efficient, it contains all the essential lipids to adapt to high light stress. Indeed, the MGDG content in *KbLT* was observed to be almost double that of *KbHT*, indicating that *KbLT* may be overcompensating for irregular qE by dedicating more energy to creating a solvation matrix for diadinoxanthin. The overall galactolipid content is also higher in *KbLT*. Notably, the proportion in which *KbLT* distributes its lipid profile is inversely proportional to *KbHT*, with 1.3-fold higher MGDG and 1.3-fold lower DGDG as a percentage of the total quantified lipid profile (Figure 3.2B). We may therefore conclude that *KbLT* has sufficient MGDG as well as *DDE* to perform qE.

Chapter 4. Redox proteomics characterization of the high and low toxic strains of *K. brevis* using fourplex IodoTMT labeling

Objective

Significant differences in the thiol content between the high and low toxic *K. brevis* indicate that the redox status of the two strains is significantly different. Due to the importance of disulfide bonds in maintaining the structure and function of proteins such as thioredoxins, kinases and xanthophyll de-epoxidases, the redox status of each strains' proteome has been characterized. This will provide important information of how thiol-disulfide dependent redox mechanisms related to light harvesting, toxin production and photo-protection may be influenced by toxin content in *K. brevis*. Specifically, in the role that various redox regulating enzymes in the thioredoxin family and their targets may be influenced by differences in the thiol redox proteome. Moreover, analysis of the relative expression of proteins such as polyketide synthases may provide useful insight on to the differences observed between the two strains' toxin production.

4.1.1 Thiol-disulfide exchange plays a key role in regulation of thylakoid proteins

Thiol-disulfide exchange is an effective post-translational modification that permits the rapid and reversible change of protein conformation and activity (Cejudo, Ojeda, Delgado-Requerey, González, & Pérez-Ruiz, 2019). Cysteine is significantly underrepresented in proteins in all life forms when compared to other amino acids. Cysteine content tends to increase with the complexity of organisms. Mammals have an average of 2.26% cysteine residues as a percentage of all amino acids, while archaea only contain 0.5% cysteine (Miseta & Csutora, 2000). This implies the possibility that as life

forms evolved, the use of cysteine to regulate the activity and structural properties of proteins became more prevalent. The observation that cysteine residues involved in thiol-disulfide exchange are highly conserved in redox sensitive proteins, such as plant Vde and dinoflagellate Dde (Figure 4.8), as well as the highly conserved CxxC motif found in various oxidoreductases and iron-sulfur proteins supports this hypothesis (Ammendola et al., 1992; Cejudo et al., 2019). Using quantitative redox proteomics, the expression and redox status of Dde, thiol-disulfide oxidoreductases and other redox dependent proteins such as kinases and MGDG synthase may be assessed between the two strains to better understand the deficiencies in NPQ experienced by *KbLT*.

4.1.1.1 Dde and MGDG synthase are disulfide regulated

The activity of Dde is regulated by several factors including luminal pH, redox state of cysteine residues and lipid composition. Vde/Dde contain thirteen conserved cysteine residues. Twelve of these residues form six disulfide bridges and the reduction of any one disulfide bridge inactivates Vde/Dde (Simionato et al., 2015). The specific binding of Vde/Dde to the MGDG rich domains of the thylakoid membrane has been proposed to be a result of the docking of the charged domain of the de-epoxidase on the polar head groups of the H_{II} lipid phase (Latowski et al., 2004; Latowski et al., 2002). The enzyme MGDG synthase is responsible for the transfer of the galactosyl moiety of UDP-Gal (Uridine diphosphate galactose) to *sn*-1,2-diacylglycerol (DAG) to produce MGDG. Like Vde/Dde, MGDG synthase activity is regulated by the TrxR/Trx system. Unlike Vde/Dde, MGDG synthase activity is enhanced by the reduction of disulfide

bonds (Geigenberger & Fernie, 2014; Nakamura, Shimojima, Ohta, & Shimojima, 2010; Yamaro, Motohashi, Takamiya, Hisabori, & Ohta, 2006).

4.1.1.2 Thioredoxins, glutaredoxins, and peroxiredoxins; important redox active proteins needed for ROS detoxification and regulation of enzyme activity.

The efficient conversion of light energy into chemical energy in chloroplasts depends on tightly regulated mechanisms that permit rapid adaptation to fluctuating light conditions. Thiol-disulfide exchange plays a critical role in this process, allowing regulation of proteins related to light harvesting and downstream biosynthetic processes. The redox regulation of proteins containing thiol-disulfide bridges is reliant on thiol oxidoreductases such as thioredoxin (Trx) and glutaredoxin (Meyer, Belin, Delorme-Hinoux, Reichheld, & Riondet, 2012). Trx and Grx share an important structural aspect, the CxxC/S redox active site, which is conserved throughout most organisms. Although various “Trx-like” and “Grx-like” proteins with atypical redox sites exist, these are not as well characterized in structure, or biochemical function (Meyer et al., 2012; Rouhier et al., 2005).

Originally, plastidic redox regulation was thought to be exclusive to the ferredoxin-FTR-Trx system in the chloroplast and it was believed that NTRs were exclusive to heterotrophic organisms. This provided a clear distinction on the source of reducing power for thioredoxin dependent redox regulation. The discovery of a plastid localized NTR containing a C-terminal Trx domain (NTRC) changed our understand of redox regulation in photosynthetic organisms (Serrato et al., 2004). It has been shown that NTRC is responsible for regulation of 2-cys-peroxiredoxin activity (2CPrx), an

effective peroxide scavenger in the chloroplast, giving rise to the hypothesis that NTRC primarily function as an antioxidant. However, several important proteins related to chlorophyll biosynthesis seem to be regulated by this oxidoreductase (Richter et al., 2013; Stenbaek et al., 2008).

Grxs are enzymes with both disulfide reductase and deglutathionylation activity that are involved in redox regulation of various target proteins (Meyer et al., 2012). The Grx system is dependent on the cascade of electrons from NADPH to glutathione disulfide (GSSG) to form reduced glutathione (GSH) via the enzyme glutathione reductase (GR). GSH can then reduce the active site of Grx which allows it to reduce/deglutathionylate its target protein (Rouhier et al., 2005).

4.1.1.3 Kinases and phosphatases

Acclimation to varying light conditions in photosynthetic organisms depends strongly on the communication between photosystem I (PS-I) and PS-II, via cytochrome-*b₆f*. One of the most crucial interactions between the two photosystems is the uncoupling of the LHC-II from PS-II which is induced by the prolonged exposure to red and far-red radiation that is preferentially absorbed by PS-II, relative to PS-I. Under conditions of prolonged PS-II excitation the plastoquinone pool resides in a more reduced state. The binding of plastoquinol (PQH₂) to the Q₀ site of cytochrome-*b₆f* leads to the activation of a protein kinase (*C. reinhardtii* Stt7) which reversibly phosphorylates LHC-II. Phosphorylated-LHC-II (P-LHC-II) uncouples from PS-II and associates itself with PS-I leading to an increase in the antenna size of PS-I, which equilibrates the light absorption between the two photosystems, in a process called state transition (Rochaix, 2007;

Rochaix et al., 2012). The exact opposite of the above process occurs under prolonged excitation of PS-I, which leads to an oxidized quinone pool and inactivation of Stt7, eventually dephosphorylation by a specific P-LHC-II phosphatase (TAP38) causes LHC-II to reassociate itself with PS-II (revert back to State 1) (Lemeille & Rochaix, 2010).

Stt7 is a unique protein in that it contains a transmembrane domain that separates its lumen localized N-terminus from the catalytic kinase domain found in the stroma. It was found that the catalytic kinase is almost always bound to cyt-*b₆f*, and can be found to be associated with LHC-II and PS-I, but not PS-II (Lemeille et al., 2009). The N-terminal side contains two conserved cysteine residues which are the only conserved cysteines in the plant orthologue STN7 (Depège, Bellafiore, & Rochaix, 2003). Site directed mutagenesis of either cysteine completely muted any kinase activity, highlighting their importance (Lemeille et al., 2009). Furthermore, preliminary evidence indicates that the two cysteines form either an intermolecular disulfide, or an intramolecular disulfide leading to dimer formation. It had been stipulated that trans-thylakoid thiol reducing proteins such as high chlorophyll protein 164 (HCF164), and cytochrome c-type biogenesis protein (CcdA) are capable of regulating Stt7/STN7 (Kang & Wang, 2016; Rochaix, 2013). However, it was not until recently that studies showing that a lumen-thiol oxidoreductase (LTO1), a thioredoxin domain containing protein, is co-expressed with plant STN7 and can oxidize the conserved lumen cysteine residues in vitro. Additionally, the loss of LTO1 decreases kinase activity of *A. thaliana* STN7 (Wu et al., 2021).

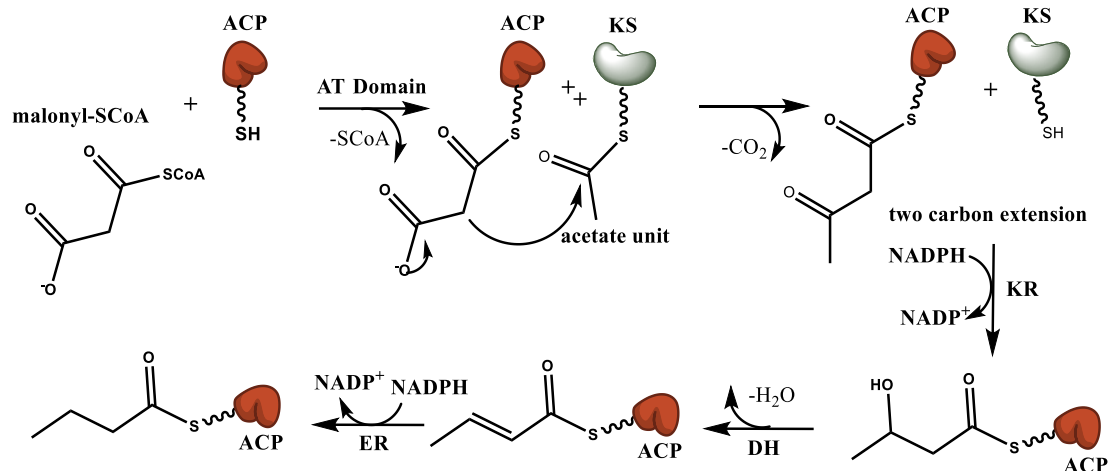
Phosphatases can also be dependent on the thiol oxidoreductases for activity. Two examples are FBPase and sedoheptulose-1,7-bisphosphatase (SBPase), proteins which function in similar aspects of the Calvin-Benson cycle, however acting on different substrates. FBPase and SBPase are similar in topology however their sequences differ significantly, and the positions of their redox active cysteine residues are in different sections of the protein (Gütle et al., 2016). Both proteins rely on reducing equivalents generated from photo-reduced ferredoxin to be relayed to them by the FTR system to activate (reduce) their disulfide bridge (Buchanan, Kalberer, & Arnon, 1967; Schürmann & Buchanan, 1975). However, it has been shown *in vivo* that FBPase activity in *A. thaliana* double mutants, having both *Trx-f* and *ntrc* deficiency, was 7% of WT. Whereas the *Trx-f* and *ntrc* single mutants had 40% and 80% activity, respectively. Demonstrating the cooperativity of NTRC and *Trx-f* to activate FBPase and respond to varying light conditions (Thormählen et al., 2015).

4.1.2 Polyketide synthases

The availability of high and low toxin producing strains of *K. brevis* could facilitate studies on the biosynthesis of the brevetoxins by revealing differentially expressed proteins that may be related to toxin biosynthesis. While not the original intent when this study was undertaken, we may have identified promising leads for such biosynthetic pathways. Stable isotope incorporation experiments, utilizing single-labeled [1-¹³C] and [2-¹³C] and double-labeled [1, 2-¹³C] sodium acetate, conducted independently by two groups in the 1980s established the biogenic origin of the brevetoxins (Chou & Shimizu, 1987; Lee, Qin, Nakanishi, & Zagorski, 1989; Lee,

Repeta, Nakanishi, & Zagorski, 1986). Although some anomalies in incorporation patterns were observed (Van Wagoner, Satake, & Wright, 2014), the overall head-to-tail arrangement of acetate units confirmed a polyketide biosynthetic pathway. Similar deviations from the incorporation patterns typical of polyketides, specifically deletions of C-1 of acetate from the parent carbon chain, have been observed in other dinoflagellate derived polyketides (Van Wagoner et al., 2014).

Polyketides are constructed by polyketide synthases (PKSs) which share a common evolutionary history with fatty acid synthases (FASs). Essential catalytic domains of FASs are the ketosynthase (KS) which catalyzes the decarboxylative condensation of malonyl-CoA with an acyl unit, extending the growing chain by two carbons with each cycle and yielding a β -keto ester, the ketoreductase (KR), the dehydratase (DH) and the enoyl reductase (ER), which respectively yield a β -hydroxy ester, an α,β -unsaturated ester and finally a fully saturated subunit. Other functional domains include the acyl transferase (AT) which selects the incoming subunit (malonyl-CoA in the case of FASs), the acyl carrier protein (ACP) which carries the growing chain as a thioester, and the thioesterase (TE) domain which hydrolyses the finished product from the ACP. Polyketides are constructed in a similar fashion, but with structural diversity resulting from the incorporation of a wider variety of subunits (selected by the AT domain) and by the omission of one or more of the KR, ER or DH steps leaving keto, alcohol or alkene functionality at specific locations along the growing chain as well as post condensation modifications (Scheme 4.1).



Scheme 4.1 Fatty acid synthase mechanism: Malonyl-CoA starter unit is selected by the AT domain, and shuttled by the ACP. An additional acetate unit is added in a decarboxylative condensation yielding a four carbon β -keto ester. NADPH provides the reducing equivalents which facilitates the reduction at the KR domain. The DH domain creates an α,β -unsaturated ester, and finally the ER domain reduces the alkene to yield the saturated fatty acid with help from NADPH. Polyketide synthases have similar mechanisms, with the exception of selected domains not being present on the protein, this leaves varying degrees of unsaturation and oxidation on the carbon chain which can later facilitate post condensation modifications. PKSs are also able to utilize different subunits, allowing for the carbon extensions of different lengths. Not shown is the TE domain, which will cleave the full-length fatty acid or polyketide from the ACP and leave the finished product as a carboxylate.

4.1.3 Redox proteomics

Due to the importance of thiol-disulfide exchange reactions and their prevalence in oxidative stress mitigation, there has been an ever increasing need to characterize their interactions and biochemical activity. Various methods of analyzing the redox status of cysteine residues in proteins have been developed over the years. These methods take advantage of the fact that thiols are good nucleophiles that can form covalent linkages with electrophiles via nucleophilic substitutions (S_N2). One of the most used reagents are isotope-coded affinity tags (ICAT, see Figure 4.1), these reagents use heavy and light isotope labels linked to a biotin affinity tag to quantitatively differentiate labeling

efficiency using affinity chromatography and mass spectrometry (Gygi et al., 1999). For example, reagents containing fluorescent linkers can be used to probe the redox status of specific proteins using western blotting (Yang, Carroll, & Liebler, 2016).

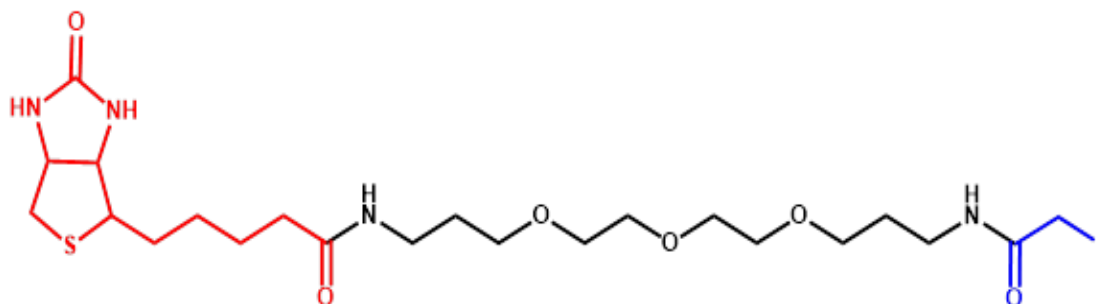


Figure 4.1 ICAT reagent depicting the three different functionalities of the molecule. In red, the biotin linker which allows for affinity purification and is cleavable. In black, the isotope coded linker (which contains either 9x ^{12}C or ^{13}C) and in blue the cysteine reactive group.

One of the newer developments in redox profiling are the tandem mass tag (TMT) reagents developed by Thompson and colleagues which improve on the sensitivity and scope of traditional ICAT reagents (Thompson et al., 2003). These reagents contain 3 separate functionalities that work to effectively label and quantitate peptides *in vitro* (Figure 4.3). First and foremost is the cysteine reactive moiety, in the case of the IodoTMT reagents this is an iodoacetamide group. Next, is a tandem mass tag fragment, which is isotopically labeled in conjunction with the final part of the molecule, the linker arm. Both the TMT fragment and the linker arm are labeled by either ^{15}N or ^{13}C (see Figure 4.3A). By adjusting the mass of the linker arm, or the TMT fragment the overall mass of the label stays the same, but the reporter ion shifts accordingly. This allows the same labeled peptide under different conditions (containing different TMT tags) to coelute, a function that is lacking in the traditional ICAT reagents. The MS signal for

each peptide pair, or multiplex is then contained within the same peak, thus improving sensitivity. Furthermore, the quantitation of each TMT fragment resulting from the collision induced dissociation (CID) of different labeled peptides happens entirely in the MS/MS mode, improving the signal-to-noise ratio, and allowing for non-labeled species to be ignored (Thompson et al., 2003). The TMT reagents, like ICAT can be purified on an affinity resin to enrich each sample to avoid competitive ionization from non-labeled peptides.

4.1.4 Multiplex labeling using IodoTMT

One of the benefits of the IodoTMT reagents is the fact that seven different isotopically labeled IodoTMT reagents are available. This allows for several experiments/treatments to be analyzed concurrently, unlike ICAT which only permits the analysis of at most two samples having either the heavy or light labels. To effectively characterize the redox status of *K. brevis*' proteome a unique method of labeling was

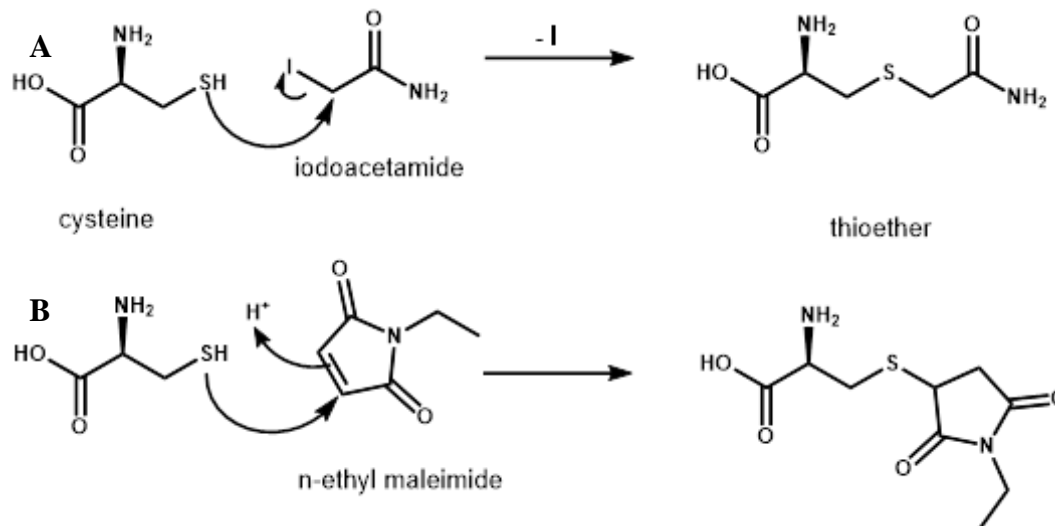


Figure 4.2 Mechanism of cysteine reactive reagents used in proteomics. **A)** nucleophilic substitution of cysteine with iodoacetamide. **B)** Michael reaction (addition) to NEM. Both reactions yield irreversible thioether bonds which effectively block any further modification of cysteine.

used. Most cysteine labeling methods require iodoacetamide (IAM) or N-ethylmaleimide (NEM) to block reduced cysteine thiols followed by reduction of oxidized cysteines with DTT or TCEP and labeling with the cysteine reactive reagent (Figure 4.2). This allows proteomes under different conditions to be compared for their oxidized cysteine content by comparing the abundance of the label contained within each respective sample.

Our unique labeling strategy ultimately provides sequence information for proteins containing initially reduced cysteine residues as a proportion of total cysteine content. Prior to reduction with DTT or TCEP, proteins are labeled with a TMT reagent. By then using a TMT label with a different isotope distribution across the reporter and equalizer, after reduction, the ratio of reduced to oxidized ($TMT_{\text{light}}/TMT_{\text{total}}$) cysteines can be obtained (Figure 4.3). The benefit of using IodoTMT to perform a preliminary labeling of reduced cysteine residues is the ability to identify residues which may be lost

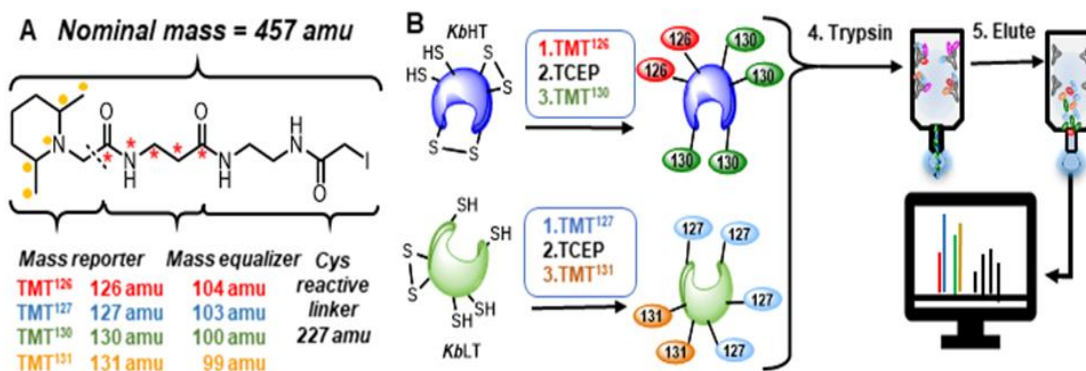


Figure 4.3 A) Isobaric iodoTMT cysteine labeling reagent. The mass of the reporter is balanced by the mass equalizer such that each label has the same nominal mass. Locations of labels are shown for TMT¹³¹ (●) and TMT¹²⁶ (*). B) Redox proteomics workflow. 1. Cysteine residues were labeled with the light label. (iodoTMT¹²⁶ and iodoTMT¹²⁷ for *KbhT* and *KblT* respectively). 2. Unlabeled cysteine residues were reduced with TCEP. 3. Heavy tags (iodoTMT¹³⁰ and iodoTMT¹³¹ for *KbhT* and *KblT*, respectively) were used to label newly reduced cysteine residues. 4. Equal amounts of labeled proteins (according to Bradford assay) were combined, trypsinized and purified using Immobilized anti-TMT resin (dark triangles represent unlabeled peptides which will not bind to the resin). 5. Purified, labeled peptides were eluted from the resin and analyzed via LC-MS/MS.

during the label enrichment step. Following traditional labeling methods with IAM or NEM, a portion of peptides, after proteolytic digestion, may not be captured by the antiTMT affinity resin. This may result in a loss of identifiable proteins limiting the scope of data analysis.

4.2 Results and Discussion

4.2.1 Simultaneous duplex IodoTMT labeling of the *K. brevis* proteome reveals that *KbLT* contains significantly more reduced cysteine residues than *KbHT*

The redox status of protein extracts was frozen by precipitation with TCA. Isolated protein was quantitated for thiol content using DTNB against cysteine standards prior to the first TMT labeling reaction. In each of the replicates, *KbHT* consistently had lower thiol concentration in the protein extract, averaging 0.61-fold lower (Figure 4.4). This difference is statistically significant ($p = 0.026$, two-tailed, paired t-test).

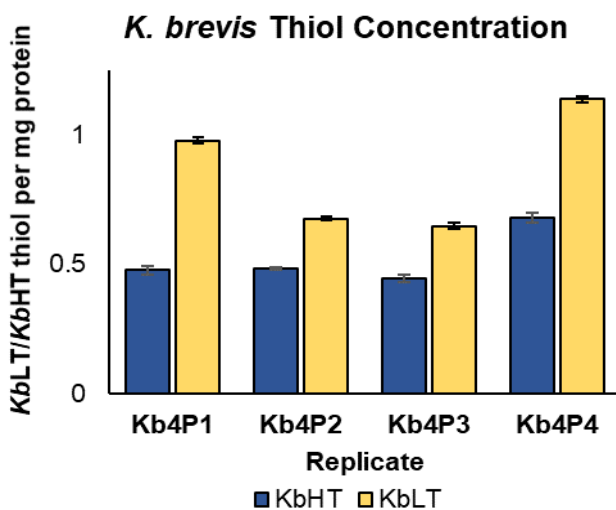


Figure 4.4 The thiol concentration of isolated proteins before labeling for each replicate. Error bars represent standard deviation of technical replicates (n=3).

The protein database of *K. brevis* was generated using EMBOSS Transeq (Madeira et al., 2019). The six-frame translation of the Wilson strain transcriptome library (Ryan et al., 2014) with stop codons removed was used as the database for peptide searches in MS analysis. Since IodoTMT labels allow for the irreversible alkylation of cysteine residues in proteins, by alkylating cysteine residues before and after reduction with TCEP and using labels containing two different reporter ions, it is possible to compare the redox status of *KbHT* and *KbLT*'s proteome simultaneously to the relative expression of each protein. By taking the amount of light label (added before reduction) and dividing it by the total incorporated (light + heavy) label, the redox status of the proteome can be assessed. *KbLT* was consistently alkylated to a greater extent before the reduction with TCEP than *KbHT* with an average redox state (incorporation of light/light+heavy labels) of 0.321 ± 0.098 (Table 4.1). *KbHT* had a lower ratio of light/total in every sample with an average of a 0.80-fold lower reduced state ($\rho = 0.025$, two-tailed paired t-test) which is consistent with the higher ratio of reduced cysteine content for *KbLT* as determined using DTNB (Figure 4.4). When looking only at proteins which appeared in at least 3 of the biological replicates we obtain 1092 (42.9%) total proteins. Of those 1092, 411 (37.6% of those with $N \geq 3$) proteins contained a significant difference in redox status between *KbHT* and *KbLT*, while 254 (23.2% of those with $N \geq 3$) proteins had significant differences in expression between the two strains based on the ρ values of their respective permutation tests (Table 4.2).

Table 4.1 The global redox status of the proteomes of *KbHT* and *KbLT*, and the ratio of redox status for the four biological replicates (ρ shown is for paired t-test).

Replicate	Light/ Light+Heavy*	
	<i>KbHT</i>	<i>KbLT</i>
<i>Kb4P1</i>	0.344	0.450
<i>Kb4P2</i>	0.273	0.319
<i>Kb4P3</i>	0.174	0.213
<i>Kb4P4</i>	0.243	0.303
Avg \pm St.Dev.	0.258 \pm 0.071	0.321 \pm 0.098
HT/LT	0.80 \pm 0.33 ($\rho= 0.025$)	

4.2.2 Cellular organelle localization of proteins

4.2.2.1 DeepLoc

In total, 2542 separate translated mRNA sequences were identified between the four replicates. Using the algorithm DeepLoc (Almagro Armenteros, S nderby, S nderby, Nielsen, & Winther, 2017) the cellular localization of each protein was predicted. The distribution of cellular localization is summarized in Table 4.2 The most predicted organelle was the nucleus (618 proteins), while the Golgi apparatus (22 proteins) was scarcely projected. DeepLoc is also capable of predicting whether a protein is soluble or membrane bound, based on the hydrophobicity of its amino acids, in total 675 proteins (26.5%) of proteins were predicted to be membrane bound.

Table 4.2 Localization predictions of all proteins identified by fourplex IodoTMT

Localization	All	$N \geq 3$	$N \geq 3$, Redox $\rho \leq 0.05$	$N \geq 3$, Expression $\rho \leq 0.05$	$N \geq 3, \rho \leq 0.05$ Rdx+Exp
Total	2542	1092	411	254	103
Nucleus	618	266	103	55	23
Cytoplasm	500	216	79	55	20
Mitochondrion	459	187	60	41	15
Plastid	369	168	67	40	15
Extracellular	285	128	58	33	18
Cell membrane	110	45	16	12	6
Peroxisome	69	28	8	5	-
Endo. retic.	65	26	9	7	4
Lysosome/vacuole	45	20	9	5	2
Golgi apparatus	22	8	2	1	-

The distribution of each localization was consistent between the global proteome and the three criteria mentioned above ($N \geq 3$, redox $\rho \leq 0.05$, expression $\rho \leq 0.05$).

Figure 4.5 shows pie charts of each of the criteria mentioned above ($N \geq 3$, with ρ value for permutation tests ≤ 0.05 for both expression and redox.) and the global proteome representing the percentage of each localization for all proteins as well as those proteins which meet all criteria.

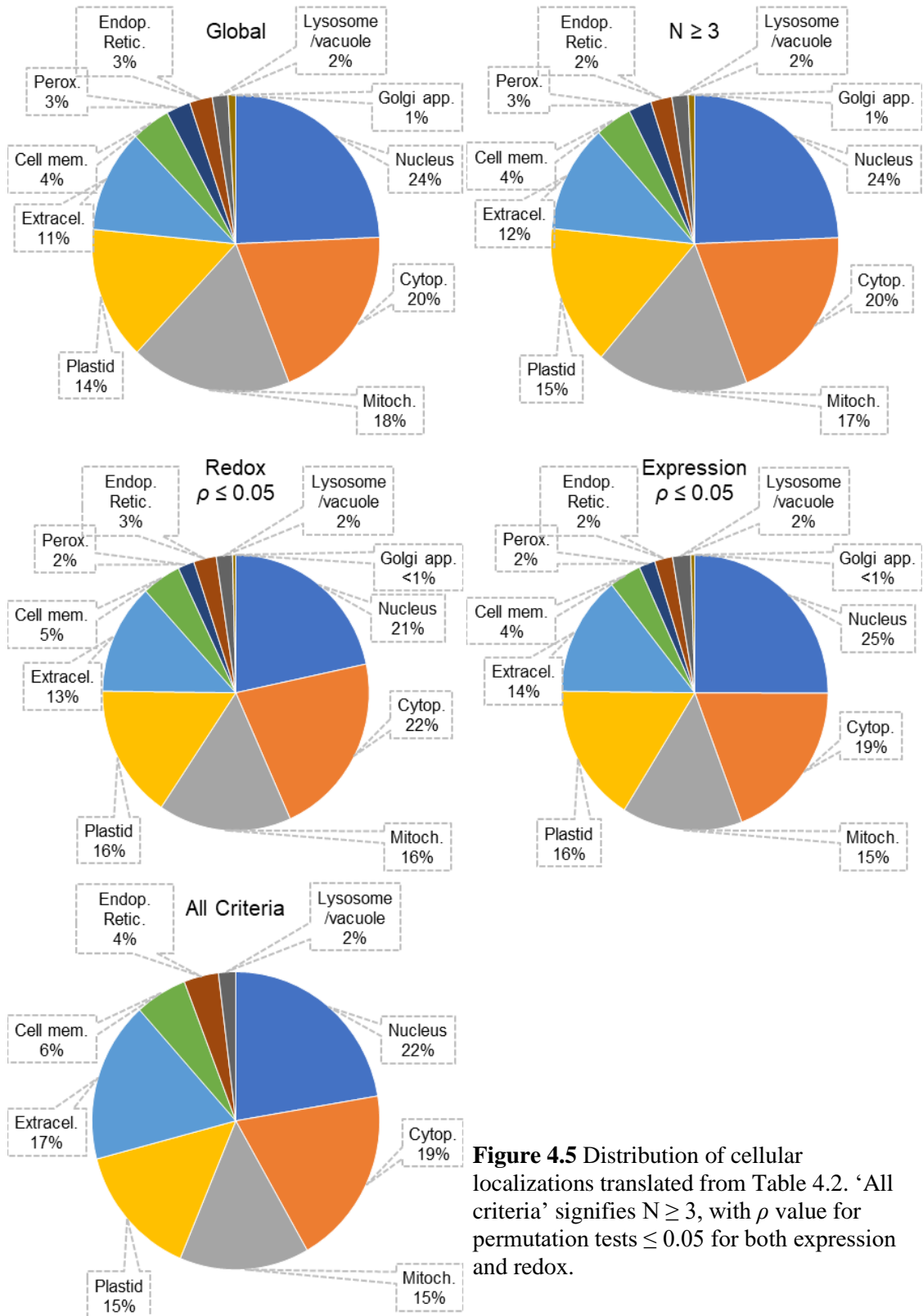


Figure 4.5 Distribution of cellular localizations translated from Table 4.2. ‘All criteria’ signifies $N \geq 3$, with ρ value for permutation tests ≤ 0.05 for both expression and redox.

4.2.2.2 ChloroP, TargetP, and SignalP; protein prediction tools

In order to analyze whether any organelle may be more affected by differences in expression status, several bioinformatics tools focused on prediction of N-terminal presequences were utilized to better characterize our identified proteins. ChloroP is an algorithm which predicts the presence of N-terminal chloroplast transit peptides (cTP) (Emanuelsson, Nielsen, & Heijne, 1999). TargetP is a similar service which predicts the presence of cTP, mitochondrial transit peptide (mTP), as well as signal peptides (SP) and thylakoid lumen transit peptides (luTP). TargetP when used for the analysis for non-plant organisms, which omits the prediction of luTPs and cTPs (Jose Juan Almagro Armenteros et al., 2019). SignalP predicts the presence of signal peptides and their cleavage sites (José Juan Almagro Armenteros et al., 2019). Table 4.3 shows the results of the four prediction tools. The redox trends for individual organelles are consistent with the global redox trends, except for proteins predicted to contain luTPs which are more reduced in *KbHT* than average when comparing to the entire global proteome within *KbHT*. However, it is still more oxidized in *KbHT* than *KbLT*

Table 4.3 Summary of predicted N-terminal presequences by ChloroP, TargetP (plant and non-plant), and SignalP.

Prediction Tool	Chloro P	TargetP Non-Plant		TargetP Plant				SignalP Euky.
	cTP	mTP	SP	cTP	mTP	SP	luTP	SP
No. of proteins	622	193	379	145	186	317	27	191
Avg Redox Ratio H/L	0.788	0.807	0.764	0.810	0.799	0.749	0.884	0.751
Avg Exp Ratio H/L	1.15	1.17	1.15	1.21	1.11	1.12	1.09	1.11

4.2.3 Functional Annotation

Functional annotation was performed using NCBI BLASTp against the non-redundant protein database using TMT-labeled protein hits with taxonomy filters including SAR supergroup and cyanobacteria (TaxID: 2698737 and 1117, respectively) (Altschul et al., 1990). Pfam, NCBI Conserved Domain Database (CDD), and BLASTKoala algorithms were also utilized for functional annotations (Kanehisa, Sato, & Morishima, 2016; Lu et al., 2020; Marchler-Bauer & Bryant, 2004; Marchler-Bauer et al., 2011; Mistry et al., 2020). Of the 2542 total proteins 2088 proteins were able to be annotated by NCBI BLASTp with confidence ($<E^{-9}$). Pfam was able to provide 1576 proteins with significant hits (bit score > 25), while NCBI CDD provided 1916 proteins with putative matches (bit score > 30). The most ineffective by far was BLASTKoala with only 800 proteins providing KEGG pathway annotations with any score >1 . In total 704 proteins were putatively identified by all 4 functional annotation algorithms. If BLASTKoala was not included in this calculation 1448 proteins could be annotated by the remaining three algorithms. Nearly all proteins annotated by Pfam were also annotated by BLASTp and CDD, with only 74 and 77 proteins missing annotations, respectively. BLASTKoala was only able to uniquely identify 5 proteins (Figure 4.6).

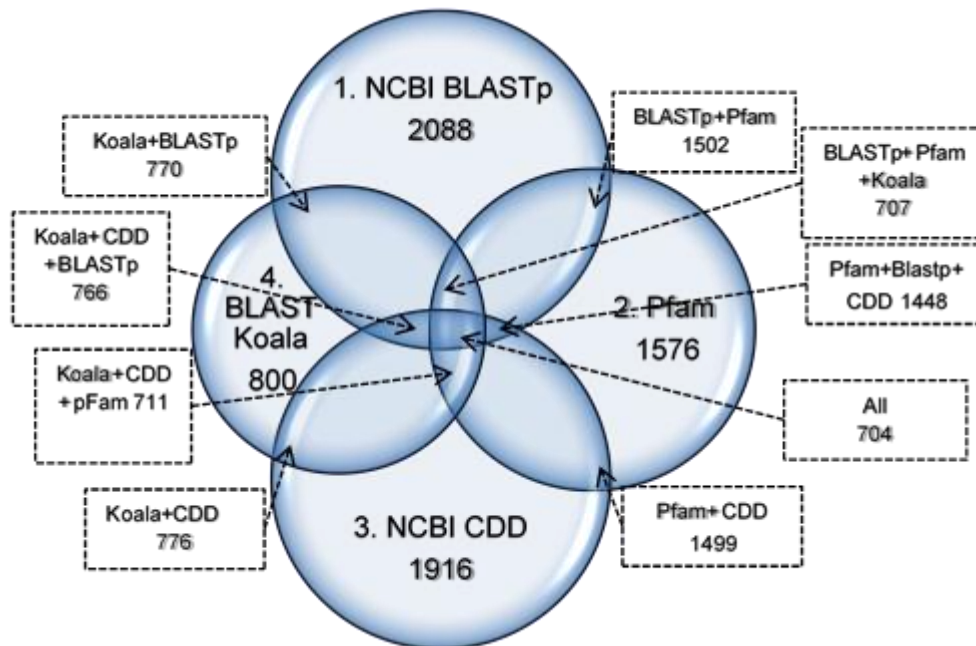


Figure 4.6 Totals of functional annotation by algorithm

4.2.4 Differences in redox state are consistent across cellular organelles.

As shown above in Figure 4.6, the distribution of cellular localizations was consistent between the global proteome when compared to proteins that appeared in multiple replicates, as well as those with significant differences in the redox ratio and expression ratio. By analyzing the distribution of average redox ratios of the global proteome and every organelle as predicted by DeepLoc, it was found that average redox ratio between the two strains was consistent across cellular organelles (Figure 4.7). The average redox ratio ($KbHT/KbLT$) for the global proteome was 0.797 ($\log_2 = -0.33$), while all organelles, except for the lysosome (0.73), endoplasmic reticulum+golgi apparatus (0.74), extracellular (0.76), and peroxisome (0.86), had values between 0.79-0.81. When examining proteins that have 2-fold greater, or 0.5-fold fewer reduced

cysteines in *KbHT* (those which are plotted in the overflow, and underflow bins, respectively) there are consistently more proteins in each organelle that are 0.5-fold as reduced (corresponding to the underflow bin). The redox ratios clearly demonstrate that *KbLT* has more reduced protein content across all cellular organelles and that no organelle is selectively affected.

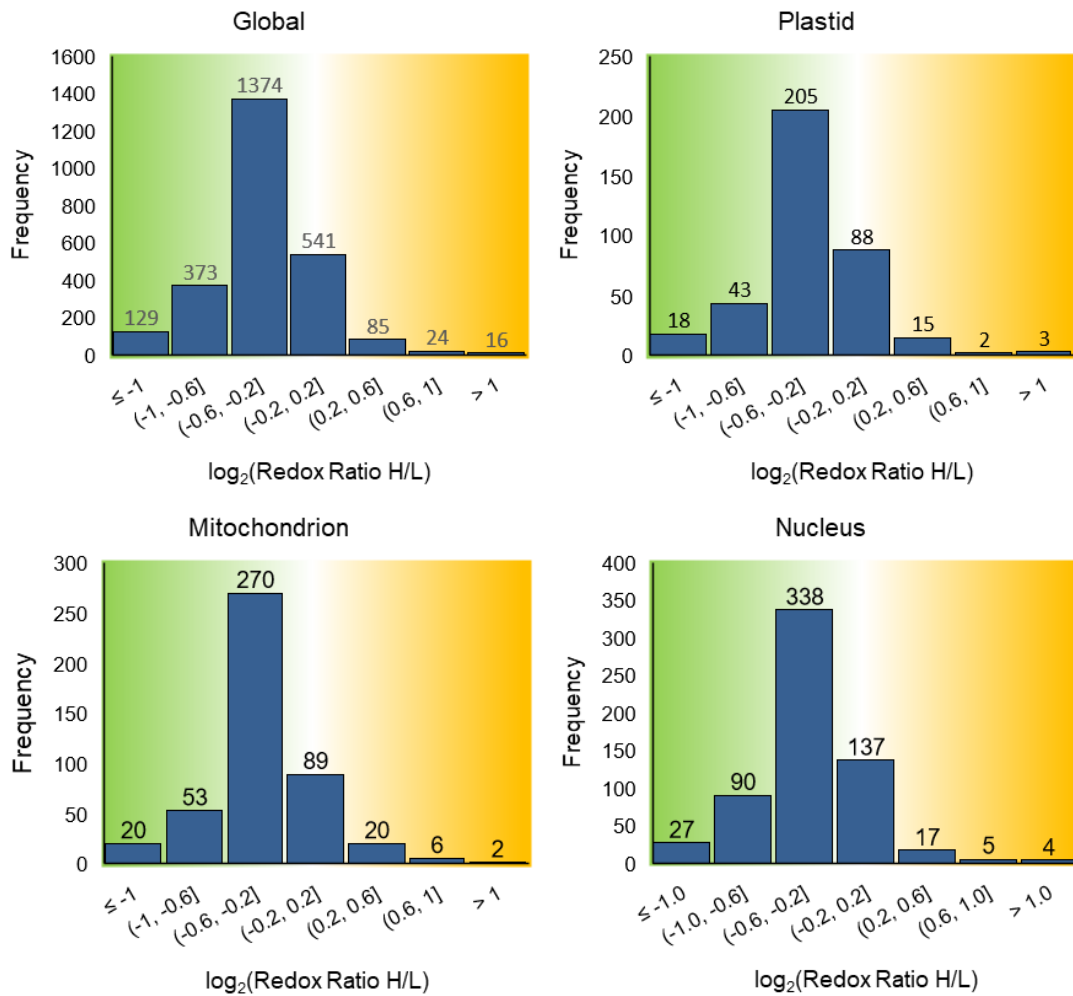


Figure 4.7A Distribution of redox status for the global proteome, plastid, mitochondrion and nucleus represented as $\log_2(\text{Redox Ratio H/L})$.

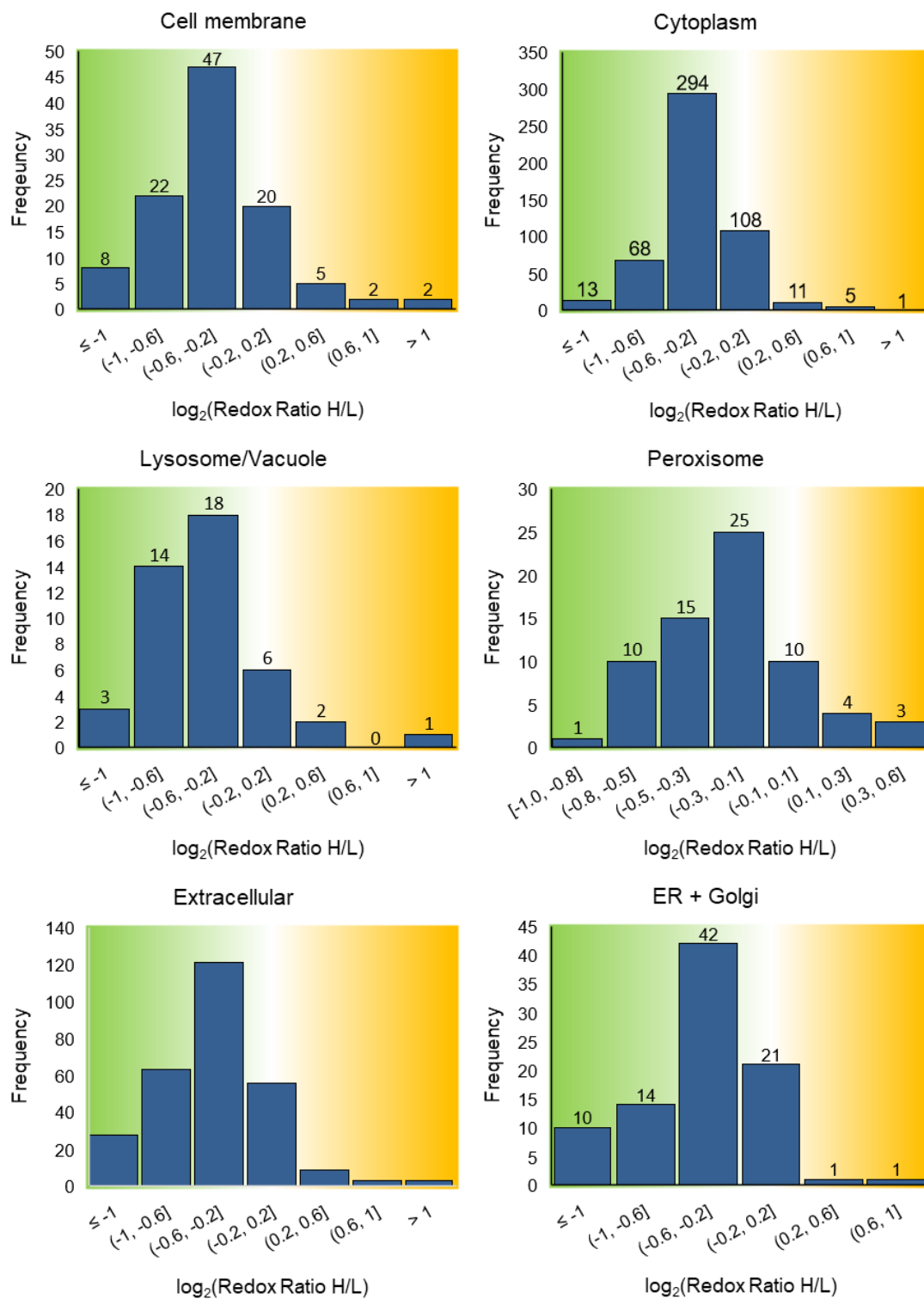


Figure 4.7B Distribution of redox status for the cell membrane, cytoplasm, lysosome/vacuole, peroxisome, extracellular, and endoplasmic reticulum + golgi apparatus represented as $\log_2(\text{Redox Ratio H/L})$.

4.2.5 The significance of expression differences between *KbHT* and *KbLT*

Expression values for each protein were calculated by dividing the number of total IodoTMT label incorporated (light + heavy) for that protein and dividing by the abundance of all labels detected for each replicate. This provides a measure of the amount of label incorporated into each protein as they relate to all proteins detected. By taking the ratio of protein expression for each protein, the fold-change in expression between the two strains can be analyzed. Furthermore, by utilizing the ρ -value of the permutation test for each protein, or t-test for larger number of replicates, and plotting against the fold-change (expression ratio) the differences in protein expression between the two strains and how significant these differences are can be assessed. To demonstrate this data in a more palatable manner, the $-\log_{10}(\rho)$ is plotted against the $\log_2(\text{Expression Ratio})$ to generate a volcano plot (Figure 4.8). In this interpretation, the expression data is centered around 0 on the x-axis and can be understood more intuitively. Additionally, since expression ratio is being plotted as a function of \log_2 , it is easy to capture large fold-changes in expression on the x-axis. By plotting the ρ -value on the y-axis as a function of $-\log_{10}$, the most similar proteins will cluster around the base of the graph near the origin, while the further a value is from the x-axis the more significant the difference becomes (smaller ρ -values) (Bailey, 2019).

A volcano plot was generated from the 1092 proteins of our proteomics data set which appeared in 3 or more biological replicates (Figure 4.8). The average expression ratio (*KbHT/KbLT*) was 1.14 ($\log_2 = 0.19$), meaning slight overexpression in the high toxic strain. Since ρ -values from the permutation test can result in a value of 0, which

would give illogical answers when calculating $-\log_{10}(0)$, the value of this calculation was substituted by 4, which represent a ρ -value = 0.0001.

When analyzing differentially expressed proteins, there were 254 individual peptides with expression ρ -value < 0.05 for their permutation tests. Of these proteins, 40 (15.7%) were plastid targeted according to DeepLoc and 69 (27.2%) were predicted to contain either a cTP or luTP based on ChloroP or TargetP (plant). From the 254 proteins with significant differences in expression 143 (56.3%) were more expressed in *KbHT*. Of the more highly expressed proteins, 7 different kinases were putatively identified, 4 of which were plastid targeted based on either DeepLoc or ChloroP. When exploring potential functions of these plastid targeted kinases, the most differentially expressed was an adenylate kinase (ADK) (ExpRatio = 2.94), followed by a 6-phosphofruktokinase (6PFK) (ExpRatio = 2.28) and a galactokinase (ExpRatio = 1.88).

Furthermore, various proteins with functions related to fatty acid or polyketide synthase were more highly expressed in *KbHT*. Various ketoreductases and ketosynthases were found to be more highly expressed in *KbHT* as well as, enoyl-CoA reductases and hydrates. These proteins ranged in expression ratio from 3.75 – 1.36. When comparing proteins related to redox homeostasis such as glutathione reductase or oxidoreductases such as glutaredoxin, and glutathione peroxidase several proteins were found to be more highly expressed with expression ratios ranging from 2.69 – 1.50. Interestingly, one of the most differentially expressed proteins was surprisingly a pyridoxal 5'-phosphate synthase (Pdx1) which had an average expression ratio of 6.61.

Pyridoxal 5'-phosphate (vitamin B6) plays roles in amino acid biosynthesis, and has been shown to be an important quencher of ROS in *A. thaliana* (Havaux et al., 2009).

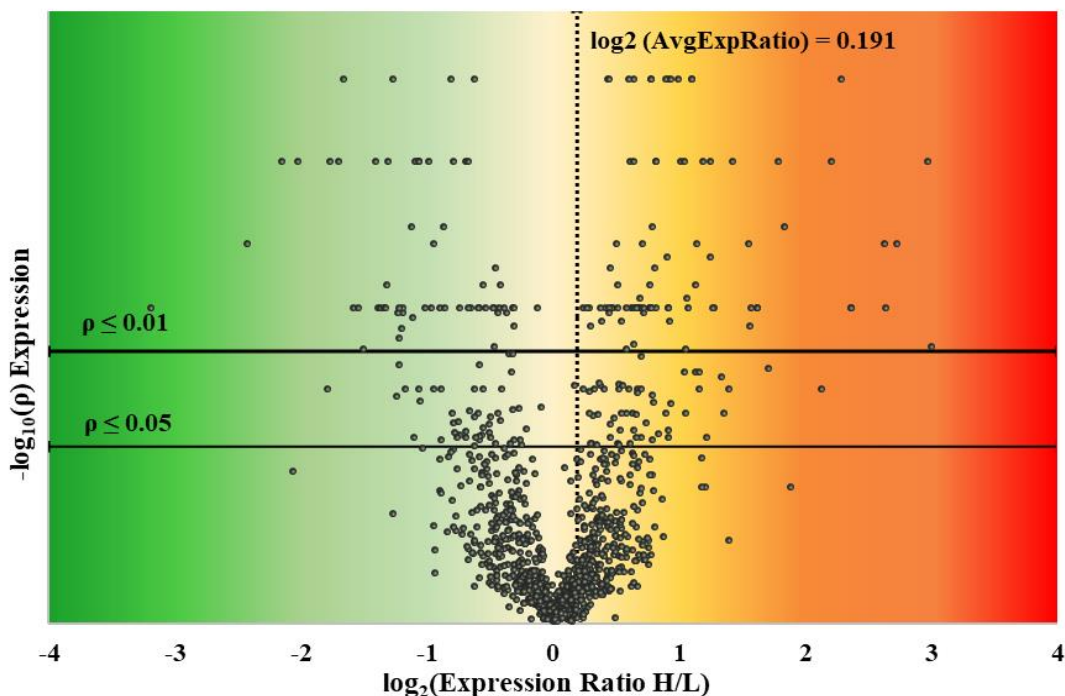


Figure 4.8 Volcano plot showing significant differences in expression as a function of fold changes in expression ($N \geq 3$, 1093 proteins total). Green represents lower expression in KbHT and red represents higher expression in KbHT. The x-axis is presented on a log₂ scale, so values of 1 and -1 represent 2-fold and 0.5-fold, respectively. Solid black lines represent the log values for permutation ρ values < 0.05 and < 0.01 . All permutation ρ values = 0 were set to equal 4 due to inability to calculate the $-\log_{10}$. Dashed vertical line represents the average expression ratio (0.19).

4.2.6 The significance of redox differences in *KbHT* and *KbLT*

Redox status was calculated as the abundance of light IodoTMT label divided by the total IodoTMT (light + heavy) label for a given protein. This calculation provides a measure of the amount of IodoTMT label that was incorporated into the protein prior to reduction with TCEP. By measuring the amount of label incorporated prior to TCEP

reduction and calculating the proportion which these labels represent relative to the total amount of label incorporated (before and after reduction), it is possible to probe the redox status of individual proteins and better understand which proteins may contain cysteine residues which may be existing as thiols, as opposed to forming disulfides or existing as oxidized forms of cysteine such as sulfenic, sulfinic and sulfonic acids. By analyzing the ratio of the cysteine proteome between *KbHT* and *KbLT* it is possible to assess which proteins' may be playing a role in the differences seen between the two strains with respect to qE, specifically the xanthophyll cycle, MGDG production, and redox homeostasis pathways involving the thioredoxin and glutaredoxin system.

Figure 4.9 shows a volcano plot of $\log_2(\text{Redox Ratio H/L})$ plotted against $-\log_{10}(\rho\text{-value})$ for all proteins detected in at least 3 replicates. Of the 1092 proteins plotted 1017 (93.1%) were more oxidized in *KbHT*. Out of 1092 proteins, 411 (37.6%) had a permutation $\rho\text{-value} \leq 0.05$. Of these 411, 67 (16.3%) were plastid targeted according to DeepLoc and 121 (23.4%) were predicted to contain either a cTP or luTP based on ChloroP or TargetP (plant). Of the proteins with significantly different redox status 407 (99.0%) were more oxidized in *KbHT* (Redox Ratio < 1). Of the 4 proteins which were more reduced in *KbHT*, the one with the highest redox ratio (3.92) was a plastid targeted ADK which is also found to be over-expressed in *KbHT*.

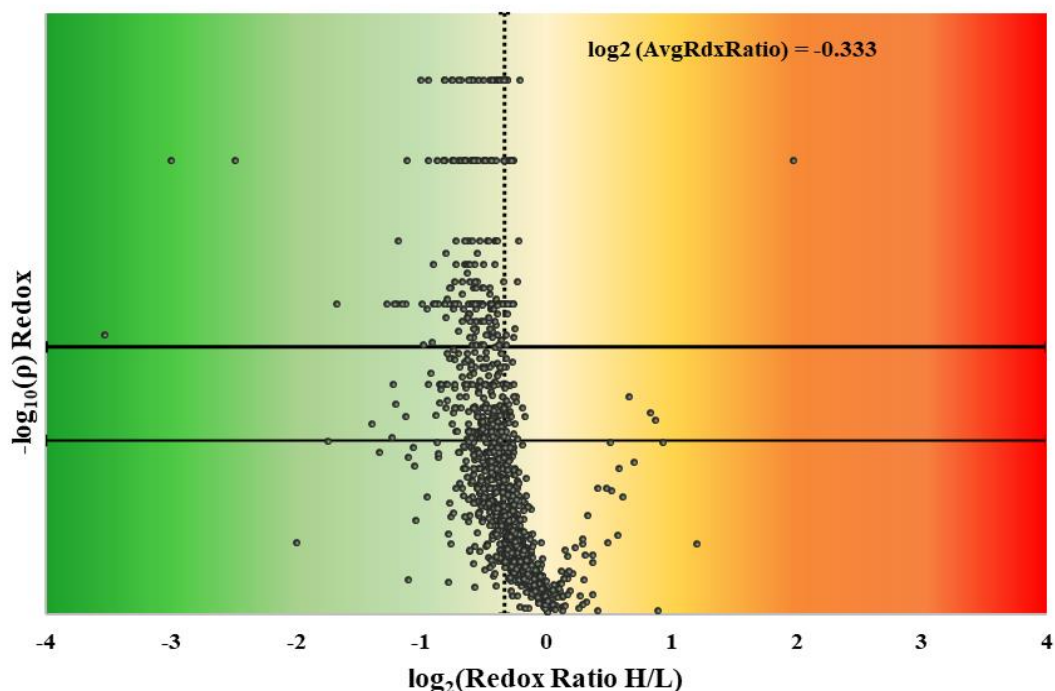


Figure 4.9 Volcano plot showing significant differences in redox status as a function of fold changes in redox status ($N \geq 3$, 1093 proteins total). Green represents proteins more oxidized in KbHT and red represents more reduced in KbHT. The x-axis is presented on a \log_2 scale, so values of 1 and -1 represent 2-fold and 0.5-fold, respectively. Solid black lines represent the log values for permutation ρ values <0.05 and <0.01 . All permutation ρ values = 0 were set to equal 4 due to inability to calculate the $-\log_{10}$. Dashed vertical line represents the average redox ratio (-0.333).

4.2.7 Diadinoxanthin de-epoxidase, and MGDG synthase are expressed similarly, but have significant differences in redox status.

Peptide fragments corresponding to ortholog Dde4 (Table 3.2) were identified in three of the four samples analyzed (*Kb4P1*, 3 and 4). This fragment corresponds to amino acids 248-260 of Dde4 (underlined in Figure 4.10). Peptide fragments from Dde1, 2, and 3 were not identified in any sample. Peptide fragments corresponding to MGDG synthase were identified in three of the four samples analyzed (*Kb4P1*, 2 and 4). Both proteins

were determined by DeepLoc to be plastid membrane localized, while Dde was predicted to have a cTP. Table 4.4 lists the ratio of the total intensities of Dde and MGDG synthase (light +heavy labels) $\times 10^4$ to the total intensity of all labeled peptides (all light + heavy) for *KbHT* and *KbLT* and is indicative of relative expression of these enzymes. In two of the three samples for which Dde4 was detected (*Kb4P3* and 4) the overall expression was slightly lower in *KbLT*, but on average, the difference was not statistically significant ($\rho=0.62$, two tailed t-test; $\rho=0.45$, permutation test). In each of the three samples, the expression of MGDG synthase was slightly lower in *KbLT* than *KbHT*, but the difference was also not statistically significant ($\rho=0.16$, two tailed t-test; $\rho=0.44$, permutation test).

Table 4.4 Relative expression of Dde and MGDG synthase expressed as ratio of total IodoTMT intensities for Dde and MGDG synthase relative to total intensities of all peptides (Light+Heavy-enzyme/Total) for each replicate of *KbLT* and *KbHT*.

Dde (replicate)	(Light+Heavy/Total) *10 ⁴		MGDG synth (replicate)	(Light+Heavy/Total) *10 ⁴	
	<i>KbHT</i>	<i>KbLT</i>		<i>KbHT</i>	<i>KbLT</i>
Dde4 (1)	5.19	6.62	MGDG synth (1)	1.30	1.26
Dde4 (2)	-	-	MGDG synth (2)	2.40	2.08
Dde4 (3)	5.25	5.00	MGDG synth (3)	-	-
Dde4 (4)	10.8	6.90	MGDG synth (4)	1.67	1.51
Avg Dde ±St.Dev.	7.08 ±3.22	6.17 ±1.03	Avg MGDG synth ±St.Dev.	1.79 ±0.56	1.61 ±0.42
HT/LT ρ (t-test) ρ (permutation test)	1.13±0.549 $\rho = 0.62$ $\rho = 0.45$		HT/LT ρ (t-test) ρ (permutation test)	1.10±0.443 $\rho = 0.16$ $\rho = 0.44$	

The ratios of light/(light+heavy) labels for Dde, and MGDG synthase, which is indicative of the redox status of the enzymes are shown in Table 4.5. In all three replicates for which Dde was identified, Dde was more reduced in *KbLT*. The average was 0.67-fold lower in *KbHT*. A two tailed t-test returned a $\rho=0.20$. However, a

permutation test, which is more appropriate for small samples, returned a $\rho = 0.052$. In all three replicates for which it was identified, MGDG synthase was also more reduced in *KbLT*. The average was 0.73-fold less reduced in *KbHT* and this difference is statistically significant ($\rho = 0.07$, two tailed t-test; $\rho = 0.005$, permutation test). A two tailed paired t-test that includes all occurrences of Dde and MGDG synthase together returns a $\rho = 0.011$.

Table 4.5 Redox status of Dde and MGDG synthase expressed as ratio of IodoTMT intensities of Light / Light+Heavy for each replicate of *KbLT* and *KbHT*

Dde (replicate)	Light / Light+Heavy		MGDG synth (replicate)	Light / Light+Heavy	
	<i>KbHT</i>	<i>KbLT</i>		<i>KbHT</i>	<i>KbLT</i>
Dde4 (1)	0.144	0.30	MGDG synth (1)	0.397	0.559
Dde4 (2)	-	-	MGDG synth (2)	0.356	0.411
Dde4 (3)	0.103	0.116	MGDG synth (3)	-	-
Dde4 (4)	0.125	0.193	MGDG synth (4)	0.251	0.408
Avg Dde ±St.Dev.	0.124 ±0.021	0.201 ±0.095	Avg MGDG synth ±St.Dev.	0.335 0.075	0.459 0.086
HT/LT ρ (t-test) ρ (permutation test)	0.672±0.325 0.20 0.052		HT/LT ρ (t-test) ρ (permutation test)	0.731±0.213 0.070 0.005	

$\rho = 0.011$ (two tailed paired t-test that includes Dde and MGDG synthase)

```

Soy 1 -----MATWGAHSMLLSHGE--GTGTPKVC---VKAGLTVRGLDRFH--RTRGFKYAPSVVV-----LKVLTAR--KPTRLRLL--RPYCS--VR--G-
Spi 1 -----MALVARSICVSYDE--IAG---IC---NNVSHR--NFKKWVQ--WKNPFLFQ-----DDAR---RNIRFNDR--KLSCTKFIG--AS
Tob 1 -----MALAPHSNFLANHE-----TIK---YYVGSKLPGHKRF--WGW--EDYFGSIVV-----AKICSSRR---IPRYFRKS--PRICCGLD--SGL
DDE1 1 MKSFLVLVLYAGH--VCRRAHTF--PSRGQQNLE---GPSGLLVGSGGQPKARSLIALGSLFLAFGPAAGWEVSSAARGYDRRLLCD--HRS--CNRRAGS--RPS
DDE2 1 -----
DDE3 1 -----MCKTALLPERLADKLPSPKPRHVCAEYKHS--GCTQ---GRALMMLCLLSDPGAGWQVVRPGLC---RGTVAAPHSPIFTRKIGRQV
DDE4 1 -----MSLS-----SCVVVC--LVCVGHGWVQSSADS---HRKTNHVQQA-----LARYL

Soy 75 -QHDHGKGYFSP--TNS---QIPR--QHILKFAAD---RMLA----FLK--DWSNLR---ITAVAGILVSV-----LMIIPPA--DAV
Spi 64 EKLQHSK---SPKS-----GLISCGWEVNSKVVUSNAV---IPK--KWNLLK--VVEVTAIVACI-----FFVMSSA--QAV
Tob 72 QLF--SHGKHNLSP--PAHSINQV--FKGNSGCKFKPKD---VALM---VWE--KWGQFA---KTAIVAF--I-----LSVASK--ADAV
DDE1 96 VVMRKVD--RL---EEDS--PRELQSV-----PSA-----QVAMRRSIIAGLGA-----AVLGPATASR
DDE2 1 -----MVRLQA--SLFLCSLA
DDE3 79 KHSSM--FNSIFANSM--LAPDRAL---MQRSHLDSESKRPAFDALN--LGALK--SLLLTVLI--SLSLASVG---VSSAQA---E-----NELSAL--ATSKST
DDE4 42 ITHSPAHA--AFNPTG--LGGHSP--TANPGPAHRSQPARTPSWLTSA--AASFAAAATLLFAMP--DITSLAMQPAAI--AATQPADRATLSAENFEKVEGFEDFA--AQQG

Soy 136 DALKTCA--CLLKD--CRIELAK--LSNPS--CAANIA--LQTCN--NRPD--ETE--QIK--CGDLF--ENS--VVD--E--FNE--CAVSR--KKCV--PKS---D--VGEF--PAPNP--DVLVNS--FNI
Spi 126 DALKTCT--CLLKE--CRIELAK--IANPS--CAANVA--LQTCN--NRPD--ETE--QIK--CGDLF--ANKV--VDE--FNE--CAVSR--KKCV--PKS---D--VGEF--PVPDP--SVLVKS--FNM
Tob 136 DALKTCT--CLLKE--CRIELAK--IANPS--CAANVA--LQTCN--NRPD--ETE--QIK--CGDLF--ENS--VVD--E--FNE--CAVSR--KKCV--PKS---D--VGD--FV--PDP--SVLV--QK--FDM
DDE1 146 AIDVDV--GCV--IKD--CACTL--AR--CTD--PT--CAELL--IQ--SNG--KPD--EGS--QIQ--CND--FND--V--VAR--FNT--CAV--SE--KKCV--PKRQ---D--DGSW--PVA--SALV--KE--FNI
DDE2 15 AVVASPL--CF--SQH--CV--SE--MWE--LR--DEK--RAV--TTC--QLG--CA--M--G--KN--F--GG--CA--M--H--Q--DH--PS--SV--D--N--M--T--A--GL--FD--NH--CM--P--V--P--F---PMV--DH--CK--T--PK--SK--PI--GI
DDE3 159 SELV--D--T--K--CL--V--N--Q--C--M--AT--TS--CA--ES--GD--T--K--G--L--L--I--AK--C--L--G--DAK---CEV--G--C--F--AR--YE--N--Q--D--L--D--N--L--L--Q--T--I--E--K--E--K--I--K--I--S--I--M--E--P--G--A--D--P--L--D--A--P--L--P--K--P--L--V--P--V--T--Q
DDE4 140 RMKADP--C--FF--N--Q--C--K--E--Q--T--T--S--FT--N--P--A--L--K--G--I--T--C--L--G--N--C--R--G--E--Q--L---CA--T--Q--C--F--AR--F--G--S--ER--I--N--A--W--L--G--T--L--E--D--K--E--C--V--T--T--G--V--K--Q--D--T--T--K--Y--Y--L---N--P--P--A--M--E--K--F--T--P

Soy 231 AEFSGKWFIT--SGLNPT--FD--FDC--QLHEFHT--ESNKLIV-----GNLSWRIRTP---DAG--FITRS--AEQRFV--QDPS--PGCILY--NH--DN--KYLHY--QDD
Spi 221 ADFNGKWFIS--SGLNPT--FDA--FDC--QLHEFHL--EDGKLV-----GNLSWRIKTP---DGG--FFTRTAV--QKFA--QDPS--PGCILY--NH--DN--AYLHY--QDD
Tob 231 KDFSGKWFIT--RGLNPT--FDA--FDC--QLHEFHT--EENKLIV-----GNLSWRIRTP---DGC--FFTRS--AVQK--FV--QD--PKY--PGCILY--NH--DN--EYLHY--QDD
DDE1 241 AEVVGWNYIT--AGLN--D--FD--T--FDC--Q--FH--K--F--T--S--P--E--P--G--K--IV---GQL--WR--IK--DP---VAG--T--N--F--I--T--K--A--T--E--Q--R--F--V--Q--D--P--K--V--G--I--F--Y--H--N--D--D--Y--L--H--Y--Q--D--D
DDE2 108 KMMQGLWTV--V--R--G--Y--D--K--I--S--D--C--Q--A--C--N--F--R--Q--W--L--P--K--P--N--S--F--W--S--Y--G--D---N--T--G--V---D--I--N--G--N--Y--N--N--F--Y--F--N--D--V--R--P--S--E--T--D--S--K--D--S--L--V--Y--H--W--G--L--E--A--G--N--M--K--E--E
DDE3 255 AEMSGDWYK--V--M--G--W--N--F--N--Y--D--C--F--Q--R--N--S--F--S--K--N--A--V--S--K--V--G--S--S--N--I--G--S--N--G--M--S--M--E--V--E--F--S--M--P--R--E--R--L--D--Q--Q--P--Q--T--Y--R--S--T--V--L--E--T--L--R--F--D--K--T--P--S--R--R--T--A--H--E--G--Q--M--F--G--V--S--F--W--E--N
DDE4 233 ADLEGK--WYK--V--L--G--Y--N--F--K--Y--D--Y--P--C--Q--T--N--E--F--T--R--K--A--D--G--A--L---N--D--I--L--R--V--P--K--P---D--G--S--G--W--Q--N--N--F--I--E--T--M--A--N--S--K--P--Q--G--K--A--S--M--I--V--E--G--K--M--F--G--L--T--F--H--E--Q

Soy 312 WYILSSKIENK--SDDY--V--F--V--Y--R--G--R--N--D---A--W--D--G--Y--G--A--V--V--Y--T--R--S--A--V--L--P--E--S--I--V---P--E--L--E--K--A--S--K--S--V--C--R--D--F--S--K--F--I--R--T--D--N--T--C--P--E--P--S--L--V--E--R--L--E--K--K--V--E--G--E--E--T--I
Spi 302 WYILSSKIENQ--PDDY--V--F--V--Y--R--G--R--N--D---A--W--D--G--Y--G--A--F--L--Y--T--R--S--A--T--V--E--N--I--V---P--E--L--N--R--A--Q--S--V--G--K--D--F--N--K--F--I--R--T--D--N--T--C--P--E--P--L--V--E--R--L--E--K--T--V--E--G--E--R--T--I
Tob 312 WYILSSKVENSP--EDY--I--F--V--Y--K--G--R--N--D---A--W--D--G--Y--G--S--V--L--Y--T--R--S--A--V--L--P--E--S--I--I---P--E--L--Q--T--A--A--Q--K--V--G--R--D--F--N--T--F--I--K--I--D--N--T--C--P--E--P--P--L--V--E--R--L--E--K--K--V--E--G--E--R--T--I
DDE1 325 WYVLA---HRPGY--F--L--V--Y--R--G--I--N--D---A--W--D--G--Y--G--A--F--L--Y--T--R--T--I--P--R--E--Y--L---P--E--L--D--A--M--Q--K--I--G--R--R--F--T--E--F--K--L--N--N--V--K--P--R--E--S--L--F--E--V--Q--N--D--V--V--Y--K--S--R--Y
DDE2 194 WVLLDE--T---E--E--Y--K--I--Y--Y--C--T--T--D--L--K--I--A--P--G--K--Q--L--E--G--L--L--S--K--T--K--D--V--T--S--N--A--A---R--I--A--D--I--F--K--E--S--A--G--L--D--Y--D--A--F--C--S--N--D--N--T--C--P--V--G--P--A--K--T--I--S--E---A--T--M--V--I
DDE3 354 WYVIGKET--GSEPE--F--R--F--I--Y--T--G--K--T---Q--L--N--R--Y--E--G--A--F--V--Y--S--R--Q--P--E--L--P--R--D--A--L---P--S--I--Y--R--I--A--R--E--A--G--I--E--P--T--G--M--C--C--D--N--K--C--F--R--E--A--E--A--K--A--S--S---P--P--P--F--V
DDE4 319 WYVVLKGC---D--N--F--R--V--V--Y--I--G--D--T---Q--Q--G--Y--D--G--A--F--V--F--I--K--E--K--D--A--L--E--G--P--S--G--S--Q--L--R--A--E--I--D--G--V--V--S--R--A--G--L--D--P--K--Q--M--R--M--I--D--N--A--C--P--E--D--A--T--K--A--G--A--S---V--E--A--A--K

Soy 404 VRE--VEQIEE---EVEKVGKTEA--I--F--Q--K--L--A--E--G--F---M--F--Q--E--D--E--N--F--L--R--L--S--K--E--E--M--I--L--D--G--L--K--M--E--A--G--E--V--E--K--L--F--G--R--A--L--P--I--R--K--L
Spi 394 IKE--VEEIEE---EVEKVRDK--E--V--T--L--F--S--K--L--F--E--G--F---E--L--Q--K--D--E--Y--F--L--K--E--L--N--K--E--R--E--L--L--E--D--L--K--M--E--A--G--E--V--E--K--L--F--G--R--A--L--P--I--R--K--L
Tob 404 IKE--VEEIEE---EVEKVRDK--E--V--T--L--F--S--K--L--F--E--G--F---E--L--Q--R--D--E--N--F--L--R--L--S--K--E--E--M--D--V--L--D--G--L--K--M--E--A--T--E--V--E--K--L--F--G--R--A--L--P--I--R--K--L
DDE1 413 -----GSLGKQLQ--Q--V--E--V--E--D--E--A--L--F--I--E--K--I--V--E--Q--E--A--K--V--E--Q--E--L--K--D--L--V--A--V--E--K--E--V--E--K--D--A--V--A--L--G--R--L--F--K--P--S--L--P--K--P--R---
DDE2 280 -----
DDE3 439 SVAVAST--L--P--G--E--A--P--K--R--T--I--L--E--S--N--L--A--P--L--R--L--E---V--D--V--R--E--Y--L--D--P--H--P--P--A--E--M--L--F--R--K--Q--R--K--M--S--E--L--L--Q--F--D--G--N--G--Y--R--V--T--S--Q--Q-
DDE4 405 E-----KLE-----WKDV-----FELTEWFRPGTIKRDIAFDPT--KM-----

```

Figure 4.10 Alignment of soybean NP_001240949.1 (Soy), spinach XP_021853497.1 (Spi) and tobacco AFP57681.1 (Tob) Vde with the four translated DDE homologues identified in the *K. brevis* transcriptome library. Multiple sequence alignments were generated using Clustal Omega, and visualized using BoxShade (Sievers et al., 2011). Red and blue amino acids represent greater than 50% identity and similarity between aligned sequences, respectively. The 12 conserved cysteine residues are highlighted in yellow. The peptide fragment identified by MS/MS (vide infra) is underlined.

In addition to Dde, diatoxanthin epoxidase (Dep) was detected in one replicate (*Kb4P3*). It was accurately predicted by DeepLoc to be a plastid membrane protein (Goss, Ann Pinto, Wilhelm, & Richter, 2006) as well as ChloroP predicting the presence of an N-terminal cTP. The redox status for Dep was found to be 0.66-fold less reduced in *KbHT*, while it was also expressed less by 0.59-fold (Table 4.6).

Table 4.6 Diatoxanthin epoxidase expression (IodoTMT Light+Heavy for Dep over abundance for all peptides*10⁴), and redox status (IodoTMT Light/(Light+Heavy)). Ratios are shown for both expression and redox status.

<i>Dep Loci</i>	Dep/Total *10⁴		<u>Light</u> (Light+Heavy)	
	<i>KbHT</i>	<i>KbLT</i>	<i>KbHT</i>	<i>KbLT</i>
57998	0.278	0.423	0.198	0.334
HT/LT	0.657		0.592	

4.2.8 Redox homeostasis mediating enzymes in the thioredoxin system, and glutaredoxin system, are significantly different in redox status.

4.2.8.1 Thioredoxins

Seven unique peptides fragments identified by MS/MS mapped to full length proteins with high homology (E-values $\leq 10^{-13}$) to thioredoxin and which localize to the plastid according to either chloroP (Emanuelsson et al., 1999) or DeepLoc (Almagro Armenteros et al., 2017) were identified by MS/MS analysis. Table S4.1 of Appendix B shows total intensities of the Trxs (light +heavy labels) x10⁴ to the total intensity of all labeled peptides (all light + heavy) for *KbHT* and *KbLT*. In nine of thirteen occurrences, Trx was more highly expressed in *KbHT*, but the difference was not statistically significant ($\rho = 0.86$, two tailed paired t-test). The intensity of the light label to the sum the light plus heavy labels (light/light+heavy) for Trx which is indicative of the redox status of these Trxs are shown in Table S4.1 of Appendix B. In ten of thirteen occurrences, Trx is more reduced in *KbLT*. Furthermore, this difference is statistically significant ($\rho = 0.006$, two tailed, paired t-test).

When taking the average of all occurrences for each unique peptide, five of seven peptides contained higher expression in *KbHT* (Figure 4.11A), although the difference was not significant ($\rho = 0.78$, two tailed, paired t-test). Conversely, when the average of all occurrences for each unique peptides' redox status is analyzed, all seven peptides had a more reduced status in *KbLT* (Figure 4.11B). The difference in redox status was once again significant ($\rho = 0.006$, two tailed, paired t-test).

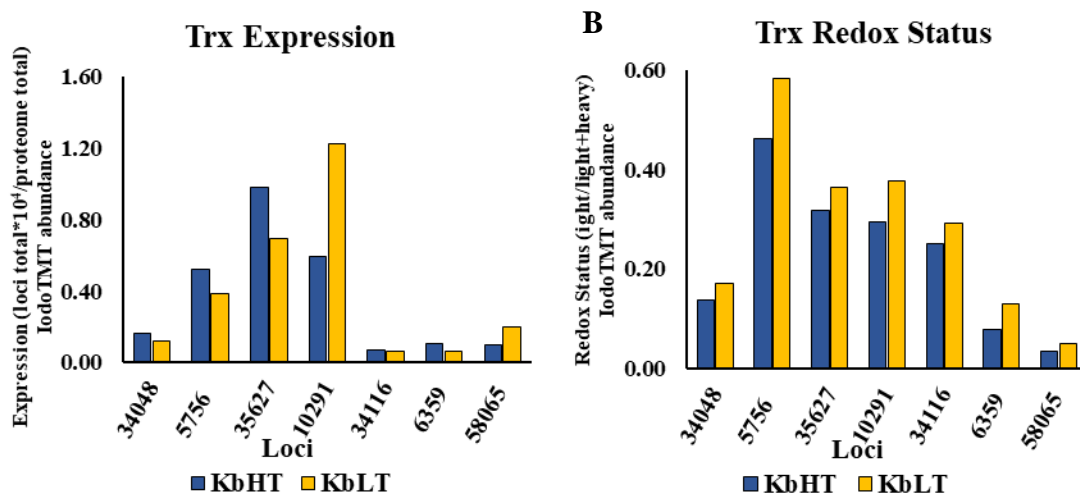


Figure 4.11 A) Average expression for plastid localized Trx. B) Average redox status for plastid localized Trx peptides

4.2.8.2 Glutaredoxins

Three unique peptides fragments identified by MS/MS mapped to full length proteins with high homology ($E\text{-values} \leq 10^{-15}$) to glutaredoxin which are targeted to the chloroplast based on ChloroP or DeepLoc predictions were identified by MS/MS analysis. Table S4.2 of Appendix B list the ratio of intensities for Grxs (light +heavy labels) $\times 10^4$ to the total intensity of all labeled peptides (all light + heavy) for *KbHT* and *KbLT*. In all twelve occurrences, Grx was more highly expressed in *KbHT*, the difference

being statistically significant ($\rho = 0.009$, two tailed, paired t-test). The ratios of the intensity of the light label to the sum the light plus heavy labels (light/light+heavy) for Grx which is indicative of the redox status of these Trxs are also shown in Table S4.2 of Appendix B. In ten of twelve occurrences, Grx is more reduced in *KbLT*, the difference being statistically significant ($\rho = 0.007$, two tailed, paired t-test).

When taking the average of all occurrences for each unique peptide, all three peptides contained higher expression in *KbHT* (Figure 4.12A), although the difference was not significant ($\rho = 0.28$, two tailed, paired t-test). When the average of all occurrences for each unique peptides' redox status is analyzed, all three peptides had a more reduced status in *KbLT* (Figure 4.12B). The difference in redox status was, however, not significant for the average ($\rho = 0.12$, two tailed, paired t-test).

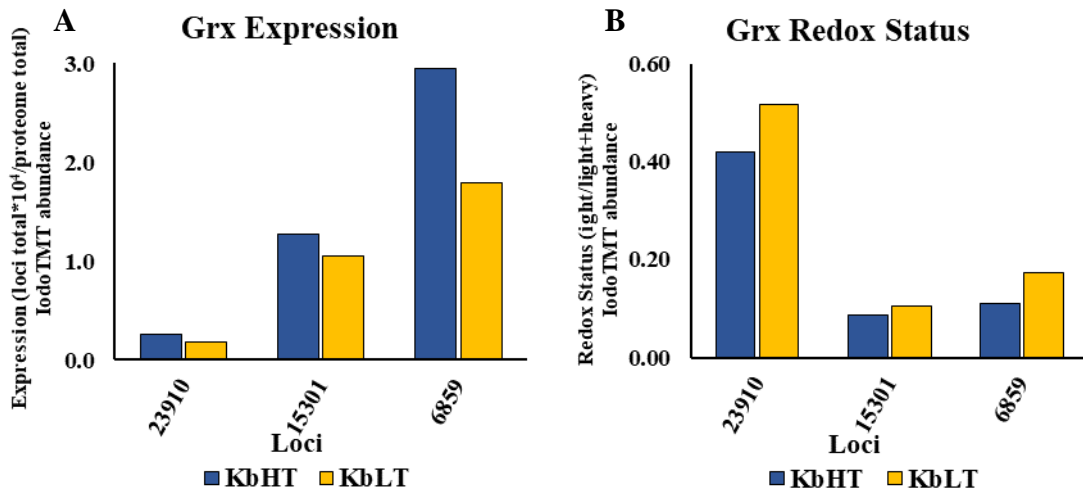


Figure 4.12 A) Average expression for plastid localized Grx. B) Average redox status for plastid localized Grx peptides

4.2.8.3 Peroxiredoxins

Five unique peptides fragments identified by MS/MS mapped to full length proteins with high homology (E-values $\leq 10^{-23}$) to Prx with plastid targeting based on predictions from ChloroP or DeepLoc were identified by MS/MS analysis. Table S4.3 of Appendix B list the ratio of intensities for Prxs (light +heavy labels) $\times 10^4$ to the total intensity of all labeled peptides (all light + heavy) for *KbHT* and *KbLT*. In seven of eleven occurrences, Prx was more highly expressed in *KbHT*, but the difference was not statistically significant ($\rho = 0.43$, two tailed paired t-test). The ratios of the intensity of the light label to the sum of the light plus heavy labels (light/light+heavy) for Prx which is indicative of the redox status of these Prxs are also shown in Table S4.3 of Appendix B. In eight of eleven occurrences, Prx is more reduced in *KbLT*, but the difference is not statistically significant ($\rho = 0.12$, two tailed, paired t-test).

When taking the average of all occurrences for each unique peptide, three of five peptides contained higher expression in *KbHT* (Figure 4.13A), although the difference was not significant ($\rho = 0.47$, two tailed, paired t-test). When the average of all occurrences for each unique peptides' redox status is analyzed, three of five peptides had a more reduced status in *KbLT* (Figure 4.13B). The difference in redox status was, however, not significant for the average of all Prx ($\rho = 0.42$, two tailed, paired t-test).

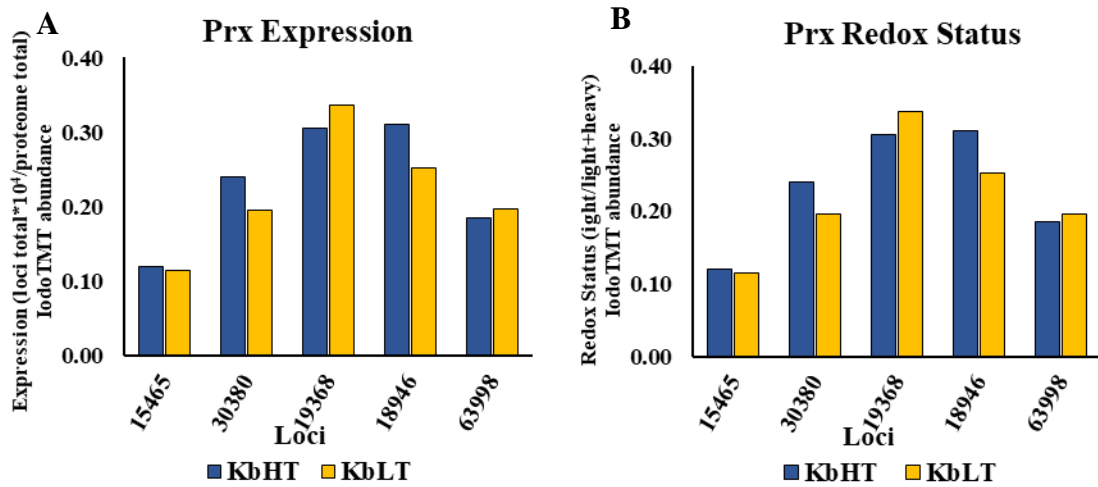


Figure 4.13 A) Average expression for plastid localized Prx. B) Average redox status for plastid localized Prx peptides

4.2.8.4 Glutathione reductases

Two peptides fragments identified by MS/MS mapped to full length proteins with high homology (E values $\leq 10^{-157}$) to glutathione reductase with plastid targeting based on predictions from ChloroP or DeepLoc were identified by MS/MS analysis. Table S4.4 of Appendix B list the ratio of intensities for GRs (light +heavy labels) $\times 10^4$ to the total intensity of all labeled peptides (all light + heavy) for *KbHT* and *KbLT*. In all five occurrences GR was more highly expressed in *KbHT*, this was statistically significant ($p = 0.041$, two tailed paired t-test). The ratios of the intensity of the light label to the sum the light plus heavy labels (light/light+heavy) for GR which is indicative of the redox status of these GRs are also shown in Table S4.4 of Appendix B. In all five occurrences, GR is more reduced in *KbLT* ($p = 3.31 \times 10^{-4}$, two tailed, paired t-test). Only one other GR, which was not plastid targeted, was detected in the proteome. The one occurrence of this mitochondrial (DeepLoc) GR was more highly expressed in *KbLT*, the opposite of what

was observed for the plastid targeted GR (Table S4.5 of Appendix B). However, it was more reduced in *KbLT*, consistent with all other GRs.

When taking the average of all occurrences for each unique peptide, all three peptides contained higher expression in *KbHT* (Figure 4.14A), although the difference was not significant ($\rho = 0.48$, two tailed, paired t-test). Conversely, when the average of all occurrences for each unique peptides' redox status is analyzed, all 3 peptides had a more reduced status in *KbLT* (Figure 4.14B). The difference in redox status was significantly different for the average of all GR ($\rho = 0.001$, two tailed, paired t-test).

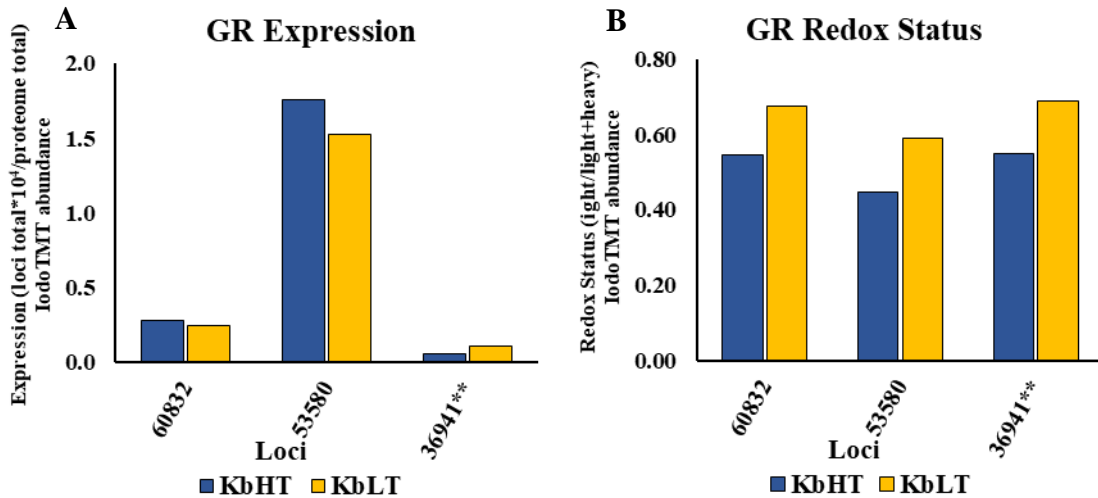


Figure 4.14 A) Average expression for GR. B) Average redox status for GR peptides. ** represents non-plastid localized, both other GR were localized to the plastid based on either DeepLoc or ChloroP

4.2.8.5 Thioredoxin reductases

Three peptides fragments identified by MS/MS mapped to full length proteins with high homology (E value $< 10^{-119}$) to thioredoxin reductases were identified by MS/MS analysis. Of these three proteins, two corresponded to Locus 29890 (*K. brevis*

large NTR shown in Table 1.2) being translated in the -three or -two frame. The peptides were detected in different replicates; however, they were both labeled at the same cysteines of the N-terminal redox center (CVNVGC) in the one occurrence for each respective peptide. Locus 29890 translated in the -two frame was targeted to the plastid membrane based on DeepLoc predictions. However, the -three frame translation of Locus 29890 was not targeted to the plastid and instead predicted to be cytoplasmic. This is likely due to differences in the N-terminal presequence used by DeepLoc to predict organellar localization as a result of different frame translations of the transcript when creating the protein database. A small NTR, Locus 21941, was also detected on one occurrence and was labeled at a cysteine that is not part of the redox center.

Table S4.5 of Appendix B list the ratio of intensities for TrxRs (light +heavy labels) $\times 10^4$ to the total intensity of all labeled peptides (all light + heavy) for *KbHT* and *KbLT*. The only occurrence of TrxR that was more highly expressed in *KbHT*, was for Locus 21941 ($\rho = 0.63$, two tailed, paired t-test). The redox status of these TrxRs are also shown in Table S4.5 of Appendix B. In two of three occurrences (one for each type of NTR), TrxR is more reduced in *KbLT* ($\rho = 0.50$, two tailed, paired t-test), but not significantly. Figure 4.15 shows both the expression and redox status for TrxR.

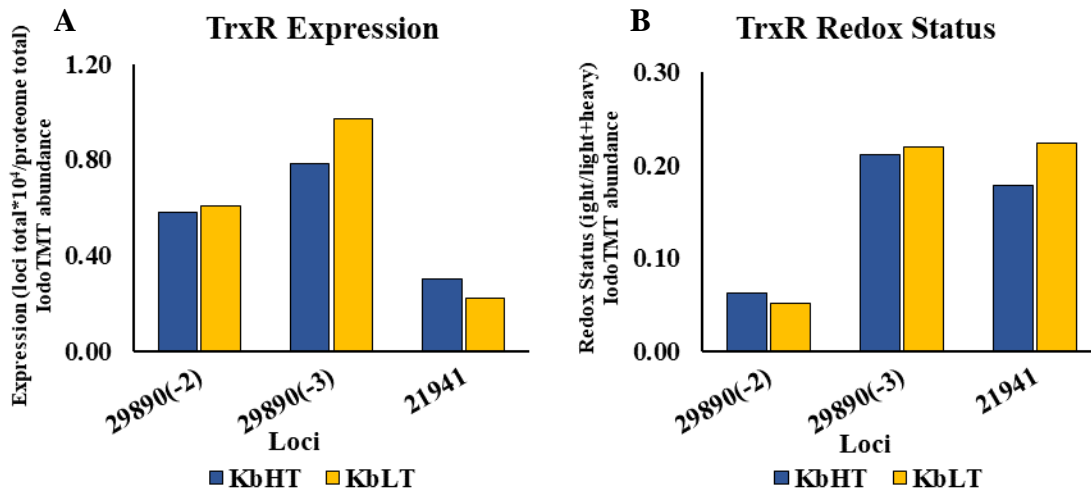


Figure 4.15 A) Average expression for plastid localized TrxR. B) Average redox status for plastid localized TrxR peptides

4.2.9 Redox status among kinases and phosphatases are significantly different.

4.2.9.1 Kinases

Forty-four peptide fragments identified by MS/MS mapped to full length proteins with high homology (E values $\leq 10^{-10}$) to plastid targeted kinases based on predictions from ChloroP or DeepLoc. Table S4.6 of Appendix B shows the intensities for kinases (light +heavy labels) $\times 10^4$ to the total intensity of all labeled peptides (all light + heavy) for *KbHT* and *KbLT*. In 37 out of 99 occurrences, kinases were more highly expressed in *KbHT*. However, this difference was not statistically significant ($\rho = 0.38$, two tailed paired t-test). The ratios of the intensity of the light label to the sum the light plus heavy labels (light/light+heavy) for kinase which is indicative of the redox status of these kinases are also shown in Table S4.6 of Appendix B. In 88 out of 99 occurrences, kinases were more reduced in *KbLT* ($\rho = 1.37 \times 10^{-20}$, two tailed, paired t-test).

When taking the average of all occurrences for each unique peptide 17 of 44 peptides contained higher expression in *KbHT* (Figure 4.16A), although the difference was not significant ($\rho = 0.53$, two tailed, paired t-test). Conversely, when the average of all occurrences for each unique peptides' redox status is analyzed, 42 of 44 peptides had a more reduced status in *KbLT* (Figure 4.16B). The difference in redox status was once again significant ($\rho = 2.84 \text{ E}^{-12}$, two tailed, paired t-test).

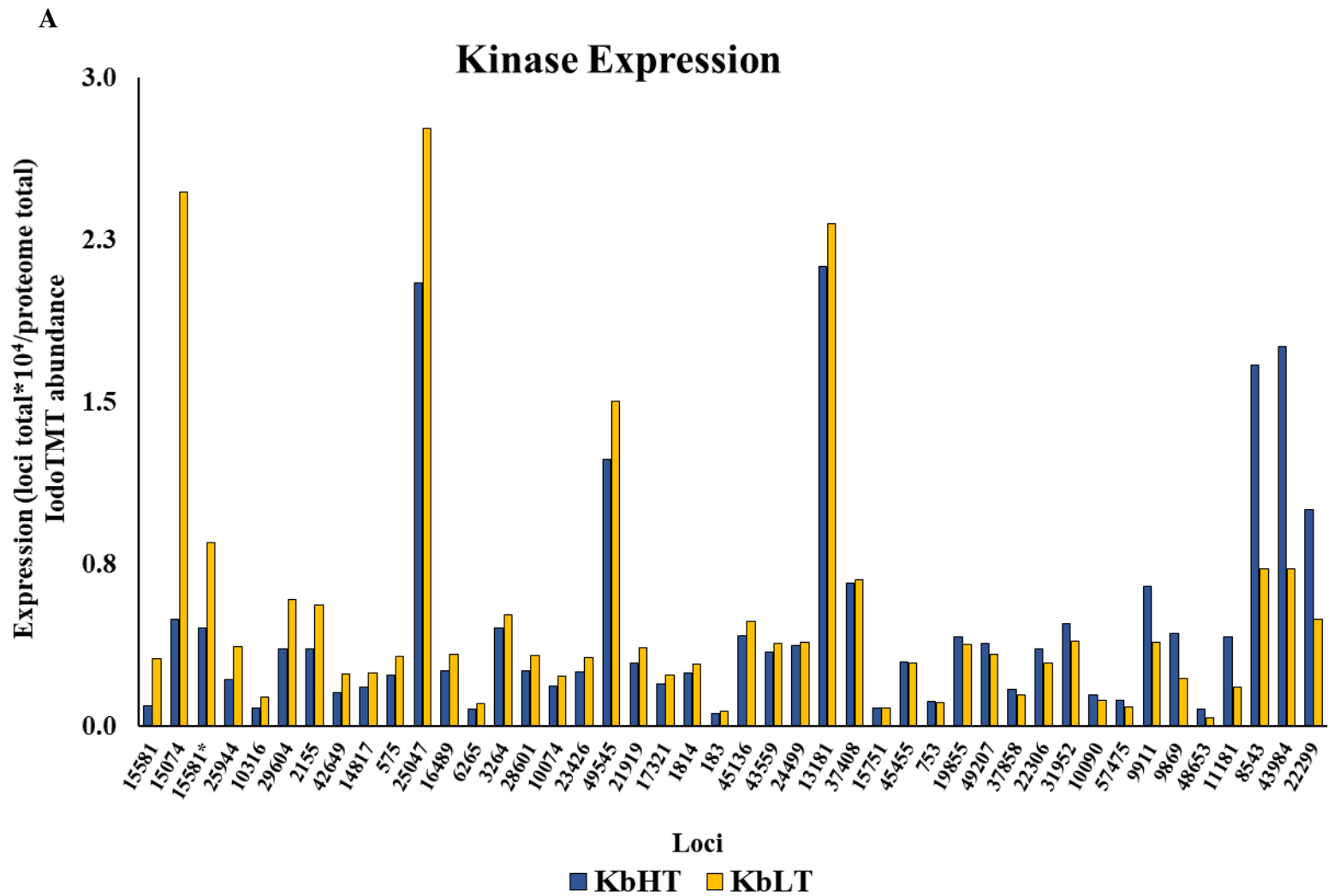


Figure 4.16A Average expression for plastid localized kinases. *represents a different frame translation of Locus 15581.

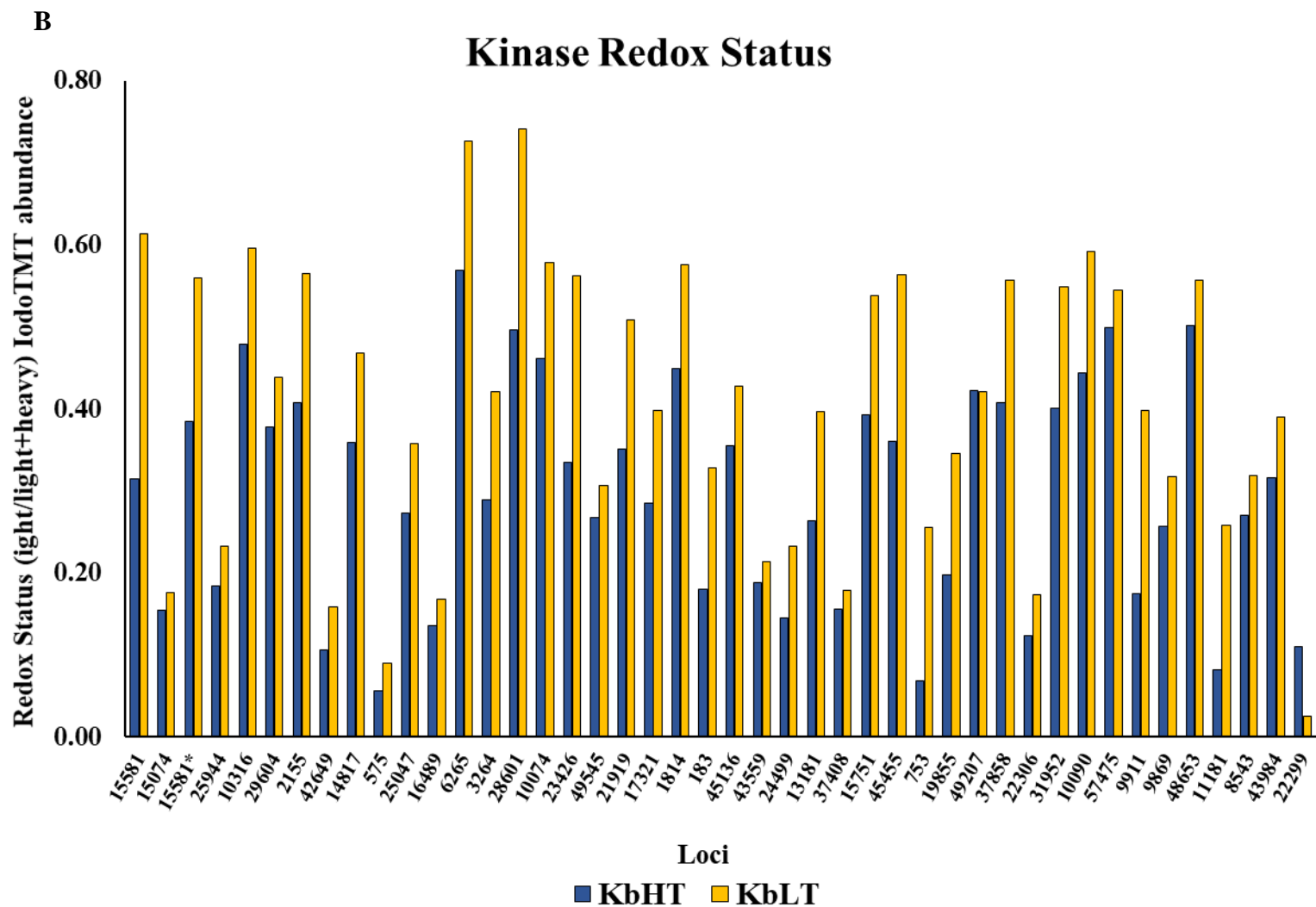


Figure 4.16B Average redox status for plastid localized kinases. *represents a different frame translation of Locus 15581.

4.2.9.2 Phosphatases

Twenty-five peptide fragments identified by MS/MS mapped to full length proteins with high homology (E values $\leq 10^{-10}$) to plastidic phosphatases on predictions from ChloroP or DeepLoc. Table S4.7 of Appendix B shows the intensities for kinases (light +heavy labels) $\times 10^4$ to the total intensity of all labeled peptides (all light + heavy) for *KbHT* and *KbLT*. In 31 of 60 occurrences phosphatases were more highly expressed in *KbHT*. However, this difference was not statistically significant ($\rho = 0.13$, two tailed paired t-test). The ratios of the intensity of the light label to the sum the light plus heavy labels (light/light+heavy) for phosphatases which is indicative of the redox status of these phosphatases are also shown in Table S4.7 of Appendix B. In 55 out of 60 occurrences, kinases were more reduced in *KbLT* ($\rho = 2.42 \text{ E}^{-14}$, two tailed, paired t-test).

When taking the average of all occurrences for each unique peptide 15 of 25 peptides contained higher expression in *KbHT*, although the difference was not significant ($\rho = 0.30$, two tailed, paired t-test) (Figure 4.17A). Conversely, when the average of all occurrences for each unique peptides' redox status is analyzed, 23 of 25 peptides had a more reduced status in *KbLT* (Figure 4.17B. The difference in redox status was once again significant ($\rho = 2.10 \text{ E}^{-6}$, two tailed, paired t-test)

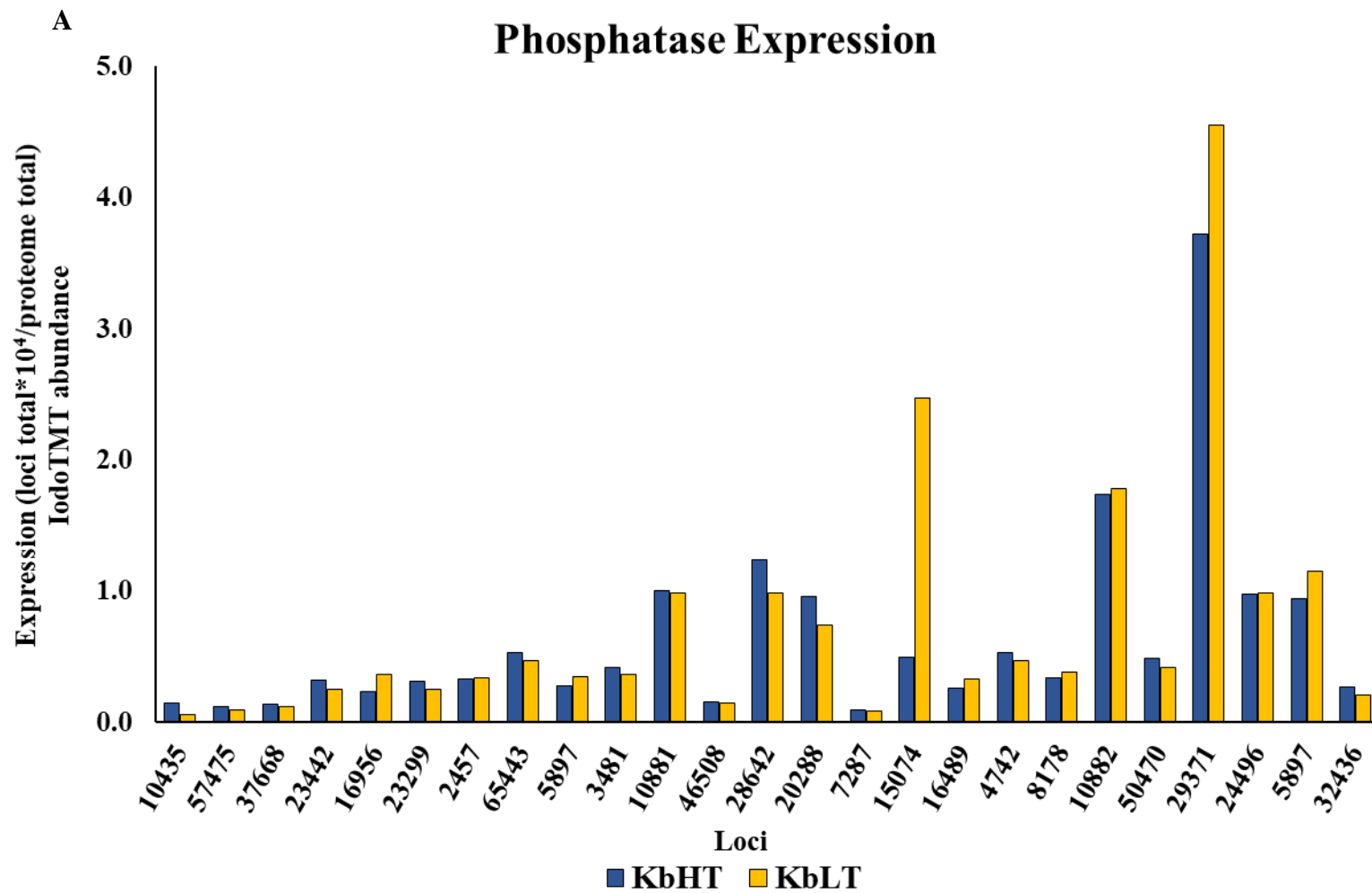


Figure 4.17A Average expression for plastid localized phosphatases.

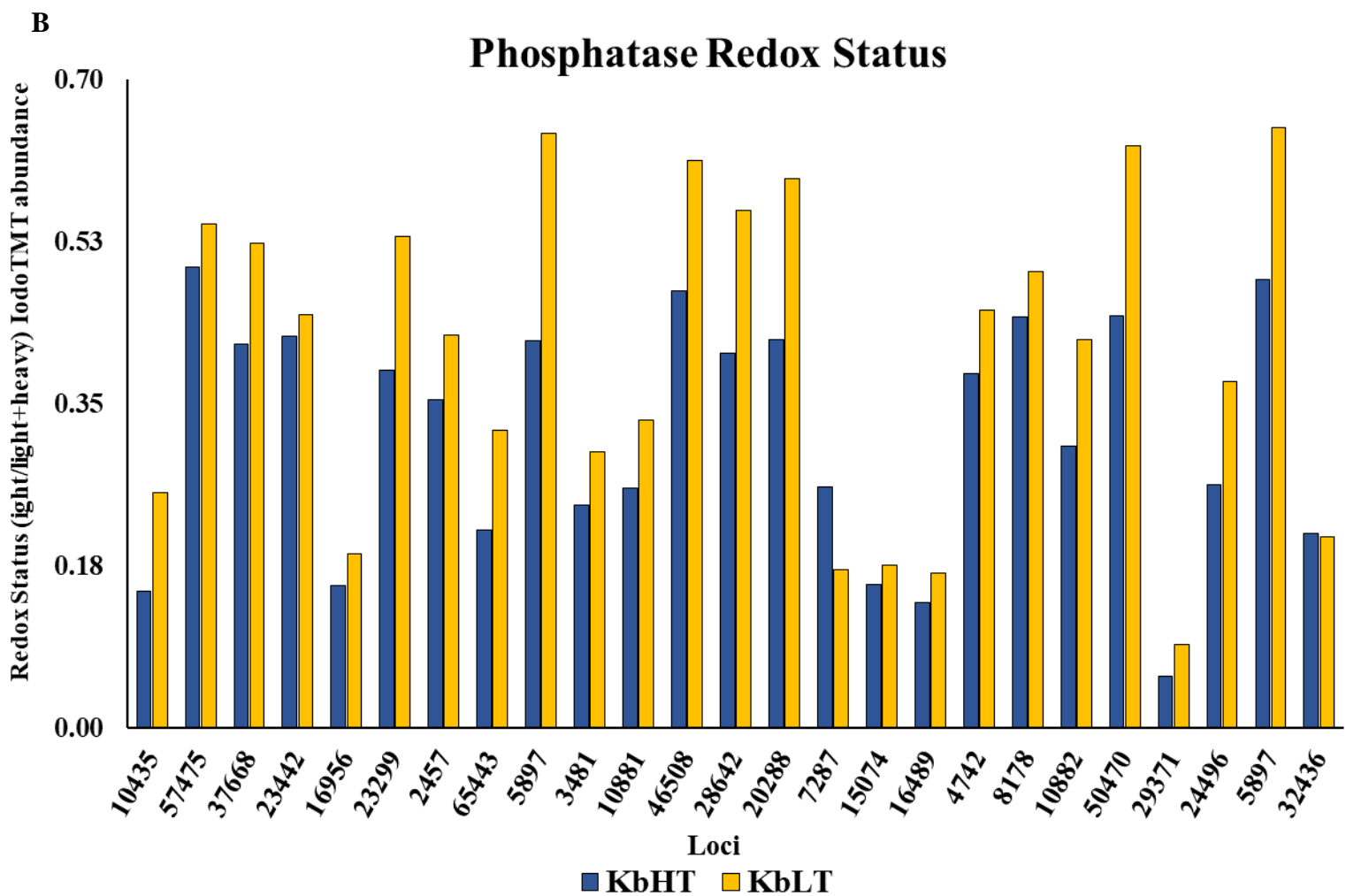


Figure 4.17B Average redox status for plastid localized phosphatases.

4.2.10 Proteins believed to be related to the biosynthesis of toxins are differentially expressed in *KbHT* and *KbLT*

4.2.10.1 Polyketide synthases: differences in expression and redox status

Redox proteomics experiments identified nineteen peptides that corresponded to PKS encoding sequences in the *K brevis* transcriptome library (Ryan et al., 2014). Each of these transcripts, listed in Table 4.7 by loci in the library, encoded for single catalytic domain enzymes and the best match in the BLASTp search also corresponded to single domain PKSs from a variety of dinoflagellates including *K. brevis*, *Gambierdiscus* (12), *Symbiodinium* and *Azadinium* all dinoflagellates known to produce polyketides. These sequences coded for KS domains (15), KR domains and an AT domain. One sequence (Locus 21608) that matched only unnamed proteins from *Symbiodinium*, was identified as a FAS dehydratase by the NCBI Conserved Domain Finder but could represent a PKS DH domain and has been included in this analysis. Table S4.8 of Appendix B also shows the intensities for PKS (light +heavy labels) $\times 10^4$ to the total intensity of all labeled peptides (all light + heavy) for *KbHT* and *KbLT*. In 30 out of 43 occurrences PKSs were more highly expressed in *KbHT*. This difference was statistically significant ($\rho = 1.36 \text{ E}^{-4}$, two tailed, paired t-test). Table S4.8 of Appendix B also lists redox status for each PKS. In 20 out of 30 occurrences PKSs were more reduced in *KbLT*. This difference was statistically significant ($\rho = 2.13 \text{ E}^{-4}$, two tailed, paired t-test).

When taking the average of all occurrences for each unique peptide thirteen of nineteen peptides contained higher expression in *KbHT* (Figure 4.18A), this difference was statistically significant ($\rho = 0.019$, two tailed, paired t-test). Conversely, when the

average of all occurrences for each unique peptides' redox status is analyzed, fifteen of nineteen peptides had a more reduced status in *KbLT* (Figure 4.18B). The difference in redox status was significant ($\rho = 0.01$, two tailed, paired t-test). Of note is the KS encoded by loci 4034 of the transcriptome reference library which we found to be 1.9-fold more expressed in the high toxin strain. This KS was first reported in 2010 (Monroe, Johnson, Wang, Pierce, & Van Dolah, 2010). Consistent with our findings of higher expression in the high toxin strain, this group reported 1.39-fold higher expression of this KS in a high toxin producing strain by Western blotting using antibodies raised to a synthetic fragment of the KS.

4.2.10.2 Cellular localization of PKS

Cellular localization by DeepLoc predicted ten of the PKSs to the peroxisome, four to the plastid, two to the nucleus, and one to each the mitochondrion, cytoplasm and extracellular. four sequences were predicted to contain cTP by either ChloroP or TargetP. Chloroplast transit peptides were not identified in any of the PKS sequences from *G. excentricus* or *G. polynesiensis* (Kohli et al., 2017) that best matched our PKS sequences. Interestingly, there seems to be little correlation between the localization results from DeepLoc with those of ChloroP or TargetP. Cellular localizations are listed in Table 4.7.

Two principle peroxisome targeting signals have been identified: the C-terminal PTS1 (Neuberger et al., 2003) and the less common, N-terminal PTS2 (Kunze, 2020) However, analysis of these sequences by the PTS1 predictor algorithm (Reumann, Buchwald, & Lingner, 2012) failed to identify PTS1, and manual inspection of the sequences failed to identify PTS1 or PTS2. Similar assignments of KS sequences from

G. polynesiensis and *G. pacificus* (Van Dolah et al., 2020) and *Ostreopsis* (Verma, Kohli, Harwood, Ralph, & Murray, 2019) have been reported. However, Van Dolah reported that KS sequences that were localized to the peroxisome by Deeploc also lacked PTS1 or PTS2 (Van Dolah et al., 2020). This group concluded that these enzymes were most likely localized to the cytosol based on the absence of PTS1 and PTS2, the small number of peroxisomal proteins in the Deeploc training set resulting in less discriminatory sensitivity and the mis-classification of known cytosolic enzymes to the peroxisome.

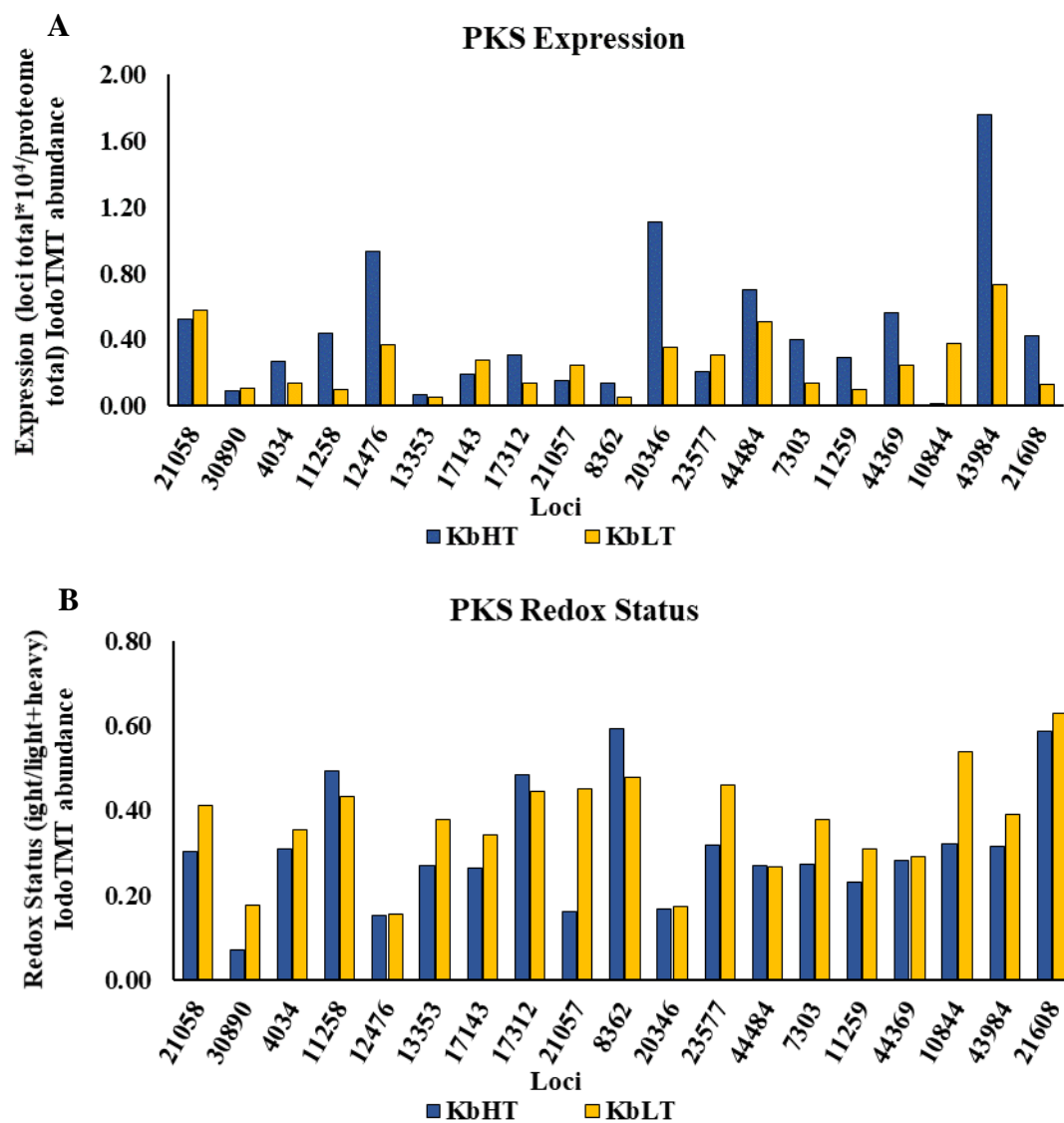


Figure 4.18 **A)** Average expression for all polyketide synthases. **B)** Average redox status for polyketide synthases.

Table 4.7 List of loci to which peptides detected in MS/MS analysis were mapped and their multiplicity (N), PKS match, cellular localization, cTP prediction, and expression ratio. E-value's shown are for BLASTp search. References: 1) Monroe et al., 2010, 2) Kohli et al., 2017.

Locus (N)	BLAST or CD Finder result Organism, Annotation, Accession, (reference)	E-value	Deeploc Prediction	cTP TargetP or ChloroP	Expression Ratio HT/LT
21058 (4)	<i>Karenia brevis</i> , PKS/single KS domain ABQ85800.1 (1)	0.0	Peroxisome		0.900
30890 (1)	<i>Karenia brevis</i> , Acyl Transferase ABQ85796.1 (1)	0.0	Plastid		0.871
4034 (2)	<i>Karenia brevis</i> , PKS/single KS domain ABQ85797.1 (1)	0.0	Nucleus		1.915
11258 (3)	<i>Gambierdiscus excentricus</i> , PKS/single KS domain AQS99208.1 (2)	0.0	Plastid	Yes	4.532
12476 (2)	<i>Gambierdiscus excentricus</i> , PKS/single KS domain AQS99217.1 (2)	0.0	Extracellular	Yes	2.556
13353 (1)	<i>Gambierdiscus excentricus</i> , PKS/single KS domain AQS99255.1 (2)	0.0	Cytoplasm	Yes	1.388
17143 (2)	<i>Gambierdiscus excentricus</i> , PKS/single KS domain AQS99239.1 (2)	0.0	Peroxisome		0.689
17312 (2)	<i>Gambierdiscus excentricus</i> , PKS/single KS domain AQS99274.1 (2)	0.0	Peroxisome		2.312
21057 (1)	<i>Gambierdiscus excentricus</i> , PKS/single KS domain AQS99208.1 (2)	0.0	Nucleus		0.605
8362 (1)	<i>Gambierdiscus excentricus</i> , PKS/single KS domain AQS99237.1 (2)	0.0	Peroxisome		2.776
20346 (2)	<i>Gambierdiscus excentricus</i> , PKS/single KS domain AQS99208.1 (2)	0.0	Peroxisome		3.124
23577 (3)	<i>Gambierdiscus polynesiensis</i> , PKS/single KS domain AQS99262.1 (2)	0.0	Peroxisome	Yes	0.677
44484 (2)	<i>Gambierdiscus polynesiensis</i> , PKS/single KR domain AQS99204.1 (2)	0.0	Peroxisome		1.374
7303 (4)	<i>Gambierdiscus polynesiensis</i> , PKS/single KS domain AQS99296.1 (2)	0.0	Mitochondria		2.902
11259 (2)	<i>Gambierdiscus polynesiensis</i> , PKS/single KS domain AQS99197.1 (2)	0.0	Peroxisome		3.054
44369 (3)	<i>Azadinium spinosum</i> , PKS/KS domain AIW63289.1	0.0	Plastid	Yes	2.257
43984 (2)	<i>Symbiodinium sp.</i> , PKS/ KR domain CAE7944839.1	3E ⁻³⁷	Peroxisome	Yes	0.043
10844 (2)	<i>Symbiodinium sp.</i> , PKS/ KS domain CAE7839101.1	1E ⁻⁵⁰	Peroxisome		2.404
21608 (4)	<i>Symbiodinium necroappetens</i> , unnamed protein, CAE7940404.1 PKS dehydratase (CD finder)	0.0	Plastid	Yes	3.269

4.3 Materials and methods

4.3.1 General

Mass spectrometry of TMT-labeled peptides was performed by the University of Texas Southwestern Proteomics Core using an Orbitrap Fusion Lumos mass spectrometer coupled to an Ultimate 3000 RSLC-Nano liquid chromatography system in positive ion mode.

4.3.2 Culture growth conditions

K. brevis culture was grown as described in 2.3.2.

4.3.3 Fourplex IodoTMT redox proteomics of *KbHT* and *KbLT*

4.3.3.1 Generation of a *K. brevis* protein database

The protein database of *K. brevis* was generated using EMBOSS Transeq (Madeira et al., 2019). The six-frame translation of the Wilson strain transcriptome library (Ryan et al., 2014) with stop codons removed was used as the database for peptide searches in MS analysis.

4.3.3.2 Lysis, protein precipitation and quantitation

K. brevis high and low toxin (*KbHT* and *KbLT*) culture (250 mL) was harvested by centrifugation (1,000 g @ 4 °C for 10 min) in five 50 mL conical tubes, and the supernatant discarded. It is important to mention that the nature of thiols makes them prone to

oxidation, which can adulterate the results of the experiment if not properly mitigated. Therefore, a critical step in the isolation of protein from *Karenia brevis* is to freeze the *in vivo* redox status by using TCA (García-Santamarina et al., 2014) . The pellets were flash frozen in liquid nitrogen and thawed a total of 4 times before being suspended in 1 mL ice-cold 20% trichloroacetic acid (TCA) in acetone (per tube), transferred to 1.5 mL Eppendorf tubes and allowed to precipitate overnight at -20 °C. The precipitated proteins were centrifuged (17,000 g @ 4 °C for 30 min) and the supernatant discarded. The pellets were washed with 1 mL (per tube) of 80% acetone to remove residual TCA and centrifuged (17,000 g @ 4 °C for 20 min) before aspirating the supernatant. Remaining pellets were washed twice with 100% acetone in the same manner, before being allowed to air dry for 5 minutes at 50 °C.

To each tube, 40 µL of hot (50 °C) 6M guanidine-HCl was added, mixed briefly and incubated at 50 °C for 5 minutes. To each tube 40 µL of hot (50 °C) HES (50 mM HEPES, 1 mM EDTA, 0.1% SDS) was added and the suspensions were mixed by pipetting up and down and incubated at 50 °C for an additional 5 minutes. Protein solutions were centrifuged (17,000 g @ RT for 5 min) to remove cellular debris and precipitated SDS. Supernatants were pooled for each respective sample and protein concentration of a 1:20 dilution was measured using Bradford reagent against a standard curve of BSA. Typical protein concentrations were in the range of 2-3 mg/mL. Reduced cysteines were quantified by combining 80 µL of the protein solutions and 20 µL of Ellman's reagent (Ellman, 1959), or DTNB (5,5-dithio-bis-(2-nitrobenzoic acid), 10 mM in 0.1 M sodium phosphate and 1 mM EDTA, pH 8.0). Absorbance was measured immediately at 412 nm. Reduced cysteine concentrations were calculated against a standard curve of *L*-cysteine HCl and normalized

to total protein. DTNB reacts with free thiols. This result reflects the reduced cysteine residues of the precipitated proteins.

4.3.3.3 Fourplex IodoTMT labeling, trypsin digestion and enrichment of labeled peptides

Protein solutions were diluted to the same concentration (1.25 mg/mL) with HES buffer and 125 µg of protein was labeled using 200 µg IodoTMT¹²⁶ and IodoTMT¹²⁷ for *KbHT* and *KbLT*, respectively. The reaction was carried out at 37 °C in the dark for 1 hour (4 mM final concentration IodoTMT). Excess IodoTMT label was removed by adding 660 µL pre-chilled (-20 °C) acetone and stored at -20 °C for a minimum of 4 hours. After resuspension of the pellet in warm (37 °C) HES buffer (100 µL), 1 µL of 0.5 M tris(2-carboxyethyl)phosphine) (TCEP) was added to the solution and the mixture incubated at 50 °C for 1 hour. To the reduced proteins 10 µL of IodoTMT¹³⁰ and IodoTMT¹³¹ (*KbHT* and *KbLT*, respectively) was added and the reaction carried out at 37 °C in the dark for 1 hour. The reaction was quenched by the addition of DTT (final concentration 20 mM) and incubation at 37 °C in the dark for 20 minutes. Excess IodoTMT was removed by acetone precipitation (6 volumes) at -20 °C for a minimum of 4 hours. The combined, fourplex labeled proteins pellets were resuspended in 100 µL warm (37 °C) TE buffer (50 mM Tris-HCl, 5mM EDTA pH 8), in a new microcentrifuge tube and trypsinized overnight at 37 °C (7 µg trypsin:250 µg protein). The digestion was stopped by the addition of 10% TFA (pH < 3). Peptides were dried and frozen in a centrifugal evaporator.

Freeze-dried, fourplex labeled peptides were resuspended in 100 µL TBS (25 mM Tris, 0.15M NaCl, pH 7.4) and loaded onto 500 µL (1 mL slurry) of Immobilized Anti-

TMT Resin (Pierce Biotechnology). The enrichment was carried out following the manufacturer's instruction (4 °C, overnight rocking). The enriched fraction was eluted with 4 column volumes of the manufacturer's TMT elution buffer and freeze dried in a centrifugal evaporator. Peptides were stored dry at -80 °C until analysis by liquid chromatography tandem mass spectrometry (LC-MS/MS)

4.3.3.4 Mass spectrometry and data processing

Affinity purified, TMT labeled peptides underwent solid-phase extraction cleanup with an Oasis HLB plate (Waters) and the resulting samples were injected onto an Orbitrap Fusion Lumos mass spectrometer coupled to an Ultimate 3000 RSLC-Nano liquid chromatography system. Samples were injected onto a 75 µm i.d., 75-cm long EasySpray column (Thermo) and eluted with a gradient from 0-28% buffer B over 180 min. Buffer A contained 2% (v/v) acetonitrile (ACN) and 0.1% formic acid in water, and buffer B contained 80% (v/v) ACN, 10% (v/v) trifluoroethanol, and 0.1% formic acid in water. The mass spectrometer operated in positive ion mode with a source voltage of 1.8 kV and an ion transfer tube temperature of 275 °C. MS scans were acquired at 120,000 resolution in the Orbitrap and top speed mode was used for SPS-MS³ analysis with a cycle time of 2.5 s. MS² was performed with collision-induced dissociation with a collision energy of 35%. The top 10 fragments were selected for MS³ fragmentation using HCD, with a collision energy of 58%. Dynamic exclusion was set for 25 s after an ion was selected for fragmentation.

Raw MS data files were analyzed using Proteome Discoverer v2.4 (Thermo), with peptide identification performed using Sequest HT searching against the *K. brevis* protein

database. Fragment and precursor tolerances of 10 ppm and 0.6 Da were specified, and three missed cleavages were allowed. Oxidation of Met and IodoTMT6plex addition on Cys were set as variable modifications. The false-discovery rate (FDR) cutoff was 1% for all peptides.

4.3.4 Bioinformatics tools and data analysis

4.3.4.1 Functional annotation using NCBI BLASTp, NCBI CDD, Pfam and BLASTKoala

Full length protein sequences identified from the *K. brevis* protein database which IodoTMT labeled peptides were mapped were analyzed by BLASTp against NCBI's non-redundant database (nr) with taxonomy filters including SAR supergroup and cyanobacteria (TaxID: 2698737 and 1117, respectively). Functional annotation was performed manually by analyzing E-values of protein hits. Proteins were annotated by BLASTp result if E-values were $<10^{-10}$ (Altschul et al., 1990).

Analysis of conserved domains was performed by NCBI Conserved Domain Tool (Lu et al., 2020; Marchler-Bauer et al., 2011). Proteins sequences were annotated based on the highest scoring conserved domain hit with bit score > 30 . Annotations were also obtained using Pfam (Mistry et al., 2020) on hits with bit score > 25 . BLASTKoala annotations were assigned by the best KO score for putative KEGG identifiers.

4.3.4.2 Cellular localization and prediction tools

Cellular localization was determined using DeepLoc (Almagro Armenteros et al., 2017), which provides organelle predictions as well as a prediction of membrane bound

or soluble based on the hydrophobicity of the amino acid sequence. Protein sequences were analyzed in batches of 50 sequences in FASTA format using the accurate prediction option. Proteins that were too long to input into DeepLoc (> 6000 amino acids) were trimmed by removing a portion of the amino acid sequence that did not contain homology to any proteins based on BLASTp results.

Prediction of N-terminal presequences coding for cTP was done by TargetP (plant) and ChloroP. TargetP was also used to predict for mTP, SP and luTP. In addition to TargetP in plant mode, it was used in non-plant mode due to the complexity of dinoflagellate genomes containing proteins with similarity to bacterial and mammalian orthologues. SignalP was used to detect for signal peptides. Protein sequences were analyzed in batches of 200 sequences in FASTA format.

4.3.4.3 Homology model of Dde4

The amino acid sequence of Dde4 was submitted to SWISS-MODEL (Waterhouse et al., 2018) against the PDB databank. The highest scoring homology model corresponding to the lipocalin domain of *Arabidopsis thaliana* Vde at pH 5 (Accession: 3CQR, (Arnoux, Morosinotto, Saga, Bassi, & Pignol, 2009) was exported as a PDB file and visualized using NCBI iCn3D (Wang et al., 2020).

4.4 Conclusion

4.4.1 Multiplex labeling of the *K. brevis* proteome

The redox proteomes of two strains of *K. brevis* with differences in toxin production, non-photochemical quenching capabilities and ROS production were examined by simultaneous duplex IodoTMT labeling. This provided both a quantitative measure of the global differences in expression within the two proteomes as well as a unique method of quantitating the cysteinyl redoxome. This provides a measure of redox status for each protein between the two strains as it relates to the relative amount of free thiols existing in a protein. Prior to labeling, both strains' thiol content was measured using Ellman's assay (Ellman, 1959). The thiol content was found to be 0.61-fold lower in *KbHT* (Figure 4.4, $\rho = 0.026$, two-tailed, paired t-test). This is consistent with previously reported thiol differences measured in *K. brevis* high and low toxin strains which detected 0.45 - 0.66-fold lower thiol content in *KbHT* (Chen et al., 2018).

Total protein was extracted, labeled, and analyzed by LC-MS/MS for four replicates. In total 2,542 proteins were labeled and identified in the *K. brevis* protein database. 1,092 proteins were identified in at least 3 replicates, with an average expression ratio (*KbHT/KbLT*) of 1.14 and an average redox ratio of 0.80. In order to increase the statistical power of our calculations a permutation test was performed on all 2,542 proteins for both expression and redox status. Proteins with ρ -values < 0.05 for their respective permutation tests were considered to have statistically significant differences in expression or redox. For expression 254 proteins (23.3%) were found to have statistically significant differences in expression, while 411 (37.6%) had statistically significant differences in redox status. Using the cellular organelle prediction algorithm

DeepLoc (Almagro Armenteros et al., 2017) proteins were localized to their respective cellular organelle. Table 4.2 summarizes these results and Figure 4.5 demonstrates that the differences observed in redox status are consistent across cellular organelles, when comparing the global proteome (all 2,542 proteins) to those that were found in a minimum of 3 replicates, or those with permutation values < 0.05 for neither expression or redox or both.

4.4.2 Enzymes related to the xanthophyll cycle and qE

4.4.2.1 Diadinoxanthin de-epoxidase

Dde4 (Table 3.2) was the only Dde homologue identified and only in three of the four replicates (*Kb4P1*, *Kb4P3*, and *Kb4P4*). The absence of the other three Dde homologs may be due to low sensitivity of the MS/MS analysis or may be in keeping with recent findings that mRNA transcripts are not always translated in dinoflagellates (Jones et al., 2015). For all replicates in which Dde4 was identified, the same peptide (underlined in Figure 4.10) was responsible for the sole hit in the MS/MS analysis. The relative expression of Dde (light+heavy/total) in *KbHT* and *KbLT* did not differ significantly ($KbHT/KbLT = 1.13 \pm 0.549$, $\rho = 0.62$, t-test: $\rho = 0.45$, permutation test: Table 4.4). The ratios ($KbHT/KbLT$) of reduced cysteine residues as determined by DTNB assay (Figure 4.4) and the fraction of reduced Dde (light/light+heavy) as determined by MS/MS analysis of labeled peptides (0.606 ± 0.209 and 0.672 ± 0.325 respectively) were gratifyingly consistent. Furthermore, the difference in reduced Dde (light/light+heavy) for *KbHT* and *KbLT* (Table 4.5) was statistically significant ($\rho = 0.052$, permutation test) when a permutation test was applied. This consistent with

sporadic functioning of qE and the xanthophyll cycle, previously observed (Cassell et al., 2015; Chen et al., 2018).

TMT labeling occurred on Cys-254 of Dde4, which forms a disulfide bridge with Cys-388. This is the only disulfide bridge that is located outside of the cysteine rich N-terminal domain. These two cysteines flank the lipocalin domain in Dde and Vde. A homology model of the lipocalin domain and C-terminus (from Glu-234) of Dde4 using the lipocalin domain of Vde from *Arabidopsis thaliana* (PDB Accession: 3CQR, QMEAN: -3.46) as the template constructed using SWISS-MODEL (Waterhouse et al., 2018) is shown in Figure 4.19. This region of Dde4 shares similarities with other lipocalins and is believed to contain the binding site for the epoxy-xanthophyll (Arnoux et al., 2009; Saga et al., 2010). Interestingly, in all 3 plant Vde sequences shown in Fig 4.10, the corresponding residue for Cys-388 is immediately followed by a Glu-rich domain (Glu-390 for *K. brevis* Dde4) considered to be critical for pH-dependent thylakoid binding and in turn, de-epoxidase activity (Bugos & Yamamoto, 1996; Hieber et al., 2002). Reduction of a disulfide bridge in this region may influence the tertiary structure of the C-terminus, disrupting xanthophyll binding and/or association with lipids, thereby lowering de-epoxidase activity, consistent with our previously reported results of xanthophyll content in *KbLT* (Chen et al., 2018).. Comparing the number of glutamate residues that are present in Dde4 vs plant Vde shows that there are significantly fewer glutamate residues in Dde4 than expected for the Glu-rich region (6 vs 24 in Vde). This may indicate that the pH dependence of Dde4 is not as critical as in plant Vde. Indeed, Jakob and colleagues have observed unusual pH dependence in the Dde of the diatom

Phaeodactylum tricornutum which reported activity at pH values as high as 7.2 (Jakob et al., 2001).

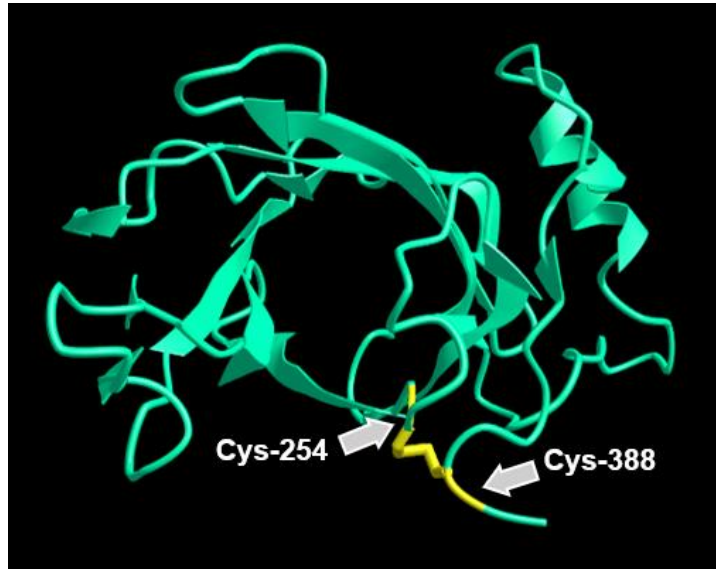


Figure 4.19 Homology model of the lipocalin domain of Dde4 based on the lipocalin domain of *Arabidopsis thaliana* Vde, indicating in yellow, the disulfide bridge formed between Cys²⁵⁴ and Cys³⁸⁸

Diatoxanthin epoxidase was also detected in one of four replicates. Both the expression ratio and redox ratio were lower in *KbHT* (0.657 and 0.592, respectively). It was only until recently that the plant orthologue zeaxanthin epoxidase (Zep) was shown to interact with Trx-*m* isoforms in *Arabidopsis*. In this study, the formation of intermolecular disulfide bonds between Zep monomers was determined to be regulated by Trx-*m*, since Trx-*m* triple silenced mutants had inhibited Zep activity (Da et al., 2018). However, prior to this no reports of thiol-based redox regulation had been reported for neither Zep or Dep (Naranjo et al., 2016).

4.4.2.2 MGDG synthase

The expression of MGDG synthase in the two cultures was similar (*KbHT/KbLT* = 1.10 ± 0.443 , $\rho = 0.16$, t-test: $\rho = 0.44$, permutation test: Table 4.4). However, in the

three samples where MGDG synthase was detected, it was more reduced in *KbLT* (0.731 ± 0.213 , $\rho = 0.070$, t-test: $\rho = 0.005$, permutation test: Table 4.5). This finding is consistent with higher levels of MGDG lipids as MGDG synthase activity is activated by reduction via Trx in vitro (Geigenberger & Fernie, 2014; Nakamura et al., 2010; Yamaryo et al., 2006). The MGDG content was in fact 30% higher in *KbLT*, while the redox status of MGDG synthase for *KbLT* was 39% more reduced (Figure 3.2B). Interestingly, the DGDG content was not also increased in *KbLT*, this is strange because MGDG is a precursor to DGDG. On the other hand, the activity of DGDG synthase is regulated by other mechanisms (Shimajima et al., 2011) not having been

4.4.3 Select plastid targeted proteins

4.4.3.1 Thiol oxidoreductases

Thioredoxins, glutaredoxins, peroxiredoxins, as well as their respective reductases all play critical roles in maintaining redox homeostasis within the photosynthetic organisms. The detoxification of reactive oxygen species by these oxidoreductases helps prevent photooxidative damage to cellular organelles and participate in regulation of thiol-disulfide exchange (Kang & Wang, 2016; Pérez-Ruiz et al., 2017; Simionato et al., 2015). Redox proteomics experiments found that the expression of Trx was not significantly different ($\rho = 0.86$, two tailed, paired t-test), although it was higher on average in *KbHT*. However, the redox status of Trx was significantly different, ranging from 16 – 63 % more reduced in *KbLT* ($\rho = 0.006$). For TrxR, expression was higher in *KbLT*, but not significantly. However, this does seem to correlate with the observation of more reduced Trx in *KbLT*, as an increase in TrxR expression could lead to increased Trx

reduction downstream. It is important to note that although Trx was more reduced in all instances in *KbLT*, we did not see a significant difference in TrxR redox status between the two strains. We do however, see that the entire proteome of *KbLT* is existing in a more reduced state, and does correlate well with the observation of more reduced Trx.

Peroxiredoxins were also observed in our redox proteomics experiment. These ROS scavenging proteins were not detected to be significantly more expressed or more reduced in either of the two strains. Similarly, glutaredoxins were not found to be significantly more highly expressed in *KbHT* ($\rho = 28$), although their expression ranged from 21 – 70% higher in *KbHT*. Moreover, they were also found to be more reduced in *KbLT* on average, albeit not significantly ($\rho = 0.12$). It is likely that large variations in the absolute redox status, and expression coupled with the small sample size inhibit the efficacy of the t-test, limiting the scope of this interpretation of their significance.

Glutathione reductase was found to be similarly expressed on average, with no significant difference between the two strains ($\rho = 0.48$). However, the redox status was found to be significantly different for both the plastid targeted and non-plastidic GR ($\rho = 0.001$). This implies that *KbLT* may experience more glutathione reductase activity, consistent with the findings of our DTNB assay (Figure 4.4) as GSH is the most abundant non-protein thiol in cells (Aoyama & Nakaki, 2015).

4.4.3.2 Kinases and phosphatases

Kinases and phosphatases provide a mechanism for critical post translation regulation of protein activity. Photosynthetically involved kinases such as Stt7 are required for the reversible phosphorylation of LHC-II upon far red illumination to induce

conformational change to improve light harvesting abilities of PS-II. The reverse reaction, the dephosphorylation of P-LHC-II is performed by the thylakoid associated phosphate/protein phosphatase 1 (TAP38/PPH1) under high light (Rantala, Lehtimäki, Aro, & Suorsa, 2016).

In our redox proteomics experiments protein kinases on average were not differentially expressed ($\rho = 0.53$). Surprisingly however, it was observed that 42 of 44 peptides which mapped to proteins with high homology to kinases were more reduced in *KbLT* ($\rho = 2.84 \text{ E}^{-12}$). *Stt7*, a plastidic kinase, activity is redox regulated by both thiol/disulfide exchange as well as the plastoquinone pool (Rochaix et al., 2012; Wu et al., 2021). *LTO1*, a lumenal oxidoreductase with a thioredoxin domain has been shown to regulate the activity of *Stt7* by oxidation of cysteine residues to form either intra- or inter-molecular disulfides with other monomers. The detection of kinases with a much higher proportion existing in a reduced state may result in an inability of *Stt7* to effectively phosphorylate LHC-II, which uncouples it from PS-II under low light conditions (Lemeille et al., 2009). Interestingly, under low light conditions *PbTx-2* has been shown to bind to a Trx-like protein. It is possible that *PbTx-2* binding to a Trx-like protein may influence the redox regulation of *Stt7* under low light conditions, by affecting the cascade of electrons conferred from Trx. The low toxin concentration of *KbLT* may not be able to influence Trx in this way and may result in higher levels of reduced *Stt7*, inactivating the enzyme. This may inhibit the photosynthetic efficiency of *KbLT* by preventing efficient light harvesting at PS-I by the binding of P-LHC-II under low light conditions. Presumably, the inability to uncouple LHC-II from PS-II may result in photooxidative

damage to LHC-II and PS-II, which is consistent with the increased ROS production observed in *KbLT* (Cassell et al., 2015; Lemeille et al., 2009).

One peptide which mapped to an ADK in our transcriptome library was identified as one of the most overexpressed in *KbHT*, as well as one of the most reduced in *KbHT*. ADKs are responsible for the conversion of 2 adenosine diphosphate (ADP) \leftrightarrow ATP + adenosine monophosphate (AMP). ADKs play an important role in balancing the energy consumption and production and are postulated to play a role in the NADPH dependent activity of glyceraldehyde-3-phosphate dehydrogenase (GAPDH). When oxidized ADK from *C. reinhardtii* has been shown to inhibit the NADPH consumption of GAPDH *in vitro*, similar to that of an intrinsically disordered protein (CP-12) which it shares > 70% identity including C-terminal conserved cysteine residues (Thieulin-Pardo et al., 2016). Like CP-12 it has been shown to stabilize GAPDH against thermal degradation. It is possible that overexpressed and reduced ADK in *KbHT* may be utilized to increase NADPH consumption by GAPDH, this can provide an electron sink during light limiting photosynthesis and facilitate CO₂ assimilation when ATP synthesis may be limited by the lack of light energy (Zhang, Launay, Liu, Lebrun, & Gontero, 2018).

Similar to kinases, plastid targeted phosphatases also had no significant difference on average for expression ($\rho = 0.30$). These same phosphatases were found to exist in a significantly more reduced state in *KbLT*, with 23 out of 25 peptides which mapped to phosphatases being more reduced ($\rho = 2.10 \text{ E}^{-6}$). Phosphatases are known to have redox regulation that can influence the activity of catalytic cysteine residues which may be sensitive to oxidation (Salmeen & Barford, 2005). Reduced cysteine residues in

phosphatases in *KbLT* may result in increased activity, however it is unclear the role that this may play for *K. brevis*.

4.4.4 Polyketide synthases

4.4.4.1 Polyketide synthases are overexpressed in *KbHT*

Over the past two decades, numerous polyketide biosynthetic pathways from bacteria and fungi have been identified at the genomic level, cloned, (Beedessee et al., 2019) and expressed in heterologous hosts. These developments have made few inroads into the study of polyketide biosynthesis by dinoflagellates. The slow progress can be largely attributed to two main factors: the large size and organization of the dinoflagellate genome and the lack of a general transformation system. Dinoflagellate genomes range from 1-270 Gbp (LaJeunesse, Lambert, Andersen, Coffroth, & Galbraith, 2005) and are composed of high copy number of genes, often arranged into tandem repeats of up to 5,000 copies (Beauchemin et al., 2012; Le, Markovic, Hastings, Jovine, & Morse, 1997).

The genomes of *Symbiodinium* sp. which are comparatively smaller than those of other dinoflagellates and have recently become available, have been shown to harbor PKSs (Beedessee, Hisata, Roy, Satoh, & Shoguchi, 2015; Beedessee et al., 2018, 2019) and a partial PKS pathway was identified by screening of a genomic library of an *Amphidinium* sp (Kubota, Inuma, & Kobayashi, 2006). None of the genes could be definitively linked to a particular polyketide product as the challenge of working with the dinoflagellate genome remains an obstacle to genetic/molecular studies. Dinoflagellate biologists have turned to transcriptomics. While, differences in expression of PKS genes

at the mRNA level between toxic and non-toxic strains of *Gambierdiscus* (Van Dolah et al., 2020; Wu et al., 2020), PKS transcripts were not differentially expressed in toxic vs non-toxic strains of *K. brevis* (Monroe et al., 2010). Given that gene expression in dinoflagellates is believed to be regulated at the translational level (Jones et al., 2015; Morey & Van Dolah, 2013; Roy et al., 2018; Roy & Morse, 2013) comparative proteomics of toxic and non-toxic strains of dinoflagellates may prove a more useful strategy for identify toxin related PKS candidates in dinoflagellates.

Herein we have identified nineteen peptide fragments which mapped to proteins having high homology to polyketide synthases. Of these nineteen, thirteen were expressed more highly in *KbHT* ($\rho = 0.019$). Although this was not an initial aim of this research, it is significant to note that this is the first ever record of high toxic and low toxic *K. brevis* differing in expression of polyketide synthases at the translational level. The data herein lays the groundwork for comparative proteomics in toxic and non-toxic dinoflagellates. It may possibly lead to new avenues of anti-PKS antibody design for detection of toxic variants of *K. brevis* or other polyether ladder toxin producing dinoflagellates. Furthermore, although the biosynthetic pathway for polyether ladder toxins has yet to be elucidated it supports the previously disputed origin of PbTx-2 deriving from a PKS pathway. There was a significant difference in redox status ($\rho = 0.01$), with *KbLT* being more reduced. However redox regulation of PKS has not been investigated, so the observation that *KbLT* contains more reduced cysteine residues in PKS is not clear.

Chapter 5. Expression of recombinant *K. brevis* NTR and characterization of its enzymatic activity in the presence of PbTx-2

Objective

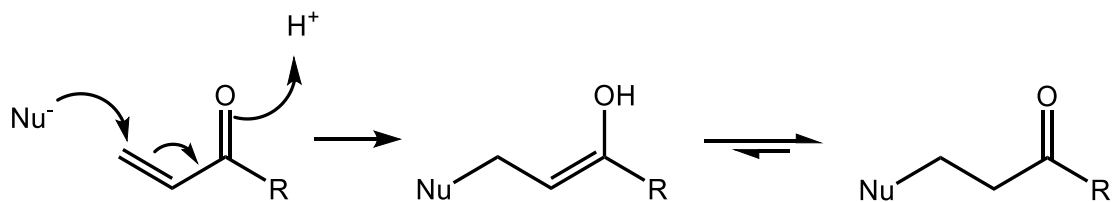
Brevetoxin (PbTx-2) has been previously shown to bind not only to LHC-II under acidic conditions simulating high-light, but to residues which appear to belong to a thioredoxin like protein under conditions of low-light (high pH). This observed interaction with a redox-active protein indicates that PbTx-2 may play a role in redox homeostasis. The objective is to clone a native *K. brevis* NTR and to characterize the effect of brevetoxin (PbTx-2) on the enzyme's activity to gain insight into the role that brevetoxin may be playing in redox homeostasis.

5.1 Thioredoxin reductase activity is influenced by α , β -unsaturated carbonyl containing compounds and other electrophiles

Recently we investigated the effects of α , β -unsaturated carbonyl compounds, including PbTx-2, on TrxR homologs/orthologs and semisynthetic mutants from organisms ranging from mammals to protists such as *Drosophila melanogaster* (*DmTrxR*) and *Plasmodium falciparum* (*PfTrxR*) (Tuladhar, Hondal, Colon, Hernandez, & Rein, 2018). These enzymes contain several different C-terminal redox centers from both the type I (xCC/Ux) and type II (CxxxxC) high MW categories. The mutants of the respective enzymes contain either functionally inactive (dead-tails) C-terminal redox centers (replacement of cysteine residues with serine (i.e xSSx), truncated C-termini (removal of either the last 7 or 8 amino acids, indicated by $\Delta 7$ or $\Delta 8$ respectively), replacement of xCUx residues by xCCx residues, and vice versa or in the case of *PfTrxR*,

which normally contains a type II C-terminus (GCGGGKCG), a chimeric type I enzyme (GCC/UG) was developed. It was observed that the effect of PbTx-2 on various TrxR mutants was dependent on the ortholog and substrate. In this way PbTx-2 is an unusual mediator of TrxR activity.

When reduced, the type I C-terminus containing Sec (type Ia) has strong intrinsic nucleophilicity which makes it susceptible to alkylation by electrophiles, such as α , β -unsaturated carbonyl containing compounds. This reaction creates a 1,4-addition product which can inactivate the C-terminal redox center (Scheme 5.1). Such compounds include curcumin (Jayakumar, Patwardhan, Pal, Sharma, & Sandur, 2016) quinones (Cai et al., 2012; Citta et al., 2014) and 4-hydroxy-2-nonenal (Ansari, Pendurthi, & Rao, 2017).



Scheme 5.1 Mechanism of a 1,4 addition of a nucleophile to an α , β unsaturated carbonyl. Nu⁻ represents the nucleophilic thiolate or selenolate (S⁻ or Se⁻) in TrxR.

5.1.1 Brevetoxin is an effector of mammalian thioredoxin reductase

PbTx-2 contains an α , β -unsaturated carbonyl functionality that is capable of acting as a Michael acceptor in a 1,4 addition of a nucleophile. In fact, it has been known for some time that the cellular mechanisms of brevetoxin detoxification involve the formation of cysteine and glutathione conjugates via 1,4 addition to this side chain (Radwan, Wang, & Ramsdell, 2005; Walsh et al., 2009). PbTx-2 inhibits the reduction of

H₂O₂ and human Trx by rat cytosolic TrxR-1 (rTrxR-1) with an IC₅₀ of 25 μM (Chen et al., 2017b; Tuladhar et al., 2018). The reduction of both of these substrates requires an intact C-terminal redox center (Zhong & Holmgren, 2000). While PbTx-2 reacts readily with selenocysteine (Chen et al., 2017a), efforts to identify a PbTx-2/rTrxR-1 adduct by LC-MS/MS have been unsuccessful as the C-terminal redox center is difficult to observe.

The hypothesis that PbTx-2 reacts with the C-terminal selenocysteine of TrxR is supported by experiments using the selenol selective probe, Sel-green (Zhang et al., 2015). The Sel-green probe undergoes nucleophilic aromatic substitution in the presence of a selenol, releasing a fluorescent coumarin reporter (Figure 5.1). Preincubation of PbTx-2 with rTrxR-1 reduces the fluorescence by >80% relative to the rTrxR-1 in the absence of PbTx-2 (Chen et al., 2017b).

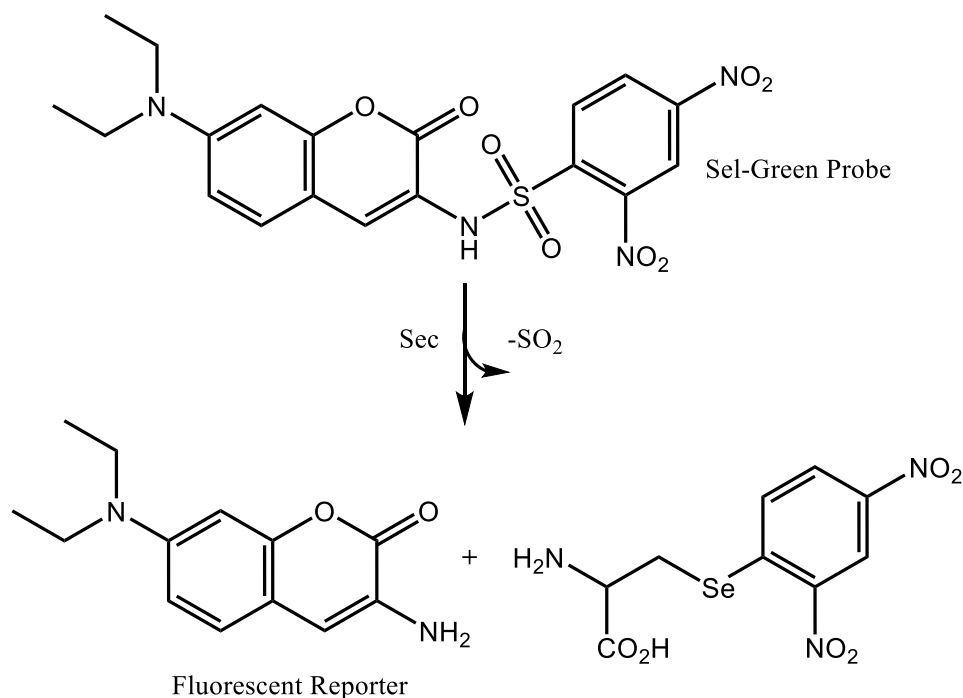


Figure 5.1 Sel-green probe reaction with selenocysteine (Sec) generates a fluorescent coumarin derivative. The inhibition of this reaction in the presence of PbTx-2 provides evidence of the reactivity of PbTx-2 with Sec residues.

PbTx-2 activates the reduction of some substrates. The reduction of DTNB by rTrxR-1, mouse mitochondrial TrxR (mTrxR-2) and mTrxR-2 mutants, as well as those of DmTrxR and PfTrxR is activated in the presence of PbTx-2. This is thought to be due to a reaction at the C-terminal redox center resulting in a conformational change which exposes the N-terminal redox center making it accessible to smaller substrates. PbTx-2 also increases the rate reduction of Trx by mTrxR-2 the opposite result when compared to rTrxR-1. PbTx-2 induced NADPH oxidase activity in dead tail and truncated mutants of mTrxR-2 as well as both the wild type rTrxR-1 and mTrxR-2 (Tuladhar et al., 2018). This activity originates from the N-terminal redox center when the C-terminal is inactive PbTx-2's effect on other TrxRs is both enzyme and substrate dependent, making it impossible to predict how it would behave towards *KbTrxR* (Lothrop, Snider, Ruggles, & Hondal, 2014). Thus, it was decided to clone and express *KbTrxR* in order to explore the effects of PbTx-2 on *K.brevis* plastid TrxR.

5.1.2 Semisynthesis of TrxR variants allows for exploration into the functionality of the C-terminus

The cloning and expression of selenoproteins is complicated by the requirement for the biosynthetic machinery that directs the incorporation of the selenocysteine residue. An alternative approach to the expression of Sec-containing TrxRs involves the application of inteine mediated semisynthetic methods to incorporate the Sec residue into the C-terminus of TrxR. In the process, one is also able to generate a truncated mutant,

which lacks a C-terminus, and facilitates characterization of the requirement for a C-terminal redox center on the enzymatic activity of the enzyme.

In short, the truncated version of the TrxR variant is cloned using the IMPACT Kit (Figure 5.2) from New England Biolabs (Evans Jr., Benner, & Xu, 1998) An expression vector containing an inducible T7 promoter, and an intein tag (a fusion protein with inducible self-cleavage bound to a chitin binding domain (CBD) which serves as an affinity tag). Once the protein expression has been optimized, the fusion protein is captured on a chitin affinity resin (step 1). Other extraneous proteins are not retained. A thiol containing cleavage reagent such as 2-mercaptoethanol (BME), or N-methyl mercaptoacetamide (NMA) is used to cleave the intein + CBD tag from the truncated TrxR as a C-terminal thioester (step 2). A full-length protein is then prepared by transthioesterification with the C-terminal cysteine containing tripeptide (step 3). This is followed by a spontaneous S to N acyl migration to create the C-terminal redox center, or mutants as desired (step 4).

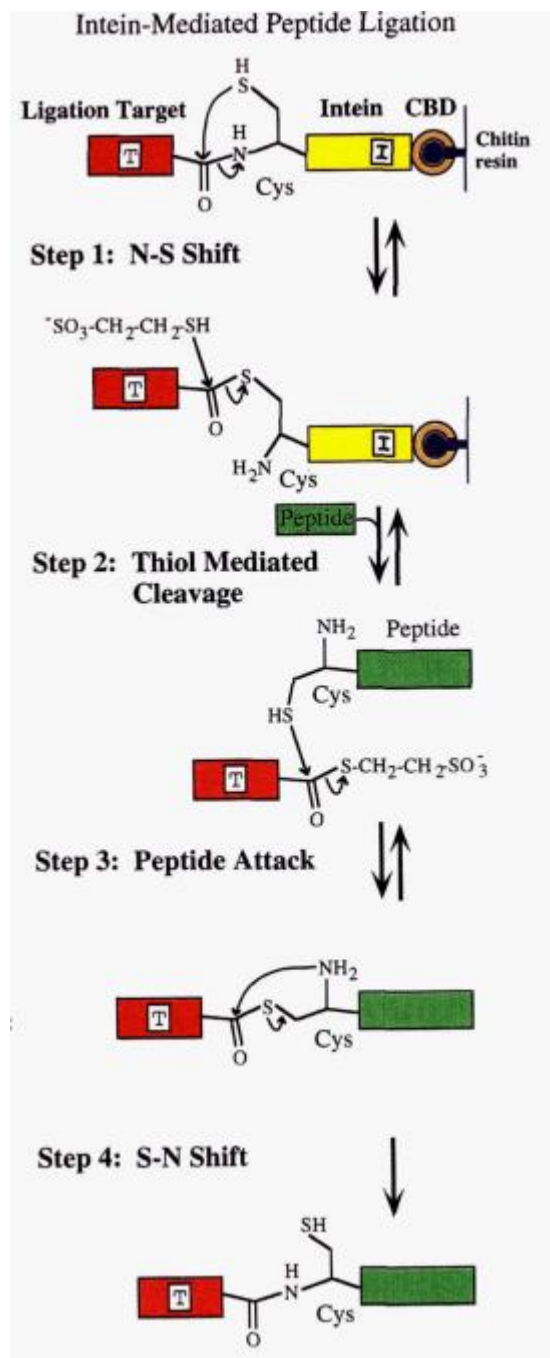


Figure 5.2 Intein mediated peptide ligation technique used to prepare TrxR. (Evans Jr, Benner, & Xu, 1998)

5.2 Results and Discussion

5.2.1 Optimization of recombinant *KbTrxR* expression

KbTrxR was prepared via semi-synthesis following the method described for mouse TrxR-2 (Eckenroth, 2006). Both the PTXB3 and PTYB3 vectors (NEB) were utilized to express *KbTrxR*. PTXB3 contains an C-terminal intein from *Mycobacterium xenobi* + CBD, while PTYB3 uses a C-terminal intein from *Saccharomyces cerevisiae* + CBD. The fusion proteins consisting of truncated *KbTrxR*, in which the three C-terminal residues (Cys-Sec-Ser) are missing, the intein and CBD were expressed in T7 Express cells (NEB). Induction of expression was initiated at OD ~0.6 and performance was compared between the two vectors. The *KbTrxR*+PTXB3 did not show significant expression when induced by 0.5 mM IPTG at either 16°C or 37°C (Figure 5.3). *KbTrxR*+PTYB3 was induced under the same conditions, as well as an additional treatment of a 5 min 42°C heat shock upon addition of IPTG for the 16°C growth treatment. Expression of the fusion protein in the PTYB3 vector showed much more promising results, especially at a 16°C growth, without heat shock (Figure 5.3). The cells were grown at 16°C for 20 hours before being harvested by centrifugation and lysed via French press. Prior to purification the lysate was centrifuged again, and the supernatant was further processed.

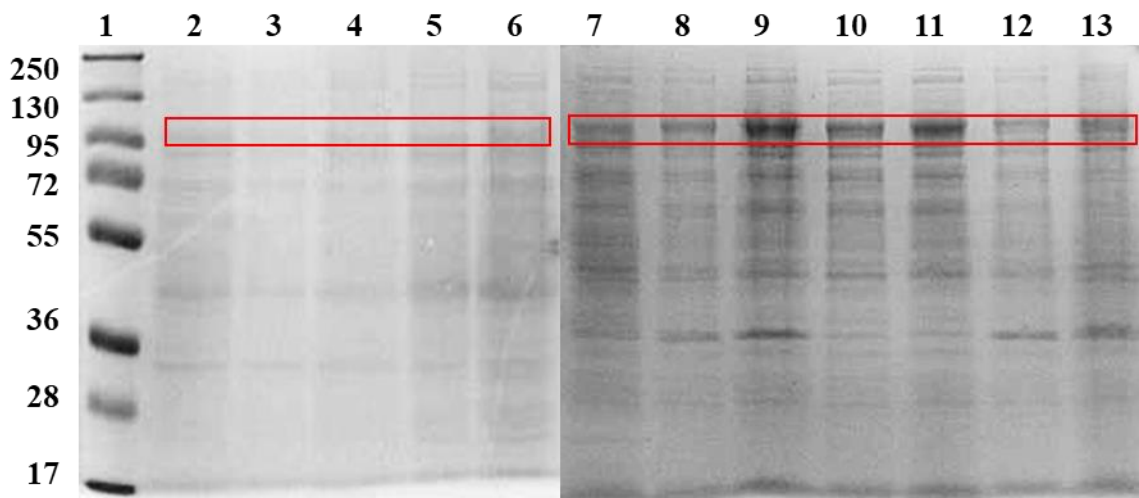


Figure 5.3 SDS-PAGE of PTXB3 (2-6) and PTYB3 (7-13) +KbTrxR expressed in T7 Express cells. 1: MW Ladder, 2: PTXB3 uninduced cells, 3: whole cell 16°C, 4: lysate 16°C, 5: whole cell 37°C, 6: lysate 37°C. 7: PTYB3 uninduced cells, 8: whole cell 16°C, 9: lysate 16°C, 10: whole cell 37°C, 11: lysate 37°C, 12: whole cell 16°C+heatshock, 13: lysate 16°C+heatshock.

Supernatant containing the fusion protein was captured on a chitin-agarose column, the inclusion of a thiol in the cleavage buffer induces excision of the intein and elution of a C-terminal thioester. Prior to cleavage 100 μ L resin was separated to compare cleavage efficiency between conditions (Figure 5.4A). Either 100 mM NMA or 100 mM BME was used at both RT and 37 °C. 100 μ L of resin from each condition (4 total) was saved for comparison of cleavage conditions on an SDS-PAGE (Figure 5.4B).

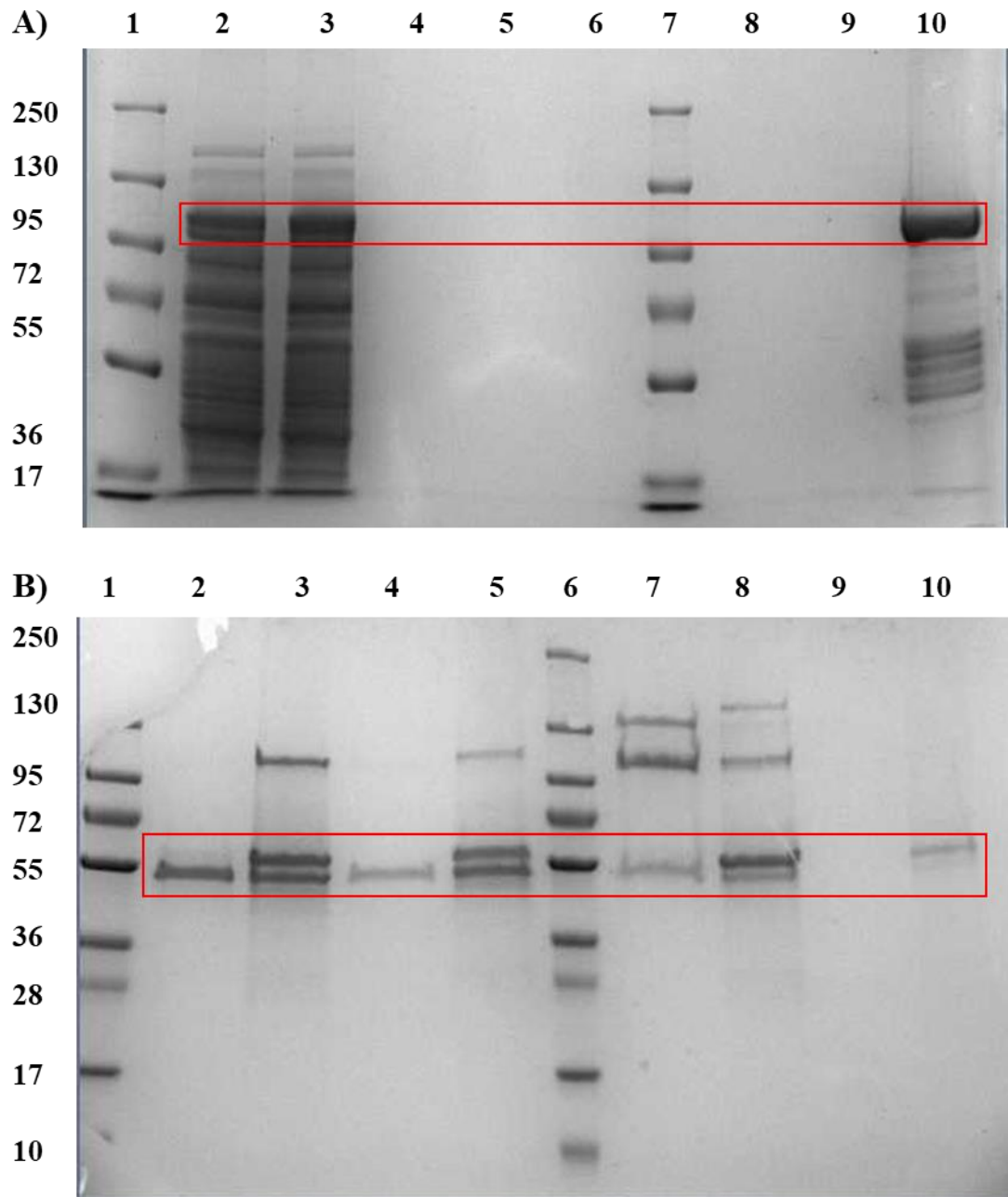


Figure 5.4 **A)** Pre-cleavage fractions of chitin agarose column. 1: MW Ladder, 2: Flow-through, 3-6: washes with Chitin Buffer , 7: MW Ladder, 8-9: washes with Chitin Buffer B, 10: Chitin resin pre-cleavage fraction. Red box signifies the fusion protein ~110 kDa. **B)** Post-cleavage fractions of chitin agarose column. 1: MW ladder, 2: Cleavage with BME (RT), 3: Resin fraction BME (RT), 4: Cleavage with BME 37°C, 5: resin fraction BME (37), 6: MW Ladder, 7: Cleavage with NMA (RT), 8: Resin fraction NMA (RT), 9: Cleavage with NMA 37°C, 10: resin fraction NMA (37).

Eluant was collected and purified via centrifugal filtration as the truncated *KbTrxR*($\Delta 3$). The absorbance spectra of the purified protein, which was yellow in color, was measured and found to contain the characteristic absorbance maxima ($\lambda_{\max} = 460 \text{ nm}$) of a flavoprotein (Figure 5.5). The concentration was determined using the molar extinction coefficient of FAD ($\epsilon = 11.3 \text{ mM}^{-1} \text{ cm}^{-1}$). A C-terminal tripeptide was installed by transesterification of the thioester with tripeptide Cys-Sec-Gly. This is followed by the spontaneous S to N acyl migration of the protein to the N-terminal residue of the tripeptide leading to full length *KbTrxR*.

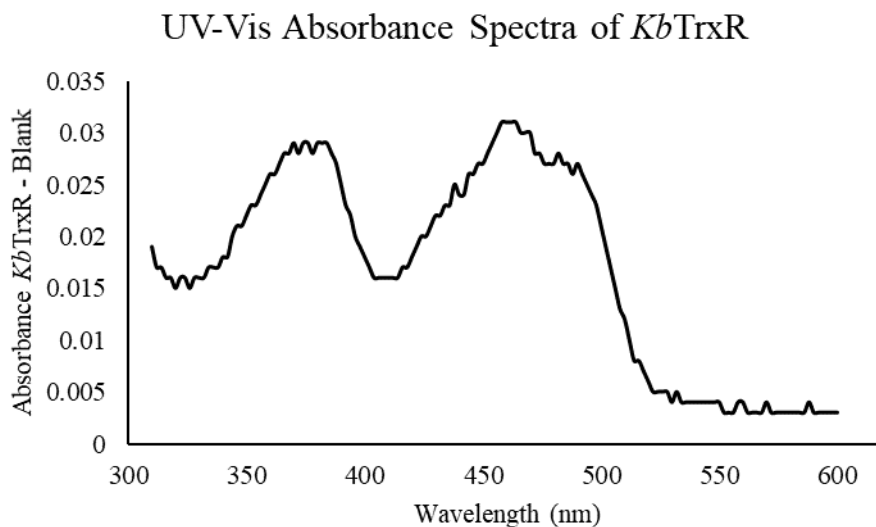


Figure 5.5 Absorbance spectra of purified *KbTrxR* shows the characteristic $\lambda_{\max} = 460 \text{ nm}$.

5.2.2 Inhibition assays with *KbTrxR* and *PbTx-2*

The activity of *KbTrxR* towards the reduction of DTNB, H_2O_2 , Trx and GSSG was evaluated in the presence of $40 \mu\text{M}$ *PbTx-2* (Table 5.1). When reduced *KbTrxR* is pre-incubated with *PbTx-2* (1 hour) the initial rates (v_0) of reduction of DTNB, H_2O_2 , Trx and GSSG are reduced by 44.7, 39.6, 34.0 and 32.5% respectively. DTNB reduction by

KbTrxR($\Delta 3$) was inhibited by 20.7%. *PbTx-2* exhibited a dose dependent inhibition of H_2O_2 reduction with an IC_{50} of $56.0 (\pm 4.67) \mu M$ (**Figure 5.6**).

Table 5.1 Initial rates (v_0) of reduction of substrates by *KbTrxR* in the presence and absence of *PbTx-2* ($40 \mu M$)

Enzyme	Substrate	mol/min-mole		% inhibition	ρ
		Control	<i>PbTx-2</i>		
<i>KbTrxR</i> (CUG)	DTNB	3519 ± 338	1947 ± 362	44.7%	$5.3 E^{-3}$
	H_2O_2	234.5 ± 6.3	141.5 ± 13.9	39.6%	$7.7 E^{-3}$
	hTrx	3.70 ± 0.55	2.45 ± 0.30	34.0%	$4.5 E^{-4}$
	GSSG	4.13 ± 0.19	2.78 ± 0.048	32.5%	$2.9 E^{-4}$
<i>KbTrxR</i> ($\Delta 3$)	DTNB	1349 ± 71	1070 ± 83	20.7%	0.011

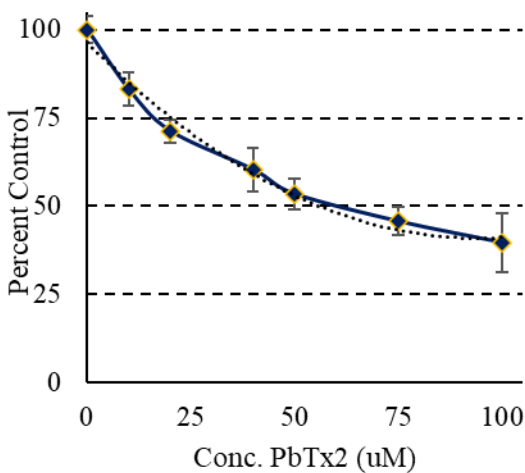


Figure 5.6 *PbTx-2* exhibits a dose dependent inhibition of H_2O_2 reduction by *KbTrxR*. $IC_{50} = 56.0 (\pm 4.67) \mu M$

5.2.3 *KbTrxR* forms a covalent adduct with PbTx-2 at the N-terminal redox center

It is interesting to note that PbTx-2 behaves differently towards rTrxR-1 with respect to reduction of the small disulfide molecule DTNB. While PbTx-2 inhibits DTNB reduction by *KbTrxR*, it activates reduction by rTrxR-1 (Chen et al., 2017a; Tuladhar et al., 2018) To establish the molecular basis for these disparate effects, we sought to determine if PbTx-2 could form a covalent adduct with *KbTrxR* and to identify the site(s) of adduction.

Reduced *KbTrxR* was incubated for 1 h with an excess of PbTx-2 (17-fold) after which the reaction mixtures was treated with NaBH₄ to reduce and stabilize any adducts that may have formed, and the enzyme was subjected to SDS PAGE. The band was excised from the gel, subjected to in-gel trypsin digestion and treated with iodoacetamide (IAC). LC-MS/MS analysis of the peptide mixture provided 90% coverage of *KbTrxR*. We had anticipated alkylation with PbTx-2 on the Sec (U) residue of the C-terminal peptide (VDDKGPAAATGGCUG). However, this peptide, either modified or unmodified, was not observed in either sample. Table 5.2 lists the identified peptide for *KbTrxR*, the *m/z*, the mass and the Δ (ppm) from the predicted mass. A single adduct was found in *KbTrxR* on Cys⁵² (Figure 5.7). Cys⁵² is one of two cysteine residues that make up the N-terminal redox center, the other being Cys⁵⁷. Adduction at this site will inhibit all activities of TrxR. It is perhaps noteworthy that the inhibition of DTNB reduction of by *KbTrxR*(Δ 3) is only half that of the full-length enzyme. This suggests that another site may be affected by PbTx-2, possibly the C-terminal Sec. We are unable to rule out this possibility as the C-terminal peptide was not identified. We do however, have indirect

evidence that the C-terminal Sec residue is compromised in rTrxR-1 which may also be the case for *Kb*TrxR (Chen et al., 2017a).

Table 5.2 Brevetoxin adducted peptides in tryptic digest of *Kb*TrxR

<i>Kb</i> TrxR	m/z (charge)	Mass	Peptide and adduct	ppm
Cys ⁵²	1023.5162 (3)	3067.5267	PSPAGTTWGLGGTC*VNVGC8IPK+896 (PbTx-2+2H)	-5.6

8Carbamidomethyl (+57)

*PbTx-2 modified

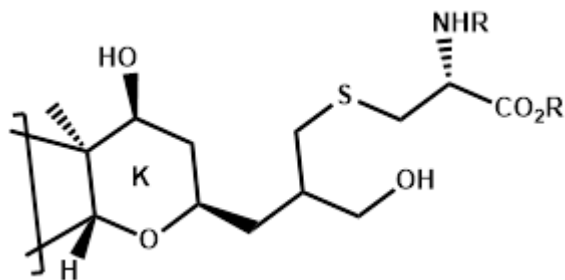


Figure 5.7 Cysteine adduct formed by *Kb*TrxR and PbTx-2 via Michael addition followed by reduction with NaBH₄

5.3 Materials and methods

5.3.1 General

Synthetic gene encoding *KbTrxR*, optimized for expression in *E. coli* and cloned into pUC57 was obtained from Genscript (Piscataway, NJ). IMPACT™ (Intein Mediated Purification with an Affinity Chitin-binding Tag) kit, restriction endonucleases *NcoI*, *SapI*, *EcoRI*, Vent DNA polymerase, T4 DNA ligase, and reaction buffers were supplied by New England Biolabs (Beverly, MA). Phusion High Fidelity PCR Master Mix, Taq polymerase, were purchased from ThermoFisher (Waltham, MA). TopoTA cloning kit and PCR primers were purchased from Invitrogen (Waltham, MA). Human thioredoxin (hTrx) and oxidized glutathione (GSSG) were supplied by Cayman Chemical (Ann Arbor, MI). Other reagents were purchased either from ThermoFisher or Sigma-Aldrich (St. Louis, MO). DNA sequencing was performed by Eurofins (Louisville, KY). Electrophoresis was performed using a mini-Protean electrophoresis system with pre-cast gradient acrylamide gels purchased from BioRad (Hercules, CA).

5.3.2 Cloning of *KbTrxR*

A *K. brevis* (Wilson strain) transcriptome library consisting of 86,580 predicted transcripts (Ryan et al., 2014) was searched by tBLASTn (Altschul et al., 1990) using a high Mr selenocysteine containing TrxR from the coccolithophore *Emiliania huxleii* (NCBI Accession number BAH20464.1) as the query. Locus 29890 of the library was returned with an expect value of $4e^{-141}$. Inspection of this locus revealed a polycistronic mRNA encoding 5 thioredoxin reductases (ORF1-5). The second ORF ends with UGC

UGA AGC UAA (Cys-Sec-Ser-Stop). The UGA codon for Sec is found at position 1453 of ORF2. After optimization of the codon usage for expression in *E. coli* and mutation of the Sec to Cys residue (TGA →TGC), the putative *K. brevis* TrxR gene was synthesized, cloned into the EcoR1 and BamH1 cloning sites of pUC57. *KbTrxR* was amplified by PCR using the Phusion High Fidelity PCR Master Mix with primers incorporating *NcoI* (forward) and *SapI* (reverse) restriction sites for in frame, directional cloning into the pTYB3 plasmid. The PCR product was purified using a PCR Kleen spin column (BioRad). 3'-A overhangs were added to the PCR product using *Taq* polymerase (1 hr at 55°C) after which it was ligated into a pCR2.1 vector following the manufacturer's instructions. Top10 *E. coli* cells were transformed with the resulting vector following the manufacturer's instructions, plated on an LB agar plate with ampicillin (100 mg/mL) and incubated for 15 h at 37 °C. A single colony was used to inoculate 10 mL of LB broth supplemented with ampicillin (100 mg/mL) and cultured 15 h at 37 °C. Plasmids were isolated from the overnight culture (QIAprep mini prep kit). Isolated plasmid was digested with *EcoR1* (2 h at 37°C). The purified *KbTrxR* band and the pTYB3 vector were digested with restriction enzymes *NcoI* and *SapI* (2 h at 37°C) followed by purification using a Qiagen spin column. The digested *KbTrxR* and pTYB3 were ligated with T4 DNA ligase (16 h at 16°C) followed by heat inactivation of the ligase (30 min at 70 °C). To the ligation reaction was added *SalI* (30 min at 37 °C) which digests only the uncut pTYB3 vector. The pTYB3-*KbTrxR* vector was transformed into competent *E. coli* (DH5α) and plasmids isolated as previously described (Eckenroth et al., 2006). The vector was sequenced using a T7 forward primer and an intein specific reverse primer to ensure the desired product was obtained.

5.3.3 *KbTrxR* inhibition assays

A stock solution of PbTx-2 (1.1 mM in 0.7% Brij in DMSO) was prepared for inhibition assays. Assays and pre-incubations were performed at ambient temperature in 384 well plates. All solutions were prepared in assay buffer (100 mM K₃PO₄, 2 mM EDTA pH 7) unless otherwise noted. Absorbance measurements were taken using a Synergy® 2 (Biotek Instruments, Inc.) microplate reader. Vehicle without PbTx-2 was added to control samples. The results of inhibition assays are represented as the average of three trials ± standard deviation.

5.3.3.1 DTNB reduction

PbTx-2 (50 μM), *KbTrxR* (7.04 nM) or *KbTrxR*(Δ3) (37.5 nM) and NADPH (64 μM) were incubated for 60 min. The reaction was initiated by the addition of DTNB (20 μL, 10 mM in 100 mM NaH₂PO₄, 1 mM Na₂EDTA pH 8.0) to 80 μL of the *KbTrxR*/PbTx-2 mixture. The absorbance at 412 nm was monitored for 5 minutes in 30 second intervals. Final concentrations: *KbTrxR* (5.6 nM), *KbTrxR*(Δ3) (30 nM) PbTx-2 (40 μM), NADPH (51 μM), DTNB (2 mM).

5.3.3.2 H₂O₂ reduction

PbTx-2 (concentrations: 125, 93.8, 62.5, 50.0, 25.0, and 12.5 μM) was incubated with a mixture of *KbTrxR* (50 nM) and NADPH (187 μM) for 60 min. To this reaction mixture (80 μL) was added 20 μL H₂O₂ (250 mM). The absorbance at 340 nm was monitored for 15 minutes in 1 min intervals. Final concentrations: *KbTrxR* (40 nM), PbTx-2 (100, 75, 50, 40, 25, and 10 μM), NADPH (150 μM), H₂O₂ (50 mM).

5.3.3.3 Trx reduction

A mixture of PbTx-2 (57 μM), *KbTrxR* (286 nM) and NADPH (305 μM) was incubated for 60 min at ambient temperature. To this mixture (70 μL) was added hTrx-insulin (30 μL , 3.33 μM hTrx, 333 μM insulin). The absorbance at 340 nm was monitored for 5 minutes in 30 second intervals. Final concentrations: *KbTrxR* (200 nM), PbTx-2 (40 μM), NADPH (213 μM), hTrx (1 μM), insulin (100 μM).

5.3.3.4 GSSG reduction

PbTx-2 (50 μM) was incubated with a mixture of *KbTrxR* (1.23 μM) and NADPH (308 μM) for 60 min. To this solution (80 μL) of the reaction mixture, GSSG (20 μL , 10 mM) was added and the absorbance at 340 nm was monitored for 30 min in 3 min intervals. Final concentrations: *KbTrxR* (1 μM), PbTx-2 (40 μM), NADPH (246 μM), GSSG (2 mM).

5.3.3.5 Preparation of PbTx-2/*KbTrxR* adducts

A solution of *KbTrxR* (4.73 μM), PbTx-2 (80.8 μM) and NADPH (592 μM) was incubated for 30 min at ambient temperature in reaction buffer (500 mM NaH_2PO_4 , 10 mM EDTA, pH 7). A stock solution of PbTx-2 (2.1 mM in DMSO with 0.3% Brij) was used to prepare this solution such that the DMSO concentration was <4% in the enzyme preparation. To the *KbTrxR* /PbTx-2 mixture, an equal volume of NaBH_4 (0.2 M in 0.2M NaOH) was added for a final concentration of 0.1 M. The reaction was incubated with gentle shaking overnight at room temperature. To this sample, 4x loading dye (250 mM Tris-HCl pH 6.8, 8% SDS, 20% βME , 40% glycerol, 0.04% bromophenol blue) was

added and the sample was heated to 95° C for 5 min and subjected to 1-D SDS PAGE using a 4-20% gradient gel along with molecular weight markers ranging from 10-250 kDa. After staining the gel with Coomassie Brilliant Blue R-250, the band of the anticipated molecular weight (~53 kDa) was excised from the gel using a clean razor blade, and stored in 100 µL of distilled water at -80°C. In-gel trypsin digestion and LC-ESI MS/MS analysis was performed by the mass spectrometry facility at the University of Massachusetts Medical School as previously described (Cassell et al., 2015).

5.3.3.6 Mass spectrometry data analysis

Scaffold (version Scaffold 4.8.4, Proteome Software Inc., Portland, OR) was used to validate MS/MS based peptide and protein identifications. Peptide identifications were accepted if they could be established at greater than 85.0% probability by the Peptide Prophet algorithm (Keller, Nesvizhskii, Kolker, & Aebersold, 2002) with Scaffold delta-mass correction. Protein identifications were accepted if they could be established at greater than 95.0% probability and contained at least 2 identified peptides. Protein probabilities were assigned by the Protein Prophet algorithm (Nesvizhskii, Keller, Kolker, & Aebersold, 2003). Proteins that contained similar peptides and could not be differentiated based on MS/MS analysis alone were grouped to satisfy the principles of parsimony. Proteins sharing significant peptide evidence were grouped into clusters.

5.4 Conclusion

5.4.1 *KbTrxR* activity is inhibited by PbTx-2

Recombinant *KbTrxR* was purified as both the native (with a substitution of a terminal serine for glycine) and truncated ($\Delta 3$) enzyme. The enzyme activity was measured for various substrates such as DTNB, H_2O_2 , Trx and GSSG. For all instances *KbTrxR* activity was inhibited (32 – 45%) by PbTx-2 (40 μ M) after 1 hour preincubation with NADPH. It is important to note, that *KbTrxR* $\Delta 3$ is void of the C-terminal redox center and cannot reduce hTrx, or H_2O_2 as these require selenocysteine for reduction (Lothrop et al., 2014). Nevertheless, DTNB reduction activity of *KbTrxR* $\Delta 3$ was inhibited by 20%. To investigate whether or not the interaction of PbTx-2 with *KbTrxR* was occurring at the N-terminal or C-terminal redox center *KbTrxR* was incubated with NADPH in the presence of PbTx-2, this reaction was reduced by $NaBH_4$ to create an irreversible 1,4 addition (see Figure 5.7). This reaction was purified by SDS-PAGE and trypsinized before being analyzed by LC-MS/MS. A single covalent modification of a cysteine residue at the N-terminal redox center was identified to have been adducted by PbTx-2. We can conclude that PbTx-2 does inhibit *KbTrxR* by covalent modification of the N-terminal redox center. However, the C-terminal redox center was not detected by MS/MS neither modified nor unmodified, there is however evidence of PbTx-2 inhibiting the C-terminal redox center due to the inhibition of Trx and H_2O_2 reduction activity. Both of these substrates require an intact C-terminal residue which contains Sec. Therefore, the greater extent of inhibition of these substrates provides indirect evidence of PbTx-2 inhibition of TrxR.

5.5 Summary

The initial aims of this work were to investigate the origin of the differences in NPQ and ROS production between the two strains of *K. brevis* with 10-fold difference in toxin production (Cassell et al., 2015). By analyzing the differences in xanthophyll cycle pigments under varying light conditions we were able to conclude that *KbLT* does not efficiently perform the qE element of NPQ which is dependent on the conversion of diadinoxanthin to diatoxanthin (see Figure 1.12) (Chen et al., 2018). Our next step was to determine if the mRNA expression of *DDE* genes was significantly different between the two strains. We also sought to compare the concentration of thylakoid lipids between *KbHT* and *KbLT*. It resulted that the mRNA expression between the two strains was not significantly different, consistent with the notion of dinoflagellate expression being regulated at the translational level (Jones et al., 2015; Morey & Van Dolah, 2013; Roy et al., 2018; Roy & Morse, 2013). Furthermore, the lipid content between the two strains was significantly different, however, the qE essential lipid MGDG was being produced by *KbLT* at 1.3-fold higher concentrations. We concluded that *KbLT* did not suffer from a lack of *DDE* expression, or a lack of fundamental lipids required for the proper functioning of the xanthophyll cycle, but instead it must result from a difference in Dde activity at the protein level. This may be a consequence of increased thiol content in *KbLT*, which is affecting the activity of the enzyme and preventing efficient qE (Colon & Rein, 2021).

To confirm our hypothesis, that Dde activity was being influenced by differences in redox status, as opposed to expression, we developed a new technique of duplex IodoTMT labeling to conduct redox proteomics experiments. *KbHT* and *KbLT* protein

was isolated and labeled by different IodoTMT labels before and after a reduction of proteinogenic disulfides with TCEP to characterize the redox proteome and quantitate the level of expression of each protein (Figure 4.2). In total we identified 2,542 peptides which were labeled by IodoTMT, many of these peptides mapped to proteins with high homology to other dinoflagellate or algal proteins. The most significant observation of our experiment was being able to conclude that Dde activity was being influenced by the abundance of free thiol residues in the *KbLT* proteome, and as a result qE was not properly functioning. This was supported by the fact that plastid localized Trxs, which have been observed to inactivate Vde *in vitro* (Hall et al., 2010), exist in a more reduced (active) state in *KbLT* (Figure 4.11). Furthermore, we also observed the redox status of MGDG synthase was influencing the activity of the enzyme, which correlated well with the observed higher concentration of MGDG in *KbLT* (Table 4.5).

The redox status of other important redox homeostasis regulating proteins was also found to be more reduced in *KbLT*, such as glutaredoxin and glutathione reductase. Similarly, we observed higher reduced status of plastid localized kinases and phosphatases, which can influence the phosphorylation of LHC-II and the generation of ATP and it's balance with NADPH production via GAPDH. A pleasant surprise, but definitely not a primary interest of this study was the observation that polyketide synthases, enzymes long thought to be responsible for the biosynthesis of polyether ladder toxins such as PbTx-2 were expressed higher in *K. brevis*, the first such observation for the dinoflagellate.

To conclude, recombinant *KbTrxR* was expressed and characterized in the presence of PbTx-2 and found to be inhibited by the toxin in its activity to reduced small disulfides (DTNB and GSSG), as well as H₂O₂, a reactive oxygen species, and human Trx, an analogue of its native substrate. Furthermore, we detected a covalent adduct formed by *KbTrxR* and PbTx-2 at the N-terminal redox center which provides strong evidence of PbTx-2 functioning as a redox homeostasis mediator in the plastid. By influencing the activity of TrxR, it can effect redox control over various photosynthetic and photooxidative functions, such as NPQ, light harvesting lipid biosynthesis, protein phosphorylation and reactive oxygen species detoxification. We believe that the data produced by our redox proteomics experiments will prove useful for years to come. Future areas of work can focus on developing antibodies specific to polyketides found in *K. brevis* to better detect harmful variants of *K. brevis* in the Gulf of Mexico. Other areas can focus on methods of mediating brevetoxicosis by targeting TrxR, or the redox regulating systems of mammals.

References

- Adarme-Vega, T. C., Lim, D. K. Y., Timmins, M., Vernen, F., Li, Y., & Schenk, P. M. (2012). Microalgal biofactories: a promising approach towards sustainable omega-3 fatty acid production. *Microbial cell factories*, *11*, 96-96. doi:10.1186/1475-2859-11-96
- Almagro Armenteros, J. J., Salvatore, M., Emanuelsson, O., Winther, O., von Heijne, G., Elofsson, A., & Nielsen, H. (2019). Detecting sequence signals in targeting peptides using deep learning. *Life Science Alliance*, *2*(5), e201900429. doi:10.26508/lsa.201900429
- Almagro Armenteros, J. J., Sønderby, C. K., Sønderby, S. K., Nielsen, H., & Winther, O. (2017). DeepLoc: prediction of protein subcellular localization using deep learning. *Bioinformatics*, *33*(21), 3387-3395. doi:10.1093/bioinformatics/btx431
- Almagro Armenteros, J. J., Tsirigos, K. D., Sønderby, C. K., Petersen, T. N., Winther, O., Brunak, S., . . . Nielsen, H. (2019). SignalP 5.0 improves signal peptide predictions using deep neural networks. *Nature Biotechnology*, *37*(4), 420-423. doi:10.1038/s41587-019-0036-z
- Altschul, S. F., Gish, W., Miller, W., Myers, E. W., & Lipman, D. J. (1990). Basic local alignment search tool. *Journal of Molecular Biology*, *215*(3), 403-410. doi:10.1016/S0022-2836(05)80360-2
- Ammendola, S., Raia, C. A., Caruso, C., Camardella, L., D'Auria, S., De Rosa, M., & Rossi, M. (1992). Thermostable NAD(+)-dependent alcohol dehydrogenase from *Sulfolobus solfataricus*: gene and protein sequence determination and relationship to other alcohol dehydrogenases. *Biochemistry*, *31*(49), 12514-12523. doi:10.1021/bi00164a031
- Andersen, R. A. (2004). Biology and systematics of heterokont and haptophyte algae. *American Journal of Botany*, *91*(10), 1508-1522. doi:10.3732/ajb.91.10.1508
- Anderson, D. M., Burkholder, J. M., Cochlan, W. P., Glibert, P. M., Gobler, C. J., Heil, C. A., . . . Vargo, G. A. (2008). Harmful algal blooms and eutrophication: Examining linkages from selected coastal regions of the United States. *Harmful Algae*, *8*(1), 39-53. doi:10.1016/j.hal.2008.08.017

Anderson, D. M., & Cheng, T. P.-O. (1988). Intracellular localization of saxitoxins in the dinoflagellate *Gonyaulax Tamarensis*. *Journal of Phycology*, 24(1), 17-22. doi:10.1111/j.1529-8817.1988.tb04451.x

Ansari, S. A., Pendurthi, U. R., & Rao, L. V. M. (2017). The lipid peroxidation product 4-hydroxy-2-nonenal induces tissue factor decryption via ROS generation and the thioredoxin system. *Blood advances*, 1(25), 2399-2413. doi:10.1182/bloodadvances.2017010132

Aoyama, K., & Nakaki, T. (2015). Glutathione in cellular redox homeostasis: Association with the excitatory amino acid carrier 1 (EAAC1). *Molecules*, 20(5), 8742-8758. doi:10.3390/molecules20058742

Araie, H., Suzuki, I., & Shiraiwa, Y. (2008). Identification and characterization of a selenoprotein, thioredoxin reductase, in a unicellular marine haptophyte alga, *Emiliania huxleyi*. *Journal of Biological Chemistry*, 283(51), 35329-35336.

Arnoux, P., Morosinotto, T., Saga, G., Bassi, R., & Pignol, D. (2009). A structural basis for the pH-dependent xanthophyll cycle in *Arabidopsis thaliana*. *The Plant Cell*, 21(7), 2036-2044. doi:10.1105/tpc.109.068007

Baden, D. G., Bourdelais, A. J., Jacocks, H., Michelliza, S., & Naar, J. (2005). Natural and derivative brevetoxins: historical background, multiplicity, and effects. *Environmental health perspectives*, 113(5), 621-625. doi:10.1289/ehp.7499

Bagu, J. R., Sykes, B. D., Craig, M. M., & Holmes, C. B. (1997). A molecular basis for different interactions of marine toxins with protein phosphatase-1: Molecular models for bound motuporin, microcystins, okadaic acid, and calyculin a. *Journal of Biological Chemistry*, 272(8), 5087-5097. doi:10.1074/jbc.272.8.5087

Bailey, A. (2019). Data Science Workshop. *British Society for Proteomic Research Meeting 2018*. Retrieved from https://ab604.github.io/docs/bspr_workshop_2018/index.html#

Barros, T., & Kühlbrandt, W. (2009). Crystallisation, structure and function of plant light-harvesting complex II. *Biochimica et Biophysica Acta (BBA) - Bioenergetics*, 1787(6), 753-772. doi:10.1016/j.bbabi.2009.03.012

- Basu, S., & Mackey, K. R. (2018). Phytoplankton as key mediators of the biological carbon pump: Their responses to a changing climate. *Sustainability*, *10*(3), 869.
- Bean, J. A., Fleming, L. E., Kirkpatrick, B., Backer, L. C., Nierenberg, K., Reich, A., . . . Baden, D. G. (2011). Florida red tide toxins (brevetoxins) and longitudinal respiratory effects in asthmatics. *Harmful Algae*, *10*(6), 744-748. doi:10.1016/j.hal.2011.06.008
- Beauchemin, M., Roy, S., Daoust, P., Dagenais-Bellefeuille, S., Bertomeu, T., Letourneau, L., . . . Morse, D. (2012). Dinoflagellate tandem array gene transcripts are highly conserved and not polycistronic. *Proceedings of the National Academy of Sciences of the United States of America*, *109*(39), 15793-15798. doi:10.1073/pnas.1206683109
- Bechard, A. (2020a). Economics losses to fishery and seafood related businesses during harmful algal blooms. *Fisheries Research*, *230*, 105678. doi:10.1016/j.fishres.2020.105678
- Bechard, A. (2020b). External costs of harmful algal blooms using hedonic valuation: The impact of *Karenia brevis* on Southwest Florida. *Environmental and Sustainability Indicators*, *5*, 100019. doi:10.1016/j.indic.2020.100019
- Beedessee, G., Hisata, K., Roy, M. C., Satoh, N., & Shoguchi, E. (2015). Multifunctional polyketide synthase genes identified by genomic survey of the symbiotic dinoflagellate, *Symbiodinium minutum*. *BMC Genomics*, *16*(1), 941. doi:10.1186/s12864-015-2195-8
- Beedessee, G., Hisata, K., Roy, M. C., Van Dolah, F. M., Satoh, N., & Shoguchi, E. (2018). Comparative genomics-first approach to understand diversification of secondary metabolite biosynthetic pathways in symbiotic dinoflagellates. *bioRxiv*, 376251. doi:10.1101/376251
- Beedessee, G., Hisata, K., Roy, M. C., Van Dolah, F. M., Satoh, N., & Shoguchi, E. (2019). Diversified secondary metabolite biosynthesis gene repertoire revealed in symbiotic dinoflagellates. *Scientific Reports*, *9*(1), 1204-1204. doi:10.1038/s41598-018-37792-0
- Beer, A., Gundermann, K., Beckmann, J., & Büchel, C. (2006). Subunit composition and pigmentation of fucoxanthin– chlorophyll proteins in diatoms: evidence for a subunit involved in diadinoxanthin and diatoxanthin binding. *Biochemistry*, *45*(43), 13046-13053.

- Bhosale, R. A., Rajabhoj, M., & Chaugule, B. (2010). *Dunaliella salina* Teod. as a prominent source of eicosapentaenoic acid. *International Journal on Algae*, 12(2).
- Binzer, S. B., Varga, E., Andersen, A. J. C., Svenssen, D. K., de Medeiros, L. S., Rasmussen, S. A., . . . Hansen, P. J. (2020). Karmitoxin production by *Karlodinium armiger* and the effects of *K. armiger* and karmitoxin towards fish. *Harmful Algae*, 99, 101905. doi:10.1016/j.hal.2020.101905
- Blanchard, J. L., & Lynch, M. (2000). Organellar genes: why do they end up in the nucleus? *Trends in Genetics*, 16(7), 315-320. doi:10.1016/S0168-9525(00)02053-9
- Bligh, E. G., & Dyer, W. J. (1959). A rapid method of total lipid extraction and purification. *Canadian journal of biochemistry and physiology*, 37(8), 911-917.
- Bossart, G. D., Baden, D. G., Ewing, R. Y., Roberts, B., & Wright, S. D. (1998). Brevetoxicosis in manatees (*Trichechus manatus latirostris*) from the 1996 Epizootic: Gross, histologic, and immunohistochemical features. *Toxicologic Pathology*, 26(2), 276-282. doi:10.1177/019262339802600214
- Bourdelais, A. J., Jacocks, H. M., Wright, J. L. C., Bigwarfe, P. M., & Baden, D. G. (2005). A new polyether ladder compound produced by the dinoflagellate *Karenia brevis*. *Journal of Natural Products*, 68(1), 2-6. doi:10.1021/np049797o
- Brunson, J. K., McKinnie, S. M. K., Chekan, J. R., McCrow, J. P., Miles, Z. D., Bertrand, E. M., . . . Moore, B. S. (2018). Biosynthesis of the neurotoxin domoic acid in a bloom-forming diatom. *Science*, 361(6409), 1356-1358. doi:10.1126/science.aau0382
- Buchanan, B. B., Kalberer, P. P., & Arnon, D. I. (1967). Ferredoxin-activated fructose diphosphatase in isolated chloroplasts. *Biochemical and Biophysical Research Communications*, 29(1), 74-79.
- Bugos, R. C., & Yamamoto, H. Y. (1996). Molecular cloning of violaxanthin de-epoxidase from romaine lettuce and expression in *Escherichia coli*. *Proceedings of the National Academy of Sciences*, 93(13), 6320-6325.
- Burki, F., Imanian, B., Hehenberger, E., Hirakawa, Y., Maruyama, S., & Keeling, P. J. (2014). Endosymbiotic gene transfer in tertiary plastid-containing dinoflagellates. *Eukaryotic cell*, 13(2), 246-255. doi:10.1128/EC.00299-13

Busch, T., Cengel, K. A., & Finlay, J. (2009). Pheophorbide a as a photosensitizer in photodynamic therapy: In vivo considerations. *Cancer Biology & Therapy*, 8(6), 540-542. doi:10.4161/cbt.8.6.8067

Cai, W., Zhang, L., Song, Y., Wang, B., Zhang, B., Cui, X., . . . Fang, J. (2012). Small molecule inhibitors of mammalian thioredoxin reductase. *Free Radical Biology and Medicine*, 52(2), 257-265. doi:10.1016/j.freeradbiomed.2011.10.447

Cassell, R. T., Chen, W., Thomas, S., Liu, L., & Rein, K. S. (2015). Brevetoxin, the dinoflagellate neurotoxin, localizes to thylakoid membranes and interacts with the Light-Harvesting Complex II (LHCII) of photosystem II. *Chembiochem*, 16(7), 1060-1067. doi:10.1002/cbic.201402669

Cavalier-Smith, T. (1999). Principles of protein and lipid targeting in secondary symbiogenesis: euglenoid, dinoflagellate, and sporozoan plastid origins and the eukaryote family tree *Journal of Eukaryotic Microbiology*, 46(4), 347-366.

Cejudo, F. J., Ojeda, V., Delgado-Requeray, V., González, M., & Pérez-Ruiz, J. M. (2019). Chloroplast redox regulatory mechanisms in plant adaptation to light and darkness. *Frontiers in plant science*, 10, 380-380. doi:10.3389/fpls.2019.00380

Chan, C. X., & Bhattacharya, D. (2010). The Origin of Plastids. In (Vol. 3).

Chapman, R. L. (2013). Algae: the world's most important "plants"—an introduction. *Mitigation and Adaptation Strategies for Global Change*, 18(1), 5-12. doi:10.1007/s11027-010-9255-9

Chen, J., Keltner, L., Christophersen, J., Zheng, F., Krouse, M., Singhal, A., & Wang, S.-s. (2002). New technology for deep light distribution in tissue for phototherapy. *The Cancer Journal*, 8(2), 154-163. Retrieved from https://journals.lww.com/journalppo/Fulltext/2002/03000/New_Technology_for_Deep_Light_Distribution_in.9.aspx

Chen, W., Colon, R., Louda, J. W., del Rey, F. R., Durham, M., & Rein, K. S. (2018). Brevetoxin (PbTx-2) influences the redox status and NPQ of *Karenia brevis* by way of thioredoxin reductase. *Harmful Algae*, 71, 29-39. doi:10.1016/j.hal.2017.11.004

Chen, W., Tuladhar, A., Rolle, S., Lai, Y., Rodriguez del Rey, F., Zavala, C. E., . . . Rein, K. S. (2017a). Brevetoxin-2, is a unique inhibitor of the C-terminal redox center of

mammalian thioredoxin reductase-1. *Toxicology and Applied Pharmacology*, 329(Supplement C), 58-66. doi:10.1016/j.taap.2017.05.027

Chen, W., Tuladhar, A., Rolle, S., Lai, Y., Rodriguez Del Rey, F., Zavala, C. E., . . . Rein, K. S. (2017b). Brevetoxin-2, is a unique inhibitor of the C-terminal redox center of mammalian thioredoxin reductase-1. *Toxicology and applied pharmacology*, 329, 58-66. doi:10.1016/j.taap.2017.05.027

Chen, Y., Shen, D., & Fang, D. (2013). Nodularins in poisoning. *Clinica Chimica Acta*, 425, 18-29. doi:10.1016/j.cca.2013.07.005

Chisti, Y. (2007). Biodiesel from microalgae. *Biotechnology Advances*, 25(3), 294-306. doi:10.1016/j.biotechadv.2007.02.001

Chorus, I., & Welker, M. (2021). *Toxic cyanobacteria in water: a guide to their public health consequences, monitoring and management*: Taylor & Francis.

Chou, H. N., & Shimizu, Y. (1987). Biosynthesis of brevetoxins. Evidence for the mixed origin of the backbone carbon chain and possible involvement of dicarboxylic acids. *J Am Chem Soc*, 109(7), 2184-2185. doi:10.1021/ja00241a048

Christensen, V. G., & Khan, E. (2020). Freshwater neurotoxins and concerns for human, animal, and ecosystem health: A review of anatoxin-a and saxitoxin. *Science of The Total Environment*, 736, 139515. doi:10.1016/j.scitotenv.2020.139515

Citta, A., Folda, A., Bindoli, A., Pigeon, P., Top, S., Vessières, A., . . . Rigobello, M. P. (2014). Evidence for targeting thioredoxin reductases with ferrocenyl quinone methides. A possible molecular basis for the antiproliferative effect of hydroxyferrocifens on cancer cells. *Journal of Medicinal Chemistry*, 57(21), 8849-8859. doi:10.1021/jm5013165

Coesel, S., Oborník, M., Varela, J., Falciatore, A., & Bowler, C. (2008). Evolutionary origins and functions of the carotenoid biosynthetic pathway in marine diatoms. *PLOS ONE*, 3(8), e2896. doi:10.1371/journal.pone.0002896

Cohen, J. H., Tester, P. A., & Forward, R. B., Jr. (2007). Sublethal effects of the toxic dinoflagellate *Karenia brevis* on marine copepod behavior. *Journal of Plankton Research*, 29(3), 301-315. doi:10.1093/plankt/fbm016

Colon, R., & Rein, K. S. (2021). Essential components of the xanthophyll cycle differ in high and low toxin *Karenia brevis*. *Harmful Algae*, *103*, 102006. doi:10.1016/j.hal.2021.102006

Cooney, M., Young, G., & Nagle, N. (2009). Extraction of bio-oils from microalgae. *Separation & Purification Reviews*, *38*(4), 291-325. doi:10.1080/15422110903327919

Da, Q., Sun, T., Wang, M., Jin, H., Li, M., Feng, D., . . . Liu, B. (2018). M-type thioredoxins are involved in the xanthophyll cycle and proton motive force to alter NPQ under low-light conditions in *Arabidopsis*. *Plant Cell Reports*, *37*(2), 279-291. doi:10.1007/s00299-017-2229-6

Dai, S., Saarinen, M., Ramaswamy, S., Meyer, Y., Jacquot, J.-P., & Eklund, H. (1996). Crystal structure of *Arabidopsis thaliana* NADPH dependent thioredoxin reductase at 2.5 Å resolution. *Journal of Molecular Biology*, *264*(5), 1044-1057. doi:10.1006/jmbi.1996.0695

de Jesus Raposo, M. F., de Morais, R. M. S. C., & de Morais, A. M. M. B. (2013). Health applications of bioactive compounds from marine microalgae. *Life Sciences*, *93*(15), 479-486. doi:10.1016/j.lfs.2013.08.002

Dechraoui, M.-Y., Naar, J., Pauillac, S., & Legrand, A.-M. (1999). Ciguatoxins and brevetoxins, neurotoxic polyether compounds active on sodium channels. *Toxicon*, *37*(1), 125-143. doi:10.1016/S0041-0101(98)00169-X

Depège, N., Bellafiore, S., & Rochaix, J.-D. (2003). Role of chloroplast protein kinase Stt7 in LHCII phosphorylation and state transition in *Chlamydomonas*. *Science*, *299*(5612), 1572. doi:10.1126/science.1081397

Duce, R. A., & Tindale, N. W. (1991). Atmospheric transport of iron and its deposition in the ocean. *Limnology and Oceanography*, *36*(8), 1715-1726. doi:10.4319/lo.1991.36.8.1715

Eckenroth, B., Harris, K., Turanov, A. A., Gladyshev, V. N., Raines, R. T., & Hondal, R. J. (2006). Semisynthesis and characterization of mammalian thioredoxin reductase. *Biochemistry*, *45*(16), 5158-5170. doi:10.1021/bi0517887

Egeland, E., Garrido, J., Clementson, L., Andresen, K., Thomas, C., Zapata, M., . . . Rodríguez, F. (2011). Data sheets aiding identification of phytoplankton carotenoids and

chlorophylls. *Phytoplankton pigments: characterization, chemotaxonomy and applications in oceanography*, 665-822.

Ellman, G. L. (1959). Tissue sulfhydryl groups. *Archives of Biochemistry and Biophysics*, 82(1), 70-77.

Emanuelsson, O., Nielsen, H., & Heijne, G. V. (1999). ChloroP, a neural network-based method for predicting chloroplast transit peptides and their cleavage sites. *Protein Science*, 8(5), 978-984. doi:10.1110/ps.8.5.978

Endo, K., Kobayashi, K., & Wada, H. (2016). Sulfoquinovosyldiacylglycerol has an essential role in *Thermosynechococcus elongatus* bp-1 under phosphate-deficient conditions. *Plant and Cell Physiology*, 57(12), 2461-2471. doi:10.1093/pcp/pcw159

Errera, R. M., Bourdelais, A., Drennan, M. A., Dodd, E. B., Henrichs, D. W., & Campbell, L. (2010). Variation in brevetoxin and brevenal content among clonal cultures of *Karenia brevis* may influence bloom toxicity. *Toxicon*, 55(2), 195-203. doi:10.1016/j.toxicon.2009.07.013

Errera, R. M., & Campbell, L. (2011). Osmotic stress triggers toxin production by the dinoflagellate *Karenia brevis*. *Proceedings of the National Academy of Sciences of the United States of America*, 108(26), 10597-10601. doi:10.1073/pnas.1104247108

Evans Jr, T. C., Benner, J., & Xu, M.-Q. (1998). Semisynthesis of cytotoxic proteins using a modified protein splicing element. *Protein Science*, 7(11), 2256-2264. doi:10.1002/pro.5560071103

Evans Jr., T. C., Benner, J., & Xu, M.-Q. (1998). Semisynthesis of cytotoxic proteins using a modified protein splicing element. *Protein Science*, 7(11), 2256-2264. doi:10.1002/pro.5560071103

Evens, T. J., Kirkpatrick, G. J., Millie, D. F., Chapman, D. J., & Schofield, O. M. E. (2001). Photophysiological responses of the toxic red-tide dinoflagellate *Gymnodinium breve* (Dinophyceae) under natural sunlight. *Journal of Plankton Research*, 23(11), 1177-1194. doi:10.1093/plankt/23.11.1177

Fassett, R. G., & Coombes, J. S. (2011). Astaxanthin: A potential therapeutic agent in cardiovascular disease. *Marine Drugs*, 9(3), 447-465. Retrieved from <https://www.mdpi.com/1660-3397/9/3/447>

FLDEP. (2021). Algal Bloom Sampling Results. *Algal Bloom Sampling Results*. Retrieved from <https://floridadep.gov/dear/algal-bloom/content/algal-bloom-sampling-results#.YKk2KYHNGwg.link>

Fleige, S., Walf, V., Huch, S., Prgomet, C., Sehm, J., & Pfaffl, M. W. (2006). Comparison of relative mRNA quantification models and the impact of RNA integrity in quantitative real-time RT-PCR. *Biotechnology Letters*, 28(19), 1601-1613. doi:10.1007/s10529-006-9127-2

Fleming, L. E., Kirkpatrick, B., Backer, L. C., Walsh, C. J., Nierenberg, K., Clark, J., . . . Baden, D. G. (2011). Review of florida red tide and human health effects. *Harmful Algae*, 10(2), 224-233. doi:10.1016/j.hal.2010.08.006

Flewelling, L. J., Naar, J. P., Abbott, J. P., Baden, D. G., Barros, N. B., Bossart, G. D., . . . Landsberg, J. H. (2005). Brevetoxicosis: red tides and marine mammal mortalities. *Nature*, 435(7043), 755-756. doi:10.1038/nature435755a

Frank, H. A., Cua, A., Chynwat, V., Young, A., Gosztola, D., & Wasielewski, M. R. (1994). Photophysics of the carotenoids associated with the xanthophyll cycle in photosynthesis. *Photosynthesis Research*, 41(3), 389-395. doi:10.1007/bf02183041

García-Santamarina, S., Boronat, S., Domènech, A., Ayté, J., Molina, H., & Hidalgo, E. (2014). Monitoring in vivo reversible cysteine oxidation in proteins using ICAT and mass spectrometry. *Nature Protocols*, 9(5), 1131-1145. doi:10.1038/nprot.2014.065

Geigenberger, P., & Fernie, A. R. (2014). Metabolic control of redox and redox control of metabolism in plants. *Antioxid Redox Signal*, 21(9), 1389-1421. doi:10.1089/ars.2014.6018

Gladyshev, V. N., Jeang, K. T., & Stadtman, T. C. (1996). Selenocysteine, identified as the penultimate C-terminal residue in human T-cell thioredoxin reductase, corresponds to TGA in the human placental gene. *Proceedings of the National Academy of Sciences*, 93(12), 6146. doi:10.1073/pnas.93.12.6146

Glazer, A. N. (1994). Phycobiliproteins—a family of valuable, widely used fluorophores. *Journal of Applied Phycology*, 6(2), 105-112.

Goss, R., Ann Pinto, E., Wilhelm, C., & Richter, M. (2006). The importance of a highly active and ΔpH-regulated diatoxanthin epoxidase for the regulation of the PS II antenna

function in diadinoxanthin cycle containing algae. *Journal of Plant Physiology*, 163(10), 1008-1021. doi:10.1016/j.jplph.2005.09.008

Goss, R., & Latowski, D. (2020). Lipid dependence of xanthophyll cycling in higher plants and algae. *Frontiers in plant science*, 11(455). doi:10.3389/fpls.2020.00455

Goss, R., Latowski, D., Grzyb, J., Vieler, A., Lohr, M., Wilhelm, C., & Strzalka, K. (2007). Lipid dependence of diadinoxanthin solubilization and de-epoxidation in artificial membrane systems resembling the lipid composition of the natural thylakoid membrane. *Biochimica et Biophysica Acta (BBA)-Biomembranes*, 1768(1), 67-75.

Goss, R., Lohr, M., Latowski, D., Grzyb, J., Vieler, A., Wilhelm, C., & Strzalka, K. (2005). Role of hexagonal structure-forming lipids in diadinoxanthin and violaxanthin solubilization and de-epoxidation. *Biochemistry*, 44(10), 4028-4036. doi:10.1021/bi047464k

Goss, R., Nerlich, J., Lepetit, B., Schaller, S., Vieler, A., & Wilhelm, C. (2009). The lipid dependence of diadinoxanthin de-epoxidation presents new evidence for a macrodomain organization of the diatom thylakoid membrane. *Journal of Plant Physiology*, 166(17), 1839-1854. doi:10.1016/j.jplph.2009.05.017

Graham, L. E., & Wilcox, L. W. (2000). *Algae*.

Gray, M., & Spencer, D. (1996). *Organellar evolution*. Paper presented at the Symposia-Society for General Microbiology.

Grouneva, I., Jakob, T., Wilhelm, C., & Goss, R. (2006). Influence of ascorbate and pH on the activity of the diatom xanthophyll cycle-enzyme diadinoxanthin de-epoxidase. *Physiologia Plantarum*, 126(2), 205-211. doi:10.1111/j.1399-3054.2006.00613.x

Guedes, A. C., Amaro, H. M., & Malcata, F. X. (2011). Microalgae as sources of carotenoids. *Marine Drugs*, 9(4), 625-644. doi:10.3390/md9040625

Guihéneuf, F., Mimouni, V., Ulmann, L., & Tremblin, G. (2009). Combined effects of irradiance level and carbon source on fatty acid and lipid class composition in the microalga *Pavlova lutheri* commonly used in mariculture. *Journal of Experimental Marine Biology and Ecology*, 369(2), 136-143. doi:10.1016/j.jembe.2008.11.009

Gundermann, K., & Büchel, C. (2012). Factors determining the fluorescence yield of fucoxanthin-chlorophyll complexes (FCP) involved in non-photochemical quenching in diatoms. *Biochimica et Biophysica Acta (BBA) - Bioenergetics*, 1817(7), 1044-1052. doi:10.1016/j.bbabi.2012.03.008

Gütle, D. D., Roret, T., Müller, S. J., Couturier, J., Lemaire, S. D., Hecker, A., . . . Jacquot, J.-P. (2016). Chloroplast FBPase and SBPase are thioredoxin-linked enzymes with similar architecture but different evolutionary histories. *Proceedings of the National Academy of Sciences of the United States of America*, 113(24), 6779-6784. doi:10.1073/pnas.1606241113

Gygi, S. P., Rist, B., Gerber, S. A., Turecek, F., Gelb, M. H., & Aebersold, R. (1999). Quantitative analysis of complex protein mixtures using isotope-coded affinity tags. *Nature Biotechnology*, 17(10), 994-999. doi:10.1038/13690

Hager, A. (1969). Lichtbedingte pH-erniedrigung in einem chloroplasten-kompartiment als ursache der enzymatischen violaxanthin-→ zeaxanthin-umwandlung; Beziehungen zur photophosphorylierung. *Planta*, 224-243.

Hagerthey, S. E., William Louda, J., & Mongkronsri, P. (2006). Evaluation of pigment extraction methods and a recommended protocol for periphyton chlorophyll a determination and chemotaxonomic assessment. *Journal of Phycology*, 42(5), 1125-1136.

Hall, M., Mata-Cabana, A., Åkerlund, H.-E., Florencio, F. J., Schröder, W. P., Lindahl, M., & Kieselbach, T. (2010). Thioredoxin targets of the plant chloroplast lumen and their implications for plastid function. *PROTEOMICS*, 10(5), 987-1001. doi:10.1002/pmic.200900654

Hallegraeff, G. M. (2010). Ocean climate change, phytoplankton community responses, and harmful algal blooms: A formidable predictive challenge. *Journal of Phycology*, 46(2), 220-235. doi:10.1111/j.1529-8817.2010.00815.x

Hannon, M., Gimpel, J., Tran, M., Rasala, B., & Mayfield, S. (2010). Biofuels from algae: challenges and potential. *Biofuels*, 1(5), 763-784. Retrieved from <http://www.ncbi.nlm.nih.gov/pmc/articles/PMC3152439/>

Hanschmann, E.-M., Godoy, J. R., Berndt, C., Hudemann, C., & Lillig, C. H. (2013). Thioredoxins, glutaredoxins, and peroxiredoxins—Molecular mechanisms and health

significance: From cofactors to antioxidants to redox signaling. *Antioxid Redox Signal*, 19(13), 1539-1605. doi:10.1089/ars.2012.4599

Hardison, D. R., Sunda, W. G., Shea, D., & Litaker, R. W. (2013). Increased toxicity of *Karenia brevis* during phosphate limited growth: Ecological and evolutionary implications. *PLOS ONE*, 8(3), e58545. doi:10.1371/journal.pone.0058545

Hardison, D. R., Sunda, W. G., Tester, P. A., Shea, D., & Litaker, W. R. (2014). Increased cellular brevetoxins in the red tide dinoflagellate *Karenia brevis* under CO₂ limitation of growth rate: Evolutionary implications and potential effects on bloom toxicity. *Limnology and Oceanography*, 59(2), 560-577. doi:10.4319/lo.2014.59.2.0560

Havaux, M., Ksas, B., Szewczyk, A., Rumeau, D., Franck, F., Caffarri, S., & Triantaphylidès, C. (2009). Vitamin B6 deficient plants display increased sensitivity to high light and photo-oxidative stress. *BMC Plant Biology*, 9(1), 130. doi:10.1186/1471-2229-9-130

Herber, S. M., & Van Elswyk, M. E. (1996). Dietary marine algae promotes efficient deposition of n-3 fatty acids for the production of enriched shell eggs. *Poultry Science*, 75(12), 1501-1507. doi:10.3382/ps.0751501

Hieber, D. A., Bugos, R. C., Verhoeven, A. S., & Yamamoto, H. Y. (2002). Overexpression of violaxanthin de-epoxidase: properties of C-terminal deletions on activity and pH-dependent lipid binding. *Planta*, 214(3), 476-483. doi:10.1007/s00425-001-0704-2

Ho-Pun-Cheung, A., Bascoul-Mollevi, C., Assenat, E., Boissière-Michot, F., Bibeau, F., Cellier, D., . . . Lopez-Crapez, E. (2009). Reverse transcription-quantitative polymerase chain reaction: description of a RIN-based algorithm for accurate data normalization. *BMC molecular biology*, 10(1), 31. doi:10.1186/1471-2199-10-31

Hoagland, P., & Scatasta, S. (2006). The Economic Effects of Harmful Algal Blooms. In E. Granéli & J. T. Turner (Eds.), *Ecology of Harmful Algae* (pp. 391-402). Berlin, Heidelberg: Springer Berlin Heidelberg.

Holmgren, A., & Bjornstedt, M. (1995). Thioredoxin and thioredoxin reductase. In *Methods in Enzymology* (Vol. 252, pp. 199-208): Academic Press.

- Hong, J., Talapatra, S., Katz, J., Tester, P. A., Waggett, R. J., & Place, A. R. (2012). Algal toxins alter copepod feeding behavior. *PLOS ONE*, 7(5), e36845-e36845. doi:10.1371/journal.pone.0036845
- Hu, H., & Gao, K. (2003). Optimization of growth and fatty acid composition of a unicellular marine picoplankton, *Nannochloropsis* sp., with enriched carbon sources. *Biotechnology Letters*, 25(5), 421-425. doi:10.1023/A:1022489108980
- Ito, E., Satake, M., & Yasumoto, T. (2002). Pathological effects of lyngbyatoxin A upon mice. *Toxicon*, 40(5), 551-556. doi:10.1016/S0041-0101(01)00251-3
- Iwai, M., Kato, N., & Minagawa, J. (2007). *Distinct physiological responses to a high light and low CO₂ environment revealed by fluorescence quenching in photoautotrophically grown Chlamydomonas reinhardtii* (Vol. 94).
- Jacquot, J.-P., Eklund, H., Rouhier, N., & Schürmann, P. (2009). Structural and evolutionary aspects of thioredoxin reductases in photosynthetic organisms. *Trends in Plant Science*, 14(6), 336-343.
- Jacquot, J.-P., Rivera-Madrid, R., Marinho, P., Kollarova, M., Le Maréchal, P., Miginiac-Maslow, M., & Meyer, Y. (1994). *Arabidopsis thaliana* NAPHP Thioredoxin Reductase: cDNA Characterization and Expression of the Recombinant Protein in *Escherichia coli*. *Journal of Molecular Biology*, 235(4), 1357-1363. doi:10.1006/jmbi.1994.1091
- Jahns, P., Latowski, D., & Strzalka, K. (2009). Mechanism and regulation of the violaxanthin cycle: The role of antenna proteins and membrane lipids. *Biochimica et Biophysica Acta (BBA) - Bioenergetics*, 1787(1), 3-14. doi:10.1016/j.bbabi.2008.09.013
- Jakob, T., Goss, R., & Wilhelm, C. (2001). Unusual pH-dependence of diadinoxanthin de-epoxidase activation causes chlororespiratory induced accumulation of diatoxanthin in the diatom *Phaeodactylum tricornerutum*. *Journal of Plant Physiology*, 158(3), 383-390. doi:10.1078/0176-1617-00288
- Järvi, S., Gollan, P. J., & Aro, E.-M. (2013). Understanding the roles of the thylakoid lumen in photosynthesis regulation. *Frontiers in plant science*, 4, 434-434. doi:10.3389/fpls.2013.00434

Jarvis, P., & Soll, J. (2002). Erratum to: "Toc, Tic, and chloroplast protein import" [Biochim. Biophys. Acta 1541 (2001) 64–79]. *Biochimica et Biophysica Acta (BBA) - Molecular Cell Research*, 1590(1), 177-189. doi:10.1016/S0167-4889(02)00176-3

Jayakumar, S., Patwardhan, R. S., Pal, D., Sharma, D., & Sandur, S. K. (2016). Dimethoxycurcumin, a metabolically stable analogue of curcumin enhances the radiosensitivity of cancer cells: Possible involvement of ROS and thioredoxin reductase. *Biochemical and Biophysical Research Communications*, 478(1), 446-454. doi:10.1016/j.bbrc.2016.06.144

Jeglitsch, G., Rein, K., Baden, D. G., & Adams, D. J. (1998). Brevetoxin-3 (PbTx-3) and its derivatives modulate single tetrodotoxin-sensitive sodium channels in rat sensory neurons. *Journal of Pharmacology and Experimental Therapeutics*, 284(2), 516. Retrieved from <http://jpet.aspetjournals.org/content/284/2/516.abstract>

Jones, G. D., Williams, E. P., Bachvaroff, T. R., Place, A. R., & Jagus, R. (2015). Translating the message: *Karlodinium veneficum* possesses an expanded toolkit of protein translation initiation factors. *Marine and freshwater harmful algae : proceedings of the 16th International Conference on Harmful Algae, 27th-31st October 2014, Wellington, New Zealand. International Conference on Harmful Algae (16th : 2014 : Wellington, N.Z.), author, 2014, 237-240*. Retrieved from

Kanehisa, M., Sato, Y., & Morishima, K. (2016). BlastKOALA and GhostKOALA: KEGG tools for functional characterization of genome and metagenome sequences. *Journal of Molecular Biology*, 428(4), 726-731. doi:10.1016/j.jmb.2015.11.006

Kang, Z.-H., & Wang, G.-X. (2016). Redox regulation in the thylakoid lumen. *Journal of Plant Physiology*, 192, 28-37. doi:10.1016/j.jplph.2015.12.012

Keeling, P. J. (2009). Chromalveolates and the evolution of plastids by secondary endosymbiosis. *Journal of Eukaryotic Microbiology*, 56(1), 1-8. doi:10.1111/j.1550-7408.2008.00371.x

Keller, A., Nesvizhskii, A. I., Kolker, E., & Aebersold, R. (2002). Empirical statistical model to estimate the accuracy of peptide identifications made by MS/MS and database search. *Analytical Chemistry*, 74(20), 5383-5392. doi:10.1021/ac025747h

Kim, S.-K. (2015). *Handbook of marine microalgae: Biotechnology Advances*: Academic Press.

Kirkpatrick, B., Bean, J. A., Fleming, L. E., Kirkpatrick, G., Grief, L., Nierenberg, K., . . . Naar, J. (2010). Gastrointestinal emergency room admissions and florida red tide blooms. *Harmful Algae*, 9(1), 82-86. doi:10.1016/j.hal.2009.08.005

Kohli, G. S., Campbell, K., John, U., Smith, K. F., Fraga, S., Rhodes, L. L., & Murray, S. A. (2017). Role of modular polyketide synthases in the production of polyether ladder compounds in ciguatoxin-producing *Gambierdiscus polynesiensis* and *G. excentricus* (Dinophyceae). *Journal of Eukaryotic Microbiology*, 64(5), 691-706. doi:10.1111/jeu.12405

Krieger-Liszak, A. (2004). Singlet oxygen production in photosynthesis. *Journal of Experimental Botany*, 56(411), 337-346. doi:10.1093/jxb/erh237

Kubota, T., Inuma, Y., & Kobayashi, J. i. (2006). Cloning of polyketide synthase genes from amphidinolide-producing dinoflagellate *Amphidinium* sp. *Biological and Pharmaceutical Bulletin*, 29(7), 1314-1318. doi:10.1248/bpb.29.1314

Kunze, M. (2020). The type-2 peroxisomal targeting signal. *Biochimica et Biophysica Acta (BBA) - Molecular Cell Research*, 1867(2), 118609. doi:10.1016/j.bbamcr.2019.118609

LaJeunesse, T. C., Lambert, G., Andersen, R. A., Coffroth, M. A., & Galbraith, D. W. (2005). *Symbiodinium* (Pyrrhophyta) genome sizes (DNA content) are smallest among dinoflagellates1. *Journal of Phycology*, 41(4), 880-886. doi:10.1111/j.0022-3646.2005.04231.x

Larkin, S. L., & Adams, C. M. (2007). Harmful algal blooms and coastal business: Economic consequences in florida. *Society & Natural Resources*, 20(9), 849-859. doi:10.1080/08941920601171683

Latowski, D., Åkerlund, H.-E., & Strzałka, K. (2004). Violaxanthin de-epoxidase, the xanthophyll cycle enzyme, requires lipid inverted hexagonal structures for its activity. *Biochemistry*, 43(15), 4417-4420. doi:10.1021/bi049652g

Latowski, D., Kostecka, A., & Strzalka, K. (2000). Effect of monogalactosyldiacylglycerol and other thylakoid lipids on violaxanthin de-epoxidation in liposomes. *Biochemical Society Transactions*, 28(6), 810-812. doi:10.1042/bst0280810

Latowski, D., Kruk, J., Burda, K., Skrzynecka-Jaskier, M., Kostecka-Gugała, A., & Strzalka, K. (2002). Kinetics of violaxanthin de-epoxidation by violaxanthin de-epoxidase, a xanthophyll cycle enzyme, is regulated by membrane fluidity in model lipid bilayers. *European Journal of Biochemistry*, 269(18), 4656-4665.

Le, Q. H., Markovic, P., Hastings, J. W., Jovine, R. V. M., & Morse, D. (1997). Structure and organization of the peridinin-chlorophyll a-binding protein gene in *Gonyaulax polyedra*. *Molecular and General Genetics MGG*, 255(6), 595-604. doi:10.1007/s004380050533

Leblond, J. D., Evans, T. J., & Chapman, P. J. (2003). The biochemistry of dinoflagellate lipids, with particular reference to the fatty acid and sterol composition of a *Karenia brevis* bloom. *Phycologia*, 42(4), 324-331. doi:10.2216/i0031-8884-42-4-324.1

Leblond, J. D., & Lasiter, A. D. (2009). Mono- and digalactosyldiacylglycerol composition of dinoflagellates. II. *Lepidodinium chlorophorum*, *Karenia brevis*, and *Kryptoperidinium foliaceum*, three dinoflagellates with aberrant plastids. *European Journal of Phycology*, 44(2), 199-205. doi:10.1080/09670260802524611

Lee, F. W.-F., Morse, D., & Lo, S. C.-L. (2009). Identification of two plastid proteins in the dinoflagellate *Alexandrium affine* that are substantially down-regulated by nitrogen-depletion. *Journal of Proteome Research*, 8(11), 5080-5092. doi:10.1021/pr900475f

Lee, M. S., Qin, G., Nakanishi, K., & Zagorski, M. G. (1989). Biosynthetic studies of brevetoxins, potent neurotoxins produced by the dinoflagellate *Gymnodinium breve*. *J Am Chem Soc*, 111(16), 6234-6241. doi:10.1021/ja00198a039

Lee, M. S., Repeta, D. J., Nakanishi, K., & Zagorski, M. G. (1986). Biosynthetic origins and assignments of carbon 13 NMR peaks of brevetoxin B. *J Am Chem Soc*, 108(24), 7855-7856.

Lemeille, S., & Rochaix, J.-D. (2010). State transitions at the crossroad of thylakoid signalling pathways. *Photosynthesis Research*, 106(1), 33-46. doi:10.1007/s11120-010-9538-8

- Lemeille, S., Willig, A., Depège-Fargeix, N., Delessert, C., Bassi, R., & Rochaix, J.-D. (2009). Analysis of the chloroplast protein kinase Stt7 during state transitions. *PLOS Biology*, 7(3), e1000045. doi:10.1371/journal.pbio.1000045
- Lewis, L. A., & McCourt, R. M. (2004). Green algae and the origin of land plants. *American Journal of Botany*, 91(10), 1535-1556. doi:10.3732/ajb.91.10.1535
- Liu, B., Lo, S. C.-L., Matton, D. P., Lang, B. F., & Morse, D. (2012). Daily changes in the phosphoproteome of the dinoflagellate *Lingulodinium*. *Protist*, 163(5), 746-754. doi:10.1016/j.protis.2011.11.001
- Liu, Z., Yan, H., Wang, K., Kuang, T., Zhang, J., Gui, L., . . . Chang, W. (2004). Crystal structure of spinach major light-harvesting complex at 2.72 Å resolution. *Nature*, 428(6980), 287-292. doi:10.1038/nature02373
- Loftin, K. A., Graham, J. L., Hilborn, E. D., Lehmann, S. C., Meyer, M. T., Dietze, J. E., & Griffith, C. B. (2016). Cyanotoxins in inland lakes of the United States: Occurrence and potential recreational health risks in the EPA National Lakes Assessment 2007. *Harmful Algae*, 56, 77-90. doi:10.1016/j.hal.2016.04.001
- Lohr, M., & Wilhelm, C. (1999). Algae displaying the diadinoxanthin cycle also possess the violaxanthin cycle. *Proceedings of the National Academy of Sciences*, 96(15), 8784-8789. doi:10.1073/pnas.96.15.8784
- Lothrop, A. P., Snider, G. W., Ruggles, E. L., & Hondal, R. J. (2014). Why is mammalian thioredoxin reductase 1 so dependent upon the use of selenium? *Biochemistry*, 53(3), 554-565. doi:10.1021/bi400651x
- Louda, J. W., Li, J., Liu, L., Winfree, M. N., & Baker, E. W. (1998). Chlorophyll-a degradation during cellular senescence and death. *Organic geochemistry*, 29(5-7), 1233-1251.
- Louda, J. W., Liu, L., & Baker, E. W. (2002). Senescence-and death-related alteration of chlorophylls and carotenoids in marine phytoplankton. *Organic geochemistry*, 33(12), 1635-1653.
- Lu, S., Wang, J., Chitsaz, F., Derbyshire, M. K., Geer, R. C., Gonzales, N. R., . . . Marchler-Bauer, A. (2020). CDD/SPARCLE: the conserved domain database in 2020. *Nucleic Acids Research*, 48(D1), D265-D268. doi:10.1093/nar/gkz991

Madeira, F., Park, Y. M., Lee, J., Buso, N., Gur, T., Madhusoodanan, N., . . . Lopez, R. (2019). The EMBL-EBI search and sequence analysis tools APIs in 2019. *Nucleic Acids Research*, *47*(W1), W636-W641. doi:10.1093/nar/gkz268

Mantoura, R., & Llewellyn, C. (1983). The rapid determination of algal chlorophyll and carotenoid pigments and their breakdown products in natural waters by reverse-phase high-performance liquid chromatography. *Analytica Chimica Acta*, *151*, 297-314.

Marchler-Bauer, A., & Bryant, S. H. (2004). CD-Search: protein domain annotations on the fly. *Nucleic Acids Research*, *32*(Web Server issue), W327-W331. doi:10.1093/nar/gkh454

Marchler-Bauer, A., Lu, S., Anderson, J. B., Chitsaz, F., Derbyshire, M. K., DeWeese-Scott, C., . . . Bryant, S. H. (2011). CDD: a Conserved Domain Database for the functional annotation of proteins. *Nucleic Acids Research*, *39*(Database issue), D225-D229. doi:10.1093/nar/gkq1189

Mariotti, M., Lobanov, A. V., Guigo, R., & Gladyshev, V. N. (2013). SECISearch3 and Seblastian: new tools for prediction of SECIS elements and selenoproteins. *Nucleic Acids Research*, *41*(15), e149-e149. doi:10.1093/nar/gkt550

Martin, W., & Herrmann, R. G. (1998). Gene transfer from organelles to the nucleus: How much, what happens, and why? *Plant Physiology*, *118*(1), 9. doi:10.1104/pp.118.1.9

McCarty, S. E., Schellenberger, A., Goodwin, D. C., Fuanta, N. R., Tekwani, B. L., & Calderón, A. I. (2015). *Plasmodium falciparum* thioredoxin reductase (PfTrxR) and its role as a target for new antimalarial discovery. *Molecules*, *20*(6), 11459-11473.

McFadden, G. I. (2001). Primary and secondary endosymbiosis and the origin of plastids. *Journal of Phycology*, *37*(6), 951-959. doi:10.1046/j.1529-8817.2001.01126.x

Menetrez, M. Y. (2012). An overview of algae biofuel production and potential environmental impact. *Environmental Science & Technology*, *46*(13), 7073-7085. doi:10.1021/es300917r

Meyer, Y., Belin, C., Delorme-Hinoux, V., Reichheld, J.-P., & Riondet, C. (2012). Thioredoxin and glutaredoxin systems in plants: Molecular mechanisms, crosstalks, and functional significance. *Antioxid Redox Signal*, *17*(8), 1124-1160. doi:10.1089/ars.2011.4327

Minoda, A., Sato, N., Nozaki, H., Okada, K., Takahashi, H., Sonoike, K., & Tsuzuki, M. (2002). Role of sulfoquinovosyl diacylglycerol for the maintenance of photosystem II in *Chlamydomonas reinhardtii*. *European Journal of Biochemistry*, 269(9), 2353-2358. doi:10.1046/j.1432-1033.2002.02896.x

Miseta, A., & Csutora, P. (2000). Relationship between the occurrence of cysteine in proteins and the complexity of organisms. *Molecular Biology and Evolution*, 17(8), 1232-1239. doi:10.1093/oxfordjournals.molbev.a026406

Mistry, J., Chuguransky, S., Williams, L., Qureshi, M., Salazar, Gustavo A., Sonnhammer, E. L. L., . . . Bateman, A. (2020). Pfam: The protein families database in 2021. *Nucleic Acids Research*, 49(D1), D412-D419. doi:10.1093/nar/gkaa913

Monroe, E. A., Johnson, J. G., Wang, Z., Pierce, R. K., & Van Dolah, F. M. (2010). Characterization and expression of nuclear-encoded polyketide synthases in the brevetoxin-producing dinoflagellate *Karenia brevis*. *Journal of Phycology*, 46(3), 541-552. doi:10.1111/j.1529-8817.2010.00837.x

Morey, J. S., & Van Dolah, F. M. (2013). Global analysis of mRNA half-lives and de novo transcription in a dinoflagellate, *Karenia brevis*. *PLOS ONE*, 8(6), e66347-e66347. doi:10.1371/journal.pone.0066347

Müller, P., Li, X.-P., & Niyogi, K. K. (2001). Non-photochemical quenching. A response to excess light energy. *Plant Physiology*, 125(4), 1558. Retrieved from <http://www.plantphysiol.org/content/125/4/1558.abstract>

Murata, N., Takahashi, S., Nishiyama, Y., & Allakhverdiev, S. I. (2007). Photoinhibition of photosystem II under environmental stress. *Biochimica et Biophysica Acta (BBA) - Bioenergetics*, 1767(6), 414-421. doi:10.1016/j.bbabi.2006.11.019

Nakajima, Y., Umena, Y., Nagao, R., Endo, K., Kobayashi, K., Akita, F., . . . Shen, J.-R. (2018). Thylakoid membrane lipid sulfoquinovosyl-diacylglycerol (SQDG) is required for full functioning of photosystem II in *Thermosynechococcus elongatus*. *The Journal of biological chemistry*, 293(38), 14786-14797. doi:10.1074/jbc.RA118.004304

Nakamura, Y., Shimojima, M., Ohta, H., & Shimojima, K. (2010). Chapter 13 Biosynthesis and Function of Monogalactosyldiacylglycerol (MGDG), the Signature Lipid of Chloroplasts. In C. A. Rebeiz, C. Benning, H. J. Bohnert, H. Daniell, J. K.

Hooper, H. K. Lichtenthaler, A. R. Portis, & B. C. Tripathy (Eds.), *The Chloroplast: Basics and Applications* (pp. 185-202). Dordrecht: Springer Netherlands.

Namikoshi, M., Murakami, T., Fujiwara, T., Nagai, H., Niki, T., Harigaya, E., . . . Tsujimura, S. (2004). Biosynthesis and transformation of homoanatoxin-a in the cyanobacterium *Raphidiopsis mediterranea skuja* and structures of three new homologues. *Chemical Research in Toxicology*, *17*(12), 1692-1696. doi:10.1021/tx0498152

Naranjo, B., Mignéé, C., Krieger-Liszkay, A., Hornero-Méndez, D., Gallardo-Guerrero, L., Cejudo, F. J., & Lindahl, M. (2016). The chloroplast NADPH thioredoxin reductase C, NTRC, controls non-photochemical quenching of light energy and photosynthetic electron transport in *Arabidopsis*. *Plant, Cell & Environment*, *39*(4), 804-822. doi:10.1111/pce.12652

Nesvizhskii, A. I., Keller, A., Kolker, E., & Aebersold, R. (2003). A statistical model for identifying proteins by tandem mass spectrometry. *Analytical Chemistry*, *75*(17), 4646-4658. doi:10.1021/ac0341261

Nikkanen, L., & Rintamäki, E. (2014). Thioredoxin-dependent regulatory networks in chloroplasts under fluctuating light conditions. *Philosophical Transactions of the Royal Society B: Biological Sciences*, *369*(1640). doi:10.1098/rstb.2013.0224

Niyogi, K. K., Grossman, A. R., & Björkman, O. (1998). *Arabidopsis* mutants define a central role for the xanthophyll cycle in the regulation of photosynthetic energy conversion. *The Plant Cell*, *10*(7), 1121-1134. Retrieved from <http://www.ncbi.nlm.nih.gov/pmc/articles/PMC144052/>

NOAA. (2021). Are all algal blooms harmful?

Novoselov, S. V., & Gladyshev, V. N. (2003). Non-animal origin of animal thioredoxin reductases: Implications for selenocysteine evolution and evolution of protein function through carboxy-terminal extensions. *Protein Science*, *12*(2), 372-378.

Oehrle, S., Rodriguez-Matos, M., Cartamil, M., Zavala, C., & Rein, K. S. (2017). Toxin composition of the 2016 *Microcystis aeruginosa* bloom in the St. Lucie Estuary, Florida. *Toxicon*, *138*, 169-172. doi:10.1016/j.toxicon.2017.09.005

- Paerl, H. W. (1997). Coastal eutrophication and harmful algal blooms: Importance of atmospheric deposition and groundwater as “new” nitrogen and other nutrient sources. *Limnology and Oceanography*, 42(5part2), 1154-1165. doi:10.4319/lo.1997.42.5_part_2.1154
- Pérez-Ruiz, J. M., Naranjo, B., Ojeda, V., Guinea, M., & Cejudo, F. J. (2017). NTRC-dependent redox balance of 2-Cys peroxiredoxins is needed for optimal function of the photosynthetic apparatus. *Proceedings of the National Academy of Sciences*, 114(45), 12069. doi:10.1073/pnas.1706003114
- Phlips, E. J., Badylak, S., Nelson, N. G., & Havens, K. E. (2020). Hurricanes, El Niño and harmful algal blooms in two sub-tropical Florida estuaries: Direct and indirect impacts. *Scientific Reports*, 10(1), 1910. doi:10.1038/s41598-020-58771-4
- Pierce, R., Henry, M., & Blum, P. (2008). Brevetoxin abundance and composition during ECOHAB-Florida field monitoring cruises in the Gulf of Mexico. *Continental Shelf Research*, 28(1), 45-58. doi:10.1016/j.csr.2007.04.012
- Pierce, R., Henry, M., Blum, P., & Payne, S. (2000). *Gymnodinium breve* toxins without cells: intra-cellular and extra-cellular toxins. *Harmful algal blooms*, 421-424.
- Pittman, J. K., Dean, A. P., & Osundeko, O. (2011). The potential of sustainable algal biofuel production using wastewater resources. *Bioresource Technology*, 102(1), 17-25. doi:10.1016/j.biortech.2010.06.035
- Poulin, R. X., Hogan, S., Poulson-Ellestad, K. L., Brown, E., Fernández, F. M., & Kubanek, J. (2018). *Karenia brevis* allelopathy compromises the lipidome, membrane integrity, and photosynthesis of competitors. *Scientific Reports*, 8(1), 9572-9572. doi:10.1038/s41598-018-27845-9
- Poulson-Ellestad, K. L., Jones, C. M., Roy, J., Viant, M. R., Fernández, F. M., Kubanek, J., & Nunn, B. L. (2014). Metabolomics and proteomics reveal impacts of chemically mediated competition on marine plankton. *Proceedings of the National Academy of Sciences*, 111(24), 9009. doi:10.1073/pnas.1402130111
- Prasad, A. V. K., & Shimizu, Y. (1989). The structure of hemibrevetoxin-B: a new type of toxin in the Gulf of Mexico red tide organism. *J Am Chem Soc*, 111(16), 6476-6477. doi:10.1021/ja00198a098

Premvardhan, L., Robert, B., Beer, A., & Büchel, C. (2010). Pigment organization in fucoxanthin chlorophyll a/c2 proteins (FCP) based on resonance Raman spectroscopy and sequence analysis. *Biochimica et Biophysica Acta (BBA) - Bioenergetics*, 1797(9), 1647-1656. doi:10.1016/j.bbabi.2010.05.002

Prince, E. K., Myers, T. L., & Kubanek, J. (2008). Effects of harmful algal blooms on competitors: Allelopathic mechanisms of the red tide dinoflagellate *Karenia brevis*. *Limnology and Oceanography*, 53(2), 531-541. doi:10.4319/lo.2008.53.2.0531

Pulido, O. M. (2008). Domoic acid toxicologic pathology: a review. *Marine Drugs*, 6(2), 180-219. doi:10.3390/md20080010

Radwan, F. F. Y., Wang, Z., & Ramsdell, J. S. (2005). Identification of a rapid detoxification mechanism for brevetoxin in rats. *Toxicological Sciences*, 85(2), 839-846. doi:10.1093/toxsci/kfi138

Ralph, S. A., van Dooren, G. G., Waller, R. F., Crawford, M. J., Fraunholz, M. J., Foth, B. J., . . . McFadden, G. I. (2004). Metabolic maps and functions of the *Plasmodium falciparum* apicoplast. *Nature Reviews Microbiology*, 2(3), 203-216. doi:10.1038/nrmicro843

Ramesh Kumar, B., Deviram, G., Mathimani, T., Duc, P. A., & Pugazhendhi, A. (2019). Microalgae as rich source of polyunsaturated fatty acids. *Biocatalysis and Agricultural Biotechnology*, 17, 583-588. doi:10.1016/j.bcab.2019.01.017

Ramos, V., & Vasconcelos, V. (2010). Palytoxin and analogs: biological and ecological effects. *Marine Drugs*, 8(7), 2021-2037. doi:10.3390/md8072021

Rantala, M., Lehtimäki, N., Aro, E.-M., & Suorsa, M. (2016). Downregulation of TAP38/PPH1 enables LHCII hyperphosphorylation in *Arabidopsis* mutant lacking LHCII docking site in PSI. *FEBS Letters*, 590(6), 787-794. doi:10.1002/1873-3468.12117

Rawat, I., Ranjith Kumar, R., Mutanda, T., & Bux, F. (2013). Biodiesel from microalgae: A critical evaluation from laboratory to large scale production. *Applied Energy*, 103, 444-467. doi:10.1016/j.apenergy.2012.10.004

Reguera, B., Riobó, P., Rodríguez, F., Díaz, P. A., Pizarro, G., Paz, B., . . . Blanco, J. (2014). Dinophysins toxins: causative organisms, distribution and fate in shellfish. *Marine Drugs*, 12(1), 394-461. doi:10.3390/md12010394

- Rengefors, K., Kremp, A., Reusch, T. B. H., & Wood, A. M. (2017). Genetic diversity and evolution in eukaryotic phytoplankton: revelations from population genetic studies. *Journal of Plankton Research*, *39*(2), 165-179. doi:10.1093/plankt/fbw098
- Reumann, S., Buchwald, D., & Lingner, T. (2012). PredPlantPTS1: A Web Server for the Prediction of Plant Peroxisomal Proteins. *Frontiers in plant science*, *3*, 194-194. doi:10.3389/fpls.2012.00194
- Reyes-Prieto, A., Yoon, H. S., & Bhattacharya, D. (2009). Marine Algal Genomics and Evolution. In J. H. Steele (Ed.), *Encyclopedia of Ocean Sciences (Second Edition)* (pp. 552-559). Oxford: Academic Press.
- Richter, A. S., Peter, E., Rothbart, M., Schlicke, H., Toivola, J., Rintamäki, E., & Grimm, B. (2013). Posttranslational influence of NADPH-dependent thioredoxin reductase C on enzymes in tetrapyrrole synthesis. *Plant Physiology*, *162*(1), 63-73. doi:10.1104/pp.113.217141
- Rinehart, K. L., Harada, K., Namikoshi, M., Chen, C., Harvis, C. A., Munro, M. H. G., . . . et al. (1988). Nodularin, microcystin, and the configuration of Adda. *J Am Chem Soc*, *110*(25), 8557-8558. doi:10.1021/ja00233a049
- Rochaix, J.-D. (2007). Role of thylakoid protein kinases in photosynthetic acclimation. *FEBS Letters*, *581*(15), 2768-2775. doi:10.1016/j.febslet.2007.04.038
- Rochaix, J.-D. (2013). Redox regulation of thylakoid protein kinases and photosynthetic gene expression. *Antioxid Redox Signal*, *18*(16), 2184-2201. doi:10.1089/ars.2012.5110
- Rochaix, J.-D., Lemeille, S., Shapiguzov, A., Samol, I., Fucile, G., Willig, A., & Goldschmidt-Clermont, M. (2012). Protein kinases and phosphatases involved in the acclimation of the photosynthetic apparatus to a changing light environment. *Philosophical Transactions of the Royal Society B: Biological Sciences*, *367*(1608), 3466-3474. doi:10.1098/rstb.2012.0064
- Rogers, M. B., Gilson, P. R., Su, V., McFadden, G. I., & Keeling, P. J. (2007). The complete chloroplast genome of the chlorarachniophyte *Bigeloviella natans*: evidence for independent origins of chlorarachniophyte and euglenid secondary endosymbionts. *Molecular Biology and Evolution*, *24*(1), 54-62.

- Rosen, B. H., Davis, T. W., Gobler, C. J., Kramer, B. J., & Loftin, K. A. (2017). *Cyanobacteria of the 2016 Lake Okeechobee and Okeechobee Waterway harmful algal bloom* (2017-1054). Retrieved from Reston, VA: <http://pubs.er.usgs.gov/publication/ofr20171054>
- Rosen, B. H., Loftin, K. A., Graham, J. L., Stahlhut, K. N., Riley, J. M., Johnston, B. D., & Senegal, S. (2018). *Understanding the effect of salinity tolerance on cyanobacteria associated with a harmful algal bloom in Lake Okeechobee, Florida* (2018-5092). Retrieved from Reston, VA: <http://pubs.er.usgs.gov/publication/sir20185092>
- Rossini, G. P., & Hess, P. (2010). Phycotoxins: chemistry, mechanisms of action and shellfish poisoning. In A. Luch (Ed.), *Molecular, Clinical and Environmental Toxicology: Volume 2: Clinical Toxicology* (pp. 65-122). Basel: Birkhäuser Basel.
- Rouhier, N., Villarejo, A., Srivastava, M., Gelhaye, E., Keech, O., Droux, M., . . . Jacquot, J.-P. (2005). Identification of plant glutaredoxin targets. *Antioxid Redox Signal*, 7(7-8), 919-929.
- Roy, S., Jagus, R., & Morse, D. (2018). Translation and translational control in dinoflagellates. *Microorganisms*, 6(2), 30.
- Roy, S., & Morse, D. (2013). Transcription and maturation of mRNA in dinoflagellates. *Microorganisms*, 1(1), 71-99. doi:10.3390/microorganisms1010071
- Ruiz-González, R., Milán, P., Bresolí-Obach, R., Stockert, J. C., Villanueva, A., Cañete, M., & Nonell, S. (2017). Photodynamic synergistic effect of pheophorbide a and doxorubicin in combined treatment against tumoral cells. *Cancers*, 9(2), 18. doi:10.3390/cancers9020018
- Ryan, D. E., Pepper, A. E., & Campbell, L. (2014). De novo assembly and characterization of the transcriptome of the toxic dinoflagellate *Karenia brevis*. *BMC Genomics*, 15(1), 888-888. doi:10.1186/1471-2164-15-888
- Saga, G., Giorgetti, A., Fufezan, C., Giacometti, G. M., Bassi, R., & Morosinotto, T. (2010). Mutation analysis of violaxanthin de-epoxidase identifies substrate-binding sites and residues involved in catalysis. *The Journal of biological chemistry*, 285(31), 23763-23770. doi:10.1074/jbc.M110.115097

- Saldarriaga, J. F., Taylor, F. J. R., Keeling, P. J., & Cavalier-Smith, T. (2001). Dinoflagellate Nuclear SSU rRNA Phylogeny Suggests Multiple Plastid Losses and Replacements. *Journal of Molecular Evolution*, 53(3), 204-213. doi:10.1007/s002390010210
- Salmeen, A., & Barford, D. (2005). Functions and mechanisms of redox regulation of cysteine-based phosphatases. *Antioxid Redox Signal*, 7(5-6), 560-577. doi:10.1089/ars.2005.7.560
- Schaller, S., Latowski, D., Jemioła-Rzemińska, M., Dawood, A., Wilhelm, C., Strzałka, K., & Goss, R. (2011). Regulation of LHCII aggregation by different thylakoid membrane lipids. *Biochimica et Biophysica Acta (BBA) - Bioenergetics*, 1807(3), 326-335. doi:10.1016/j.bbabi.2010.12.017
- Schaller, S., Latowski, D., Jemioła-Rzemińska, M., Wilhelm, C., Strzałka, K., & Goss, R. (2010). The main thylakoid membrane lipid monogalactosyldiacylglycerol (MGDG) promotes the de-epoxidation of violaxanthin associated with the light-harvesting complex of photosystem II (LHCII). *Biochimica et Biophysica Acta (BBA) - Bioenergetics*, 1797(3), 414-424. doi:10.1016/j.bbabi.2009.12.011
- Schoepp, N. G., Stewart, R. L., Sun, V., Quigley, A. J., Mendola, D., Mayfield, S. P., & Burkart, M. D. (2014). System and method for research-scale outdoor production of microalgae and cyanobacteria. *Bioresource Technology*, 166, 273-281. doi:10.1016/j.biortech.2014.05.046
- Schroeder, A., Mueller, O., Stocker, S., Salowsky, R., Leiber, M., Gassmann, M., . . . Ragg, T. (2006). The RIN: an RNA integrity number for assigning integrity values to RNA measurements. *BMC molecular biology*, 7, 3-3. doi:10.1186/1471-2199-7-3
- Schürmann, P., & Buchanan, B. B. (1975). Role of ferredoxin in the activation of sedoheptulose diphosphatase in isolated chloroplasts. *Biochimica et Biophysica Acta (BBA)-Bioenergetics*, 376(1), 189-192.
- Schürmann, P., & Buchanan, B. B. (2008). The ferredoxin/thioredoxin system of oxygenic photosynthesis. *Antioxid Redox Signal*, 10(7), 1235-1274.
- Seiwert, D., Witt, H., Janshoff, A., & Paulsen, H. (2017). The non-bilayer lipid MGDG stabilizes the major light-harvesting complex (LHCII) against unfolding. *Scientific Reports*, 7, 5158. doi:10.1038/s41598-017-05328-7

Serrato, A. J., Pérez-Ruiz, J. M., Spínola, M. C., & Cejudo, F. J. (2004). A novel NADPH thioredoxin reductase, localized in the chloroplast, which deficiency causes hypersensitivity to abiotic stress in *Arabidopsis thaliana*. *Journal of Biological Chemistry*, 279(42), 43821-43827. doi:10.1074/jbc.M404696200

Sibbald, S. J., & Archibald, J. M. (2020). Genomic Insights into Plastid Evolution. *Genome biology and evolution*, 12(7), 978-990. doi:10.1093/gbe/evaa096

Siefermann, D., & Yamamoto, H. Y. (1974). Light-induced de-epoxidation of violaxanthin in lettuce chloroplasts. III. Reaction kinetics and effect of light intensity on de-epoxidase activity and substrate availability. *Biochimica et Biophysica Acta (BBA) - Bioenergetics*, 357(1), 144-150. doi:10.1016/0005-2728(74)90119-4

Sievers, F., Wilm, A., Dineen, D., Gibson, T. J., Karplus, K., Li, W., . . . Higgins, D. G. (2011). Fast, scalable generation of high-quality protein multiple sequence alignments using Clustal Omega. *Molecular Systems Biology*, 7(1), 539. doi:10.1038/msb.2011.75

Simionato, D., Basso, S., Zaffagnini, M., Lana, T., Marzotto, F., Trost, P., & Morosinotto, T. (2015). Protein redox regulation in the thylakoid lumen: The importance of disulfide bonds for violaxanthin de-epoxidase. *FEBS Letters*, 589(8), 919-923. doi:10.1016/j.febslet.2015.02.033

Singh, N. K., Sonani, R. R., Rastogi, R. P., & Madamwar, D. (2015). The phycobilisomes: an early requisite for efficient photosynthesis in cyanobacteria. *EXCLI journal*, 14, 268-289. doi:10.17179/excli2014-723

Sinkins, W. G., Estacion, M., Prasad, V., Goel, M., Shull, G. E., Kunze, D. L., & Schilling, W. P. (2009). Maitotoxin converts the plasmalemmal Ca(2+) pump into a Ca(2+)-permeable nonselective cation channel. *American journal of physiology. Cell physiology*, 297(6), C1533-C1543. doi:10.1152/ajpcell.00252.2009

Spolaore, P., Joannis-Cassan, C., Duran, E., & Isambert, A. (2006). Commercial applications of microalgae. *Journal of Bioscience and Bioengineering*, 101(2), 87-96. doi:10.1263/jbb.101.87

Standfuss, J., Terwisscha van Scheltinga, A. C., Lamborghini, M., & Kühlbrandt, W. (2005). Mechanisms of photoprotection and nonphotochemical quenching in pea light-harvesting complex at 2.5 Å resolution. *The EMBO journal*, 24(5), 919-928. doi:10.1038/sj.emboj.7600585

- Steiner, J. M., & Löffelhardt, W. (2002). Protein import into cyanelles. *Trends in Plant Science*, 7(2), 72-77.
- Stenbaek, A., Hansson, A., Wulff, R. P., Hansson, M., Dietz, K.-J., & Jensen, P. E. (2008). NADPH-dependent thioredoxin reductase and 2-Cys peroxiredoxins are needed for the protection of Mg-protoporphyrin monomethyl ester cyclase. *FEBS Letters*, 582(18), 2773-2778. doi:10.1016/j.febslet.2008.07.006
- Sun, P., Leeson, C., Zhi, X., Leng, F., Pierce, R. H., Henry, M. S., & Rein, K. S. (2016). Characterization of an epoxide hydrolase from the Florida Red tide dinoflagellate, *Karenia brevis*. *Phytochemistry*, 122, 11-21. doi:10.1016/j.phytochem.2015.11.002
- Sunda, W. G., Burleson, C., Hardison, D. R., Morey, J. S., Wang, Z., Wolny, J., . . . Van Dolah, F. M. (2013). Osmotic stress does not trigger brevetoxin production in the dinoflagellate *Karenia brevis*. *Proceedings of the National Academy of Sciences of the United States of America*, 110(25), 10223-10228. doi:10.1073/pnas.1217716110
- Tengs, T., Dahlberg, O. J., Shalchian-Tabrizi, K., Klaveness, D., Rudi, K., Delwiche, C. F., & Jakobsen, K. S. (2000). Phylogenetic analyses indicate that the 19' hexanoyloxy-fucoxanthin-containing dinoflagellates have tertiary plastids of haptophyte origin. *Molecular Biology and Evolution*, 17(5), 718-729.
- Tester, P. A., Turner, J. T., & Shea, D. (2000). Vectorial transport of toxins from the dinoflagellate *Gymnodinium breve* through copepods to fish. *Journal of Plankton Research*, 22(1), 47-62. doi:10.1093/plankt/22.1.47
- Thieulin-Pardo, G., Schramm, A., Lignon, S., Lebrun, R., Kojadinovic, M., & Gontero, B. (2016). The intriguing CP12-like tail of adenylate kinase 3 from *Chlamydomonas reinhardtii*. *The FEBS Journal*, 283(18), 3389-3407. doi:10.1111/febs.13814
- Thompson, A., Schäfer, J., Kuhn, K., Kienle, S., Schwarz, J., Schmidt, G., . . . Hamon, C. (2003). Tandem mass tags: A novel quantification strategy for comparative analysis of complex protein mixtures by MS/MS. *Analytical Chemistry*, 75(8), 1895-1904. doi:10.1021/ac0262560
- Thormählen, I., Meitzel, T., Groysman, J., Öchsner, A. B., von Roepenack-Lahaye, E., Naranjo, B., . . . Geigenberger, P. (2015). Thioredoxin *fl* and NADPH-dependent thioredoxin reductase *c* have overlapping functions in regulating photosynthetic

metabolism and plant growth in response to varying light conditions. *Plant Physiology*, 169(3), 1766-1786. doi:10.1104/pp.15.01122

Tiselius, P., Saiz, E., & Kiørboe, T. (2013). Sensory capabilities and food capture of two small copepods, *Paracalanus parvus* and *Pseudocalanus sp.* *Limnology and Oceanography*, 58(5), 1657-1666. doi:10.4319/lo.2013.58.5.1657

Tominack, S. A., Coffey, K. Z., Yoskowitz, D., Sutton, G., & Wetz, M. S. (2020). An assessment of trends in the frequency and duration of *Karenia brevis* red tide blooms on the South Texas coast (western Gulf of Mexico). *PLOS ONE*, 15(9), e0239309. doi:10.1371/journal.pone.0239309

Townhill, B. L., Tinker, J., Jones, M., Pitois, S., Creach, V., Simpson, S. D., . . . Pinnegar, J. K. (2018). Harmful algal blooms and climate change: exploring future distribution changes. *ICES Journal of Marine Science*, 75(6), 1882-1893. doi:10.1093/icesjms/fsy113

Tuladhar, A., Hondal, R. J., Colon, R., Hernandez, E. L., & Rein, K. S. (2018). Effectors of thioredoxin reductase: Brevetoxins and manumycin-A. *Comparative Biochemistry and Physiology Part C: Toxicology & Pharmacology*. doi:10.1016/j.cbpc.2018.11.015

Twiner, M. J., Rehmann, N., Hess, P., & Doucette, G. J. (2008). Azaspiracid shellfish poisoning: a review on the chemistry, ecology, and toxicology with an emphasis on human health impacts. *Marine Drugs*, 6(2), 39-72. doi:10.3390/md20080004

Untergasser, A., Cutcutache, I., Koressaar, T., Ye, J., Faircloth, B. C., Remm, M., & Rozen, S. G. (2012). Primer3--new capabilities and interfaces. *Nucleic Acids Research*, 40(15), e115-e115. doi:10.1093/nar/gks596

Van Dolah, F. M., Morey, J. S., Milne, S., Ung, A., Anderson, P. E., & Chinain, M. (2020). Transcriptomic analysis of polyketide synthases in a highly ciguatoxic dinoflagellate, *Gambierdiscus polynesiensis* and low toxicity *Gambierdiscus pacificus*, from French Polynesia. *PLOS ONE*, 15(4), e0231400. doi:10.1371/journal.pone.0231400

Van Dolah, F. M., Zippay, M. L., Pezzolesi, L., Rein, K. S., Johnson, J. G., Morey, J. S., . . . Pistocchi, R. (2013). Subcellular localization of dinoflagellate polyketide synthases and fatty acid synthase activity. *Journal of Phycology*, 49(6), 1118-1127. doi:10.1111/jpy.12120

- Van Wagoner, R. M., Satake, M., & Wright, J. L. C. (2014). Polyketide biosynthesis in dinoflagellates: what makes it different? *Natural Product Reports*, *31*(9), 1101-1137. doi:10.1039/C4NP00016A
- Verma, A., Kohli, G. S., Harwood, D. T., Ralph, P. J., & Murray, S. A. (2019). Transcriptomic investigation into polyketide toxin synthesis in *Ostreopsis* (Dinophyceae) species. *Environmental Microbiology*, *21*(11), 4196-4211. doi:10.1111/1462-2920.14780
- Vigna, K. L., Quesada, I., & Verdugo, P. (2012). Exocytic mechanisms of storage and release of brevetoxin in the dinoflagellate *Karenia brevis*. *Biophysical Journal*, *102*(3, Supplement 1), 319a-320a. doi:10.1016/j.bpj.2011.11.1755
- Waggett, R. J., Hardison, D. R., & Tester, P. A. (2012). Toxicity and nutritional inadequacy of *Karenia brevis*: synergistic mechanisms disrupt top-down grazer control. *Marine Ecology Progress Series*, *444*, 15-30. Retrieved from <https://www.int-res.com/abstracts/meps/v444/p15-30/>
- Walsby, A. E. (1981). Cyanobacteria: Planktonic Gas-Vacuolate Forms. In M. P. Starr, H. Stolp, H. G. Trüper, A. Balows, & H. G. Schlegel (Eds.), *The Prokaryotes: A Handbook on Habitats, Isolation, and Identification of Bacteria* (pp. 224-235). Berlin, Heidelberg: Springer Berlin Heidelberg.
- Walsh, C. J., Leggett, S. R., Henry, M. S., Blum, P. C., Osborn, S., & Pierce, R. H. (2009). Cellular metabolism of brevetoxin (PbTx-2) by a monocyte cell line (U-937). *Toxicon*, *53*(1), 135-145. doi:10.1016/j.toxicon.2008.10.024
- Walsh, J. J., Lenes, J. M., Weisberg, R. H., Zheng, L., Hu, C., Fanning, K. A., . . . Smith, J. (2017). More surprises in the global greenhouse: Human health impacts from recent toxic marine aerosol formations, due to centennial alterations of world-wide coastal food webs. *Marine Pollution Bulletin*, *116*(1), 9-40. doi:10.1016/j.marpolbul.2016.12.053
- Wan, X., Yao, G., Liu, Y., Chen, J., & Jiang, H. (2019). Research progress in the biosynthetic mechanisms of marine polyether toxins. *Marine Drugs*, *17*(10), 594. doi:10.3390/md17100594
- Wang, J., Youkharibache, P., Zhang, D., Lanczycki, C. J., Geer, R. C., Madej, T., . . . Marchler-Bauer, A. (2020). iCn3D, a web-based 3D viewer for sharing 1D/2D/3D representations of biomolecular structures. *Bioinformatics*, *36*(1), 131-135. doi:10.1093/bioinformatics/btz502

- Waterhouse, A., Bertoni, M., Bienert, S., Studer, G., Tauriello, G., Gumienny, R., . . . Schwede, T. (2018). SWISS-MODEL: homology modelling of protein structures and complexes. *Nucleic Acids Research*, *46*(W1), W296-W303. doi:10.1093/nar/gky427
- Wheeler, D. L., Church, D. M., Federhen, S., Lash, A. E., Madden, T. L., Pontius, J. U., . . . Wagner, L. (2003). Database resources of the National Center for Biotechnology. *Nucleic acids research*, *31*(1), 28-33. doi:10.1093/nar/gkg033
- Wiese, M., D'Agostino, P. M., Mihali, T. K., Moffitt, M. C., & Neilan, B. A. (2010). Neurotoxic alkaloids: saxitoxin and its analogs. *Marine Drugs*, *8*(7), 2185-2211. doi:10.3390/md8072185
- Witman, S. (2017). World's biggest oxygen producers living in the swirling ocean waters. *Eos*, *98*. doi:10.1029/2017EO081067
- Wollast, R. (1991). Ocean margin processes in global change. *New York, Wiley*, 365-381.
- Wu, J., Rong, L., Lin, W., Kong, L., Wei, D., Zhang, L., . . . Xu, X. (2021). Functional redox links between lumen thiol oxidoreductase1 and serine/threonine-protein kinase STN7. *Plant Physiology*. doi:10.1093/plphys/kiab091
- Wu, Z., Luo, H., Yu, L., Lee, W. H., Li, L., Mak, Y. L., . . . Lam, P. K. S. (2020). Characterizing ciguatoxin (CTX)- and Non-CTX-producing strains of *Gambierdiscus balechii* using comparative transcriptomics. *Science of The Total Environment*, *717*, 137184. doi:10.1016/j.scitotenv.2020.137184
- Xiao, S., Gao, W., Chen, Q.-F., Chan, S.-W., Zheng, S.-X., Ma, J., . . . Chye, M.-L. (2010). Overexpression of *Arabidopsis* acyl-CoA binding protein ACBP3 promotes starvation-induced and age-dependent leaf senescence. *The Plant Cell*, *22*(5), 1463-1482. doi:10.1105/tpc.110.075333
- Xu, J., & Kiørboe, T. (2018). Toxic dinoflagellates produce true grazer deterrents. *Ecology*, *99*(10), 2240-2249. doi:10.1002/ecy.2479
- Yamamoto H.Y., C. E. E., Yamada D.K. (1974). Effect of chloroplast lipids on violaxanthin de-epoxidase activity. *Proc. 3rd Int. Cong. Photosyn.*, 1999–2006.

- Yamamoto, H. Y. (2006). Functional roles of the major chloroplast lipids in the violaxanthin cycle. *Planta*, 224(3), 719-724. doi:10.1007/s00425-006-0257-5
- Yamamoto, H. Y., Higashi, R. M. (1978). Violaxanthin de-epoxidase: Lipid composition and substrate specificity. *Archives of Biochemistry and Biophysics*, 190(2), 514-522. doi:10.1016/0003-9861(78)90305-3
- Yamaryo, Y., Motohashi, K., Takamiya, K.-i., Hisabori, T., & Ohta, H. (2006). In vitro reconstitution of monogalactosyldiacylglycerol (MGDG) synthase regulation by thioredoxin. *FEBS Letters*, 580(17), 4086-4090. doi:10.1016/j.febslet.2006.06.050
- Yang, J., Carroll, K. S., & Liebler, D. C. (2016). The expanding landscape of the thiol redox proteome. *Molecular & cellular proteomics : MCP*, 15(1), 1-11. doi:10.1074/mcp.O115.056051
- Yen, H.-W., Hu, I. C., Chen, C.-Y., Ho, S.-H., Lee, D.-J., & Chang, J.-S. (2013). Microalgae-based biorefinery – From biofuels to natural products. *Bioresource Technology*, 135, 166-174. doi:10.1016/j.biortech.2012.10.099
- Yoon, H. S., Hackett, J. D., & Bhattacharya, D. (2002). A single origin of the peridinin- and fucoxanthin-containing plastids in dinoflagellates through tertiary endosymbiosis. *Proceedings of the National Academy of Sciences of the United States of America*, 99(18), 11724-11729. Retrieved from <http://www.jstor.org.ezproxy.fiu.edu/stable/3073106>
- Zhang, B., Ge, C., Yao, J., Liu, Y., Xie, H., & Fang, J. (2015). Selective selenol fluorescent probes: Design, synthesis, structural determinants, and biological applications. *J Am Chem Soc*, 137(2), 757-769. doi:10.1021/ja5099676
- Zhang, Y., Launay, H., Liu, F., Lebrun, R., & Gontero, B. (2018). Interaction between adenylate kinase 3 and glyceraldehyde-3-phosphate dehydrogenase from *Chlamydomonas reinhardtii*. *The FEBS Journal*, 285(13), 2495-2503. doi:10.1111/febs.14494
- Zhong, L., & Holmgren, A. (2000). Essential role of selenium in the catalytic activities of mammalian thioredoxin reductase revealed by characterization of recombinant enzymes with selenocysteine mutations *Journal of Biological Chemistry*, 275(24), 18121-18128. doi:10.1074/jbc.M000690200

Zhou, J., & Fritz, L. (1994). Okadaic acid antibody localizes to chloroplasts in the DSP-toxin-producing dinoflagellates *Prorocentrum lima* and *Prorocentrum maculosum*. *Phycologia*, 33(6), 455-461. doi:10.2216/i0031-8884-33-6-455.1

APPENDIX

APPENDIX A: CHAPTER 3 SUPPORTING INFORMATION

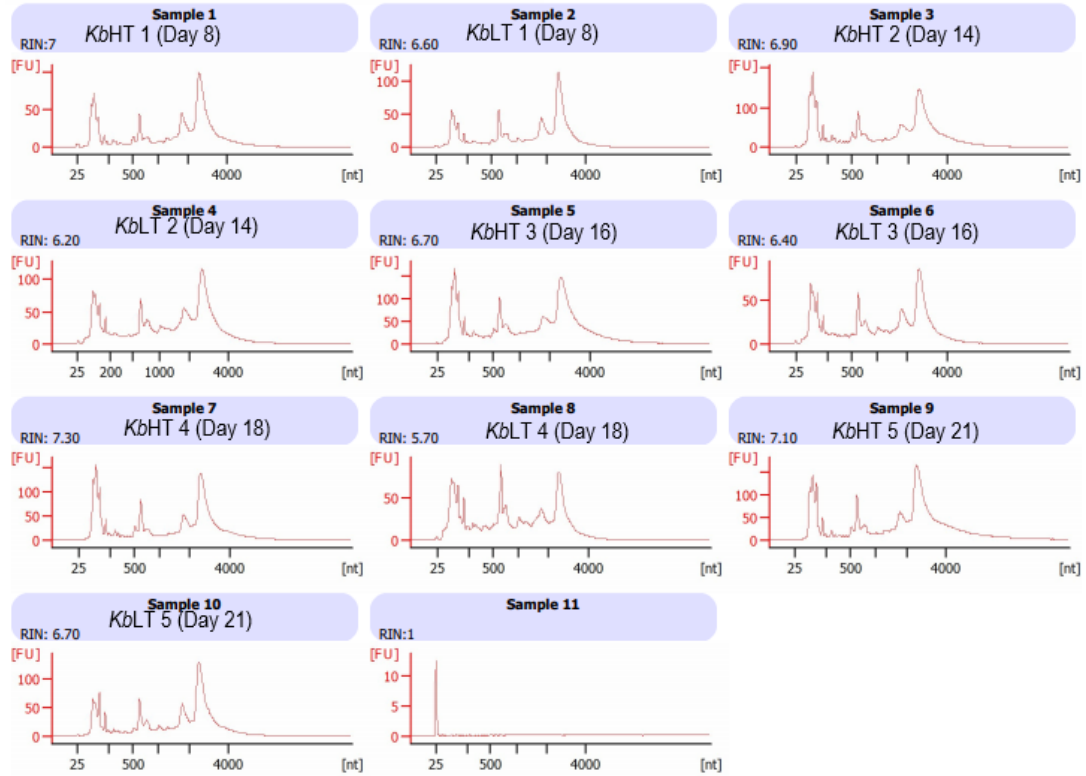


Figure S3.1 Capillary electrophoresis data for each q-RT-PCR sample demonstrating the RIN values calculated

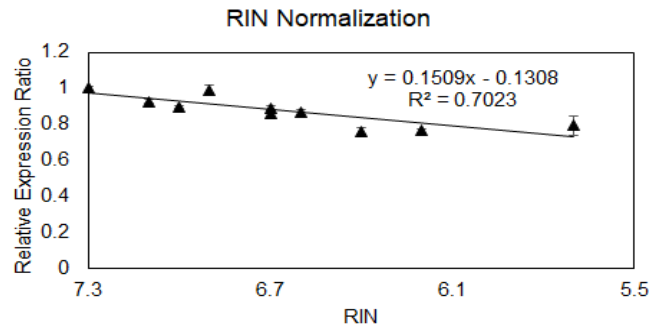


Figure S3.2 RIN Correction of relative expression for q-RT-PCR. RIN correction was performed by plotting a linear regression of relative expression ratio (RER) for all biological replicates of both low and high toxic vs RIN. RER was found using the equation $RER(n) = \frac{C_{t(RuBisCO)}_n}{C_{t(RuBisCO)}_\alpha}$ for each technical replicate within the 5 pairs of biological replicates ($y = 0.1509x - 0.1308$). Where

n = sample number, and α = sample number H4 (the sample with the highest quality RNA). The RER(calculated) was found by substituting the RIN for x in the above equation. RER(calculated) was used as a coefficient for each samples C_i to account for differing RNA quality.

Table S3.1 Relative expression ratio vs RIN calculations

Sample	RIN	Relative Expression Ratio			AVG RER	SD RER	Relative Expression Ratio (Calculated)
H4	7.3	1.009943	0.994371	0.995833	1.000049	0.012103	0.970884
H5	7.1	0.926357	0.930174	0.923829	0.926787	0.00855	0.9407
H1	7	0.897504	0.900488	0.893949	0.897314	0.008348	0.925608
H2	6.9	0.99001	0.959839	1.011451	0.9871	0.027386	0.910515
L5	6.7	0.896316	0.891595	0.878297	0.888736	0.01208	0.880331
H3	6.7	0.882877	0.842771	0.855008	0.860219	0.021673	0.880331
L1	6.6	0.870954	0.875458	0.855549	0.86732	0.012857	0.865239
L3	6.4	0.777459	0.751572	0.755766	0.761599	0.015229	0.835055
L2	6.2	0.769945	0.763435	0.754924	0.762768	0.009975	0.804871
L4	5.7	0.735651	0.830879	0.806631	0.791054	0.051334	0.729411

Table S3.2 All lipid species quantified (nmol per mg protein)

Compound Name	Average nmol lipid per mg protein (n=4)		T.Test
	KbHT(SD)	KbLT(SD)	
DGDG(28:0)	0.252(0.0262)	0.266(0.0346)	0.5374
DGDG(30:1)	0.015(0.0057)	0.016(0.0081)	0.8182
DGDG(30:0)	1.278(0.1638)	1.211(0.2054)	0.6261
DGDG(32:4)	2.475(0.2475)	2.746(0.5118)	0.3769
DGDG(32:1)	0.263(0.0349)	0.186(0.0253)	0.0117
DGDG(32:0)	0.651(0.0992)	0.851(0.1349)	0.0540
DGDG(34:5)	0.014(0.0056)	0.036(0.0164)	0.0468
DGDG(34:4)	0.013(0.0027)	0.024(0.0108)	0.0766
DGDG(34:3)	0.044(0.0091)	0.055(0.0127)	0.1924

DGDG(34:2)	0.184(0.0213)	0.285(0.0371)	0.0032
DGDG(34:1)	0.251(0.0147)	0.467(0.0697)	0.0009
DGDG(36:6)	0.022(0.0149)	0.037(0.0066)	0.1172
DGDG(36:3)	0.014(0.0092)	0.003(0.0036)	0.0665
AVG DGDG	5.474(0.5027)	6.184(0.6599)	0.1381
MGDG(30:1)	0.408(0.0409)	0.859(0.3617)	0.0478
MGDG(32:5)	2.245(0.4907)	4.375(0.6300)	0.0018
MGDG(32:0)	0.012(0.0074)	0.026(0.0066)	0.0389
MGDG(34:6)	0.104(0.0346)	0.113(0.0161)	0.6540
MGDG(34:5)	0.020(0.0061)	0.123(0.0452)	0.0041
MGDG(34:2)	0.046(0.0209)	0.028(0.0110)	0.1728
MGDG(34:1)	0.019(0.0086)	0.031(0.0108)	0.1377
MGDG(36:10)	1.112(0.3076)	2.003(0.3025)	0.0061
MGDG(36:9)	0.162(0.0411)	0.500(0.1150)	0.0015
MGDG(36:8)	0.014(0.0025)	0.093(0.0373)	0.0056
MGDG(36:6)	0.011(0.0063)	0.006(0.0039)	0.2059
MGDG(36:3)	0.028(0.0132)	0.015(0.0067)	0.1540
AVG MGDG	4.182(0.4877)	8.172(0.8352)	0.0002
Total Galactolipids	9.656(0.0966)	14.355(1.4334)	0.0006
PG(34:0)	0.000(0.0004)	0.001(0.0012)	0.2152
PG(36:7)	0.212(0.0739)	0.497(0.1424)	0.0120
PG(36:2)	0.071(0.0446)	0.044(0.0808)	0.5872
AVG PG	0.283(0.0561)	0.543(0.1350)	0.0120
TOTAL	9.939(0.1219)	14.898(1.4539)	0.0005

Table S3.3 All SQDG species analyzed (signal per mg protein)

Compound Formula	Average signal per mg protein (n=4)		T.Test
	KbHT(SD)	KbLT(SD)	
SQDG(28:1)	71.98(7.80)	48.13(5.99)	0.00285
SQDG(28:0)	399.65(48.60)	426.69(51.48)	0.473948
SQDG(30:2)	18.36(7.13)	10.14(2.69)	0.07439
SQDG(30:1)	162.24(11.46)	75.46(13.68)	6.79E-05
SQDG(30:0)	31.65(10.19)	27.89(7.69)	0.576891
SQDG(32:3)	6.04(2.99)	1.72(1.37)	0.039266
SQDG(32:2)	13.83(5.21)	7.44(1.75)	0.059083
SQDG(32:1)	211.84(25.82)	90.99(16.63)	0.000223
SQDG(32:0)	35.08(12.51)	17.43(11.74)	0.085377
SQDG(34:1)	7.95(3.55)	7.57(2.66)	0.869934
SQDG(36:2)	8.52(1.65)	4.89(1.99)	0.031012

SQDG(38:6)	96.89(17.00)	110.81(5.45)	0.169811
TOTAL SQDG	1064.05(91.98)	829.17(76.24)	0.007694

APPENDIX B: CHAPTER 4 SUPPORTING INFORMATION

Table S4.1 Ratios of IodoTMT intensities for plastid localized Trx in *KbLT* and *KbHT*

<i>Trx Loci</i>	Trx/Total *10⁴		<u>Light</u> (Light+Heavy)	
	<i>KbHT</i>	<i>KbLT</i>	<i>KbHT</i>	<i>KbLT</i>
34048	0.142	0.104	0.121	0.229
	0.178	0.138	0.154	0.114
5756	0.405	0.371	0.472	0.620
	0.641	0.396	0.449	0.545
35627	0.878	0.755	0.343	0.390
	1.09	0.748	0.317	0.384
	0.974	0.586	0.292	0.319
10291	0.696	1.45	0.317	0.490
	0.483	0.995	0.274	0.265
34116	0.0705	0.065	0.25	0.292
6359	0.105	0.064	0.079	0.129
58065	0.116	0.239	0.072	0.065
	0.0835	0.161	0.00	0.034
ρ (t-test)	0.86		0.006	

Table S4.2 Ratios of IodoTMT intensities for plastid localized Grx in *KbLT* and *KbHT*

<i>Grx Loci</i>	Grx/Total *10⁴		<u>Light</u> (Light+Heavy)	
	<i>KbHT</i>	<i>KbLT</i>	<i>KbHT</i>	<i>KbLT</i>
23910	0.289	0.233	0.473	0.623
	0.245	0.148	0.504	0.523
	0.332	0.189	0.325	0.455
	0.191	0.128	0.381	0.469
15301	0.816	0.705	0.042	0.038
	1.179	0.992	0.090	0.120
	1.820	1.548	0.055	0.051
	1.270	0.949	0.159	0.212
6859	3.386	2.267	0.041	0.046
	2.103	1.139	0.059	0.117
	3.512	2.326	0.032	0.038
	2.790	1.419	0.306	0.497
ρ (t-test)	0.009		0.007	

Table S4.3 Ratios of IodoTMT intensities for plastid localized Prx in *KbLT* and *KbHT*

<i>Prx Loci</i>	Prx/Total *10⁴		<u>Light</u> (Light+Heavy)	
	<i>KbHT</i>	<i>KbLT</i>	<i>KbHT</i>	<i>KbLT</i>
15465	0.168	0.166	0.186	0.235
	0.072	0.062	0.192	0.205
30380	0.240	0.196	0.205	0.190
19368	0.522	0.564	0.292	0.361
	0.307	0.352	0.443	0.621
	0.087	0.094	0.330	0.376
18946	0.598	0.517	0.402	0.447
	0.185	0.156	0.273	0.282
	0.149	0.083	0.194	0.221
63998	0.164	0.152	0.196	0.193
	0.207	0.240	0.250	0.180
ρ (t-test)	0.43		0.12	

Table S4.4 Ratios of IodoTMT intensities for plastid localized GR in KbLT and KbHT

<i>GR Loci</i>	GR/Total *10⁴		<u>Light</u> (Light+Heavy)	
	<i>KbHT</i>	<i>KbLT</i>	<i>KbHT</i>	<i>KbLT</i>
60832	0.277	0.243	0.547	0.675
53580	2.218	1.972	0.400	0.505
	1.022	0.862	0.493	0.626
	2.341	1.932	0.384	0.555
	1.441	1.332	0.510	0.676
ρ (t-test)	0.041		3.31 E ⁻⁴	

Table S4.5 Ratios of IodoTMT intensities for non-plastid localized GR in *KbLT* and *KbHT*

<i>Non-plastid GR Loci</i>	GR/Total *10⁴		<u>Light</u> (Light+Heavy)	
	<i>KbHT</i>	<i>KbLT</i>	<i>KbHT</i>	<i>KbLT</i>
36941	0.059	0.108	0.550	0.688
HT/LT	0.545		0.799	

Table S4.6 Ratios of IodoTMT intensities for plastid localized TrxR in KbLT and KbHT

<i>TrxR Loci</i>	TrxR/Total *10⁴		<u>Light</u> (Light+Heavy)	
	<i>KbHT</i>	<i>KbLT</i>	<i>KbHT</i>	<i>KbLT</i>
29890 (-2)	0.580	0.606	0.064	0.051
29890 (-3)	0.786	0.968	0.212	0.220
21941	0.301	0.222	0.178	0.224
ρ (t-test)	0.63		0.50	

Table S4.7 Ratios of IodoTMT intensities for plastid localized TrxR in KbLT and KbHT

<i>Kinase Loci</i>	Kinase/Total *10⁴		Light (Light+Heavy)	
	<i>KbHT</i>	<i>KbLT</i>	<i>KbHT</i>	<i>KbLT</i>
15581	0.097	0.314	0.314	0.613
15074	0.160	0.342	0.127	0.111
	0.831	4.597	0.184	0.242
15581	0.452	0.845	0.449	0.643
	0.410	0.606	0.404	0.545
	0.628	0.991	0.236	0.423
	0.337	0.956	0.447	0.628
25944	0.206	0.351	0.231	0.295
	0.231	0.391	0.138	0.169
10316	0.096	0.152	0.404	0.654
	0.075	0.124	0.553	0.537
29604	0.410	0.738	0.486	0.575
	0.158	0.277	0.412	0.429
	0.387	0.495	0.240	0.315
	0.480	0.839	0.373	0.434
2155	0.316	0.435	0.466	0.671
	0.402	0.686	0.350	0.459
42649	0.086	0.136	0.098	0.187
	0.086	0.109	0.096	0.063
	0.303	0.484	0.125	0.226
14817	0.180	0.245	0.359	0.468
575	0.238	0.321	0.057	0.089
25047	1.788	2.819	0.340	0.399
	3.179	4.185	0.302	0.345
	0.811	0.931	0.218	0.299
	2.417	3.131	0.233	0.387
16489	0.256	0.333	0.136	0.168
6265	0.081	0.104	0.568	0.726
3264	0.090	0.133	0.484	0.690
	0.421	0.590	0.269	0.401
	0.217	0.335	0.144	0.200
	1.086	0.999	0.259	0.394
28601	0.200	0.261	0.642	0.812

	0.311	0.332	0.363	0.636
	0.259	0.388	0.485	0.775
10074	0.184	0.233	0.461	0.579
23426	0.253	0.318	0.335	0.562
49545	1.336	1.716	0.400	0.511
	1.930	2.253	0.292	0.306
	0.441	0.548	0.111	0.103
21919	0.248	0.322	0.402	0.573
	0.361	0.575	0.465	0.578
	0.309	0.281	0.213	0.358
	0.256	0.281	0.325	0.524
17321	0.151	0.188	0.478	0.633
	0.329	0.383	0.310	0.355
	0.178	0.160	0.164	0.246
	0.132	0.209	0.189	0.356
1814	0.219	0.272	0.528	0.699
	0.273	0.302	0.371	0.453
183	0.062	0.069	0.180	0.328
45136	0.472	0.673	0.428	0.529
	0.352	0.399	0.331	0.382
	0.433	0.379	0.304	0.374
43559	0.321	0.334	0.250	0.301
	0.390	0.488	0.174	0.212
	0.309	0.301	0.136	0.168
	0.363	0.419	0.190	0.173
24499	0.481	0.449	0.120	0.274
	0.271	0.334	0.171	0.191
13181	0.509	0.526	0.345	0.517
	2.847	3.072	0.313	0.415
	1.533	1.413	0.161	0.273
	3.618	4.282	0.236	0.382
37408	0.666	0.680	0.143	0.160
	0.654	0.675	0.169	0.198
15751	0.086	0.085	0.392	0.539
45455	0.247	0.249	0.481	0.688
	0.408	0.362	0.429	0.546
	0.247	0.340	0.205	0.420
	0.298	0.216	0.323	0.602

753	0.118	0.109	0.068	0.255
19855	0.291	0.344	0.218	0.474
	0.682	0.590	0.185	0.229
	0.270	0.199	0.189	0.332
49207	0.383	0.331	0.422	0.421
37858	0.132	0.128	0.517	0.673
	0.265	0.229	0.451	0.555
	0.113	0.080	0.253	0.444
22306	0.357	0.293	0.123	0.173
31952	0.477	0.392	0.401	0.548
10090	0.148	0.121	0.444	0.592
57475	0.121	0.092	0.498	0.544
9911	0.646	0.391	0.175	0.398
9869	0.300	0.189	0.332	0.435
	0.354	0.201	0.270	0.364
	0.629	0.271	0.168	0.155
48653	0.078	0.039	0.501	0.557
11181	0.416	0.183	0.081	0.258
8543	1.142	0.554	0.355	0.447
	2.032	0.936	0.329	0.320

	2.108	0.734	0.157	0.204
	1.394	0.684	0.241	0.303
43984	1.691	0.680	0.355	0.474
	1.819	0.781	0.278	0.306
22299	1.163	0.703	0.127	0.050
	1.271	0.733	0.086	0.039
	1.061	0.452	0.084	0.012
	0.510	0.085	0.146	0.00
ρ (t-test)	0.38		1.37 E ⁻²⁰	

Table S4.8 Ratios of IodoTMT intensities for plastid localized kinases in KbLT and KbHT

<i>Phosphatase Loci</i>	Kinase/Total *10⁴		Light (Light+Heavy)				
	<i>KbHT</i>	<i>KbLT</i>	<i>KbHT</i>	<i>KbLT</i>			
			10074	0.184	0.233	0.461	0.579
			23426	0.253	0.318	0.335	0.562
			49545	1.336	1.716	0.400	0.511
				1.930	2.253	0.292	0.306
				0.441	0.548	0.111	0.103
			21919	0.248	0.322	0.402	0.573
				0.361	0.575	0.465	0.578
				0.309	0.281	0.213	0.358
				0.256	0.281	0.325	0.524
			17321	0.151	0.188	0.478	0.633
				0.329	0.383	0.310	0.355
				0.178	0.160	0.164	0.246
				0.132	0.209	0.189	0.356
			1814	0.219	0.272	0.528	0.699
				0.273	0.302	0.371	0.453
			183	0.062	0.069	0.180	0.328
			45136	0.472	0.673	0.428	0.529
				0.352	0.399	0.331	0.382
				0.433	0.379	0.304	0.374
			43559	0.321	0.334	0.250	0.301
				0.390	0.488	0.174	0.212
				0.309	0.301	0.136	0.168
				0.363	0.419	0.190	0.173
			24499	0.481	0.449	0.120	0.274
				0.271	0.334	0.171	0.191
			13181	0.509	0.526	0.345	0.517
				2.847	3.072	0.313	0.415
				1.533	1.413	0.161	0.273
				3.618	4.282	0.236	0.382
			37408	0.666	0.680	0.143	0.160
				0.654	0.675	0.169	0.198
			15751	0.086	0.085	0.392	0.539
			45455	0.247	0.249	0.481	0.688
				0.408	0.362	0.429	0.546
				0.247	0.340	0.205	0.420
				0.298	0.216	0.323	0.602
			753	0.118	0.109	0.068	0.255
			19855	0.291	0.344	0.218	0.474
				0.682	0.590	0.185	0.229
15581	0.097	0.314	0.314	0.613			
15074	0.160	0.342	0.127	0.111			
	0.831	4.597	0.184	0.242			
15581	0.452	0.845	0.449	0.643			
	0.410	0.606	0.404	0.545			
	0.628	0.991	0.236	0.423			
	0.337	0.956	0.447	0.628			
25944	0.206	0.351	0.231	0.295			
	0.231	0.391	0.138	0.169			
10316	0.096	0.152	0.404	0.654			
	0.075	0.124	0.553	0.537			
29604	0.410	0.738	0.486	0.575			
	0.158	0.277	0.412	0.429			
	0.387	0.495	0.240	0.315			
	0.480	0.839	0.373	0.434			
2155	0.316	0.435	0.466	0.671			
	0.402	0.686	0.350	0.459			
42649	0.086	0.136	0.098	0.187			
	0.086	0.109	0.096	0.063			
	0.303	0.484	0.125	0.226			
14817	0.180	0.245	0.359	0.468			
575	0.238	0.321	0.057	0.089			
25047	1.788	2.819	0.340	0.399			
	3.179	4.185	0.302	0.345			
	0.811	0.931	0.218	0.299			
	2.417	3.131	0.233	0.387			
16489	0.256	0.333	0.136	0.168			
6265	0.081	0.104	0.568	0.726			
3264	0.090	0.133	0.484	0.690			
	0.421	0.590	0.269	0.401			
	0.217	0.335	0.144	0.200			
	1.086	0.999	0.259	0.394			
28601	0.200	0.261	0.642	0.812			
	0.311	0.332	0.363	0.636			
	0.259	0.388	0.485	0.775			

	0.270	0.199	0.189	0.332
49207	0.383	0.331	0.422	0.421
37858	0.132	0.128	0.517	0.673
	0.265	0.229	0.451	0.555
	0.113	0.080	0.253	0.444
22306	0.357	0.293	0.123	0.173
31952	0.477	0.392	0.401	0.548
10090	0.148	0.121	0.444	0.592
57475	0.121	0.092	0.498	0.544
9911	0.646	0.391	0.175	0.398
9869	0.300	0.189	0.332	0.435
	0.354	0.201	0.270	0.364
	0.629	0.271	0.168	0.155

48653	0.078	0.039	0.501	0.557
11181	0.416	0.183	0.081	0.258
8543	1.142	0.554	0.355	0.447
	2.032	0.936	0.329	0.320
	2.108	0.734	0.157	0.204
	1.394	0.684	0.241	0.303
43984	1.691	0.680	0.355	0.474
	1.819	0.781	0.278	0.306
22299	1.163	0.703	0.127	0.050
	1.271	0.733	0.086	0.039
	1.061	0.452	0.084	0.012
	0.510	0.085	0.146	0.00
ρ (t-test)	0.38		1.37 E ⁻²⁰	

VITA
RICARDO COLON

EDUCATION

2012 – 2016

B.S. Chemistry

Florida International University

Miami, FL

2016 – 2021

Doctoral Candidate, Chemistry

Florida International University

Miami, FL

PUBLICATIONS

Chen, W., Colon, R., Louda, J. W., del Rey, F. R., Durham, M., & Rein, K. S. (2018).

Brevetoxin (PbTx-2) influences the redox status and NPQ of *Karenia brevis* by way of thioredoxin reductase. *Harmful Algae*, 71, 29-39.

Colon, R., & Rein, K. S. (2021). Essential components of the xanthophyll cycle differ in high and low toxin *Karenia brevis*. *Harmful Algae*, 103, 102006.

Tuladhar, A., Hondal, R. J., Colon, R., Hernandez, E. L., & Rein, K. S. (2018). Effectors of thioredoxin reductase: Brevetoxins and manumycin-A. *Comparative Biochemistry and Physiology Part C: Toxicology & Pharmacology*.